Close coupling calculations of dimer energy levels

Danby, Grahame

CLOSE COUPLING CALCULATIONS OF DIMER ENERGY LEVELS

by

Grahame Danby

A Thesis submitted to the University of Durham in candidature for the Degree of Doctor of Philosophy

September 1985

ABSTRACT

The aim of this thesis is to calculate the bound state energies of molecular dimers. The problem is formulated for a system consisting of any two $^1\Sigma$ diatomic molecules, treated as rigid rotors. Simplifications which arise from symmetry considerations are fully discussed. The de Vogelaere and R-matrix propagator algorithms have been used to solve the resulting systems of coupled second order differential equations. Their numerical convergence properties are compared in test calculations on the Ar-HCl system.

The above methods are used to calculate the bound state energies of H_2-H_2, using four separate ab initio potentials. The CI potential of Meyer, Schaefer and Liu (designated "M80") is found to give the best agreement with spectroscopic measurements, though a small shift in the position of the repulsive wall is indicated. The M80 potential is then used in the remaining calculations; these include the evaluation of the energies of resonances and bound states lying above the dissociation limit of the dimer, corresponding to rotationally excited H_2. The results of these calculations are used to assess the validity of approximations made in the proposed identification of H_2-H_2 features in the far infrared spectra of the Jovian atmosphere.

The Born-Oppenheimer approximation permits the use of the M80 potential to calculate the bound states and resonances of D_2-D_2. That some of these resonances have dual Feshbach/shape character is noted. The dimer structure, accompanying the observed near infrared $S_1(0)$ and $Q_1(0)$ + $S_o(0)$ spectra in ortho-deuterium, is modelled by treating the two D_2 molecules as distinguishable rigid rotors. We conclude that the experiments provide evidence both for rotational splitting of the levels and for internal rotational predissociation. Alternative line assignments to those hitherto made are also suggested.

We end with a general discussion in which suggestions for future work are made.

ACKNOWLEDGEMENTS

I am indebted to my Ph.D. supervisor, Dr. D.R. Flower, for his interest, assistance and stoicism over the years. I also thank him, together with Professor B.H. Bransden and Dr. J.V. Major, for accepting me as a Research Student in Durham.

I have had many useful discussions with my Molecular Physics Colleagues : Dr. D.J. Baker, Dr. D.P. Dewangan and Dr. D.J. Kirkpatrick. It is also a pleasure to thank the following for their interest in my progress : Professor A.W. Wolfendale, Dr. R. Shingal, Dr. C.W. Newby and Mr. R.N. Hewitt.

The staff of Durham University Computer Unit have been extremely helpful. Financial support for this work was provided by the S.E.R.C. Finally, I should like to thank Mrs. M. Chipchase both for her patience and her efficient typing of the manuscript.

CONTENTS

CHAPTER ONE

INTRODUCTION

1.1 Motivation

The complementarity of studies of low energy scattering of electrons, e^-, on positive ions, X^{m+}, and of the electronic structure of the corresponding bound state system, $X^{(m-1)+}$, has been recognised for many years. Very similar numerical techniques may be applied to both the bound state and scattering problems (e.g. Seaton and Wilson 1972, Seaton 1974). By following this approach information derived from spectroscopic measurements on $X^{(m-1)+}$ may be used to obtain accurate values of the cross-sections for the excitation process

$$X^{m+} + e^- \longrightarrow (X^{m+})^* + e^- \qquad (1.1)$$

near threshold. The results of these calculations find important applications in the studies of many types of astrophysical plasmas.

In the dense molecular clouds of interstellar space, rotational excitation of molecules, M, occurs principally in collisions with molecular hydrogen,

$$M(j) + H_2 \longrightarrow M(j') + H_2 \qquad (1.2)$$

at energies close to the rotational excitation thresholds. The corresponding cross-sections are required to interpret the microwave spectra of the molecular clouds.

A prerequisite in calculations of cross-sections for processes of type (1.2) is a knowledge of the relevant $M\text{-}H_2$ electronic potential energy surfaces (e.g. Green and Thaddeus 1976, Green et al. 1978). The $M\text{-}H_2$ interaction is, for non-reactive systems, strongly repulsive at

short range, where the electron charge distributions of M and H_2 overlap, and weakly attractive at long range, owing to the dispersion (van der Waals) interaction. The other contributions at long range are the interaction between the permanent electrostatic multipole moments of the molecules, and that between the permanent and induced multipoles. The latter interaction, called the induction energy, is generally unimportant in neutral systems. The long range permanent electrostatic energy is dominated by the dispersion energy except in highly polar systems such as H_2O - H_2O. At some intermediate distance, there is a potential minimum, where the attractive and repulsive forces cancel. The values of rotational excitation cross-sections, at low collision energies, are particularly sensitive to the form of the M-H_2 interaction in the region of this potential well.

If the potential well is sufficiently deep, it can support bound states of the M-H_2 system. It follows that spectroscopy of the molecular dimer, M-H_2, can yield valuable information on the M-H_2 interaction in the region of the well. It is this part of the interaction which is the most difficult to determine theoretically; spectroscopy should thus also be helpful in assessing the relative merits of different approximations used in any such potential calculations. Given the potential, the bound state eigenenergies may be calculated and the resulting transition frequencies compared with experiment. These calculations may be carried out using numerical

techniques similar to those employed in studies of rotational excitation. Le Roy and Carley (1980) have reviewed calculations on atom-diatom systems. The problem of a dimer consisting of two diatoms is receiving growing attention, and the work reported in this thesis will reflect that trend.

A more direct motivation for the study of van der Waals molecules is the possibility of observing their spectra in the interstellar medium. Of the sixty or so molecular species observed to date, some, such as H_2CO and HCO, have low thermochemical stability (Dalgarno 1975; Millar and Williams 1985). Most of these molecules are observed in the cold dark clouds of interstellar gas and their higher density cores. Storey and Cheung (1978) have carried out a search, at radio wavelengths, for evidence of the HCN - HCN dimer in several interstellar clouds. No such evidence was found, and they were able to place an upper limit of around 1% for the abundance of the dimer relative to the monomer. A similar conclusion was reached by Vanden Bout et al. (1979) regarding the concentration of the CO -CO dimer. They searched 11 interstellar clouds at the frequency 1.458 GHz (0.0486 cm^{-1}), which is an observed laboratory transition of the dimer. Vanden Bout et al. also suggested that a similar search for the H_2 - CO dimer could well be more fruitful; however, they were prevented from carrying out such a search because of difficulties in obtaining either parallel laboratory radio-frequency measurements or accurate

theoretical results.

The preponderance of H_2 in the interstellar medium makes the associated dimer another candidate, though the binding energy of $H_2 - H_2$ is only about 2.4 cm^{-1}. It had been suggested that collision induced dipole radiation arising from the radiative association process

$$H_2 + H_2 \longrightarrow H_2 - H_2 + h\nu \qquad (1.3)$$

could be important in interstellar Hydrogen gas (Schaefer 1982a, Schaefer and Meyer 1983). Indeed it was claimed that radiation from this process could account for an observed excess in the cosmic microwave background between 14 and 20 cm^{-1} (Gush 1981). However, it was subsequently realised (e.g. Frommhold et al. 1985, and references therein) that the original calculations predicted a hugely inflated dimer formation rate by the process (1.3). Recently, a more plausible explanation for the observations of Gush (1981) has emerged: de Bernardis et al. (1985) have proposed the existence of far infrared emission from extragalactic dust, heated by a near infrared cosmological background.

Humphries and Horton (1977) have argued that structure accompanying Lyman absorption lines of H_2 may be due to the presence of the H_4 dimer in diffuse interstellar clouds. Even allowing for some enhancement of the formation process (1.3), due to the presence in these clouds of rotationally excited H_2, it seems unlikely that sufficiently high concentrations of the dimer could exist. Spitzer

and Morton (1976) have attributed this structure, observed by the Copernicus satellite, to a Doppler effect resulting from components of the interstellar clouds moving with different velocities.

Convincing astronomical evidence of H_4 dimers has, however, come from another source : the far infrared observations by the Voyager spacecraft of the atmospheres of Jupiter and Saturn (Hanel et al. 1979, Gautier et al. 1983). These observations, which will be discussed elsewhere in this thesis, provide information on the ortho-H_2 to para-H_2 ratio as well as on the general physical conditions in these planetary atmospheres. The questions of whether van der Waals molecules exist in measurable quantities in the interstellar medium, and if observations of their spectra could yield useful information on physical conditions there, remain open.

1.2 Potential energy surfaces

1.2.1 The ab initio calculation of potential energy surfaces. Implicit in the above reference to potential energy surfaces is the assumption of the Born-Oppenheimer approximation. This permits a separation of the motions of the rapidly moving electrons from those of the nuclei (e.g. Green 1974, Gianturco 1980). Most of this thesis will be concerned with the nuclear dynamics; here we briefly outline the solution of the electronic Schroedinger equation, the eigenenergies of which provide the potential surfaces on which the nuclei move. A large number of excellent reviews of this subject exist; the author

found the short articles by Green (1974), Balint-Kurti (1975a) and Pople (1982) particularly helpful.

If the nuclei, α, are fixed at a geometry, denoted by the coordinates Q_α, the total Hamiltonian of the system reduces to an effective electronic Hamiltonian. The terms in this are the kinetic energy of the electrons, i, and the Coulomb interactions, involving the electrons and nuclei: $V_{\alpha\alpha'}$, $V_{ii'}$, and $V_{i\alpha}$. For a system consisting of two closed shell molecules, spin-orbit coupling terms may be neglected. The Schroedinger equation for the motion of the electrons in a system of two interacting molecules, A and B, is written as

$$\left[H^{AB}(q_i ; Q_\alpha) - E^{AB}(Q_\alpha) \right] \psi^{AB}(q_i ; Q_\alpha) = 0 \quad (1.4)$$

To map out a potential energy surface, (1.4) must be solved for several values of the nuclear coordinates, Q_α. The interaction energy is found by subtracting the electronic energies of the isolated molecules, E^A and E^B, from the total electronic energy, E^{AB}. Great care must be taken to reduce cancellation errors in this procedure.

This cancellation problem can be avoided, for large intermolecular separations, by calculating the (small) interaction energy directly using perturbation theory (Buckingham 1967, Leavitt 1980). The perturbation Hamiltonian, V_{AB} is given by

$$V_{AB} = H^{AB} - (H^A + H^B) \quad (1.5)$$

where H^A and H^B are the (electronic) Hamiltonians of the two isolated molecules, A and B. If the wavefunctions of the isolated, ground state, molecules are known, we can write down the first order contribution to the interaction energy:

$$V_{int}^{(1)} = \langle A_o B_o | V_{AB} | A_o B_o \rangle \qquad (1.6)$$

The zeroth order wavefunction is just a product of those for the isolated systems, reflecting an assumption that the charge clouds do not overlap. Alternatively, a multipole expansion of V_{AB} may be performed, leading to an expression for the long-range first-order interaction in terms of the permanent multipoles of A and B (Gray 1968, Maitland et al. 1981). These may be obtained either experimentally or by quantum mechanical calculations on the individual molecules. We have thus obtained the permanent electrostatic energy contribution to the long range interaction.

The induction and dispersion terms are found by going to second order, the Rayleigh-Schroedinger expression being given by

$$V_{int}^{(2)} = \sum_{i,j \neq o,o} \sum |\langle A_o B_o | V_{AB} | A_i B_j \rangle|^2 / (E_o^A + E_o^B - E_i^A - E_j^B) \qquad (1.7)$$

A_i is the i^{th} excited state of molecule A with eigenenergy E_i^A. The ground state terms and those applying to molecule B are similarly defined. The dominant dispersion contribution, which is due to the correlation of charge density fluctuations in A and B, is given by the sum of the terms in (1.7) excluding those for which either i or j corresponds to a ground electronic state (o). As in the electrostatic case, an explicit form for the dispersion energy can be written, as a power series in 1/R, in terms of the properties of A and B. By way of example, the leading term in the dispersion interaction between two rare gas atoms is given by (Buckingham 1967)

$$V_{disp}(R) = -\left\{ \frac{3\, U_A U_B \quad \alpha_A \alpha_B}{2\,(U_A + U_B)} \right\} R^{-6} \qquad (1.8)$$

where U and α are respectively the ionisation potentials and the polarisabilities of the interacting atoms, separated by a distance R. This provides the theoretical basis for the attractive contribution to the well known Lennard-Jones 6-12 potential:

$$V(R) = c R^{-12} - d R^{-6} \qquad (1.9)$$

For a system of two interacting molecules, the coefficient d will be geometry dependent. No justification for the R^{-12} behaviour exists, other than the empirical presence of a strong short-range repulsive barrier.

The short-range forces arise from the overlapping charge distributions of the interacting molecules. As alluded to in equation (1.4), the system can be treated as a single supermolecule using the same techniques as for many-electron atoms and molecules (H.F. Schaefer 1972). The interaction energy is given by the following expression

$$V_{int} = \langle \Psi^{AB} | H^{AB} | \Psi^{AB} \rangle - \langle A_o | H^A | A_o \rangle - \langle B_o | H^B | B_o \rangle \qquad (1.10)$$

where the integrations are performed over the coordinates of all electrons. The three terms on the right hand side of (1.10) should all be calculated in the same way so that any errors approximately cancel. Consider the first term, which is the energy, E^{AB}, of the supermolecule in its ground electronic state. We know from

the variational theorem that a normalised trial wavefunction may be used to provide an upper limit to this:

$$\langle \Psi^{trial} | H^{AB} | \Psi^{trial} \rangle \geq \langle \Psi^{AB} | H^{AB} | \Psi^{AB} \rangle = E^{AB} \qquad (1.11)$$

In the Hartree-Fock (HF) method, the compound trial wavefunction is taken to be a single Slater determinant of molecular spin-orbitals. For a closed shell supermolecule with N electrons, this is written

$$\Psi^{HF} = (N!)^{-1/2} \begin{vmatrix} \phi_1(q_1)\uparrow & \phi_1(q_2)\uparrow & \cdots & \phi_1(q_N)\uparrow \\ \phi_1(q_1)\downarrow & \phi_1(q_2)\downarrow & \cdots & \phi_1(q_N)\downarrow \\ \phi_2(q_1)\uparrow & \phi_2(q_2)\uparrow & \cdots & \phi_2(q_N)\uparrow \\ \vdots & \vdots & & \vdots \\ \phi_{N/2}(q_1)\downarrow & \phi_{N/2}(q_2)\downarrow & \cdots & \phi_{N/2}(q_N)\downarrow \end{vmatrix} \qquad (1.12)$$

The $(N!)^{-\frac{1}{2}}$ factor is a normalisation factor arising from the fact that the Slater determinant is an antisymmetric combination of all possible (N!) permutations of simple products of N spin-orbitals. The Pauli exclusion principle is automatically satisfied by such a determinantal wavefunction. The arrows denote the spin functions of the electrons. The (space) orbitals ϕ are defined as functions of the coordinates of a single electron. These molecular orbitals are varied so as to minimise the energy, in keeping with the variational principle (1.11). The condition that this energy be a minimum leads to the Hartree-Fock equations, which each of the individual molecular orbitals satisfy:

$$F(q_i ; Q_\alpha)\,\phi_i(q_i) = \varepsilon_i\,\phi_i(q_i) \qquad (1.13)$$

These equations describe the motion of a single electron, assigned to the orbital ϕ_i, moving in the averaged field of the other electrons. The Fock Hamiltonian, F, is itself dependent on the orbitals themselves due to the presence of a direct Coulomb interaction and an exchange interaction; the latter term arising from the antisymmetry of the Hartree-Fock wavefunction. The HF equations (1.13) must thus be solved iteratively. Starting with an educated guess for all of the molecular orbitals ϕ_i, F is evaluated. Equation (1.13) is then used to calculate a new set of ϕ_i, which in turn are used to calculate an improved F. This cycle is repeated until F does not change to within an acceptable tolerance. The orbitals thus determined can then be substituted in (1.12) and thence in (1.11) to yield the self-consistent field (SCF) energy, a term which is self-explanatory given the above procedure. Although there is no universally recognised convention, the term "Hartree-Fock energy" is usually reserved for the exact solution of the HF equations.

It is not practicable to obtain a numerical solution of the HF equations for systems consisting of more than two atoms. They may, however, be solved by expressing the molecular orbitals as a linear combination of atomic orbitals (LCAO) centred on each of the nuclei (e.g. Bunker 1979a):

$$\phi_i = \sum_j C_{ij} \chi_j \qquad (1.14)$$

The coefficients, C_{ij}, of this expansion are varied so as to find the best solutions of (1.13). The accuracy of the final results will clearly depend on the atomic orbital basis set used. Each atomic orbital, χ_j, is generally represented by a number of either Slater type functions or the computationally convenient, though less realistic, Gaussian type. The basis set "quality" is determined by four factors : the type of functions, the level of optimisation of the parameters of these functions, the number of functions used to describe each atomic orbital, and the number of polarisation functions per orbital. Polarisation functions are functions with higher quantum numbers than the occupied atomic orbitals. A more systematic approach to assessing the basis set quality has been investigated by Burton et al. (1982).

We note at this point that an incomplete basis set will lead to a contribution to the interaction energy known as the basis set superposition error (e.g. van der Avoird et al. 1980). This is purely an artefact of the calculation. The energy of the supermolecule is artificially lowered (though it is still above the true value) due to the admixture of basis functions centred on one molecule with those of the other. A concurrent lowering is absent from the energies of the isolated molecules, calculated with the same atomic

orbital basis set. The result is to make V_{int} too low, thus overestimating the well depth. This problem can be circumvented by introducing a similar degree of basis flexibility in the calculation of the isolated molecule energies. The energy of each isolated molecule is calculated, for every point on the potential energy surface, with so-called ghost orbitals placed at the position occupied by the other molecule in the corresponding supermolecule calculation . The basis set superposition errors, which are then present in all three terms on the right hand side of (1.10), hopefully cancel. This is known as the function counterpoise method (Boys and Bernardi 1970, Wells and Wilson 1983).

The SCF method is reliable for computing the short range part of the potential as it accurately describes the dominant Coulomb and exchange interactions associated with the overlapping charge clouds. Unfortunately, the situation is rather different for intermediate intermolecular distances. This is because a single Slater determinant cannot account for the simultaneous correlation of two (or more) electrons. The dispersion energy, which is generally relatively important at intermediate range, is the intermolecular contribution to the correlation energy. The correlation energy is defined in terms of the exact solution of (1.4), E^{AB}, and the HF energy, E^{HF}:

$$E^{corr} = E^{AB} - E^{HF} \qquad (1.15)$$

This definition differs from that of Green (1974) only by a minus sign. Some kind of post HF procedure is necessary to obtain the interaction energy accurately in the well region.

One way to improve on the HF or SCF results is to take a linear combination of Slater determinants, differing in the choice of molecular orbitals which the electrons are assumed to occupy. Each Slater determinant therefore, corresponds to a different electronic configuration. If, for the sake of argument, we define the ground state HF wavefunction (1.12) as our reference (or root) configuration, then we can form all single excitations (or substitutions) by replacing one occupied molecular orbital with an unoccupied one. The maximum number of such excitations that we can make will be determined by the available atomic orbital basis. Higher order excitations are similarly defined. The resulting trial wavefunction to use in the variational procedure is known as a configuration interaction (CI) wavefunction:

$$\psi^{CI} = \sum_k a_k \psi_k^{HF} \qquad (1.16)$$

The variational parameters a_k which minimise the energy are obtained by diagonalising the matrix of the Hamiltonian H^{AB} in the basis of the functions ψ_k^{HF}. This approach, which is known as the CI method, yields in principle an exact solution of (1.4) providing that a large enough number of Slater determinants are used in the expansion (1.16).

As indicated in (1.16), we have used HF molecular orbitals to construct the Slater determinants. A much better expansion would result if the so-called natural orbitals (Löwdin 1955) were used instead. Unfortunately, to determine these requires advance knowledge of the exact wavefunction. Approximate natural orbitals may, however, be constructed either iteratively (Bender and Davidson 1966) or by using pseudonatural orbitals (PNO's) (Edmiston and Krauss 1966). The PNO's are determined for selected electron pairs moving in the HF field of the remaining electrons; the method utilises the fact that approximate natural orbitals can be determined relatively straightforwardly for the simple two electron problem. By using such orbitals, the number of Slater determinants in the CI expansion can be reduced, typically by a factor of ten, without compromising the accuracy of the final results.

The CI method can be used for all values of the intermolecular distance, though it does require a large number of configurations even if approximate natural orbitals are used. The consequential computational expense of the CI method has encouraged the development of approximate methods for treating electron correlation. Pair theories are based on estimating the energy arising from the correlated motion of two electrons at a time. The resulting pair correlation energies may then be either simply added, or coupling terms can be introduced (H.F. Schaefer 1972, Kutzelnigg 1977a). We may expect this to be a reasonable approach both because the Hamiltonian

in (1.4) contains only one and two electron operators, and because the Pauli exclusion principle prevents more than two electrons from occupying the same point in space.

Ab initio methods for calculating points on a potential energy surface form a large and active field of research. Only some of the general ideas have been discussed here. The potential may be empirically improved by comparing experimental observations with calculations of the nuclear dynamics on which they depend. The relevant experimental observables (Maitland et al. 1981) include the non-ideal behaviour and transport properties of gases, molecular beam scattering measurements and, of course, the spectroscopy of van der Waals molecules.

1.2.2 Fitting potential energy surfaces. In order to carry out dynamical calculations on an ab initio potential surface, it is necessary to fit the computed points to a suitable functional form. Analytic functions for describing the angular dependence of the interaction between two rigid diatoms will be presented in the following chapter. Here we shall discuss the problem in general terms.

The interaction potential for a system of any two rigid molecules is a function of the separation of their centres of mass, R, and of their relative orientation. The latter is defined by a number of angles (three are needed for a diatom-diatom system), collectively denoted by Ω_α. For a given radial separation, the angular

dependence can be expanded in terms of a convenient set of functions f_a:

$$V(R, \Omega_\alpha) = \sum_a V_a(R) f_a(\Omega_\alpha) \qquad (1.17)$$

If the index α has N values, then a least squares fit to an n term expansion (each term denoted by the index a) may be attempted, providing of course, that $N \geqslant n$. Thus, at each value of R we minimise the quantity

$$D = \sum_\alpha \left\{ \sum_a V_a(R) f_a(\Omega_\alpha) - V(R, \Omega_\alpha) \right\}^2 \qquad (1.18)$$

A necessary condition for D to be a minimum is that, for all b, $\partial D / \partial V_b(R) = 0$. This condition leads to a system of linear equations, which may be solved to obtain the potential expansion coefficients, $V_a(R)$ (Alexander and De Pristo 1976):

$$\sum_\alpha f_b(\Omega_\alpha) V(R, \Omega_\alpha) = \sum_\alpha f_b(\Omega_\alpha) \left\{ \sum_a f_a(\Omega_\alpha) V_a(R) \right\} \qquad (1.19)$$

If (1.19) can be solved for a number of terms, n, equal to the number of geometries, N, then the latter may be said to have been "optimally chosen". In this case, the solution of (1.19) is equivalent to solving (1.17) for the $V_a(R)$ by direct inversion of the matrix $f_a(\Omega_\alpha)$.

We note, in passing, that for large systems of such equations, computer routines for matrix inversion tend to be numerically less stable than those which solve the linear equations directly.

If the angular functions, f_a, form a complete orthonormal set, then the radial expansion coefficients may also be obtained by numerical quadrature over all angles:

$$V_a(R) = \langle f_a(\Omega_\alpha) \mid V(R, \Omega_\alpha) \rangle \qquad (1.20)$$

The only disadvantage of this alternative method, employed by Berns and van der Avoird (1980) and Tennyson (1984), is that the ab initio potential is needed at a large number of geometries. Such large numbers (typically 100) of points are often unavailable.

Once the potential expansion coefficients have been obtained on a radial grid, using either of the above procedures, they may be fitted using some form of polynomial interpolation. Green (1977) has discussed the relative merits of cubic spline and 5th order Lagrange interpolation in this context.

1.3 van der Waals molecules

1.3.1 Experimental The spectroscopy of van der Waals molecules forms a substantial part of this thesis. Nevertheless, it is pertinent to make a few general comments here. The molecular dimers discussed in later chapters have been observed either in gas cell absorption or molecular beam experiments. The former method involves conventional spectroscopy of a bulk sample of gas containing the constituent molecules of the dimer in question (e.g. Blaney and Ewing 1976).

Dimer transitions are observed as fine structure accompanying absorption of infrared radiation due, typically

to vibrational excitation of one of the monomers. The gas sample is cooled to enhance the dimer concentration. The dimers are formed mainly in 3-body collisions, a mechanism which is insignificant in the rarefied conditions of the interstellar medium. In order to reduce the component of the line widths due to pressure broadening, low gas densities are nevertheless required. This necessitates a long optical path length, generally achieved by multiple traversal of the sample using a system of mirrors. Typical experimental configurations have been illustrated by Watanabe and Welsh (1965) and McKellar and Welsh (1972).

Molecular beam spectroscopy is a more recent development, using supersonic nozzles to produce a much higher concentration of dimers than is possible with the more conventional approach above. A gas at high pressure is allowed to expand, through a nozzle, into a vacuum. The resulting adiabatic expansion cools the gas, producing a beam of molecules with a very narrow spread of velocities. This can correspond to an effective translational temperature which is often less than 1K (Howard 1981) and sometimes as low as 0.05K (Levy 1981). As the gas emerges from the nozzle, 3-body collisions produce van der Waals molecules which are stable with respect to (the less frequent) collisions further downstream. Highly excited rotational and vibrational states of the monomers are depopulated at the low ambient temperatures leading to a simplification of the observed spectrum.

A variety of spectroscopic techniques may be used in conjunction with molecular beams. Perhaps the most important to date has been molecular beam electric resonance (MBER) spectroscopy (Klemperer 1977, Howard 1981). Initially, beam molecules, in a particular quantum state, pass through two focussing fields onto the entrance slit of a mass spectrometer detector. Microwave or radiofrequency radiation is then applied to the beam between the two focussing fields. Absorption of this radiation changes the quantum state, and hence the dipole moment, of the molecule concerned. This leads to a concurrent decrease in beam intensity arriving at the mass spectrometer.

The complementary technique of molecular beam magnetic resonance spectroscopy has been used in radiofrequency studies of rare gas-H_2 (Waaijer and Reuss 1981) and H_2 - H_2 (Verberne and Reuss 1980) complexes. MBER spectroscopy cannot be used in such instances as H_2 does not possess an electric dipole moment.

Other spectroscopic techniques which have been used with molecular beams include laser induced fluorescence and bolometric spectroscopy (Le Roy and Carley 1980). In the former, the beam molecules are electronically excited by a continuous wave dye laser; photodetectors monitor the resulting fluorescence. In the bolometric method, one of the constituent monomers of the dimer is excited using an infrared laser. The energy absorbed is converted to heat as the beam strikes the bolometer.

Should the dimer predissociate during transit (by transferring the monomer excitation energy to the van der Waals bond), the fragments are scattered out of the beam and a "negative signal" results.

1.3.2 Classification. For the interpretation and assignment of experimental lines, a system of classifying van der Waals molecules is desirable. Ewing (1976) has devised a classification scheme for van der Waals complexes of the type X_2 - Y. The scheme, which can be extended to more complex systems, is based on how strongly the angle dependent part of the potential couples the rotational states of the diatom.

We begin by defining a quantity $\overline{\Delta V}$ which is an "average effective anisotropy" (Le Roy and Carley 1980). A reasonable way of obtaining this would be to fix the intermolecular separation at some suitable average value, and then to sum the expansion coefficients $V_a(R)$ corresponding to non-isotropic terms $f_a(\omega_\alpha)$ (see equation (1.17) and also equation (2.21) in the following chapter). Weakly coupled complexes are defined as those having $\overline{\Delta V} \ll \Delta E(j)$, where $\Delta E(j)$ represents the rotational level spacing of the isolated diatom. In strongly coupled dimers, this spacing is of the same magnitude, or somewhat smaller, than the average effective anisotropy. The rotor states of the dimer will then be strongly mixed, and j is not even approximately a good quantum number as it is in the weak coupling case. Ashton et al. (1983) have noted that, in the Ar - HCl dimer, there is a

gradual transition from strong to weak coupling for higher bound states. This is because $\Delta E(j)$ is larger for levels correlating with higher j.

When $\overline{\Delta V} \gg \Delta E(j)$, a high potential barrier to internal rotation exists and the complex is said to be semi-rigid. These systems have a well defined structure, and it is more appropriate to associate a bending vibration, rather than a rotation, with the (rigid) diatom.

The structure of a variety of van der Waals molecules has been illustrated by Hobza and Zahradnik (1980). J. Tennyson has coined the term "floppy" to describe both van der Waals molecules in general, together with conventional (chemically bound) species undergoing large internal bending motion. This thesis deals with the former, though it should be borne in mind that similar techniques can be used to determine the bound state energies of the latter.

CHAPTER TWO

THEORY

2.1 Introduction

In the previous chapter we showed how to solve the Schroedinger equation for the electronic energy. The result depends parametrically on the positions of the nuclei. The rest of this thesis is concerned with the solution of the equations of motion of the nuclei moving on this electronic potential energy surface.

We shall work in a body-fixed frame of reference in which the intermolecular vector $\underset{\sim}{R}$, joining the centres of mass of the two diatoms (see Figure 2.1), is taken as the z axis. Its position relative to the space-fixed z axis is given by the Euler angles $(\phi, \theta, 0)$. The third Euler angle is arbitrary and is set equal to 0. A more formal definition of the body-fixed frame has been given by Tennyson and Sutcliffe (1982). We shall see that the problem reduces to a set of coupled second order differential equations. Initially the coupled equations and matrix elements for a system of two distinguishable heteronuclear $^1\Sigma$ diatomic molecules, treated as rigid rotors, will be given. The equivalence of the space-fixed and body-fixed basis sets and of the respective representations of the intermolecular potential will be demonstrated. Starting from this general system, we shall use any additional symmetries to reduce the number of basis states in the expansion of the total wave function and hence the number of coupled equations which must be solved. The cases where one

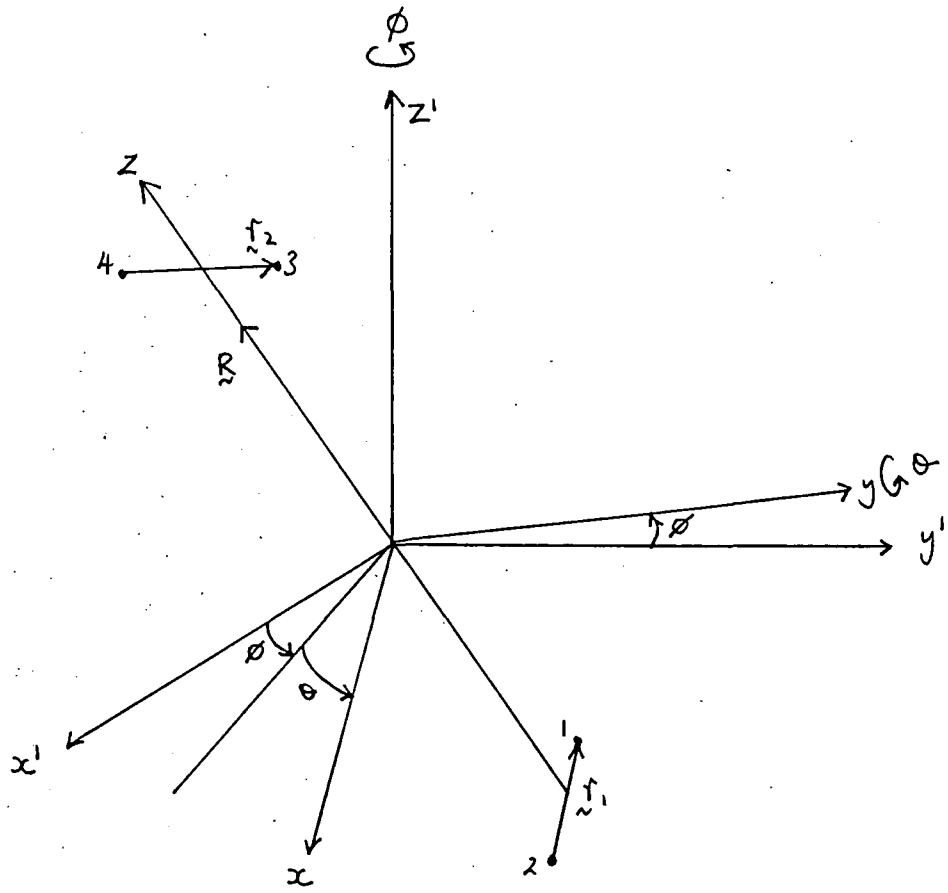

Figure 2.1

Definition of the reference frames used in this thesis. z' is the space-fixed and z the body-fixed z axis. The orientations of the two diatoms, referred to the body-fixed frame, are $\hat{r}_1 = (\theta_1,\phi_1)$ and $\hat{r}_2 = (\theta_2,\phi_2)$. r_1 is the intramolecular vector joining the nuclei 2 and 1. A rotation through the Euler angles $(\phi,\theta,0)$ takes the space-fixed into the body-fixed frame.

The nuclei are numbered according to the convention of Bunker (1979b) (see section 2.6).

or both molecules are homonuclear and where the molecules are identical are discussed. A number of workers have effected such reductions in basis dimensionality for specific systems by using the appropriate molecular symmetry group (e.g. Dyke et al. 1972, Tennyson and van der Avoird 1982a, 1984a). We shall illustrate the connection between this and the present approach, which is more in keeping with that adopted by Alexander and De Pristo (1977) and Heil et al. (1978).

We shall ignore nuclear spin, but note that this determines the multiplicity of the energy states and can, in the case of identical molecules, lead to the exclusion of some such states through considerations of the symmetry of the entire system. Inclusion of nuclear spin in the calculations would lead to a hyperfine splitting of the rovibrational energy levels of the dimer (Verberne and Reuss 1981). Calculations involving molecules with nonvanishing electronic spin and orbital angular momentum along the intramolecular axis (i.e. not $^1\Sigma$) are more complex, introducing further angular momenta couplings. To date, calculations of this type, whether scattering or bound state, appear to have been restricted to systems comprising a diatom and a structureless particle. The study by Tennyson and van der Avoird (1984b) of the He-O_2 van der Waals molecule, with oxygen in its ground $^3\Sigma$ state, is an example.

2.2 Two distinguishable diatomic molecules

The Schroedinger equation for the system in Figure 2.1 is written as

$$(H - E)\Psi = 0 \qquad (2.1)$$

In an inertial frame moving with the centre of mass of the complex, the Hamiltonian is, in atomic units,

$$H = h_1 + h_2 - \frac{1}{2\mu}\nabla_R^2 + V(\hat{r}_1, \hat{r}_2, R) \qquad (2.2)$$

In equation (2.2) h_1 and h_2 are the rotational Hamiltonians of the two isolated rigid rotors, and the kinetic energy operator can be expressed in the following form:

$$-\frac{1}{2\mu}\nabla_R^2 = -\frac{1}{2\mu R}\frac{\partial^2}{\partial R^2}R + \frac{\underset{\sim}{l}^2}{2\mu R^2} \qquad (2.3)$$

$\underset{\sim}{l}$ is the angular momentum operator associated with the intermolecular vector $\underset{\sim}{R}$. μ is the reduced mass of the system of four nuclei:

$$\mu = \frac{(m_1 + m_2)(m_3 + m_4)}{m_1 + m_2 + m_3 + m_4} \qquad (2.4)$$

We start by expanding Ψ in a rotational basis:

$$\Psi(JM|\hat{r}_1, \hat{r}_2, R) = \sum_{j_1 j_2 j_{12} \Omega} \frac{1}{R} F(j_1 j_2 j_{12} \Omega JM|R)\, \mathcal{Y}(j_1 j_2 j_{12} \Omega JM|\hat{r}_1, \hat{r}_2, \hat{R}) \qquad (2.5)$$

Here J is the total angular momentum with a projection, M, on the space-fixed z axis. j_{12} is the coupled value of the angular momenta, j_1 and j_2, of the two rotors, with a projection Ω on the body-fixed z axis. The rotational basis function, which defines a channel, is given by (cf. van der Avoird 1982)

$$\mathcal{Y}(j_1 j_2 j_{12} \Omega J M | \hat{r}_1, \hat{r}_2, \hat{R}) = \Psi(j_1 j_2 j_{12} \Omega | \hat{r}_1, \hat{r}_2) N^J_{M\Omega}(\hat{R}) \qquad (2.6)$$

where

$$\Psi(j_1 j_2 j_{12} \Omega | \hat{r}_1, \hat{r}_2, \hat{R}) = \sum_{\Omega_1 \Omega_2} C^{j_1 j_2 j_{12}}_{\Omega_1 \Omega_2 \Omega} Y_{j_1 \Omega_1}(\hat{r}_1) Y_{j_2 \Omega_2}(\hat{r}_2) \qquad (2.7)$$

and

$$N^J_{M\Omega}(\hat{R}) = \left(\frac{2J+1}{4\pi}\right)^{1/2} D^{J*}_{M\Omega}(\phi, \theta, 0) \qquad (2.8)$$

The function $Y_{j_1 \Omega_1}(\hat{r}_1)$ in equation (2.7) is a spherical harmonic, satisfying the eigenvalue equation

$$h_1 Y_{j_1 \Omega_1}(\hat{r}_1) \equiv \frac{j_1^2}{2\mu_1 r_1^2} Y_{j_1 \Omega_1}(\hat{r}_1) = B_1 j_1(j_1+1) Y_{j_1 \Omega_1}(\hat{r}_1) \qquad (2.9)$$

μ_1 is the reduced mass of the nuclei in the isolated diatom, and r_1 is a constant since we assume the rigid rotor approximation to be valid (see Section 2.5). B_1 is the rotational constant of diatom 1. $C^{j_1 j_2 j_{12}}_{\Omega_1 \Omega_2 \Omega}$

is a Clebsch-Gordan coefficient. In equation (2.8), $N^{J}_{M\Omega}$ is a normalised symmetric top eigenfunction (Rose 1957) and $D^{J*}_{M\Omega}$ is a rotation matrix element. Note in equation (2.9) that the angular momentum operator $\underset{\sim}{j}_1^2$ behaves in the same way as it would in a space-fixed frame (Brocks et al., 1983). The form of the basis functions (2.6) could be justified by noting that they are eigenfunctions of the body-fixed Hamiltonian with all coupling terms removed, as Le Roy and Carley (1980) have done in the atom-diatom case. Had we adopted a space-fixed reference frame then we would have written the rotational basis functions in the usual way (see e.g. Alexander and De Pristo 1977):

$$\mathcal{Y}(j_1 j_2 j_{12} l J M \varepsilon | \hat{\underset{\sim}{r}}_1', \hat{\underset{\sim}{r}}_2', \hat{\underset{\sim}{R}}) = \sum_{m_1 m_2 m m_l} C^{j_{12}\, l\, J}_{m\ m_l M} C^{j_1 j_2 j_{12}}_{m_1 m_2 m} Y_{j_1 m_1}(\hat{\underset{\sim}{r}}_1') Y_{j_2 m_2}(\hat{\underset{\sim}{r}}_2') Y_{l m_l}(\hat{\underset{\sim}{R}}) \qquad (2.10)$$

where l is the end-over-end angular momentum of the whole complex. The angular momentum projections now refer, of course, to the space-fixed z axis. The wave-functions, (2.6) and (2.10), are related through the unitary transformation (Launay 1977)

$$\mathcal{Y}(j_1 j_2 j_{12} \Omega J M | \hat{\underset{\sim}{r}}_1, \hat{\underset{\sim}{r}}_2, \hat{\underset{\sim}{R}}) = \sum_{l} \left(\frac{2l+1}{2J+1}\right)^{1/2} C^{j_{12}\, l\, J}_{\Omega\ 0\ \Omega} \mathcal{Y}(j_1 j_2 j_{12} l J M \varepsilon | \hat{\underset{\sim}{r}}_1', \hat{\underset{\sim}{r}}_2', \hat{\underset{\sim}{R}}) \qquad (2.11)$$

The effect of the parity operator, P, is to invert the space-fixed coordinates in the origin $(\hat{\underset{\sim}{r}}_1', \hat{\underset{\sim}{r}}_2', \hat{\underset{\sim}{R}} \rightarrow -\hat{\underset{\sim}{r}}_1', -\hat{\underset{\sim}{r}}_2', -\hat{\underset{\sim}{R}})$,

leading to the result that the parity of the space-fixed functions (2.10) is

$$\mathcal{E} = (-)^{j_1 + j_2 + l} \tag{2.12}$$

Acting on the right hand side of equation (2.11) with P we find that the rotational functions (2.6) are not eigenfunctions of parity, transforming thus:

$$P\,\mathcal{Y}(j_1 j_2 j_{12} \Omega J M | \hat{\underset{\sim}{r}}_1, \hat{\underset{\sim}{r}}_2, \hat{\underset{\sim}{R}})$$
$$= (-)^{J + j_{12} + j_1 + j_2}\, \mathcal{Y}(j_1 j_2 j_{12} -\Omega J M | \hat{\underset{\sim}{r}}_1, \hat{\underset{\sim}{r}}_2, \hat{\underset{\sim}{R}}) \tag{2.13}$$

Note that, as we only deal with integer angular momenta, we can set

$$(-)^{-J} = (-)^{J} \tag{2.14}$$

Functions with well defined parity, $\mathcal{E}$, are constructed by taking linear combinations of (2.6) and normalising:

$$\mathcal{Y}(j_1 j_2 j_{12} \bar{\Omega} J M \mathcal{E} | \hat{\underset{\sim}{r}}_1, \hat{\underset{\sim}{r}}_2, \hat{\underset{\sim}{R}})$$
$$= \left[\mathcal{Y}(j_1 j_2 j_{12} \bar{\Omega} J M | \hat{\underset{\sim}{r}}_1, \hat{\underset{\sim}{r}}_2, \hat{\underset{\sim}{R}}) + \mathcal{E}(-)^{J + j_{12} + j_1 + j_2} \right. \tag{2.15}$$
$$\left. \times\, \mathcal{Y}(j_1 j_2 j_{12} -\bar{\Omega} J M | \hat{\underset{\sim}{r}}_1, \hat{\underset{\sim}{r}}_2, \hat{\underset{\sim}{R}}) \right] \left[2(1 + \delta_{\bar{\Omega} 0})\right]^{-1/2}$$

where $\bar{\Omega} \equiv |\Omega|$. These functions vanish when $\bar{\Omega} = 0$ and $\mathcal{E}(-)^{J + j_{12} + j_1 + j_2} = -1$. The functions (2.10) and (2.15) form an equivalent basis, the unitary transformation between them following directly from (2.11) and (2.15) (Launay 1977):

$$\mathcal{Y}(j_1 j_2 j_{12}\,\pi\, J M \varepsilon\,|\hat{\underset{\sim}{r}}_1, \hat{\underset{\sim}{r}}_2, \hat{\underset{\sim}{R}})$$

$$= \sum_{l} \left(\frac{(1+\delta_{\pi 0})(2l+1)}{2(2J+1)} \right)^{1/2} C^{j_{12}\, l\, J}_{\pi\, 0\, \pi}\; \mathcal{Y}(j_1 j_2 j_{12}\, l\, J M \varepsilon\,|\hat{\underset{\sim}{r}}_1, \hat{\underset{\sim}{r}}_2, \hat{\underset{\sim}{R}}) \qquad (2.16)$$

Expanding the total wavefunction Ψ in the set of basis functions (2.15) we have

$$\Psi(JM\varepsilon|\hat{\underset{\sim}{r}}_1, \hat{\underset{\sim}{r}}_2, \underset{\sim}{R}) = \sum_{j_1 j_2 j_{12}\pi} \frac{1}{R} F(j_1 j_2 j_{12}\,\pi\, J M \varepsilon|R)\, \mathcal{Y}(j_1 j_2 j_{12}\,\pi\, J M \varepsilon|\hat{\underset{\sim}{r}}_1, \hat{\underset{\sim}{r}}_2, \hat{\underset{\sim}{R}}) \qquad (2.17)$$

Using (2.17), (2.3) and (2.2), equation (2.1) becomes

$$\left(h_1 + h_2 - \frac{1}{2\mu R}\frac{\partial^2}{\partial R^2} R + \frac{\underset{\sim}{l}^2}{2\mu R^2} + V(\hat{\underset{\sim}{r}}_1, \hat{\underset{\sim}{r}}_2, R) - E\right)$$

$$\times \sum_{j_1' j_2' j_{12}' \pi'} \frac{1}{R} F(j_1' j_2' j_{12}'\,\pi'\, J M \varepsilon|R)\, \mathcal{Y}(j_1' j_2' j_{12}'\,\pi'\, J M \varepsilon|\hat{\underset{\sim}{r}}_1, \hat{\underset{\sim}{r}}_2, \hat{\underset{\sim}{R}}) = 0 \qquad (2.18)$$

from which we may derive an infinite set of coupled second-order differential equations (Arthurs and Dalgarno 1960) for the radial functions, F(R):

$$\frac{d^2}{dR^2} F(j_1 j_2 j_{12}\,\pi\, J M \varepsilon|R)$$

$$= \sum_{j_1' j_2' j_{12}' \pi'} W(j_1 j_2 j_{12}\,\pi\,;\, j_1' j_2' j_{12}'\,\pi'\, J M \varepsilon|R) F(j_1' j_2' j_{12}'\,\pi'\, J M \varepsilon|R) \qquad (2.19)$$

The close-coupling method involves truncating the above set of equations by restricting the values of j_1' and j_2', and allowing the values of j_{12}' and π' permitted by the good quantum numbers (J and ε). The equations are independent of M. The coupling matrix, $\underset{\sim}{W}$, is

$$W(j_1 j_2 j_{12}\,\pi\,;\, j_1' j_2' j_{12}'\,\pi'\, J M \varepsilon|R) = \delta_{j_1 j_1'}\,\delta_{j_2 j_2'}\,\delta_{j_{12} j_{12}'}\,\delta_{\pi\pi'}\, 2\mu$$

$$\times \left[B_1 j_1(j_1+1) + B_2 j_2(j_2+1) - E\right] \qquad (2.20)$$

$$+ \frac{1}{R^2} \langle j_1 j_2 j_{12}\,\pi\, J M \varepsilon\,|\underset{\sim}{l}^2|\, j_1' j_2' j_{12}'\,\pi'\, J M \varepsilon\rangle_{\hat{\underset{\sim}{r}}_1, \hat{\underset{\sim}{r}}_2, \hat{\underset{\sim}{R}}}$$

$$+ 2\mu \langle j_1 j_2 j_{12}\,\pi\, J M \varepsilon\,|V(\hat{\underset{\sim}{r}}_1, \hat{\underset{\sim}{r}}_2, R)|\, j_1' j_2' j_{12}'\,\pi'\, J M \varepsilon\rangle_{\hat{\underset{\sim}{r}}_1, \hat{\underset{\sim}{r}}_2, \hat{\underset{\sim}{R}}}$$

A suitable expansion for the intermolecular potential must now be chosen to make possible the evaluation of the V-matrix elements in equation (2.20). Gioumousis and Curtiss (1961) proposed the following (body-fixed) expansion:

$$V(\hat{r}_1,\hat{r}_2,R) = 4\pi \sum_{q_1 q_2 \mu} V_{q_1 q_2 \mu}(R)\, Y_{q_1 \mu}(\hat{r}_1)\, Y_{q_2 -\mu}(\hat{r}_2) \qquad (2.21)$$

which is invariant under rotations about the z axis. The condition that the potential must be invariant under the parity operator implies that (Dyke et al. 1972)

$$V_{q_1 q_2 \mu}(R) = V_{q_1 q_2 -\mu}(R) \qquad (2.22)$$

Taking this inversion symmetry into account we may expand the potential in the following way:

$$V(\hat{r}_1,\hat{r}_2,R) = \sum_{q_1 q_2 \mu \geq 0} V_{q_1 q_2 \mu}(R)\, Y_{q_1 q_2 \mu}(\hat{r}_1,\hat{r}_2) \qquad (2.23)$$

where

$$Y_{q_1 q_2 \mu}(\hat{r}_1,\hat{r}_2) = 4\pi \left(Y_{q_1 \mu}(\hat{r}_1) Y_{q_2 -\mu}(\hat{r}_2) + Y_{q_1 -\mu}(\hat{r}_1) Y_{q_2 \mu}(\hat{r}_2) \right) \times (1+\delta_{\mu 0})^{-1} \qquad (2.24)$$

The index μ is now restricted to the range $0 \leq \mu \leq \min(q_1, q_2)$, where the function min means "smallest argument". $V_{000}(R)$ is the isotropic part of the potential. If the electronic potential energy surface at a given R

is known for n carefully chosen orientations, $V(\hat{\underset{\sim}{r}}_1, \hat{\underset{\sim}{r}}_2, R)$, we can use (2.23) to obtain a set of linear inhomogeneous algebraic equations for n potential expansion coefficients $V_{q_1 q_2 \mu}(R)$.

The intermolecular potential is frequently expanded in a space-fixed frame (cf. Green 1977) thus:

$$V(\hat{\underset{\sim}{r}}_1', \hat{\underset{\sim}{r}}_2', \underset{\sim}{R}) = \sum_{q_1 q_2 q_{12}} A_{q_1 q_2 q_{12}}(R)\; I_{q_1 q_2 q_{12}}(\hat{\underset{\sim}{r}}_1', \hat{\underset{\sim}{r}}_2', \hat{\underset{\sim}{R}}) \qquad (2.25)$$

where

$$I_{q_1 q_2 q_{12}} = \sum_{m_1 m_2 m_{12}} C^{q_1 q_2 q_{12}}_{m_1 m_2 m_{12}}\; Y_{q_1 m_1}(\hat{\underset{\sim}{r}}_1')\, Y_{q_2 m_2}(\hat{\underset{\sim}{r}}_2')\, Y^{*}_{q_{12} m_{12}}(\hat{\underset{\sim}{R}}) \qquad (2.26)$$

As Flower et al. (1979) point out, the two representations of the potential are equivalent, related through the transformation

$$V_{q_1 q_2 \mu}(R) = \frac{1}{(4\pi)^{3/2}} \sum_{q_{12}} (2q_{12}+1)^{1/2} A_{q_1 q_2 q_{12}}(R)\, C^{q_1 q_2 q_{12}}_{\mu\, -\mu\, 0} \qquad (2.27)$$

where $(q_1 + q_2 + q_{12})$ is even. This restriction is a direct consequence of the invariance of the potential under the parity operator, and it also ensures that the intermolecular potential (2.23) is a real quantity (Green 1975).

We are now in a position to give expressions for the matrix elements in equation (2.20). Using equation (2.23) and the normalisation properties of the symmetric top wavefunction (2.8) to perform the integration over

$\hat{\underset{\sim}{R}}$, we have

$$\left\langle j_1 j_2 j_{12} \bar{\alpha} \, J M \varepsilon \,\middle|\, V(\hat{\underset{\sim}{r}}_1, \hat{\underset{\sim}{r}}_2, R) \,\middle|\, j_1' j_2' j_{12}' \bar{\alpha}' \, J M \varepsilon \right\rangle_{\hat{\underset{\sim}{r}}_1, \hat{\underset{\sim}{r}}_2, \hat{\underset{\sim}{R}}}$$

$$= \sum_{q_1 q_2 \mu \geq 0} V_{q_1 q_2 \mu}(R) \left\langle j_1 j_2 j_{12} \bar{\alpha} \,\middle|\, Y_{q_1 q_2 \mu}(\hat{\underset{\sim}{r}}_1, \hat{\underset{\sim}{r}}_2) \,\middle|\, j_1' j_2' j_{12}' \bar{\alpha}' \right\rangle_{\hat{\underset{\sim}{r}}_1, \hat{\underset{\sim}{r}}_2} \qquad (2.28)$$

Using standard techniques of Racah algebra (Messiah 1962, Cowan 1981) we obtain

$$\left\langle j_1 j_2 j_{12} \bar{\alpha} \,\middle|\, Y_{q_1 q_2 \mu}(\hat{\underset{\sim}{r}}_1, \hat{\underset{\sim}{r}}_2) \,\middle|\, j_1' j_2' j_{12}' \bar{\alpha}' \right\rangle$$

$$= \delta_{\bar{\alpha} \bar{\alpha}'} (-)^{j_1 + j_2 + j_{12} + \bar{\alpha}} \left(\frac{2}{1+\delta_{\mu 0}} \right) \left\{ j_1, j_2, j_{12}, j_1', j_2', j_{12}', q_1, q_2 \right\}^{1/2}$$

$$\times \begin{pmatrix} j_1 & q_1 & j_1' \\ 0 & 0 & 0 \end{pmatrix} \begin{pmatrix} j_2 & q_2 & j_2' \\ 0 & 0 & 0 \end{pmatrix} \qquad (2.29)$$

$$\times \sum_{q_{12}} (-)^{q_{12}} (2q_{12}+1) \begin{pmatrix} q_1 & q_2 & q_{12} \\ -\mu & \mu & 0 \end{pmatrix} \begin{pmatrix} j_{12} & q_{12} & j_{12}' \\ -\bar{\alpha} & 0 & \bar{\alpha} \end{pmatrix} \begin{Bmatrix} j_1 & j_2 & j_{12} \\ j_1' & j_2' & j_{12}' \\ q_1 & q_2 & q_{12} \end{Bmatrix}$$

In equation (2.29),

$$\begin{pmatrix} j_1 & q_1 & j_1' \\ 0 & 0 & 0 \end{pmatrix}$$

is a 3-j symbol,

$$\begin{Bmatrix} j_1 & j_2 & j_{12} \\ j_1' & j_2' & j_{12}' \\ q_1 & q_2 & q_{12} \end{Bmatrix}$$

is a 9-j symbol (Messiah 1962), and $\{j_1, j_2, \ldots\}$ is a shorthand for $(2j_1+1)(2j_2+1)\ldots$ The delta function, $\delta_{\bar{\Omega}\bar{\Omega}'}$, ensures diagonality of the V-matrix elements in the $\bar{\Omega}$ index; this is a consequence of the invariance of the potential under rotations about $\underset{\sim}{R}$. The summation over q_{12} is such that $(q_1 + q_2 + q_{12})$ is even. Equation (2.29) is a special case of the expression given by Launay (1977), as can be shown by making use of the symmetry properties of the 6-j symbols that appear in the latter, and by noting the slightly different definition of $Y_{q_1 q_2 \mu}$.

The $\underset{\sim}{\ell}^2$-matrix elements in equation (2.20) may be evaluated by setting

$$\underset{\sim}{\ell}^2 = (\underset{\sim}{J} - \underset{\sim}{j}_{12})^2$$

$$= \underset{\sim}{J}^2 + \underset{\sim}{j}_{12}^2 - 2(j_{12})_z J_z - (j_{12})_+ J_- - (j_{12})_- J_+ \qquad (2.30)$$

In the body-fixed frame the components of $\underset{\sim}{J}$ do not obey the normal angular momentum commutation relations and Brocks et al. (1983), who study this in detail, call $\underset{\sim}{J}$ a pseudo-angular momentum operator. This introduces a negative sign when the angular momentum ladder operator, $J_{\pm}$, acts on the body-fixed basis functions (2.15), leading to the following non-zero matrix elements (Launay 1976):

$$\langle j_1 j_2 j_{12} \bar{\Omega} J M \varepsilon | \underset{\sim}{\ell}^2 | j_1 j_2 j_{12} \bar{\Omega} J M \varepsilon \rangle$$

$$= j_{12}(j_{12}+1) + J(J+1) - 2\bar{\Omega}^2 \qquad (2.31)$$

and

$$\langle j_1 j_2 j_{12}\, \Omega\, JM\varepsilon \,|\, \underset{\sim}{\mathcal{L}}^2 \,|\, j_1 j_2 j_{12}\, \Omega\pm 1\, JM\varepsilon\rangle$$
$$= -(1+\delta_{\Omega 0})^{1/2}(1+\delta_{\Omega\pm 1,0})^{1/2}\left[j_{12}(j_{12}+1) - \Omega(\Omega\pm 1)\right]^{1/2} \qquad (2.32)$$
$$\times \left[J(J+1) - \Omega(\Omega\pm 1)\right]^{1/2}$$

In writing down (2.32) it has been assumed that any $\Omega = 0$ basis function which vanishes has been excluded from the basis set. We note that in the body-fixed coordinate system the $\underset{\sim}{\mathcal{L}}^2$-matrix elements are not diagonal, with coriolis terms (2.32) which can change the value of Ω. However, the potential is more naturally expressed in this frame, a fact exemplified by the diagonality of the matrix elements (2.29) in the Ω index. The overall result is that, unlike the space-fixed case (Rabitz 1975), many of the elements of the body-fixed coupling matrix are identically zero; this may be exploited when solving the coupled equations (see Chapter 3).

The differential equations (2.19) may now be integrated numerically subject to bound state (Chapter 3) or scattering (Chapter 5) boundary conditions. The next two sections are concerned with additional symmetries that arise in special cases of this general problem, which may be exploited to achieve substantial savings in computer time.

2.3 Two identical heteronuclear diatomic molecules

The wavefunction describing two identical molecules has a well defined symmetry under the interchange trans-

formation I($\hat{\underset{\sim}{r}}_1'$, $\hat{\underset{\sim}{r}}_2'$, $\hat{\underset{\sim}{R}} \rightarrow$ $\hat{\underset{\sim}{r}}_2'$, $\hat{\underset{\sim}{r}}_1'$, $-\hat{\underset{\sim}{R}}$) (Takayanagi 1965, Heil et al. 1978).

Applying this operator to the space-fixed basis functions (2.10) we get

$$I\,\mathcal{Y}(j_1 j_2 j_{12}\, l\, J M \varepsilon | \hat{\underset{\sim}{r}}_1', \hat{\underset{\sim}{r}}_2', \hat{\underset{\sim}{R}}) = (-)^{j_1+j_2+j_{12}+l}\,\mathcal{Y}(j_2 j_1 j_{12}\, l\, J M \varepsilon | \hat{\underset{\sim}{r}}_1', \hat{\underset{\sim}{r}}_2', \hat{\underset{\sim}{R}}) \qquad (2.33)$$

Note that, as j_1 and j_2 are interchanged on the right hand side, this is not an eigenvalue equation. From the unitary transformation (2.11) it can be shown that the body-fixed basis functions (2.15) behave as follows under interchange:

$$I\,\mathcal{Y}(j_1 j_2 j_{12}\, \pi\, J M \varepsilon | \hat{\underset{\sim}{r}}_1, \hat{\underset{\sim}{r}}_2, \hat{\underset{\sim}{R}}) = \varepsilon (-)^{j_{12}}\,\mathcal{Y}(j_2 j_1 j_{12}\, \pi\, J M \varepsilon | \hat{\underset{\sim}{r}}_1, \hat{\underset{\sim}{r}}_2, \hat{\underset{\sim}{R}}) \qquad (2.34)$$

Functions with well defined interchange symmetry, $i\,(= \pm 1)$, are obtained by taking linear combinations of (2.15) and normalising:

$$\mathcal{Y}(j_1 j_2 j_{12}\, \pi\, J M \varepsilon\, i | \hat{\underset{\sim}{r}}_1, \hat{\underset{\sim}{r}}_2, \hat{\underset{\sim}{R}}) = [2(1+\delta_{j_1 j_2})]^{-1/2} \left[\mathcal{Y}(j_1 j_2 j_{12}\, \pi\, J M \varepsilon | \hat{\underset{\sim}{r}}_1, \hat{\underset{\sim}{r}}_2, \hat{\underset{\sim}{R}}) + i\varepsilon (-)^{j_{12}}\,\mathcal{Y}(j_2 j_1 j_{12}\, \pi\, J M \varepsilon | \hat{\underset{\sim}{r}}_1, \hat{\underset{\sim}{r}}_2, \hat{\underset{\sim}{R}}) \right] \qquad (2.35)$$

We effect a reduction in the basis set by excluding those functions (2.35) for which $j_2 > j_1$, and for which $j_1 = j_2$ and $i\varepsilon(-)^{j_{12}} = -1$. In this latter case the functions (2.35) vanish.

The invariance of the potential (2.23) under the interchange transformation leads to the conclusion that

$$V_{q_2 q_1 \mu}(R) = (-)^{q_1+q_2} V_{q_1 q_2 \mu}(R) \qquad (2.36)$$

This can be seen by operating on equation (2.25) with I, and then using the relation (2.27). The fully symmetrised potential may thus be written as

$$V(\hat{r}_1, \hat{r}_2, R) = \sum_{q_1 \geq q_2} \sum_{\mu \geq 0} V_{q_1 q_2 \mu}(R)\, Y^{+}_{q_1 q_2 \mu}(\hat{r}_1, \hat{r}_2) \qquad (2.37)$$

where

$$Y^{+}_{q_1 q_2 \mu}(\hat{r}_1, \hat{r}_2) = \left[Y_{q_1 q_2 \mu}(\hat{r}_1, \hat{r}_2) + (-)^{q_1+q_2} Y_{q_2 q_1 \mu}(\hat{r}_1, \hat{r}_2) \right] \times (1 + \delta_{q_1 q_2})^{-1} \qquad (2.38)$$

We thus have fewer terms in our potential expansion. The derivation of the coupled equations (2.19) is identical to that already given except for the restrictions on the basis set and the potential given above. Given the relationship between the functions (2.15) and those with well defined interchange symmetry (i.e. equation (2.35)) it is possible to write the V-matrix elements in terms of equations (2.28) and (2.29). Specifically the symmetry properties of the 9-j symbol (Messiah 1962) in (2.29), together with the restriction of $(q_1 + q_2 + q_{12})$ to even values, are used to deduce

$$\langle j_1 j_2 j_{12} \Pi | Y_{q_1 q_2 \mu} | j_1' j_2' j_{12}' \Pi' \rangle$$

$$= (-)^{j_1+j_2+j_{12}+j_1'+j_2'+j_{12}'} \langle j_2 j_1 j_{12} \Pi | Y_{q_2 q_1 \mu} | j_2' j_1' j_{12}' \Pi' \rangle \qquad (2.39)$$

With this and the potential expansion (2.37) we obtain

$$\langle j_1 j_2 j_{12} \pi \, J M \varepsilon i | V(\hat{r}_1, \hat{r}_2, R) | j_1' j_2' j_{12}' \pi' \, J M \varepsilon i \rangle$$

$$= 2\left[2(1+\delta_{j_1 j_2})\right]^{-1/2}\left[2(1+\delta_{j_1' j_2'})\right] \sum_{q_1 \geq q_2} \sum_{\mu \geq 0} V_{q_1 q_2 \mu}(R)\,(1+\delta_{q_1 q_2})^{-1} \tag{2.40}$$

$$\times \Big\{ \langle j_1 j_2 j_{12} \pi | Y_{q_1 q_2 \mu} | j_1' j_2' j_{12}' \pi' \rangle + i\varepsilon(-)^{j_{12}'} \langle j_1 j_2 j_{12} \pi | Y_{q_1 q_2 \mu} | j_2' j_1' j_{12}' \pi' \rangle$$

$$+ (-)^{q_1+q_2} \Big[\langle j_1 j_2 j_{12} \pi | Y_{q_2 q_1 \mu} | j_1' j_2' j_{12}' \pi' \rangle$$

$$+ i\varepsilon(-)^{j_{12}'} \langle j_1 j_2 j_{12} \pi | Y_{q_2 q_1 \mu} | j_2' j_1' j_{12}' \pi' \rangle \Big] \Big\}$$

where use has been made of the symmetries of the 3-j symbols to halve the number of terms in this expression. While substantial savings in computer time are possible by using the basis (2.35) (because of the consequent reduction in the number of coupled equations), it is usually more convenient to retain the non-symmetrised (with respect to interchange) potential (2.23) and simply set

$$V_{q_2 q_1 \mu}(R) = (-)^{q_1+q_2} V_{q_1 q_2 \mu}(R) \tag{2.36}$$

This gives a less unwieldy expression for the potential matrix elements:

$$\langle j_1 j_2 j_{12} \pi \, J M \varepsilon i | V(\hat{r}_1, \hat{r}_2, R) | j_1' j_2' j_{12}' \pi' \, J M \varepsilon i \rangle$$

$$= 2\left[2(1+\delta_{j_1 j_2})\right]^{-1/2}\left[2(1+\delta_{j_1' j_2'})\right]^{-1/2} \sum_{q_1 q_2 \mu \geq 0} V_{q_1 q_2 \mu}(R) \tag{2.41}$$

$$\times \Big[\langle j_1 j_2 j_{12} \pi | Y_{q_1 q_2 \mu} | j_1' j_2' j_{12}' \pi' \rangle + i\varepsilon(-)^{j_{12}'} \langle j_1 j_2 j_{12} \pi | Y_{q_1 q_2 \mu} | j_2' j_1' j_{12}' \pi' \rangle \Big]$$

The $\underset{\sim}{\ell}^2$-matrix elements for $\mathcal{Y}(j_1 j_2 j_{12} \pi J M \varepsilon i | \hat{\underset{\sim}{r}}_1, \hat{\underset{\sim}{r}}_2, \hat{\underset{\sim}{R}})$ can, in a similar fashion, be written in terms of those for $\mathcal{Y}(j_1 j_2 j_{12} \pi J M \varepsilon | \hat{\underset{\sim}{r}}_1, \hat{\underset{\sim}{r}}_2, \hat{\underset{\sim}{R}})$. The restrictions placed on the basis (2.35) lead to expressions for the non-zero matrix elements which we are identical to (2.31) and (2.32), i.e.

$$\langle j_1 j_2 j_{12} \pi J M \varepsilon i | \underset{\sim}{\ell}^2 | j_1 j_2 j_{12} \pi' J M \varepsilon i \rangle$$

$$= \langle j_1 j_2 j_{12} \pi J M \varepsilon | \underset{\sim}{\ell}^2 | j_1 j_2 j_{12} \pi' J M \varepsilon \rangle \qquad (2.42)$$

By taking account of the restrictions on the basis set, simpler expressions to those given by Danby (1983) and Alexander and De Pristo (1977) are thus obtained.

Before continuing with a discussion of the further symmetry reductions possible when one or both of the diatoms is homonuclear, we give an example of the basis reductions that have occupied us for much of this Chapter. Table 2.1 gives the basis sets (2.6), (2.15) and (2.35) for two identical heteronuclear rotors, each possessing the range of possible angular momenta j = 0,1. The corresponding space-fixed basis set (2.10) is given, together with eigenfunctions of I, constructed in an analogous way to their body-fixed counterparts (2.35); relation (2.33) would be used to achieve this. In this example the total angular momentum, J = 1. The coupled equations are seen to separate into 4 blocks, corresponding to the possible combinations of ε and i .

Body-fixed basis															Space-fixed basis										
(i)				(ii)					(iii)						(iv)					(v)					
j_1	j_2	j_{12}	Ω	j_1	j_2	j_{12}	$\bar{\Omega}$	ϵ	j_1	j_2	j_{12}	$\bar{\Omega}$	ϵ	i	j_1	j_2	j_{12}	ℓ	ϵ	j_1	j_2	j_{12}	ℓ	ϵ	i
0	0	0	0	0	0	0	0	-1	0	0	0	0	-1	-1	0	0	0	1	-1	0	0	0	1	-1	-1
0	1	1	-1	0	1	1	0		1	0	1	0			0	1	1	0		1	0	1	0		
0	1	1	0	0	1	1	1		1	0	1	1			0	1	1	2		1	0	1	2		
0	1	1	1	1	0	1	0		1	1	0	0			1	0	1	0		1	1	0	1		
1	0	1	-1	1	0	1	1		1	1	2	0			1	0	1	2		1	1	2	1		
1	0	1	0	1	1	0	0		1	1	2	1			1	1	0	1		1	1	2	3		
1	0	1	1	1	1	1	1		1	0	1	0	-1	1	1	1	1	1		1	0	1	0	-1	1
1	1	0	0	1	1	2	0		1	0	1	1			1	1	2	1		1	0	1	2		
1	1	1	-1	1	1	2	1		1	1	1	1			1	1	2	3		1	1	1	1		
1	1	1	0	0	1	1	1	1	1	0	1	1	1	-1	0	1	1	1	1	1	0	1	1	1	-1
1	1	1	1	1	0	1	1		1	1	1	0			1	0	1	1		1	1	1	0		
1	1	2	-1	1	1	1	0		1	1	1	1			1	1	1	0		1	1	1	2		
1	1	2	0	1	1	1	1		1	0	1	1	1	1	1	1	1	2		1	0	1	1	1	1
1	1	2	1	1	1	2	1		1	1	2	1			1	1	2	2		1	1	2	2		

TABLE 2.1

The body-fixed and space-fixed basis sets for 2 identical heteronuclear diatomics, with j = 0,1. The total angular momentum, J = 1. Columns (iv) and (v) represent the analogous space-fixed basis sets to the body-fixed in (ii) and (iii) respectively.

2.4 Homonuclear molecules

The angular momentum, j_i, of a homonuclear diatomic molecule can only take values which are either all odd or all even. This is a consequence of the symmetry of the total molecular wavefunction under the interchange of two identical nuclei. The coupled equations therefore separate further into blocks corresponding to even or odd j_i.

If the rotor i is homonuclear, then the intermolecular potential (2.25) is invariant under the transformation

$$\hat{\underset{\sim}{r}}_i' \longrightarrow -\hat{\underset{\sim}{r}}_i'$$

It follows directly from this and equation (2.27) that the q_i indices in the body-fixed expansion of the intermolecular potential (2.23), (2.37) may only take even values. This is consistent with the restrictions on j_i as can be seen from the symmetry properties of the 3-j symbols

$$\begin{pmatrix} j_i & q_i & j_i' \\ 0 & 0 & 0 \end{pmatrix}$$

in equation (2.29).

Two homonuclear molecules of the same species (e.g. H_2 - H_2) but with one diatom restricted to even j (e.g. para-H_2) and the other to odd j (e.g. ortho-H_2) are distinct, and the treatment in section 2.2 applies. It is interesting to note that in the case of nuclei with zero spin (e.g. ^{16}O) the corresponding diatom (e.g. $^{16}O_2$) cannot exist in one of these j modifications (for a fixed electronic state). This is because the nuclear spin state can only be symmetric with respect to interchange

of the nuclei (Bransden and Joachain 1983).

We summarise the results obtained in sections 2.2, 2.3 and 2.4 in Table 2.2, referencing the optimum (fully symmetrised) basis sets and potential expansions.

2.5 The effects of monomer vibration

All of the calculations reported in this thesis treat the diatomic molecules in the van der Waals complex as rigid rotors. However, the experimental spectra with which we will compare our results involve the vibrational excitation of one of the diatoms. It is therefore important to indicate how intramolecular stretch may be incorporated into the close-coupling formulation of the preceding sections, and to understand the effects of its neglect.

The rigid rotor approximation involves freezing the bond length of the diatom at an equilibrium value r_{eq} ideally defined by the equation

$$B = \frac{1}{2\mu r_{eq}^2} = \int \chi^*(00|r) \frac{1}{2\mu r^2} \chi(00|r)\, dr \qquad (2.43)$$

where B is the rotational constant which we met in equation (2.9), and $\chi(00|r)$ is the (normalised) wavefunction of the ground vibrational state of the diatom which we shall return to presently. Classically we can think of this as taking an average value of r over the vibrational motion, which is much faster than the rotational motion. Usually, r_{eq} is set equal to r^o, the expectation value of r in the ground vibrational state. Sometimes r^e,

System	potential expansion	basis set	V-matrix elements	$\underset{\sim}{l}^2$-matrix elements	good quantum numbers
AB-CD	(2.23)	(2.15)	(2.28),(2.29)	(2.31),(2.32)	J,M,$\mathcal{E}$
AB-AB	(2.37)	(2.35)	(2.40),(2.29)	(2.42)	J,M,$\mathcal{E}$,i
A_2-AB	(2.23) q_1=0,2,4 ...	(2.15) j_1=1,3,5 ... or 0,2,4 ...	(2.28),(2.29)	(2.31),(2.32)	J,M,$\mathcal{E}$
A_2-B_2	(2.23) q_1=q_2=0,2,4 ...	(2.15) j_1=1,3,5 ... or 0,2,4 ... ditto j_2	(2.28),(2.29)	(2.31),(2.32)	J,M,$\mathcal{E}$
A_2-A_2	(2.37) q_1=q_2=0,2,4 ...	(2.35) j_1=j_2=1,3,5 ... or 0,2,4 ...	(2.40),(2.29)	(2.42)	J,M,$\mathcal{E}$,i
	(2.23)* q_1=q_2=0,2,4	(2.15) j_1=1,3,5 ... and j_2=0,2,4 ...	(2.28),(2.29)	(2.31),(2.32)	J,M,$\mathcal{E}$

TABLE 2.2

A summary of the results obtained in sections 2.2, 2.3 and 2.4. The optimum basis set, potential expansion, and the corresponding matrix elements are referenced.

* The fully symmetrised rigid rotor potential expansion is in fact (2.37), but it is more convenient to use expansion (2.23) and set $V_{q_2 q_1 \mu} = (-1)^{q_1+q_2} V_{q_1 q_2 \mu}$.

the position of the minimum of the intramolecular potential is used (Tennyson and Sutcliffe 1983a). It is usually possible to evaluate diatomic rotational energies either by ab initio calculations (e.g. Wolniewicz 1983) or by reference to observed spectra (Herzberg 1950, Herman and Short 1968) so it is not necessary to assume the same rotational constant for all j, and in this way the effects of centrifugal distortion may be taken into account (Lester and Schaefer 1973). We still neglect the effects of any vibrationally excited monomer states and in this sense the rigid rotor approximation may be regarded as a basis set truncation (Green 1974). Perturbation theory tells us that this truncation is justified if the energy difference between the ground and first excited vibrational state is large and the potential coupling between them is small.

We now consider the effects of intramolecular stretch on the intermolecular potential. As the bond length of a diatom increases, the repulsive wall of the intermolecular interaction is shifted to larger values of R, the separation of the monomer centres of mass. This is because of the earlier onset of exchange repulsion as the molecules approach one another. If this was the only effect then the resulting potential well would also be shallower. However, an increase in the diatom bond length results in an increase in its polarisability and thus an increase in the attractive dispersion interaction

(Le Roy et al. 1977). Though these simplified arguments neglect the effects of monomer orientation (Tennyson and Sutcliffe 1983a) it is generally true that an increase in r shifts the repulsive wall outwards and increases the well depth.

In ab initio calculations of the electronic potential energy surface, the diatom bond length is usually fixed at r^o, giving the potential

$$V(\underset{\sim}{r}_1^o, \underset{\sim}{r}_2^o, R). \qquad (2.44)$$

Even in the case of the H_2 - H_2 dimer, in which the light nuclei may be expected to perform large amplitude vibrations, (2.44) has been shown to be a good approximation to the vibrationally averaged potential (Burton and Senff 1982):

$$\int \chi^*(00|r_1)\, \chi^*(00|r_2)\, V(\underset{\sim}{r}_1, \underset{\sim}{r}_2, R)\, \chi(00|r_1)\, \chi(00|r_2)\, dr_1\, dr_2 \qquad (2.45)$$

So far in this section we have discussed the validity of the rigid rotor approximation. We now outline the modifications necessary to the close-coupling formalism if the diatoms are allowed to vibrate. The total wave function of the complex is expanded as before in a set of diabatic (R-independent) basis states (c.f. equation (2.17)):

$$\Psi(JM\varepsilon|\underset{\sim}{r}_1, \underset{\sim}{r}_2, R) = \sum_{v_1 v_2 j_1 j_2 j_{12} \pi} \frac{1}{R} F(v_1 v_2 j_1 j_2 j_{12} \pi JM\varepsilon|R)\, \Phi(v_1 v_2 j_1 j_2 j_{12} \pi JM\varepsilon|\underset{\sim}{r}_1, \underset{\sim}{r}_2, \hat{\underset{\sim}{R}}) \qquad (2.46)$$

where

$$\phi = \chi(v_1 j_1 | r_1)\, \chi(v_2 j_2 | r_2)\, \mathcal{Y}(j_1 j_2 j_{12} \pi J M \varepsilon | \hat{\underset{\sim}{r}}_1, \hat{\underset{\sim}{r}}_2, \hat{\underset{\sim}{R}}) \qquad (2.47)$$

$\mathcal{Y}$ is the rotational basis function defined in equation (2.15). $\chi(vj|r)$ is a solution of the radial Schroedinger equation describing the nuclear motion of an isolated diatom (Le Roy and Carley 1980):

$$\left\{ -\frac{1}{2\mu r} \frac{d^2}{dr^2} r + v(r) - \left(E_{vj} - \frac{j(j+1)}{2\mu r^2} \right) \right\} \chi(vj|r) = 0 \qquad (2.48)$$

Here, $v(r)$ is the intramolecular potential (i.e. the electronic energy of the diatom) and v is the vibrational quantum number. E_{vj} is the rotation-vibration energy of the isolated molecule. It is worth noting that implicit in (2.48) is the fact that a complete set of orthonormal vibrational functions may be generated for any one value of j. Rather than numerically solving (2.48) it is usual to replace χ by analytical functions such as Morse oscillators (Tennyson and Sutcliffe 1982).

For identical molecules undergoing internal vibration, the interchange operator, I, of section 2.3 may be generalised as follows:

$$I\left(r_1 \hat{\underset{\sim}{r}}_1', r_2 \hat{\underset{\sim}{r}}_2', R\hat{\underset{\sim}{R}} \rightarrow r_2 \hat{\underset{\sim}{r}}_2', r_1 \hat{\underset{\sim}{r}}_1', R(-\hat{\underset{\sim}{R}}) \right) \qquad (2.49)$$

From equation (2.34) we see that the effect of the interchange operator on ϕ is as follows:

$$I\,\phi(v_1 v_2 j_1 j_2 j_{12} \pi J M \varepsilon | \underset{\sim}{r}_1, \underset{\sim}{r}_2, \hat{\underset{\sim}{R}})$$

$$= \varepsilon(-)^{j_{12}} \phi(v_2 v_1 j_2 j_1 j_{12} \pi J M \varepsilon | \underset{\sim}{r}_1, \underset{\sim}{r}_2, \hat{\underset{\sim}{R}}) \qquad (2.50)$$

Proceeding as in section 2.3 we construct basis states which have a well defined interchange symmetry, i.

$$\phi(v_1 v_2 j_1 j_2 j_{12} \pi J M \varepsilon i | \underset{\sim}{r}_1, \underset{\sim}{r}_2, \hat{\underset{\sim}{R}})$$

$$= [2(1+\delta_{v_1 v_2}\delta_{j_1 j_2})]^{-1/2} [\phi(v_1 v_2 j_1 j_2 j_{12} \pi J M \varepsilon | \underset{\sim}{r}_1, \underset{\sim}{r}_2, \hat{\underset{\sim}{R}}) \qquad (2.51)$$

$$+ i\varepsilon(-)^{j_{12}} \phi(v_2 v_1 j_2 j_1 j_{12} \pi J M \varepsilon | \underset{\sim}{r}_1, \underset{\sim}{r}_2, \hat{\underset{\sim}{R}}) \;]$$

States with different interchange symmetry are decoupled. Linear independence among each set of basis states is achieved by omitting those functions (2.51) for which

(i) $v_1 = v_2$ and $j_2 > j_1$

(ii) $v_2 > v_1$ for all j_1, j_2

(iii) $v_1 = v_2$, $j_1 = j_2$ and $i\varepsilon(-)^{j_{12}} = -1$ (2.52)

(i) and (ii) are the 'well-ordering' conditions of Takayanagi (1965). States for which (iii) is satisfied vanish. When $v_1 = v_2 = 0$ the conditions (2.52) are seen to reduce to those for the case of two rigid rotors.

There are no restrictions on the vibrational quantum number, v, of an isolated homonuclear diatom, analogous to those on j discussed in section 2.4. This is because interchanging the two identical nuclei does not affect the magnitude of the intramolecular vector.

The derivation of the coupled equations is similar to the rotor-rotor case except the matrix elements now involve integrations over r_1 and r_2 as well as $\hat{\underset{\sim}{r}}_1$,

$\hat{r}_2$ and $\hat{R}$. The only addditional difficulty is in the evaluation of the V-matrix elements. Values of the interaction potential are needed not only for a range of geometries ($\hat{r}_1, \hat{r}_2$) and intermolecular separations (R), but also for a number of r_1, r_2 values. Once we have these the potential surface must be fitted in a way that makes possible the evaluation of the V-matrix elements. A convenient way of doing this is to describe the intramolecular dependence of the potential using a power series in the diatom stretching coordinate (Le Roy and Van Kranendonk 1974)

$$\xi(r) = (r - r^\circ) / r^\circ \qquad (2.53)$$

The intermolecular potential between two vibrotors could thus be fitted to an expression of the form (c.f. equation (2.23)).

$$V(\hat{r}_1, \hat{r}_2, R) = \sum_{m\,n} \sum_{q_1 q_2 \mu \geq 0} V_{m n q_1 q_2 \mu}(R)\, \xi^m(r_1)\, \xi^n(r_2)\, Y_{q_1 q_2 \mu}(\hat{r}_1, \hat{r}_2) \qquad (2.54)$$

To date, such calculations have been restricted to atom-diatom systems. Tennyson and Sutcliffe (1983a) have carried out two sets of calculations on the He-HF van der Waals molecule; one treating HF as a rigid rotor, the other with the vibrational degree of freedom included. In this way they were able to directly verify the validity of the rigid rotor assumption which is made throughout the present work.

2.6 Group theoretical note

A large part of the preceding sections of this Chapter has been devoted to constructing rotational basis functions which fully reflect all symmetries in the problem. Any treatment of symmetry is underpinned by the mathematical theory of groups (Hamermesh 1962), and we end this Chapter by outlining the methods of obtaining such symmetrised basis functions. The relevant concepts will be introduced as we go along, though most can be found in the concise introduction to the subject given in Chapter 7 of Atkins (1983).

It will be convenient to discuss the case of two identical heteronuclear diatoms and then to indicate the further steps necessary when the molecules are homonuclear. The symmetry of the system under rotations about a space-fixed axis leads to the constancy of J and M, and this has already been accounted for in the basis functions (2.6). We need therefore only consider the symmetry under the inversion and interchange (permutation) operations. The relevant group is the permutation-inversion group PI(4) (Metropoulos and Chiu 1978), which consists of the complete set of <u>feasible</u> (Ezra 1982, Bunker 1979a) operations that leave the Hamiltonian (2.2) invariant.

The four symmetry operations (or elements) of PI(4) are $\{ E, P_{13,24}, E^*, P^*_{13,24} \}$. E is the identity

which leaves the system unchanged. $P_{13,24}$ is the simultaneous permutation of identical nuclei 1 with 3 and 2 with 4. E^* inverts all the nuclei in the origin of a space-fixed coordinate system which is coincident with the centre of mass of the complex. $P^*_{13,24}$ simultaneously permutes identical and inverts all nuclei ($P^*_{13,24} \equiv P_{13,24}E^* \equiv E^*P_{13,24}$). E^* and $P_{13,24}$ are respectively the active analogues of the passive operations P and I introduced in sections 2.2′ and 2.3 (Bunker 1979a). The above will be clarified by reference to Figure 2.2. Note that operations such as P_{13} are not feasible, an assumption reflected in the "collision complex" form of the Hamiltonian. The permutation-inversion group which omits such operations (PI(4)) is the molecular symmetry group (G_4) of Longuet-Higgins (1963).

Having determined the appropriate group, the next step is to establish a matrix representation of this group. To do this we need the effects of the PI(4) operations, $\mathcal{R}$, on the (unsymmetrised) basis function (2.6):

$$E\,\mathcal{Y}(j_1 j_2 j_{12} \alpha J M|\hat{r}_1,\hat{r}_2,\hat{R}) = \mathcal{Y}(j_1 j_2 j_{12} \alpha J M|\hat{r}_1,\hat{r}_2,\hat{R}) \equiv \mathcal{Y}_1$$

$$P_{13,24}\,\mathcal{Y}(j_1 j_2 j_{12} \alpha J M|\hat{r}_1,\hat{r}_2,\hat{R}) = (-)^{j_1+j_2+J}\mathcal{Y}(j_2 j_1 j_{12} \alpha J M|\hat{r}_1,\hat{r}_2,\hat{R}) \equiv \mathcal{Y}_2$$

$$E^*\,\mathcal{Y}(j_1 j_2 j_{12} \alpha J M|\hat{r}_1,\hat{r}_2,\hat{R}) = (-)^{J+j_{12}+j_1+j_2}\mathcal{Y}(j_1 j_2 j_{12} -\alpha J M|\hat{r}_1,\hat{r}_2,\hat{R}) \equiv \mathcal{Y}_3$$

$$P^*_{13,24}\,\mathcal{Y}(j_1 j_2 j_{12} \alpha J M|\hat{r}_1,\hat{r}_2,\hat{R}) = (-)^{j_{12}}\mathcal{Y}(j_2 j_1 j_{12} \alpha J M|\hat{r}_1,\hat{r}_2,\hat{R}) \equiv \mathcal{Y}_4 \qquad (2.55)$$

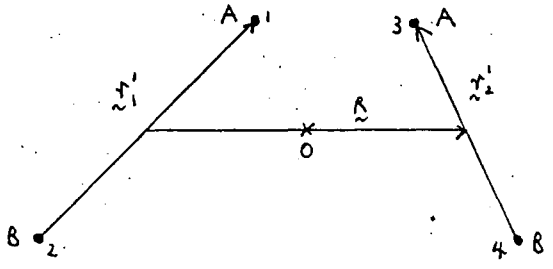

(i) E

(ii) $(\underset{\sim}{r}_1', \underset{\sim}{r}_2', \underset{\sim}{R} \rightarrow \underset{\sim}{r}_1', \underset{\sim}{r}_2', \underset{\sim}{R})$

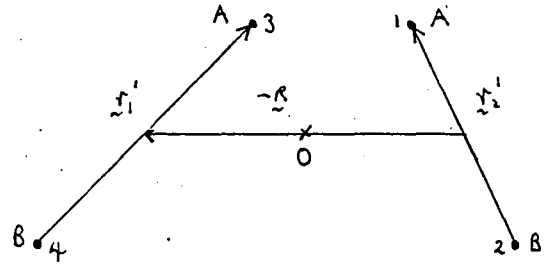

(i) $P_{13,24}$

(ii) $(\underset{\sim}{r}_1', \underset{\sim}{r}_2', \underset{\sim}{R} \xrightarrow{I} \underset{\sim}{r}_2', \underset{\sim}{r}_1', -\underset{\sim}{R})$

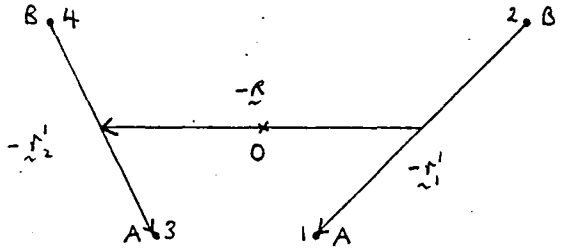

(i) E^*

(ii) $(\underset{\sim}{r}_1', \underset{\sim}{r}_2', \underset{\sim}{R} \xrightarrow{\rho} -\underset{\sim}{r}_1', -\underset{\sim}{r}_2', -\underset{\sim}{R})$

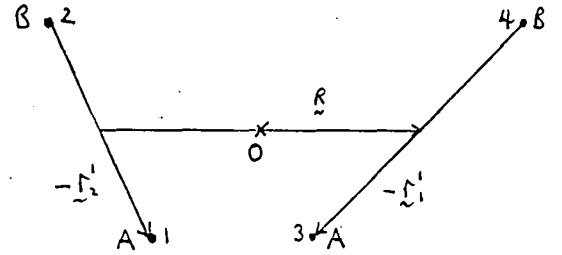

(i) $P^*_{13,24}$

(ii) $(\underset{\sim}{r}_1', \underset{\sim}{r}_2', \underset{\sim}{R} \longrightarrow -\underset{\sim}{r}_2', -\underset{\sim}{r}_1', \underset{\sim}{R})$

Figure 2.2

The elements of the group PI(4) (G_4) for the system $(AB)_2$. O is both the centre of mass of the system and the origin of an inertial space-fixed reference frame. Also given are the active (i) elements which act on the nuclei, and the equivalent passive (ii) elements which act on the coordinates.

Because the action of symmetry operations is most easily visualised in the space-fixed reference frame (Tennyson and Sutcliffe 1984), we obtain (2.55) by operating on the space-fixed basis function (2.10) and then using the unitary transformation (2.11). If $j_1 \neq j_2$ and $\Omega \neq 0$, the functions ψ_n are orthogonal and form a 4-dimensional basis (row-) vector spanning the regular matrix representation (Hamermesh 1962) of PI(4) thus:

$$E(\psi_1,\psi_2,\psi_3,\psi_4) = (\psi_1,\psi_2,\psi_3,\psi_4)\begin{pmatrix}1&0&0&0\\0&1&0&0\\0&0&1&0\\0&0&0&1\end{pmatrix}$$

$$P_{13,24}(\psi_1,\psi_2,\psi_3,\psi_4) = (\psi_1,\psi_2,\psi_3,\psi_4)\begin{pmatrix}0&1&0&0\\1&0&0&0\\0&0&0&1\\0&0&1&0\end{pmatrix}$$

$$E^*(\psi_1,\psi_2,\psi_3,\psi_4) = (\psi_1,\psi_2,\psi_3,\psi_4)\begin{pmatrix}0&0&1&0\\0&0&0&1\\1&0&0&0\\0&1&0&0\end{pmatrix}$$

$$P^*_{13,24}(\psi_1,\psi_2,\psi_3,\psi_4) = (\psi_1,\psi_2,\psi_3,\psi_4)\begin{pmatrix}0&0&0&1\\0&0&1&0\\0&1&0&0\\1&0&0&0\end{pmatrix} \qquad (2.56)$$

The matrices in (2.56), under the normal rules of matrix multiplication, may be shown to satisfy the multiplication table of the PI(4) group (Metropoulos and Chiu 1980). We give below the traces (characters), $\chi(R)$, of the representation matrices in (2.56) which will be needed later:

$$\chi(E) = 4 \;, \quad \chi(P_{13,24}) = \chi(E^*) = \chi(P^*_{13,24}) = 0 \qquad (2.57)$$

Note that the dimensionality of the representation is given by $\chi(E)$.

By applying a similarity transformation (Atkins 1983) to the four matrices in (2.56) it is possible to reduce them to block-diagonal form. This set of matrices thus forms a reducible representation, Γ , of the group. An irreducible matrix representation is one that cannot be so reduced. In order to determine which irreducible representations, Γ_k , are contained in Γ it is necessary to know the character table of the group. This is given by Metropoulos and Chiu (1978) and Bunker (1979b) and is reproduced in table 2.3. The character table for PI(4) may be simply obtained by following a set of rules given by Boardman et al. (1973). Table 2.3 tells us that four inequivalent (not related by a similarity transformation) irreducible representations exist in the group PI(4). The importance of this lies in the fact that basis functions belonging to different irreducible representations are orthogonal and cannot be coupled by the Hamiltonian which belongs to the completely symmetric irreducible representation Γ_1 . This is the vanishing integral rule (Bunker 1979a). We conclude that the close-coupled equations for the system $(AB)_2$ will separate into four blocks, as indicated in Table 2.1.

	E	$P_{13,24}$	E^*	$P^*_{13,24}$
Γ_1	1	1	1	1
Γ_2	1	1	-1	-1
Γ_3	1	-1	-1	1
Γ_4	1	-1	1	-1

Table 2.3 The character table of the group PI(4).

The reduction of the representation, Γ , may be represented by the equation

$$\Gamma = \sum_k{}' a_k \Gamma_k \tag{2.58}$$

where we take a direct sum (Boardman et al. 1973) of the irreducible representations Γ_k. The reduction coefficients, a_k, are given by (Boardman et al. 1973).

$$a_k = \left(\frac{1}{h}\right) \sum_{\mathcal{R}} \chi^k(\mathcal{R})^* \chi(\mathcal{R}) \tag{2.59}$$

h is the order of the group (the number of elements). $\chi^k(\mathcal{R})$ is the character of Γ_k corresponding to the element $\mathcal{R}$. We thus obtain

$$\Gamma = \Gamma_1 \oplus \Gamma_2 \oplus \Gamma_3 \oplus \Gamma_4 \tag{2.60}$$

The symbol $\oplus$ means a direct sum (Boardman et al. 1973). It is a feature of the regular representation that, on reduction, each irreducible representation appears a number of times equal to its dimensionality (Hamermesh 1962, Weissbluth 1978).

We may construct basis functions, y_m^k, of the irreducible representations, Γ_k, by taking linear combinations of the functions y_n. The formal procedure is based on the projection operator, P^k, defined as follows:

$$P^k = \left(\frac{d_k}{h}\right) \sum_R \chi^k(R)^* R \qquad (2.61)$$

where d_k is the dimensionality of Γ_k. The effect of P^k operating on y_n is to produce a sum of the functions y_m^k (Atkins 1983):

$$P^k y_n = \sum_{m=1}^{d_k} y_m^k \qquad (2.62)$$

As all of the irreducible representations are one-dimensional it is necessary to apply the projection operator to only one of the functions y_n. Choosing y_1 (see equation (2.55)) we obtain symmetrised basis functions spanning each of the irreducible representations:

$$\begin{aligned}
P^1 y_1 &= \tfrac{1}{4}(y_1 + y_2 + y_3 + y_4) \equiv y^1 \\
P^2 y_1 &= \tfrac{1}{4}(y_1 + y_2 - y_3 - y_4) \equiv y^2 \\
P^3 y_1 &= \tfrac{1}{4}(y_1 - y_2 - y_3 + y_4) \equiv y^3 \\
P^4 y_1 &= \tfrac{1}{4}(y_1 - y_2 + y_3 - y_4) \equiv y^4
\end{aligned} \qquad (2.63)$$

The subscript m in (2.62) is redundant for one-dimensional representations and has been omitted. By referring to equations (2.55), (2.15), and (2.35) we see that

$$\mathcal{Y}^k = \frac{1}{2}\,\mathcal{Y}(j_1 j_2 j_{12}\, \pi\, J M \varepsilon i \,|\, \hat{\underset{\sim}{r}}_1, \hat{\underset{\sim}{r}}_2, \hat{\underset{\sim}{R}}) \qquad (2.64)$$

where ε and i are given by the characters $\chi^k(E^*)$ and $\chi^k(P_{13,24})$ respectively. Projection operators do not in general give symmetrised functions that are normalised. It is now timely to recall that in the derivation of $\mathcal{Y}^k$ we assumed that $j_1 \neq j_2$ and $\pi \neq 0$. When either or both of these conditions no longer hold, the original basis functions (2.6) are partly symmetrised (Tennyson and van der Avoird 1982a) and do not therefore span all of the irreducible representations of PI(4). Because all of the irreducible representations are one-dimensional, the characters give the effect of the corresponding operation on the symmetrised basis function. We could then have shown that the functions $\mathcal{Y}(j_1 j_2 j_{12}\, \pi\, J M \varepsilon i \,|\, \hat{\underset{\sim}{r}}_1, \hat{\underset{\sim}{r}}_2, \hat{\underset{\sim}{R}})$ are also eigenfunctions of $P^*_{13,24}$ and hence are bases for the irreducible representations. The above, however, demonstrates general principles which may be used for higher order groups.

The system $(A_2)_2$ is particularly relevant to the present work. Our approach, outlined in the preceding sections, is to use the basis functions for two identical heteronuclear diatoms, restricting the values of j (see

Table 2.2). The relevant group is PI(16) (Metropoulos 1981). The main complication is that two of the ten irreducible representations are two-dimensional; reducing the regular representation would lead to these appearing twice. The coupled equations would therefore separate into 12 blocks of which only 10 need be solved (Tennyson and van der Avoird 1982 a,b). The two-dimensional irreducible representations are spanned by two orthogonal and degenerate basis functions (Atkins 1983). To obtain these formally, one would have to apply the projection operator (2.61) to two of the unsymmetrised functions $\mathcal{Y}_n$. The resulting symmetrised functions, $P^k \mathcal{Y}_n$ and $P^k \mathcal{Y}_{n'}$, would not in general be orthogonal. This problem can be surmounted by using Schmidt orthogonalisation (Bunker 1979a). For the $(A_2)_2$ system, however, the form of these functions is intuitively obvious; they correspond to $\mathcal{Y}(j_1 j_2 j_{12} \pi JM\varepsilon | \hat{r}_1, \hat{r}_2, \hat{R})$ one with (j_1, j_2) = (odd, even) and the other with (j_1, j_2) = (even, odd) (Metropoulos 1981).

To summarise the contents of this section: we first establish a (reducible) representation of the symmetry group of the Hamiltonian by applying the group elements to a set of (unsymmetrised) basis functions. With a knowledge of the character table we can find which inequivalent irreducible representations are contained in the reducible one - all are if we set up the regular representation. The linear combinations of basis states that reduce the representation are then found using

projection operators. The vanishing integral rule tells us that the coupling matrix elements (2.20) between two basis states belonging to different irreducible representations vanish.

CHAPTER THREE

SOLUTION OF THE CLOSE-COUPLED EQUATIONS

3.1 Introduction

In this chapter we shall consider the solution of the coupled differential equations (2.19) written below in matrix form

$$\frac{d^2}{dR^2} F_j(R) = W_{jk}(R)\, F_k(R) \qquad (3.1)$$

There are two basic approaches to solving these. The radial functions $\underset{\sim}{F}(R)$ could be expanded in terms of an appropriate set of basis functions and the resulting secular equation solved (Le Roy and Carley 1980). This technique has been applied to calculations of the bound states of molecular dimers by Verberne and Reuss (1981) and Tennyson and van der Avoird (1982a). Similar ideas have also been applied to scattering problems by Bocchetta and Gerratt (1985) in their implementation of the Wigner R-matrix method. In this thesis, we shall adopt the other, more direct approach : numerical integration of the differential equations.

The coupled equations are identical for the bound state and collision problems; only the boundary conditions differ. A large number of numerical methods have been developed for scattering problems and Thomas et al. (1981) have carried out comparative test calculations on eleven of these. These methods, however, may be classified depending on whether they approximate $\underset{\sim}{F}(R)$ or $\underset{\sim}{W}(R)$.

In the approximate solution approach, the "scattering coordinate" R is divided into sectors and the solution $\underset{\sim}{F}$ assumed to possess some simple polynomial form in each sector. The approximate potential (or piecewise analytic) approach assumes that the coupling matrix $\underset{\sim}{W}$ has a simple form such that in each sector the differential equations may be solved analytically. Mattson and Anderson (1984) have studied such methods assuming the potential to be either constant, linear or quadratic across individual radial sectors.

Secrest (1979) has further subdivided these two approaches according to the way the solution is developed from one sector to the next. The first of these subdivisions is the common solution following approach in which the values of $\underset{\sim}{F}$ and $d\underset{\sim}{F}/dR$ at one end of the sector are used to obtain those at the other. This process is continued recursively with each sector being treated as an initial value problem. Because of the exponential behaviour of the radial wave functions in the classically forbidden regions, solution-following methods suffer from inherent instability. This problem led to the development of the invariant imbedding technique. In a scattering context this involves setting the potential to zero at the sector boundaries. A full scattering problem may then be solved for each sector and the S-matrices matched across the sector boundaries. The

S-matrix is thus propagated to large R at which point the potential vanishes. Because the equations for the S-matrix do not suffer from the instabilities of those for the wavefunction, the invariant imbedding method is inherently stable. Invariant imbedding was originally developed for solving the differential equations which arise in neutron transport and illustrations from this and other physical problems have been given by Scott (1973). In general terms the method involves reformulating the problem so that the quantity of interest is calculated directly at each stage of the calculation.

In sections 3.2 and 3.3 we shall consider in turn our implementation of two numerical methods : the de Vogelaere method which is based on approximate solution/solution following, and the R-matrix propagator method based on approximate potential/invariant imbedding. Using the results of test calculations (section 3.4) we shall be able to indicate the relative merits of the different numerical approaches, much of which has been discussed by Secrest (1979, 1983) within a collision calculation framework.

Thomas et al. (1981) considered the efficiency in terms of computer time of a number of numerical methods. Alexander (1984) has shown that significant improvements are possible by adopting hybrid methods. Despite this, computational speed may still be an inhibiting drawback

of direct numerical methods either when very large numbers of coupled equations must be solved or if we are interested in inverting intermolecular potentials by least squares fitting to experimental data. In the latter case, repeated calculations of the eigenenergies are needed. We could try to counter this speed problem using decoupling methods valid under special conditions. Our options, though, are rather limited as it is in general necessary to retain the full Hamiltonian for bound state problems. Methods involving the neglect of Coriolis terms in the coupling matrix and the decoupling of angular and radial motions have been used. We shall discuss these and the other alternative methods for calculating bound states in section 3.5.

3.2 The de Vogelaere method

3.2.1 Derivation

We begin by outlining the derivation of the method of de Vogelaere (1955) for a single second order differential equation of the type

$$\frac{d^2}{dR^2} F(R) = W(R) F(R) \qquad (3.2)$$

The central ideas of the method and an estimate of the truncation error can all be illustrated by reference to this "single channel" case. The extension to a system of coupled differential equations is immediate. We

partition the radial coordinate into sectors, denoting the boundaries of an arbitrary one by R_i and R_{i+1} (see figure 3.1). The wavefunctions at the boundaries are related by the Taylor series expansion:

$$F(R_{i+1}) = F(R_i) + hF'(R_i) + \frac{h^2}{2}F''(R_i) + \frac{h^3}{6}F'''(R_i) + \frac{h^4}{24}F^{IV}(R_i) + O(h^5) \tag{3.3}$$

$h(= R_{i+1} - R_i)$ is the sector length, F^i denotes the i-th derivative with respect to R, and the $O(h^5)$ term shows that we are approximating the solution to a 4th order polynomial. Using (3.2) we may re-write (3.3) as

$$F(R_{i+1}) = F(R_i) + hF'(R_i) + \frac{h^2}{2}W(R_i)F(R_i) + \frac{h^2}{3}\left\{\frac{h}{2}\left[W(R_i)F(R_i)\right]' + \frac{h^2}{8}\left[W(R_i)F(R_i)\right]''\right\} + O(h^5) \tag{3.4}$$

Using the Taylor expansion for $W(R_{i+\frac{1}{2}})F(R_{i+\frac{1}{2}})$ about R_i, the term in curly brackets may be written as

$$\{\quad\} = W(R_{i+\frac{1}{2}})F(R_{i+\frac{1}{2}}) - W(R_i)F(R_i) + O(h^3) \tag{3.5}$$

Substituting this into (3.4) and rearranging we obtain

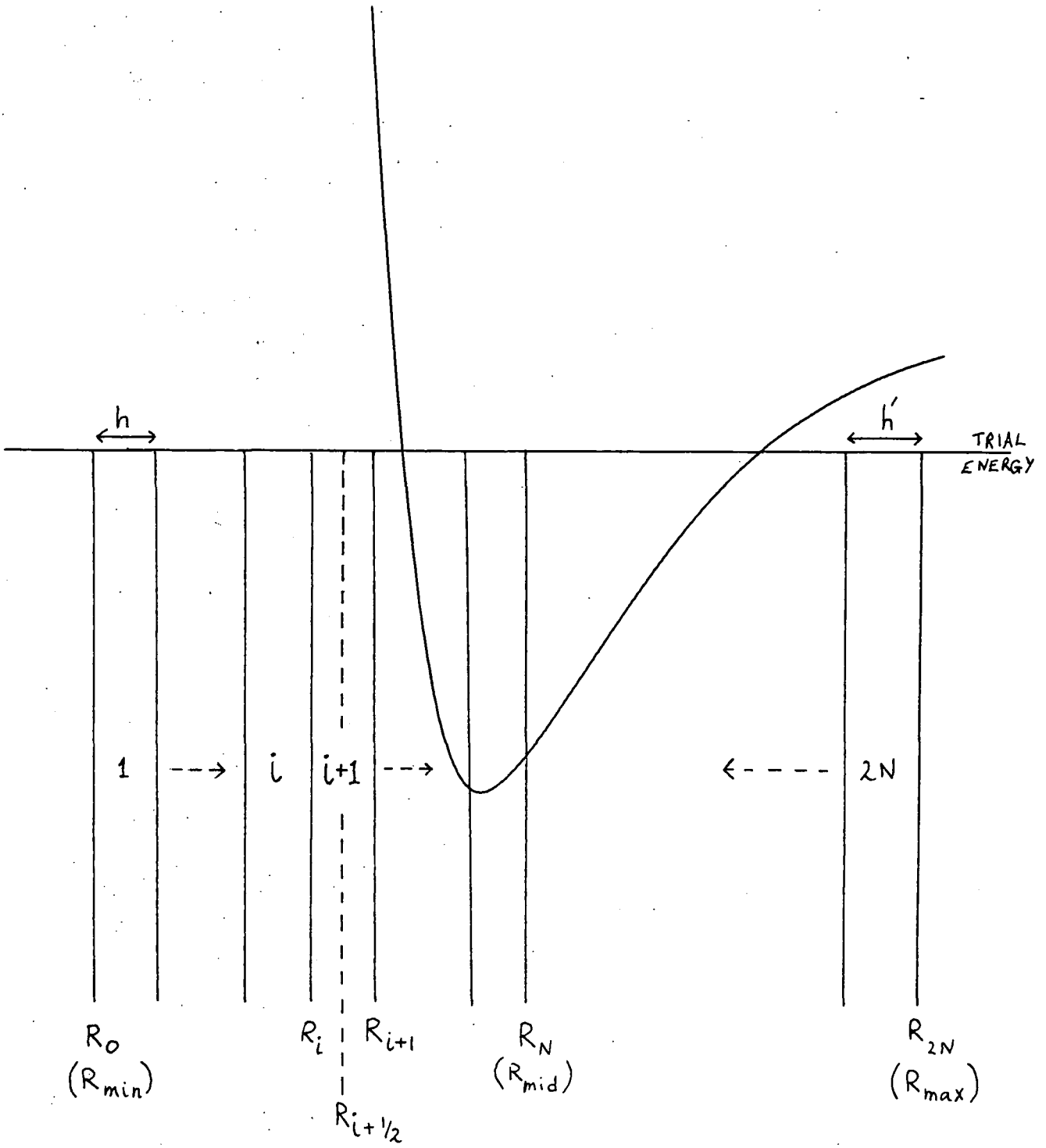

Figure 3.1

Definition of the integration parameters and sector labelling conventions used in the discussion of the de Vogelaere and R-matrix propagator algorithms. R_{min} and R_{max} are the limits of the integration range, and R_{mid} is the matching point.

$$F(R_{i+1}) = F(R_i) + hF'(R_i) + \frac{h^2}{6}\left\{W(R_i)F(R_i) + 2W(R_{i+\frac{1}{2}})F(R_{i+\frac{1}{2}})\right\} + O(h^5) \tag{3.6}$$

It is clear that we need an expression for the wavefunction at the midpoint $R_{i+\frac{1}{2}}(=R_i + \frac{h}{2})$ of the sector across which we hope to develop the solution. We use the Taylor series for $F(R_{i+\frac{1}{2}})$ to obtain an expression analogous to (3.4). Making use of the Taylor expansion about R_i for $W(R_{i-\frac{1}{2}})F(R_{i-\frac{1}{2}})$ to eliminate derivatives of WF, we obtain the intermediate step in the de Vogelaere algorithm (Coleman and Mohamed 1978):

$$F(R_{i+\frac{1}{2}}) = F(R_i) + \frac{h}{2}F'(R_i) + \frac{h^2}{24}\left\{4W(R_i)F(R_i) - W(R_{i-\frac{1}{2}})F(R_{i-\frac{1}{2}})\right\} + O(h^4) \tag{3.7}$$

The $O(h^4)$ truncation error of this step contributes an error of only $O(h^6)$ in propagating the solution across the sector because $W(R_{i+\frac{1}{2}})F(R_{i+\frac{1}{2}})$ is multiplied by an h^2 term in (3.6).

Finally we have to find the solution derivative $F'(R_i)$ which appears in the propagation equations. A fourth order approximation to this is obtained by applying Simpson's rule directly to the Schroedinger equation (3.2).

$$F'(R_{i+1}) = F'(R_i) +$$

$$\frac{h}{6}\left\{W(R_i)F(R_i) + 4\,W(R_{i+\frac{1}{2}})F(R_{i+\frac{1}{2}}) + W(R_{i+1})F(R_{i+1})\right\} + O(h^5) \quad (3.8)$$

Cyclic use of equations (3.6), (3.7) and (3.8) constitutes de Vogelaere's algorithm. Note that these equations are slightly different from those given by Launay (1976) because of a different sign convention for the coupling matrix. The method is not self-starting as we need to supply $F(R_{-\frac{1}{2}})$ to begin the integration at R_o. We use an expression which is adequate provided the wavefunction has effectively decayed to zero at R_o (Lester 1968, Coleman and Mohamed 1979).

$$F(R_{-1/2}) = -\frac{h}{2}F'(R_o) \quad (3.9)$$

It can now be seen why this method is classified as solution following; the wavefunction and its derivative are both propagated sector by sector. Because we have not made any approximation to W(R), the extension to a system of coupled differential equations is immediate (Lester 1968, Mohamed 1984). For an n-channel problem, W becomes an n x n matrix and F,F' column vectors of length n.

As we have already seen, the local (sector) truncation error of this method is, as $h \to o$, $O(h^5)$. To obtain the global (total) truncation error, we multiply

the local error by the number of sectors which is proportional to $^1/h$ for constant h. The global error is thus $O(h^4)$, a fact confirmed by Coleman and Mohamed (1978) who used more rigorous arguments. h should be sufficiently small to accurately represent the solution. For weakly bound van der Waals molecules, the radial wavefunction does not rapidly oscillate and this requirement presents no problem.

Each step in de Vogelaere's method involves two matrix multiplications which take up most of the computer time. However, because of the diagonality of the V-matrix elements in the $\bar{\Omega}$ index (see equation (2.29)), the body-fixed coupling matrix contains many identically zero elements. This is in contrast to the space-fixed coupling matrix, a point illustrated graphically by Rabitz (1975). Launay (1976) pointed out that this results in the faster integration of the body-fixed equations, in comparison to the space-fixed, as there are fewer matrix elements to multiply and add.

3.2.2. Boundary and matching conditions

The boundary conditions for energies below the dissociation limit may be written as

$$\underset{\sim}{F}(R) \rightarrow \underset{\sim}{0} \quad \text{as} \quad R \rightarrow 0 \text{ and } \infty \tag{3.10}$$

Here $\underset{\sim}{F}$ is a column vector denoting the complete set of radial functions that appear in (3.1). In practice we take as end points of the integration range the values $R_{min}(> 0)$ and $R_{max}(< \infty)$, both determined empirically. Our computer programme contains an option for finding estimates of R_{min} and R_{max} based on the decay of the radial solution in the classically forbidden regions.

A system of n coupled second order differential equations has 2n linearly independent solutions. The boundary conditions (3.10) eliminate the n irregular solutions, Lester (1971). A problem arises in specifying the starting values of the derivative vector since the homogeneity of the Schroedinger equation permits only one of the elements to be chosen arbitrarily. We avoid an iterative search over the n-1 non-arbitrary components by making use of the fact that any n-vector in Hilbert space may be described as a linear combination of n linearly independent n-vectors. This is the superposition principle. Following Gordon (1969) we propagate an (n x n) solution matrix, each column of which represents a solution vector; n is the dimensionality of the basis set. The boundary conditions appropriate to the de Vogelaere, and other similar algorithms, may be taken as follows:

$$\underset{\sim}{F}_1(R_{min}) = \underset{\sim}{0} \qquad \underset{\sim}{F}_1'(R_{min}) = \underset{\sim}{I}$$

$$\underset{\sim}{F}_2(R_{max}) = \underset{\sim}{0} \qquad \underset{\sim}{F}_2'(R_{max}) = \underset{\sim}{I} \qquad (3.11)$$

$\underset{\sim}{F}$ is now an (n x n) solution matrix. For $\underset{\sim}{F}'$, its derivative with respect to R, we may take any non-singular matrix but the identity $\underset{\sim}{I}$ is the one most commonly used. The subscripts 1 and 2 serve only to distinguish between the solutions started at R_{min} and R_{max} respectively. The solution and its derivative are propagated from R_{min} and R_{max} towards a point in the region of the potential minimum, R_{mid} (Dunker and Gordon 1976a). The backward propagation from R_{max} is simply achieved by replacing h by -h in the de Vogelaere algorithm.

At R_{mid} the true solution is some linear combination of the n solution vectors propagated from R_{min} :

$$\underset{\sim}{F}(R_{mid}) = \underset{\sim}{F}_1(R_{mid})\ \underset{\sim}{C}_1$$

$$\underset{\sim}{F}'(R_{mid}) = \underset{\sim}{F}_1'(R_{mid})\ \underset{\sim}{C}_1 \qquad (3.12)$$

$\underset{\sim}{C}_1$ is a vector of n unknown coefficients. Similar expressions hold for the solutions propagated from R_{max} except that the linear combination $\underset{\sim}{C}_2$ is in general different. If the total energy E corresponds to an eigenvalue then the wavefunction and its derivative must match at R_{mid}.

$$\underset{\sim}{F}_1(R_{mid})\ \underset{\sim}{C}_1 = \underset{\sim}{F}_2(R_{mid})\ \underset{\sim}{C}_2$$

$$\underset{\sim}{F}_1'(R_{mid})\ \underset{\sim}{C}_1 = \underset{\sim}{F}_2'(R_{mid})\ \underset{\sim}{C}_2 \qquad (3.13)$$

This may be rewritten as one matrix equation

$$\begin{pmatrix} \underset{\sim}{F}_1(R_{mid}) & \underset{\sim}{F}_2(R_{mid}) \\ \underset{\sim}{F}_1'(R_{mid}) & \underset{\sim}{F}_2'(R_{mid}) \end{pmatrix} \begin{pmatrix} \underset{\sim}{C}_1 \\ -\underset{\sim}{C}_2 \end{pmatrix} = \underset{\sim}{O} \qquad (3.14)$$

A non-trivial solution to these 2n homogeneous linear equations exists only if the following matching condition at the midpoint is satisfied:

$$\begin{vmatrix} \underset{\sim}{F}_1(R_{mid}) & \underset{\sim}{F}_2(R_{mid}) \\ \underset{\sim}{F}_1'(R_{mid}) & \underset{\sim}{F}_2'(R_{mid}) \end{vmatrix} = 0 \qquad (3.15)$$

The eigenvalue problem thus reduces to one of finding the zeroes of the determinant of a (2n x 2n) matrix. We found our eigenvalues using a simple search procedure, involving repeated calculation of the determinant in (3.15) at a number of trial energies. Linear interpolation between two determinants of different sign was generally adequate to obtain rapid convergence to an eigenenergy.

Having determined the eigenenergy we may then wish to evaluate the radial solution vector, either to assign quantum numbers or as a first step towards calculating matrix elements of operators corresponding to physical observables. In principle this is achieved by assuming that we have located the precise position of the zero of the determinant in (3.15). Gauss elimination (Kreyzig

1972) could then be used to obtain the eigenvector $\begin{pmatrix} \underset{\sim}{c}_1 \\ -\underset{\sim}{c}_2 \end{pmatrix}$ corresponding to the zero eigenvalue of the matrix in equation (3.14). In practice this method may sometimes be unstable because one cannot in general locate the precise zero of the matching determinant. This means that none of the matrix eigenvalues are zero, as required by equation (3.14). Dunker and Gordon (1976a) have found it more satisfactory to solve, instead of (3.14), the matrix eigenvalue equation

$$\begin{pmatrix} \underset{\sim}{F}_1(R_{mid}) & \underset{\sim}{F}_2(R_{mid}) \\ \underset{\sim}{F}_1'(R_{mid}) & \underset{\sim}{F}_2'(R_{mid}) \end{pmatrix} \begin{pmatrix} \underset{\sim}{c}_1 \\ -\underset{\sim}{c}_2 \end{pmatrix} = \varepsilon \begin{pmatrix} \underset{\sim}{c}_1 \\ -\underset{\sim}{c}_2 \end{pmatrix} \qquad (3.16)$$

where ε is the smallest matrix eigenvalue.

The evaluation of the wavefunction is complicated still further by the introduction of the stabilising transformations, to be discussed in the next section. Detailed schemes for the calculation of wavefunctions have been developed by Dunker and Gordon (1976a) and Rosenthal and Gordon (1976). These authors used an approximate potential method for solving the close-coupled equations. This has an advantage over approximate solution methods, such as de Vogelaere, when evaluating matrix elements of operators between wavefunctions. If a polynomial form is assumed for the operator then the contribution to the matrix element in each sector may be obtained

analytically (Dunker and Gordon 1976a). For highly oscillatory radial wavefunctions a very fine grid would be required by the de Vogelaere method to represent the wavefunction accurately. Approximate solution techniques are unlikely to be the method of choice for evaluating matrix elements. In this context it is interesting to note a development by Kidd and Balint-Kurti (1985) which permits the evaluation of matrix elements directly by incorporating the relevant operator in a modified coupling matrix. The close-coupled equations may then be integrated without any need to evaluate the wavefunctions explicitly.

Knowledge of the wavefunction does, however, provide a rigorous way of determining the quantum numbers of a state. Good quantum numbers, such as the total angular momentum and the parity, are of course assigned at the outset as discussed in Chapter 2. Even without a knowledge of the wavefunction it is usually possible to assign additional approximate quantum numbers such as the end-over-end rotation of the dimer (ℓ) or the projection of the total angular momentum on the intermolecular axis ($\overline{\Omega}$). The basis states used in the expansion of the total wavefunction (see equation (2.17)) are eigenfunctions of the Hamiltonian if all coupling terms are set to zero. These provide suitable approximate or "asymptotic" quantum numbers if the corresponding eigenenergies deviate only slightly from those obtained with the full coupling matrix.

Dunker and Gordon (1976b), who used space-fixed basis functions, produced plots of the eigenenergies of Ar-HCl versus an anisotropy factor (lying between 0 and 1) by which they multiplied W_{jk}, $j \neq k$. In this way they were able to uniquely assign all of the energy levels. Their plots showed a number of avoided crossings which implies that the quantum numbers assigned, notably the space-fixed l, were not a suitable choice. Kidd et al. (1981) went on to show that the body-fixed quantum number, Ω, is more appropriate for the lower bound states of this system. The vibrational quantum number of the van der Waals bond, n, is easily assigned according to the ordering of levels with the same asymptotic angular quantum numbers.

It will suffice for our present purposes to assign asymptotic quantum numbers to energy levels rather than give accurate contributions from all of the basis states. Furthermore, as we have not concerned ourselves with the evaluation of physical observables other than the transition frequencies, we need consider the calculation of eigenfunctions no further.

3.2.3 Numerical stability

The de Vogelaere method, like all other solution following techniques, is inherently unstable (Secrest 1979). This is due to the exponential rise of the wave-function in the classically forbidden regions. A stabilising

transformation must periodically be applied both to prevent numerical round-off errors and to maintain the linear independence of the n solution vectors (Dunker and Gordon 1976a). During propagation through a non-classical region, the component of each solution vector corresponding to the most locally closed channel will tend to grow much faster than the others. Due to the finite precision of the computer, all n solution vectors thus tend towards the same vector and linear independence is lost. In this eventuality the bound state matching condition (3.15) is no longer valid. It is also important to ensure that all solution vectors have roughly the same magnitude. Failure to do this will lead at first to round-off error as one solution vector becomes more important than the others, and ultimately to floating point overflow.

A number of different stabilisation techniques are in everyday use (Gordon 1969, Wagner and McKoy 1973) but they all have in common the periodic replacement of the solution matrix by a linear combination of the constituent column vectors. The various stabilisation methods differ largely in their adopted criterion for linear independence. We have used the simplest method which is to replace $\underset{\sim}{F}$, $\underset{\sim}{F}'$ by $\underset{\sim}{F}\underset{\sim}{F}^{-1} = \underset{\sim}{I}$, $\underset{\sim}{F}'\underset{\sim}{F}^{-1}$ every 5 to 10 integration steps (Riley and Kuppermann 1968, Launay 1978). The modified solution matrix is then perfectly

linearly independent and normalised. The inverse of the derivative matrix, $\underset{\sim}{F'}^{-1}$, may also be used to stabilise. The drawback with such transformations is that they are expensive in terms of computer time, and must be applied across the entire integration range when strongly closed channels are included in the basis expansion.

3.3 The R-matrix propagator method

In this method the quantity that is propagated is the Wigner R-matrix, related to the (n x n) solution and derivative matrices by the expression

$$\underset{\sim}{R} = \underset{\sim}{F}(\underset{\sim}{F'})^{-1} \qquad (3.17)$$

The exponential build up of the wavefunction in the classically forbidden regions is, therefore, cancelled and the method is inherently stable. Quite apart from the fact that no stabilising transformation is needed, the R-matrix contains the minimum amount of information for the determination of bound state energies. As has already been mentioned, the principles behind this technique are very different from those of the de Vogelaere method. The coupled equations are solved exactly for an approximate coupling matrix $\underset{\sim}{W}$. This is known as the piecewise analytic or approximate potential approach. Dividing the radial coordinate into sectors, we first diagonalise the "true" coupling matrix at the centre of each sector. This effectively transforms the basis set into one in which

there is no coupling. The resulting set of n one-dimensional Schroedinger equations may then be solved analytically if a simple form for $\underset{\sim}{W}$ is assumed over the rest of the sector (Stechel et al. 1978, De Vries and George 1980). For the present calculations we assumed a constant (and diagonal) $\underset{\sim}{W}$ within a given sector. Schneider and Walker (1979) have expanded the radial dependence of the total wavefunction in a basis, thereby combining ideas from square integrable methods and direct numerical integration.

Secrest (1979) has classified the propagation technique in this method as invariant imbedding, and his derivation makes direct use of this concept. We shall show in the following section that it is not necessary to do so; the R-matrix propagator method will be derived by a straightforward rearrangement of the propagation equations of what is essentially the solution following method of Light (1971).

3.3.1 Derivation

The system of n coupled differential equations (3.1) may be rewritten as

$$\underset{\sim}{T}^{-1}(R)\,\underset{\sim}{F}''(R) = \left(\underset{\sim}{T}^{-1}(R)\,\underset{\sim}{W}(R)\,\underset{\sim}{T}(R)\right)\underset{\sim}{T}^{-1}(R)\,\underset{\sim}{F}(R) \qquad (3.18)$$

If $\underset{\sim}{T}$ is chosen such that $\underset{\sim}{T}^{-1}\ \underset{\sim}{W}\ \underset{\sim}{T}$ is a diagonal matrix, then we have converted the problem to a set of n single channel Schroedinger equations which can then be solved

individually. The transformed radial functions are accordingly $\underset{\sim}{T}^{-1}(R)\underset{\sim}{F}(R)$. Since $\underset{\sim}{W}$ is symmetric the transformation matrix $\underset{\sim}{T}$ is orthogonal (Boardman et al. 1973) and thus its inverse may be replaced by its transpose $\underset{\sim}{T}^{T}$.

Taking an arbitrary radial sector, i + 1, we diagonalise $\underset{\sim}{W}$ at the centre of this sector, $R_{i+\frac{1}{2}}$ (see Figure 3.1):

$$\underset{\sim}{T}^{T}(i+1)\,\underset{\sim}{W}(R_{i+\frac{1}{2}})\,\underset{\sim}{T}(i+1) = \underset{\sim}{\lambda}^{2}(i+1) \qquad (3.19)$$

$\underset{\sim}{\lambda}^{2}(i + 1)$ is a diagonal matrix whose elements are the eigenvalues of the matrix $\underset{\sim}{W}$. As indicated, the diagonalising transformation is taken to be sector dependent but indepedent of R within each sector. The elements of $\underset{\sim}{\lambda}^{2}$ are, in the present work, assumed to be constant throughout the sector in question, each "corresponding" to the local value of the negative of the wavevector in each channel (see equation 2.20). These approximations imply both that the departure from diagonality and the variation of the potential, as we move away from the centre of the sector, are both negligible (Light et al. 1979). The latter condition implies that small step lengths must be taken at short range, where the potential is varying rapidly, to preserve accuracy.

Although the diagonalising transformation is computationally expensive it is energy independent. Hence, once a calculation has been completed for one trial

energy, subsequent energies are much cheaper. In a bound state problem, which involves complete calculations at a number of "trial" and "iterated" energies, this is clearly a good feature. The consequent saving in CPU time is at the expense of increased storage needed for the matrices which diagonalise $\underset{\sim}{W}$. The matrix eigenvalues for each sector are also all stored for the first energy; subsequent changes in the total energy ΔE alter all of these by the same amount $(-2\mu \Delta E)$ (Light 1971).

To begin with we consider the numerical solution of the single Schroedinger equation

$$F''(R) = \lambda^2 F(R) \tag{3.20}$$

As in the derivation of the de Vogelaere method, a Taylor series is used to expand the solution and its derivative.

$$F(R_{i+1}) = F(R_i) + hF'(R_i) + \frac{h^2}{2} F''(R_i) + \frac{h^3}{6} F'''(R_i) + \ldots \tag{3.21a}$$

$$F'(R_{i+1}) = F'(R_i) + hF''(R_i) + \frac{h^2}{2} F'''(R_i) + \ldots \tag{3.21b}$$

Using (3.20) we can write

$$F'''(R_i) = (\lambda^2)' F(R_i) + \lambda^2 F'(R_i) \tag{3.22}$$

The approximation that λ^2 is constant throughout the

sector means that the first term on the right hand side of this equation vanishes. This introduces a local error of $O(h^2)$ in the solution derivative F' and consequently an error of $O(h^3)$ in the solution, as can be seen by reference to equations (3.21). We conclude that the local error is $O(h^3)$ in agreement with Light (1971) whose arguments were based on the Magnus exponentiation method (Magnus 1954). Using the same simple arguments as in section 3.2.1, we arrive at a global error of $O(h^2)$. This result is borne out empirically as will be seen in Section 3.4.1.

Expressions similar to (3.22) for higher derivatives of F are readily obtained, and from (3.20) it is seen that they may all be expressed in terms of F and F'. Substituting these relations into the Taylor expansions (3.21) and neglecting all derivatives of λ^2, we obtain in matrix form:

$$\begin{pmatrix} F(R_{i+1}) \\ F'(R_{i+1}) \end{pmatrix} = \begin{pmatrix} P_1 & P_2 \\ P_3 & P_4 \end{pmatrix} \begin{pmatrix} F(R_i) \\ F'(R_i) \end{pmatrix} \qquad (3.23)$$

The form of the sector <u>propagators</u> P_k depends on whether the channel is open ($\lambda^2 < 0$) or closed ($\lambda^2 > 0$):

$$P_1 = P_4 = 1 + \frac{h^2}{2}\lambda^2 + \ldots = \begin{cases} \cosh(h|\lambda|) & , \lambda^2 > 0 \\ \cos(h|\lambda|), & \lambda^2 < 0 \end{cases} \qquad (3.24a)$$

$$p_2 = h + \frac{h^3}{6}\lambda^2 + \ldots = \begin{cases} \sinh(h|\lambda|)/|\lambda|, & \lambda^2 > 0 \\ \sin(h|\lambda|)/|\lambda|, & \lambda^2 < 0 \end{cases} \tag{3.24b}$$

$$p_3 = h\lambda^2 + \frac{h^3}{6}\lambda^4 + \ldots = \begin{cases} |\lambda| \sinh(h|\lambda|), & \lambda^2 > 0 \\ -|\lambda| \sin(h|\lambda|), & \lambda^2 < 0 \end{cases} \tag{3.24c}$$

Equation (3.23) is the core of a piecewise analytic, solution following algorithm. Given initial values of the solution and its derivative at one end of the sector (R_i) we can propagate to the other end (R_{i+1}).

By multiplying out (3.23), the resulting two equations may be rearranged to obtain expressions for $F(R_i)$ and $F(R_{i+1})$ in terms of $F'(R_i)$ and $F'(R_{i+1})$:

$$\begin{pmatrix} F(R_i) \\ F(R_{i+1}) \end{pmatrix} = \begin{pmatrix} r_1 & r_2 \\ r_3 & r_4 \end{pmatrix} \begin{pmatrix} -F'(R_i) \\ F'(R_{i+1}) \end{pmatrix} \tag{3.25}$$

All we have done is to restate an initial value problem as a boundary value problem, expressing the solutions at the sector boundaries in terms of their derivatives (Light and Walker 1976). $F'(R_i)$ has been multiplied by -1 to retain the convention of Stechel et al. (1978) in which the derivatives at the sector boundaries are outwardly normal. It is important to take note of this derivative convention when implementing boundary conditions

as we shall see in the following section. Equation (3.25) defines the sector R-matrix $\underset{\sim}{r}$ whose elements are given by:

$$r_1 = P_3^{-1} P_4 = \begin{cases} \coth(h|\lambda|)/|\lambda| , & \lambda^2 > 0 \\ -\cot(h|\lambda|)/|\lambda| , & \lambda^2 < 0 \end{cases} \qquad (3.26a)$$

$$r_2 = P_3^{-1} = \begin{cases} \operatorname{csch}(h|\lambda|)/|\lambda| , & \lambda^2 > 0 \\ -\csc(h|\lambda|)/|\lambda| , & \lambda^2 < 0 \end{cases} \qquad (3.26b)$$

$$r_3 = -P_2 + P_1 P_3^{-1} P_4 = \begin{cases} \operatorname{csch}(h|\lambda|)/|\lambda|, & \lambda^2 > 0 \\ -\csc(h|\lambda|)/|\lambda|, & \lambda^2 < 0 \end{cases} \qquad (3.26c)$$

$$r_4 = P_1 P_3^{-1} = \begin{cases} \coth(h|\lambda|)/|\lambda| , & \lambda^2 > 0 \\ -\cot(h|\lambda|)/|\lambda| , & \lambda^2 < 0 \end{cases} \qquad (3.26d)$$

Note that $r_1 = r_4$ and $r_2 = r_3$. To avoid ambiguity we shall, whenever necessary, refer to the R-matrix defined by equation (3.17) as the global R-matrix. Combining the definition of the global (3.17) with that of the sector (3.25) R-matrix, the radial wavefunctions can be eliminated to obtain two simultaneous equations relating $F'(R_i)$ and $F'(R_{i+1})$. $F'(R_i)$ may then be eliminated to obtain the following propagation equation for the global R-matrix (Light et al. 1979):

$$R(R_{i+1}) = r_4 - r_3\left(R(R_i) + r_1\right)^{-1} r_2 \qquad (3.27)$$

The first step in generalising this expression to a system of n(> 1) differential equations is trivial. The elements of the sector R-matrix become (n x n) diagonal matrices, the elements of which are obtained from equations (3.26) by replacing $|\lambda|$ with $|\lambda_{jj}|$. The second step involves accounting for the fact that $\underset{\sim}{R}(R_{i+1})$ and $\underset{\sim}{R}(R_i)$ refer to the bases which diagonalise the coupling matrix in sectors i + 1 and i respectively (Figure 3.1). The transformation which first takes the uncoupled basis of sector i into the original coupled basis, and from this into the uncoupled basis of sector i + 1 is given by the product $\underset{\sim}{T}^T(i+1)\underset{\sim}{T}(i)$. It follows that the R-matrix propagator equation, generalised to the n-channel problem, may be written

$$\underset{\sim}{R}(R_{i+1}) = \underset{\sim}{r}_4 - \underset{\sim}{r}_3\left(\underset{\sim}{T}^T(i+1)\,\underset{\sim}{T}(i)\,\underset{\sim}{R}(R_i)\,\underset{\sim}{T}^T(i)\,\underset{\sim}{T}(i+1) + \underset{\sim}{r}_1\right)^{-1}\underset{\sim}{r}_2 \qquad (3.28)$$

The transformation which takes the global R-matrix at the right hand boundary of sector i to that at the left hand boundary of sector i + 1 ensures continuity of the wavefunction and its derivative across the sector wall (Light and Walker 1976). Equation (3.28) is a statement

of the R-matrix propagator algorithm. It is seen that at no stage are the wavefunction or its derivative evaluated so the method is stable, even in the classically forbidden regions.

Once the end of the integration range (the right hand side of the Nth sector) is reached, the final global R-matrix is obtained by transforming from the locally diagonal basis back to the original

$$\underset{\sim}{R}^{f}(R_N) = \underset{\sim}{T}(N)\ \underset{\sim}{R}(R_N)\ \underset{\sim}{T}^{T}(N) \qquad (3.29)$$

We shall now consider the implementation of the boundary conditions appropriate to bound state problems.

3.3.2 Boundary and matching conditions

To start the R-matrix propagation, the global R-matrix at the right hand boundary of the first sector must be specified. Similarly the calculation must be initialised for the propagation from R_{max} to R_{mid}. The boundary conditions reflect the exponential behaviour of the wavefunction in the classically forbidden regions:

$$\left[\underset{\sim}{R}_1(R_{min}+h)\right]_{jk} = \delta_{jk}\,|\lambda_{jj}|^{-1} \qquad (3.30a)$$

$$\left[\underset{\sim}{R}_2(R_{max}-h')\right]_{jk} = \delta_{jk}\,|\lambda'_{jj}|^{-1} \qquad (3.30b)$$

λ^2_{jj} and λ'^2_{jj} are the eigenvalues of the coupling matrices $\underset{\sim}{W}(R_{min} + h/2)$ and $\underset{\sim}{W}(R_{max} - h'/2)$ respectively. h and h' are the lengths of the first sector at either end of the integration range (refer to Figure 3.1). These boundary conditions are less "severe" than the corresponding de Vogelaere ones (3.11) which are equivalent to assuming an infinite wall potential at R_{min} and R_{max}. The R-matrix boundary conditions only assume a constant effective potential for $R \leqslant R_{min}$ and $R \geqslant R_{max}$, and a consequence of this is that a smaller integration range may be sufficient.

As with the de Vogelaere method we must integrate from both R_{min} and R_{max} to R_{mid}. For the sector R-matrices given in (3.26) the inward propagation may simply be achieved, as in the de Vogelaere case, by replacing h by -h in the R-matrix propagator algorithm. In general one can always explicitly use the inverse of (3.28), obtaining $\underset{\sim}{R}(R_i)$ in terms of $\underset{\sim}{R}(R_{i+1})$ (Baluja et al., 1983). Because the R-matrix computer programme available to us was a straightforward implementation of the algorithm of Stechel et al. (1978), where h is assumed to be positive, an alternative but equivalent method of inward integration was adopted. This involved making the simple transformation $R' = R_{max} - R$ with $\underset{\sim}{W}(R') = \underset{\sim}{W}(R)$. This converts a backward to a forward problem.

Having obtained the final (in the original coupled basis) global R-matrix at R_{mid}, an analogous matching

condition to (3.15) is obtained

$$\begin{vmatrix} \underset{\sim}{R}_1^f(R_{mid}) & -\underset{\sim}{R}_2^f(R_{mid}) \\ \underset{\sim}{I} & \underset{\sim}{I} \end{vmatrix} = 0 \qquad (3.31)$$

The subscript 1(2) denotes propagation from $R_{min}(R_{max})$ and the minus sign of $\underset{\sim}{R}_2^f$ is a consequence of the derivative convention of Stechel et al. (1978). The identity matrices $\underset{\sim}{I}$ may be eliminated to obtain the R-matrix matching condition for an eigenenergy:

$$\left| \underset{\sim}{R}_1^f(R_{mid}) + \underset{\sim}{R}_2^f(R_{mid}) \right| = 0 \qquad (3.32)$$

where we now have to evaluate the determinant of an (n x n) matrix. That (3.32) follows from (3.31) is immediately apparent for a single Schroedinger equation. The validity of this expression for the general n-channel case follows from mathematical induction. Alternatively, (3.32) can be justified physically by stating that for an eigenenergy the two R-matrices are identical at the matching point. Note that had we used the same convention for the derivatives as we did in the de Vogelaere method (always measured with respect to increasing R), then the R-matrix matching condition would involve the difference rather than the sum of $\underset{\sim}{R}_1^f$ and $\underset{\sim}{R}_2^f$. This convention was adopted in an earlier presentation (Danby 1983).

An example of the behaviour of the determinant (3.32) in the region of an eigenenergy is shown in Figure 3.2(a). Also shown are the corresponding plots of the de Vogelaere matching determinant (3.15). The matrices $\underset{\sim}{F}^{-1}$ and $\underset{\sim}{F}'^{-1}$ were used to stabilise in Figure 3.2(b) and 3.2(c) respectively. The origin of the poles in Figures 3.2(a) and 3.2(c) is easily understood in terms of the single channel case as occurring when either $\underset{\sim}{R}_1^f(R_{mid})$ or $\underset{\sim}{R}_2^f(R_{mid})$ becomes infinite; in other words when the derivative of the radial wavefunction becomes zero. The similarity of these two figures, as distinct from 3.2(b), should not be surprising. Frequent stabilisation with $\underset{\sim}{F}'^{-1}$ is rather like propagating the R-matrix.

3.4 Tests of the numerical methods

To date, no independent calculations on the bound states of a molecular dimer, using direct numerical integration of the close-coupled equations, have been published. Extensive results have been reported for the Ar-HCl dimer, and this is, therefore, a convenient system on which to test the accuracy of the numerical methods we employ. The HCl is treated as a rigid rotor and the problem is thus a special case of the 2-rotor algebra presented in Chapter 2. For these tests we used the empirical potential, I, of Dunker and Gordon (1976b). The potential expansion coefficients $V_{q1q2\mu}(R)$ are plotted in Figure 3.3. In the atom-rotor problem $q_2 = \mu = 0$ and the potential

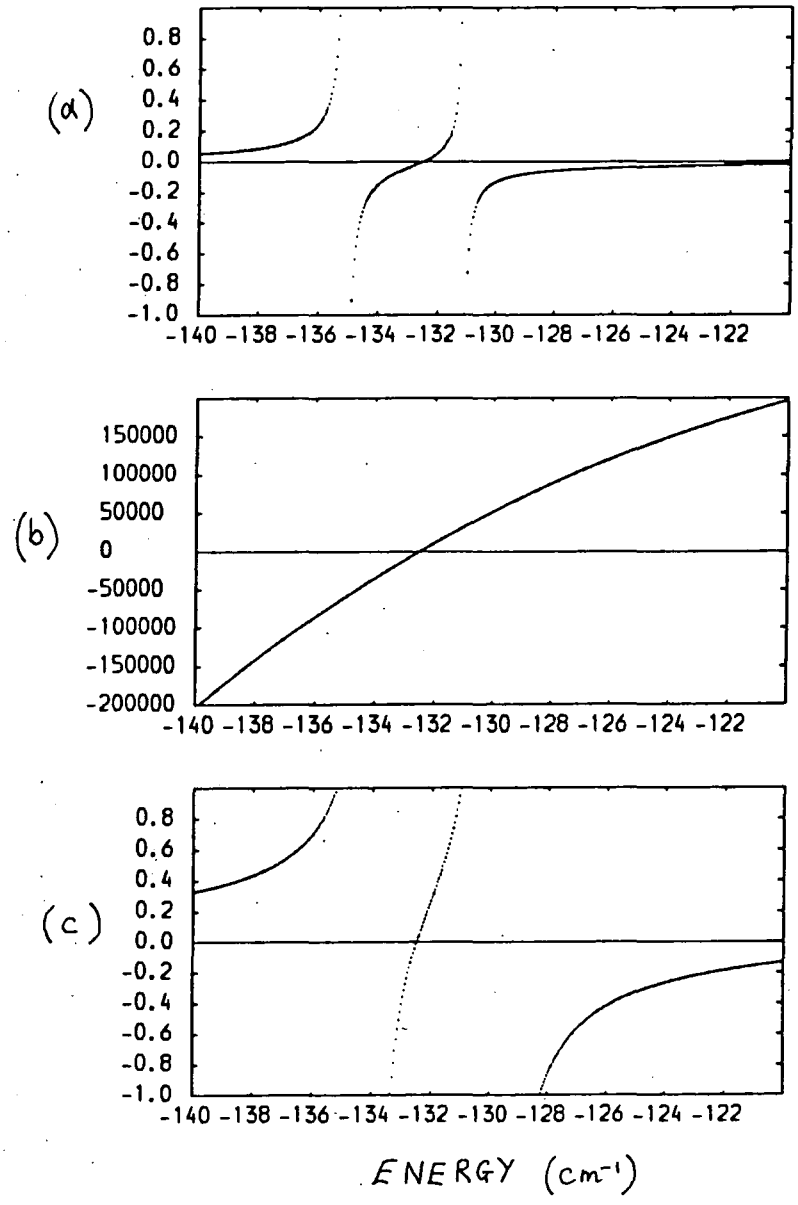

Figure 3.2

Illustration of the matching condition in the region of an eigenenergy. (a) is a plot of the R-matrix matching determinant (3.32) as a function of trial energy. The corresponding de Vogelaere determinant (3.15) is also plotted where the matrices (b) $\underset{\sim}{F}^{-1}$ and (c) $\underset{\sim}{F}'^{-1}$ were used to stabilise during propagation. The eigenenergy in question is the ground rovibrational state of the Dunker and Gordon (1976b) potential I (see Section 3.4).

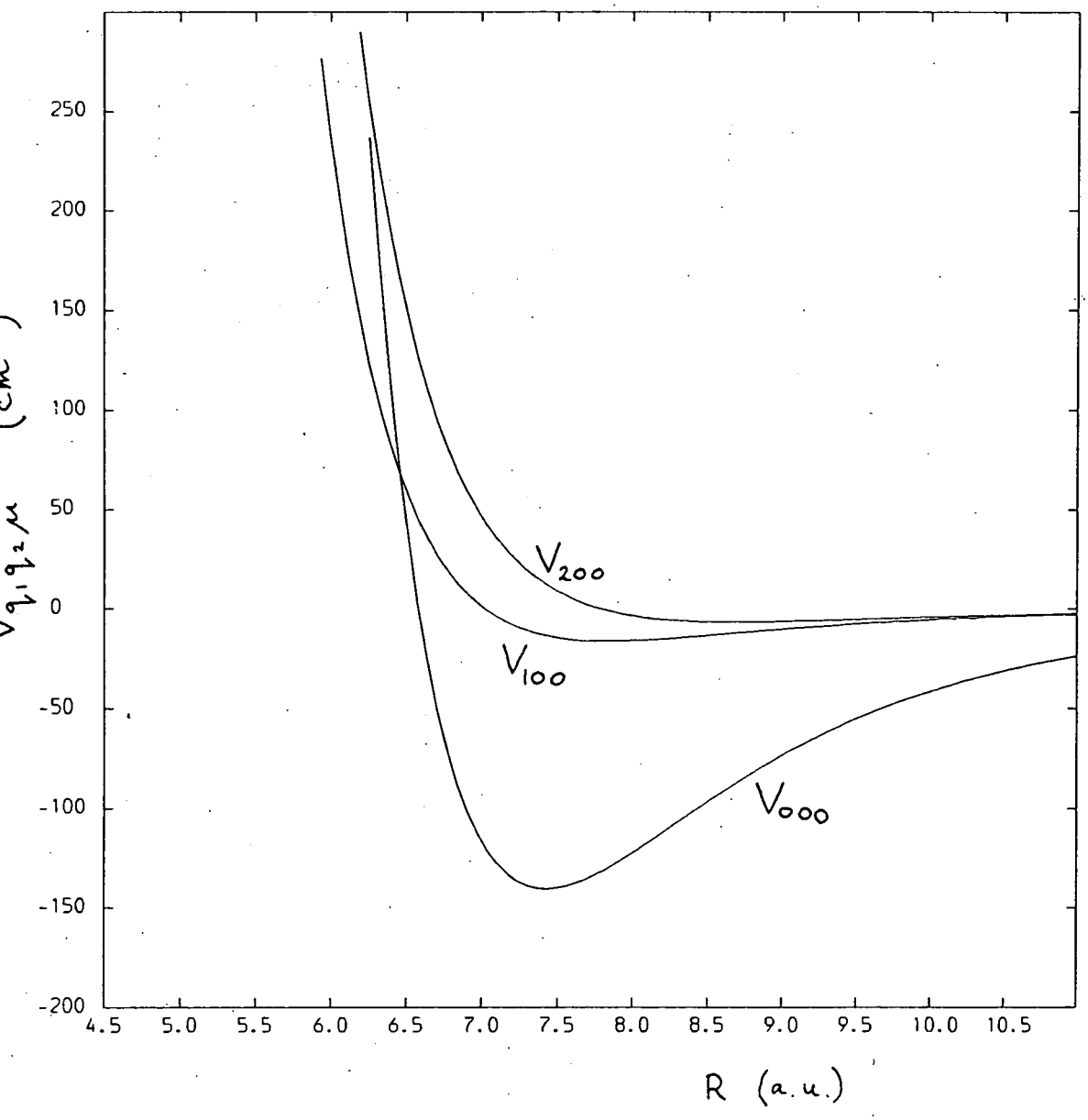

Figure 3.3

The variation with the Ar-HCl centre-of-mass separation of the body-fixed potential expansion coefficients (cf. equation (3.33)) for potential I of Dunker and Gordon (1976b).

expansion (2.23) reduces to

$$V(\hat{r}_1, R) = \sum_{q_2} V_{q_1 00}(R) \sqrt{2q_1+1}\, P_{q_1}(\cos\theta_1) \qquad (3.33)$$

where P_{q1} is a Legendre polynomial. All calculations with this potential were carried out with five rotational states, j = 0 - 4, on the HCl. The corresponding channel energies were determined from the rotational constant of HCl, 10.44019 cm^{-1}. We illustrate the convergence properties of the numerical methods with reference to the ground rovibrational state of the Ar-HCl system.

3.4.1 Convergence properties

In examining the numerical convergence properties, the parameters of interest are the integration range, $R_{max} - R_{min}$, and the number of integration steps per "half-range", N. We took the same number of steps integrating the equations from R_{min} to R_{mid} as we did from R_{max} to R_{mid}, and the step length was kept constant in each half-range, thus:

$$R_{max} - R_{mid} = Nh' \qquad (3.34a)$$

$$R_{mid} - R_{min} = Nh \qquad (3.34b)$$

This has the desirable properties of both being easy to programme and of having smaller sector widths, h,

in the region where the potential is more rapidly varying. The latter is important in the R-matrix propagator method and also helpful from the point of view of stabilisation in the de Vogelaere method. Furthermore, the global error of the results can be expected to behave monotonically with decreasing step length. This is in contrast to the erratic behaviour which can result from the use of step length algorithms (Light 1983, Mattson et al. 1983, Mattson and Anderson 1984).

In Table 3.1, the convergence of the ground state eigenenergy with respect to the number of integration steps per half-range is illustrated. R_{min} and R_{max} are held constant at 5.5 a.u. (Bohr) and 10.0 a.u. respectively. The matching point, R_{mid} = 7.4266 a.u. For N = 100, the de Vogelaere method has converged to eight significant figures, while the R-matrix propagator has to five. Given the errors inherent in the interaction potential, these levels of precision are both more than adequate. The agreement between the two methods is good; six significant figures for N = 400. Analysis of the results in Table 3.1 shows that the error in the eigenenergies obtained with the R-matrix propagator method is proportional to $(1/N)^2$. This is seen by noting that for a $(1/N)^2$ error,

$$\left(E(N) - E(2N)\right) \Big/ \left(E(2N) - E(4N)\right) = 4 \qquad (3.35)$$

	Eigenenergy (cm^{-1})	
N	de Vogelaere	R-matrix propagator
50	-132.495 07	-132.480 62
100	-132.495 08	-132.491 47
200	-132.495 08	-132.494 18
400	-132.495 08	-132.494 86

TABLE 3.1

Convergence of the ground rovibrational state of Ar-HC1 (Dunker and Gordon potential) as a function of the number of integration steps per half range, N. R_{min} = 5.5 au, R_{max} = 10.0 au, R_{mid} = 7.4266 au.

This ratio of eigenenergy differences is equal to 3.985 for N = 50 and 4.060 for N = 100. Following a suggestion by Hutson (1983a) this error can be eliminated using Richardson h^2 extrapolation (Hartree 1958). The corrected eigenenergy, E, obtained from the eigenenergies for N = 50 and N = 100 is given by

$$E = E(N=100) - \frac{1}{3}\left(E(N=50) - E(N=100)\right) \quad (3.36)$$

We thus obtain E = -132.49509 cm^{-1}, in very good agreement with the converged de Vogelaere result. Expressions analogous to (3.36) for global errors other than $O(h^2)$ may readily be derived (Mattson and Anderson 1984). Keeping h fixed in each half-range and halving it in successive calculations ensures that the global truncation error decreases monotonically as a simple power of $(1/N)$, guaranteeing the success of Richardson extrapolation.

In examining the convergence with respect to increasing the integration range, we must be aware of the loss of numerical accuracy resulting from a corresponding increase in the step length. In Table 3.2 we keep R_{min} constant at 5.5 a.u. and N at 400. This large N value ensures that changes in the de Vogelaere eigenenergies reflect variations due solely to the position of the outer starting point, R_{max}. At R_{max} = 9 a.u., the de Vogelaere method

	Eigenenergy (cm^{-1})	
R_{max}(au)	de Vogelaere	R-matrix propagator
8.5	-131.879 38	-132.540 51
9.0	-132.475 74	-132.495 42
9.5	-132.494 85	-132.494 90
10.0	-132.495 08	-132.494 86

TABLE 3.2

Convergence of the ground rovibrational state of Ar-HCl (Dunker and Gordon potential) as a function of the outer limit of the integration range, R_{max}. R_{min} = 5.5 au, R_{mid} = 7.4266 au, N = 400.

has converged to four significant figures, the R-matrix propagator to six. The differences between the two methods in convergence with respect to the inner starting point, R_{min}, are less marked, but the better convergence properties of the R-matrix propagator method are still evident (Table 3.3).

To summarise, rapid convergence with respect to the number of sectors is attained using the de Vogelaere method, but the R-matrix propagator method requires smaller penetration into the classically forbidden regions. This, as was indicated in section 3.3.2, is due to the less severe boundary conditions (3.30). In bound state problems for weakly bound van der Waals dimers, where there are few oscillations in the radial wavefunction, solution following techniques will have faster convergence properties. However, the advantage of the R-matrix propagator method in requiring a smaller integration range may prove useful where reasonably accurate eigenenergies are required for states lying close to the dissociation limit.

3.4.2 Comparison with other calculations

In the paper of Kidd et al. (1981), comparison was made with the close-coupling calculations performed by Dunker and Gordon (1976b) on Ar-HCl. Dunker and Gordon used a piecewise analytic method, described by Gordon (1971) and Dunker and Gordon (1976a). Kidd et al. used the "amplitude density" method of Johnson and Secrest

	Eigenenergy (cm^{-1})	
R_{min}(au)	de Vogelaere	R-matrix propagator
6.5	-132.214 54	-132.526 02
6.0	-132.494 89	-132.494 92
5.5	-132.495 08	-132.494 86
5.0	-132.495 08	-132.494 79
4.5	-132.495 08	-132.494 70

TABLE 3.3

Convergence of the ground rovibrational state of Ar-HCl (Dunker and Gordon potential) as a function of the inner limit of the integration range, R_{min}. R_{max} = 10.0 au, R_{mid} = 7.4266 au, N = 400.

(1968) to solve the coupled equations. This is an approximate solution approach and so might be expected to have convergence properties closer to those of the de Vogelaere than the R-matrix propagator method.

In Table 3.4 we give the eigenenergies of the ground rovibrational state at different values of the total angular momentum, J. The only other good quantum number, the parity $\mathcal{E}$, is also given. The values obtained with the R-matrix propagator and de Vogelaere methods are compared with the results of Kidd et al. (1981) and Dunker and Gordon (1976b). For comparison purposes the same integration parameters were used in our two methods; R_{min} = 5.5 a.u., R_{max} = 10.00 a.u. and N = 200. The matching point, R_{mid} = 7.4266 a.u. The potential energy parameters, HCl rotational constant, and conversion factors used were those given by Kidd et al. (1981).

The agreement we obtain with Kidd et al. is very good; to within two in the sixth significant figure. The de Vogelaere results are in rather better agreement than those using the R-matrix propagator method because of the poorer convergence properties of the latter with respect to number of sectors. The calculations of Dunker and Gordon were in single precision arithmetic, and this is a likely cause of the discrepancies with their results. The computer time, per trial energy, required by our two methods, with N = 200, is similar : about 2.5 s for

			Present calculations			
n	J	ε	de Vogelaere	R-matrix	Kidd et al.	Dunker and Gordon
5	0	1	-132.4951	-132.4942	-132.4954	-132.436
9	1	-1	-132.3821	-132.3812	-132.3824	-132.315
12	2	1	-132.1561	-132.1552	-132.1566	-132.092
14	3	-1	-131.8173	-131.8164	-131.8178	-
15	4	1	-131.3656	-131.3647	-131.3663	-
15	5	-1	-130.8013	-131.8004	-130.8022	-

TABLE 3.4

Ground-state eigenenergies (cm^{-1}) at different total angular momentum, J. The parity, ε, and the dimensionality, n, of the basis set which includes rotor states j = 0-4 are also given. For the present calculations, the integration parameters used were: N = 200, R_{min} = 5.5 au, R_{max} = 10.0 au, R_{mid} = 7.4266 au. Potential I of Dunker and Gordon (1976b) was used.

n = 5 (J = 0) and about 35s for n = 15 (J = 4,5). The calculations were performed on an IBM 370/168 machine.

So far all of our tests have been carried out using the Dunker and Gordon potential plotted in Figure 3.3. This section will be concluded with the results of some calculations on an Ar-HCl potential with a significantly shallower well and more anisotropic terms. The number and size of the anisotropic terms, together with the relatively small HCl rotational constant, lead to the basis (j) states being strongly coupled. The potential is due to J.A. Vliegenthart and A. Rozendaal, full details of which are given by Kidd et al. (1981). The expansion coefficients $V_{q_1 q_2 \mu}(R)$ for this potential are plotted in Figure 3.4, which may be compared to Figure 3.3. In Table 3.5 we present the results of calculations on two levels using the R-matrix propagator method. The energy levels chosen are those for which Kidd et al. carried out detailed convergence tests, enabling them to give definite error estimates. These calculations are for J = 0 and a basis expansion j = 0-9. The parity, $\mathcal{E} = (-)^{j+\ell} = +1$. We took the same integration range (2 - 21 a.u.) as Kidd et al. Eigenenergy 1 is the ground rovibrational state of Ar - HCl (some 37 cm^{-1} higher than the value obtained with the Dunker and Gordon potential in this section). Eigenenergy 2 is a state lying close to the dissociation

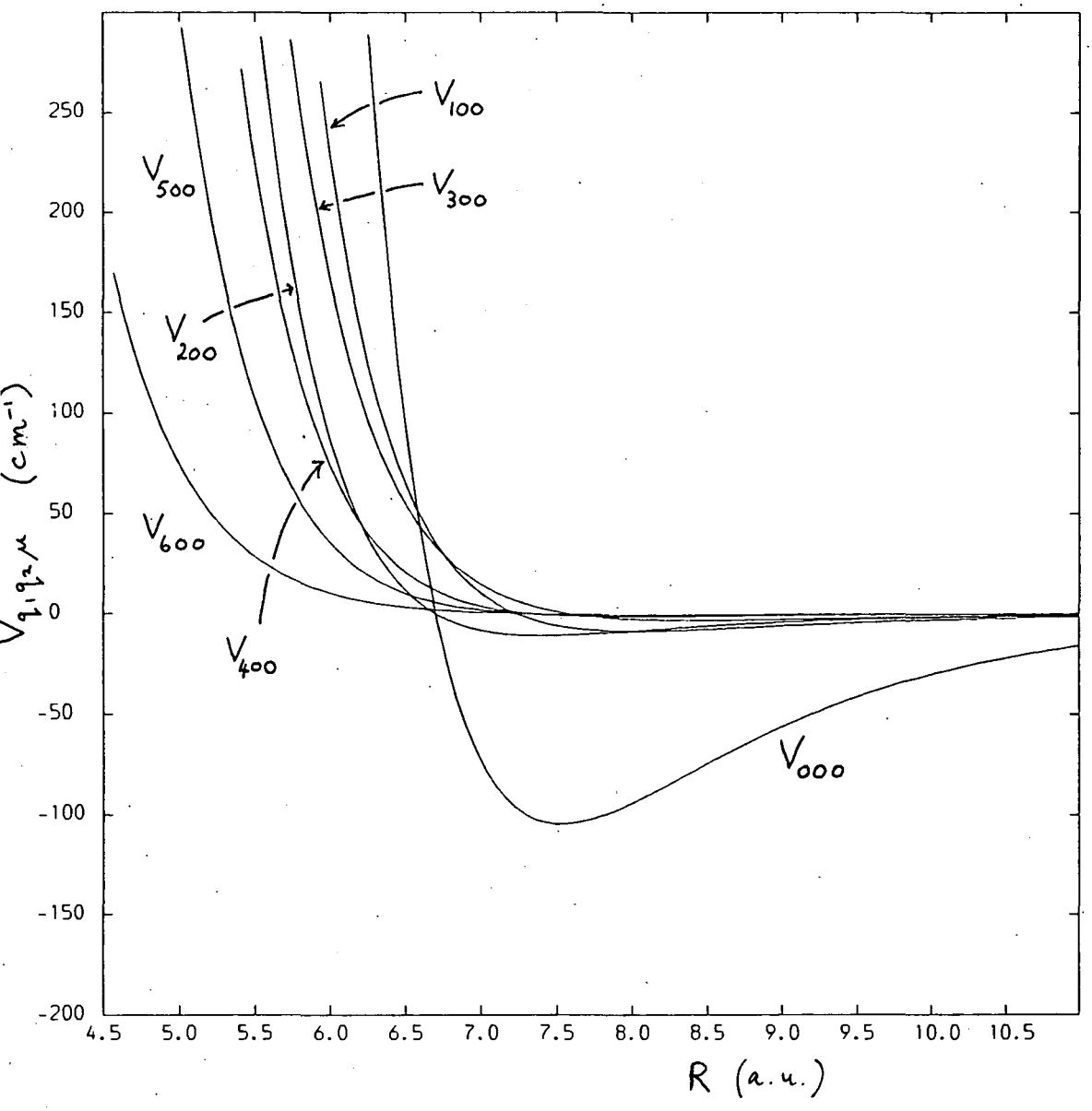

Figure 3.4

The variation with the Ar-HCl centre-of-mass separation of the body-fixed potential expansion coefficients for the Vliegenthart and Rozendaal potential described in Table 1 of Kidd et al. (1981).

	Eigenenergy 1	Eigenenergy 2
N = 100	-95.289707	-5.0057807
N = 200	-95.329388	-4.9895762
Richardson h^2 extrapolate	-95.3429	-4.9845
Kidd et al.	-95.3429 ± 0.001	-4.9854 ± 0.02

TABLE 3.5

Calculations of two rovibrational states of the Vliegenthart and Rozendaal Ar-HCl potential in Figure 3.4. A Richardson h^2 extrapolate was obtained from calculations employing a total of 200 (N = 100) and 400 (N = 200) steps. Also presented are the results and error bounds of Kidd et al. (1981) who used a total of 400 integration steps. All energies are in cm^{-1}.

limit. It is seen that in both cases, our estimate of the eigenenergy, using a Richardson h^2 extrapolation of the results for N = 100 and N = 200, lies well within the error bounds quoted by Kidd et al. Their results were obtained using a total of 400 sectors, presumably requiring similar computational effort to our N = 200 calculation.

The high level of agreement between the R-matrix propagator, de Vogelaere and Johnson and Secrest algorithms is encouraging. The results of this section allay the reservations expressed by Light and Walker (1976) about the suitability of the R-matrix propagator method for use in coupled channel bound state problems. It should be emphasised that all of the calculations described in this chapter are purely for test purposes. Close-coupled bound state calculations on the Ar-HCl dimer using more realistic potentials have been performed by Hutson and Howard (1982) and Hutson (1984).

In the following chapter we shall apply the numerical methods of the present chapter and the algebraic methods of Chapter 2 to the H_2 - H_2 dimer. Before doing so, alternative approaches to finding the bound states of van der Waals molecules will be discussed.

3.5 Alternative methods for finding bound states

3.5.1 Matching conditions

The implementation of the boundary conditions of the bound state problem for a single Schroedinger equation is considerably simpler than the more general n channel case presented so far. It is well established that a shooting procedure is a satisfactory way of finding the eigenenergies (Eisberg 1961). A trial energy is chosen and the solution F(R) propagated from R_{min} into the right hand side classically forbidden region. Unless an eigenenergy was fortuitously chosen, the wavefunction will either approach the axis before rising exponentially in magnitude, or it will cross the axis and continue exponentially. One eigenenergy (or some other odd number) lies between two trial energies for which the trial solutions differ in sign at large R. The eigenenergy may be located using Bolzano's method (taking the next trial energy to be midway between the first two). For a single Schroedinger equation the time consuming integration is, therefore, taken no further than necessary, and there is no need to carry out tests to determine either a suitable matching point R_{mid} or upper limit to the integration range R_{max}. The behaviour of the wavefunction as the trial energy passes through an eigenenergy has been nicely illustrated by Hajj (1980). A number of highly automated computer programmes adopting

the above shooting approach for a single Schroedinger equation have been written and are suitable for use as "black boxes" (e.g. Foglia 1984). An exception is the work of Cooley (1961) who preferred the forward and backward propagation, for solving a single Schroedinger equation, as this enabled him to develop a particularly efficient method for iterating to an eigenvalue.

It is instructive to consider the difficulties encountered when we try to apply the shooting technique to systems of coupled equations. Consider the simplest case of equation (3.1) with two coupled channels.

$$\frac{d^2}{dR^2} F_j(R) = \sum_k W_{jk}(R) F_k(R)$$

$$j = 1, 2 \quad \text{and} \quad k = 1, 2 \qquad (3.37)$$

At $R = R_{min}$ we set $F_1 = F_2 = 0$ and we are free, because of the homogeneity of the Schroedinger equation, to specify an arbitrary value for <u>one</u> of the initial derivatives, say $F_1'(R_{min})(= \frac{dF_1}{dR}(R_{min}))$. We now have to search over two unknowns, $F_2'(R_{min})$ and E, in order to find the eigen-energies for which $F_1(R_{max}) = F_2(R_{max}) = 0$. In principle the differential equations (3.37) may be integrated for trial values of these unknowns and some form of inverse interpolation used, guided by the form of the solutions in the asymptotic region. A more systematic method

based on Newton's process has been described by Fox (1960). For the problem at hand, Newton's process gives rise to two simultaneous equations for the corrections, $\delta F_2'(R_{min})$ and δE, to the trial values of $F_2'(R_{min})$ and E:

$$\delta E \frac{\partial F_1}{\partial E}(R_{max}) + \delta F_2' \frac{\partial F_1}{\partial F_2'}(R_{max}) + F_1(R_{max}) = 0$$

$$\delta E \frac{\partial F_2}{\partial E}(R_{max}) + \delta F_2' \frac{\partial F_2}{\partial F_2'}(R_{max}) + F_2(R_{max}) = 0 \quad (3.38)$$

For clarity the R_{min} argument has been dropped. $F_1(R_{max})$ and $F_2(R_{max})$ are found by numerically integrating the coupled equations. The coefficients of δE and $\delta F_2'$ have to be found by numerical integration of differential equations obtained by differentiating the Schroedinger equation with respect to E and F_2'. The boundary conditions for these at R_{min} are obtained directly from those for (3.37). Once E and F_2' have been corrected using (3.38) the procedure is repeated until E and F_2' no longer change to within a specified tolerance. It is clear that this procedure will become very complicated for large systems of coupled equations, though it does avoid the need for propagating a matrix of solutions rather than a single column. If the iterative procedure was efficient then this would result in a saving of CPU time. A good initial estimate of the eigenenergy as well as the starting

solution derivatives is critical to the method's efficiency. In addition, Fox (1960) sometimes obtained false eigenvalues when he failed to choose a large enough value of R_{max}. This occurred when one of the components of the solution happened to cross the axis, changing sign at R_{max}. Fox attempted to solve a maximum of 3 coupled equations. With these problems in mind, we opted to follow Gordon (1969) in propagating a set of solution vectors in both the forward and backward directions, and matching at R_{mid}.

The backward propagation is avoided in an important technique, devised by Shapiro (1972) and developed for bound state calculations by Shapiro and Balint-Kurti (1979), known as the artificial channels method. This involves converting the bound state problem into a scattering calculation by the addition of two unphysical channels which are open at large R. These channels, which we denote by β and γ, are not directly coupled to each other but are coupled to the (closed) channels of the bound state problem, collectively denoted by α. The augmented coupling matrix has a special asymmetric form which permits coupling of γ to β via α but not β to γ.

$$\underset{\sim}{W}(R) = \begin{pmatrix} V_{\alpha\alpha} - E & 0 & V_{\alpha\gamma} \\ V_{\beta\alpha} & V_{\beta\beta} - E & 0 \\ 0 & 0 & V_{\gamma\gamma} - E \end{pmatrix} \times 2\mu \qquad (3.39)$$

Shapiro and Balint-Kurti (1979) chose exponentially decaying forms, ae^{-bR}, for $V_{\beta\beta}$, $V_{\gamma\gamma}$, $V_{\beta\alpha}$ and $V_{\alpha\gamma}$. They pointed out, however, that the bound state energies yielded by their method were completely insensitive to the values of a and b chosen. Figure 3.5 is a schematic representation of the diagonal elements of the augmented effective potential matrix for the example of a single Schroedinger equation (Shapiro and Balint-Kurti 1977). Using numerical methods, such as those described in Sections 3.2 and 3.3, the coupled equations may be integrated outwards into the asymptotic region. At this point, scattering boundary conditions (see Chapter 5) may be applied. The transition probability or T-matrix element, $T_{\beta\leftarrow\gamma}$, may thus be obtained. It has been shown that this T-matrix element may be written as a sum of contributions from all of the bound states, $\phi_b(R)$, of $V_{\alpha\alpha}(R)$ plus an integral over the continuum states (Shapiro and Balint-Kurti 1979):

$$T_{\beta\leftarrow\gamma} \sim \sum_b \langle \chi_\beta | V_{\beta\alpha} | \phi_b \rangle_R \frac{1}{E-\varepsilon_b} \langle \phi_b | V_{\alpha\gamma} | \chi_\gamma \rangle_R$$

$$+ \text{ continuum contributions} \qquad (3.40)$$

χ_β and χ_γ are the scattering states of channels β and γ in the zero coupling limit. (3.40) shows that $T_{\beta\leftarrow\gamma}$ has a pole whenever the total energy E is

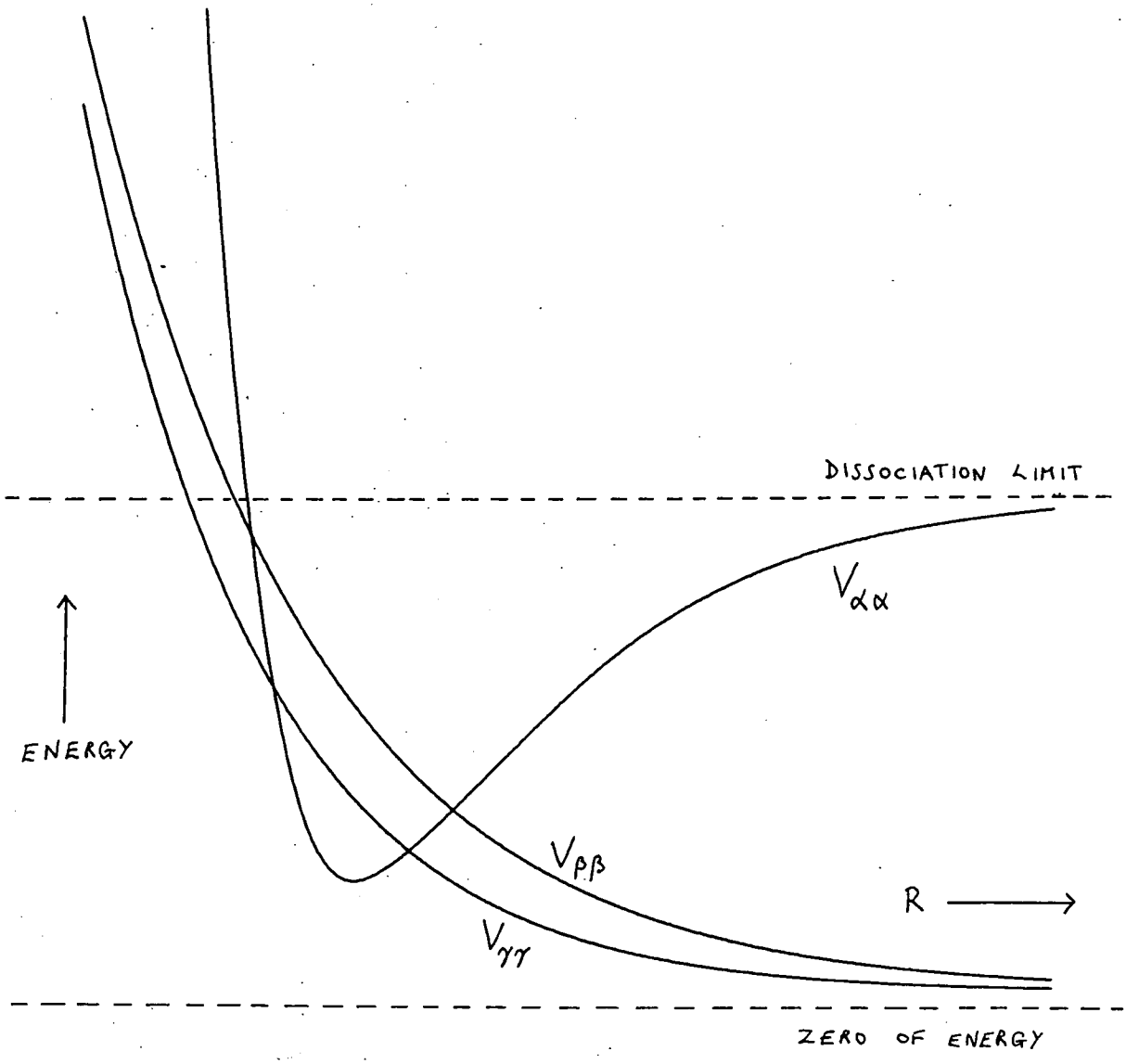

Figure 3.5

The diagonal elements of the 3 x 3 effective potential matrix corresponding to a single channel (α) bound state problem (Shapiro and Balint-Kurti 1977).

equal to a bound state energy $\mathcal{E}_b$. The bound state problem has thus been reduced to one of calculating the T-matrix at a range of trial energies and locating the poles in $T_{\beta \leftarrow \gamma}$.

It may be observed that the artificial scattering problem constructed above bears a striking resemblance to the physical problem of the Raman scattering of light by molecules (Weissbluth 1978). In this analogy β and γ correspond to the final and initial molecular states. These are not directly coupled by the transition dipole moment induced by the incoming photon, but only indirectly via intermediate states (α). An expression similar to (3.40) is obtained for the transition matrix element which, if the finite widths of the intermediate states are unaccounted for, possesses similar poles (Bransden and Joachain 1983).

In order to construct the appropriate scattering boundary conditions in the artificial channels method it is necessary, as with bound state boundary conditions, to propagate a matrix of solution vectors. In this case each column vector represents an initial state of the system. Thomas (1979, 1982) has had considerable success with an iterative approach in which scattering from a single initial state only is considered. This yields a single column of the T-matrix. Though Thomas

solved the problem in integral form, it is equivalent to propagating a single solution vector and iteratively searching for the correct starting derivatives. The method gains in speed over conventional methods providing the total number of iterations is much smaller than the dimensionality of the problem. 510 close-coupled equations have been solved by the Thomas (1982) method.

In the artificial channels approach, one is not interested in the whole T-matrix; just a single element. The bringing together of Thomas' work on scattering calculations with the artificial channels method, heeding the lessons of Fox (1960), could produce a useful method for calculating bound states. Furthermore, information gleaned at the first trial energy could be used to reduce the number of iterations needed to find the correct scattering solution at subsequent energies. The method could find application in calculating the bound states of systems requiring very large numbers of coupled equations. Examples of such systems are provided by semi-rigid van der Waals molecules (e.g. He-I_2) or conventional "floppy" systems such as H_3^+ and KCN.

3.5.2 The centrifugal decoupling method

So far in this chapter, we have discussed the solution of the bound state problem using the full close-coupling (cc) method. We now outline an approximate method which

requires a body-fixed formulation for its implementation. In the body-fixed frame the potential matrix elements are diagonal in the $\bar{\Omega}$ quantum number; only the coriolis interactions couple states of different $\bar{\Omega}$ (see equation (2.32)). The centrifugal decoupling (CD) or coupled states method involves neglecting these coriolis terms. In scattering calculations, for which this approximation has been widely made (e.g. Dickinson 1979), the diagonal $\underset{\sim}{l}^2$ matrix elements (equation (2.31)) are also sometimes approximated. The true values should be retained when calculating bound states. The CD approximation thus leads to a coupling matrix W which is block diagonal in $\bar{\Omega}$ (Rabitz 1975). The bound state problem may thus be solved separately for each block resulting in a saving in CPU time. Within the CD approximation $\bar{\Omega}$ becomes a good quantum number and may be used for bound state assignments. Furthermore, as can be seen from equation (2.15), the basis set for $\bar{\Omega} \neq 0$ is independent of the parity ε . In other words, for $\bar{\Omega} \neq 0$, the coupled equations need only be solved for one parity; levels differing only in ε thus become degenerate (Tennyson and van der Avoird 1982a).

The CD method has been applied to the Ar-HCl dimer by Kidd et al. (1981). This is a favourable system both because the strong potential coupling makes the coriolis terms relatively unimportant, and because the

dimer is a near symmetric top (for which $\bar{J}$ is a good quantum number). Kidd et al. (1981) compared CD with cc calculations of the ground state eigenenergy for a range of total angular momenta, J. The error in the CD results was found to increase with increasing J, reflecting the growing importance of the coriolis coupling.

The range of systems which could be studied by the CD method could be extended in a number of ways. Rabitz (1975) has suggested including only selected coriolis couplings, while Hutson and Howard (1980) have used perturbation theory to correct for neglect of these terms. Perturbative correction of CD results has also been applied to scattering problems by Secrest (1983).

The CD method has been applied in bound state calculations of the strongly coupled molecular dimers $(HF)_2$ (Barton and Howard 1982) and $(N_2)_2$ (Tennyson and van der Avoird 1982a). In the latter example, eigenvalues accurate to within 0.1 cm^{-1} were obtained for states where the full coupling matrix was too large to allow more accurate cc calculations to be made. Tennyson and van der Avoird solved these CD equations not by numerical integration, but by the secular equation method which we now describe.

3.5.3 The secular equation method

So far we have solved the coupled equations for the radial wavefunctions by direct numerical integration. Alternatively we may use the variational principle and expand the radial coordinate in terms of an orthonormal set of states (Le Roy and van Kranendonk 1974):

$$F_k(R) = \sum_n a_{nk} \psi_n(R) \qquad (3.41)$$

n represents the stretching quantum number of the van der Waals bond. It is more convenient to define $\psi_n(R)$ as being the same for all radial channels k, though the radial expansion coefficients a_{nk} will, as indicated, generally differ. Substituting (3.41) into the close-coupled equations (3.1), and projecting with $\psi_m(R)$ yields a set of linear equations of the following form:

$$\left(H_{mj,nk} - E\,\delta_{mj,nk}\right) a_{nk} = 0 \qquad (3.42)$$

In the notation of Chapter 2, the Hamiltonian matrix is given by

$$H_{mj,nk} = \int \psi_m^*(R) \left\{ \delta_{jk} \left[-\frac{1}{2\mu} \frac{d^2}{dR^2} + E \right] + \frac{W_{jk}(R)}{2\mu} \right\} \psi_n(R)\, dR \qquad (3.43)$$

Unique solutions of (3.42) exist only if the determinant of the matrix in brackets is zero, and this condition yields a secular equation for E. The problem of solving

the close-coupled equations thus reduces to one of diagonalising the Hamiltonian matrix. The eigenenergies E and eigenvectors $\underset{\sim}{a}$ thus obtained are frequently labelled with a set of quantum numbers α ($\equiv n j_1 j_2 j_{12} \Omega$) representing the basis state to which they correlate in the isotropic limit (Le Roy and Carley 1980). Tennyson and van der Avoird (1982a) have coined the term LC-RAMP (Linear Combination of Radial and Angular Momentum functions Products) to distinguish the secular equation method outlined here from its implementations in other types of problems (e.g. in electronic structure calculations).

In order to generate the Hamiltonian matrix it is necessary to perform radial integrations over d^2/dR^2, $1/R^2$ and $V_{q_1 q_2 \mu}(R)$. It is important to choose radial basis states for which these matrix elements are straightforward to evaluate. The number of terms in the expansion (3.41) required to provide an accurate representation of the wavefunction should be as small as possible, to avoid having to diagonalise an unwieldly Hamiltonian matrix. One possibility is to define $\psi_n(R)$ to be the bound eigenstates of a single radial Schroedinger equation:

$$\left\{ -\frac{1}{2\mu}\frac{d^2}{dR^2} + \frac{l(l+1)}{2\mu R^2} + V_{000}(R) - E(n,l) \right\} \psi_n(R) = 0 \qquad (3.44)$$

This equation may be obtained from the close-coupled equations in the body-fixed frame by setting J = 0 and neglecting the potential anisotropy. In this case $\ell = j_{12}$.

The "basis generating potential" (Le Roy and Carley 1980) is taken to be the isotropic part of the diatom-diatom interaction, though other choices are possible. For complexes undergoing strongly hindered internal rotation, the radial potential obtained by fixing the monomer orientations at their equilibrium values may lead to fewer $\psi_n(R)$ being needed (Tennyson and van der Avoird 1982c). Numerical solution of the basis generating equation (3.44) can yield a complete set of orthonormal states for any single value of ℓ. In the weakly coupled hydrogen-rare gas systems, where ℓ is approximately conserved, a value corresponding to the dimer state of interest was chosen by Le Roy and Carley (1980). Tennyson and van der Avoird (1982c) chose $\ell = 0$ for all their calculations on the strongly bound floppy molecule KCN. This gave rapid convergence as the effective radial potential was quite insensitive to changes in ℓ.

In strongly bound conventional molecules which have a large number of bound states, or in weakly coupled van der Waals systems when ℓ is approximately conserved, the above approach has been shown to be satisfactory.

For strongly coupled van der Waals molecules, l is no longer good and there may not exist a sufficiently large number of bound solutions of (3.44) to achieve convergence. This problem can be overcome by placing an infinite wall in the basis generating potential at some large radial separation R_w. R_w should be beyond the classical turning point of the highest eigenstate of interest, if the radial behaviour of the dimer wavefunction is to be properly represented in a physically important region. However, if R_w is too large the positive eigenenergies of (3.44) representing the continuum become more closely bunched. Relatively more terms are then needed to achieve a given degree of flexibility in the description of $\underset{\sim}{F}(R)$. In general some experimentation is necessary to establish a suitable compromise, though a more formal procedure of minimising the dimer eigenvalues with respect to R_w, for a fixed basis set size, could be used. Le Roy et al. (1982) chose R_w to maximise the amplitude of the dimer eigenfunctions. Le Roy et al. (1977) have used the infinite wall approach to calculate the ground rovibrational state of the Ar-HCl dimer, using the potential of Figure 3.3. They obtained a value of $-132.497\ cm^{-1}$ which differs from the true value by only $0.002\ cm^{-1}$ (see Tables 3.1, 3.2 and 3.3). This method has also been used by Tennyson (1982) in his study of the very weakly bound H_3 molecule.

The use of numerical radial basis states has been reviewed by Le Roy and Carley (1980). A final point is that the numerical solution for $\psi_n(R)$ yields the matrix elements over d^2/dR^2 in (3.43) directly. This is because the total Hamiltonian may be written in terms of the basis generating Hamiltonian plus the anisotropic potential terms and terms in $1/R^2$.

An alternative approach is to use a set of analytic polynomial functions in the radial coordinate. This avoids having both to perform numerical integrations of (3.44) and the need to retain the basis states, over a fine grid, in storage. Tennyson and Sutcliffe (1982) introduced the use of Morse oscillators which are based on associated Laguerre polynomials, for finding the bound states of KCN and H_2-Ne. For these functions the matrix elements over d^2/dR^2 are analytic while the others must be evaluated by numerical quadrature. Associated with a single complete set of oscillators are 3 parameters; these are related to those of the associated Morse potential, namely the dissociation energy (D_e), the fundamental vibration frequency (W_e) and the position of the potential minimum (R_e). These may be adjusted so as to minimise selected dimer eigenvalues for a small radial and angular basis set calculation. A larger basis, using these optimised parameters, may then be used for production runs. For the KCN molecule, Tennyson and Sutcliffe

(1982) found that a basis set of Morse oscillators, variationally optimised in this way, required the same number of terms to give converged results as earlier calculations using a numerically generated basis (Tennyson and van der Avoird 1982c). Furthermore, the 444 dimensional Hamiltonian matrix took only a tenth of the CPU time to construct.

Spherical oscillator-like functions have also been used (Tennyson and Sutcliffe 1983b). For these functions, which have 2 adjustable parameters, the matrix elements over $1/R^2$ as well as d^2/dR^2 are analytic. In their work on H_3^+, Tennyson and Sutcliffe (1984) compared the performance of these with Morse oscillators and found the latter to be better. This they attributed to the additional flexibility provided by the extra adjustable parameter in the Morse case.

Two "black box" computer programmes have been produced to study atom-diatom (or triatomics in general) systems. One uses Morse oscillators (Tennyson 1983), the other spherical oscillators (Tennyson 1984). The latter has been used in studies of the CH_2^+ molecule for which the linear H-C-H configuration is important (Tennyson and Sutcliffe 1983b). This corresponds to R = 0, for which Morse functions do not obey the correct (vanishing) boundary conditions.

The secular equation method has been applied to the diatom-diatom system N_2-N_2 (Tennyson and van der Avoird 1982a) using an extension of the first of the computer codes referred to above. They were able to solve up to 675 close-coupled equations with this method, an order of magnitude larger than the number feasible with the de Vogelaere and R-matrix propagators. However, it should be clear from the discussion above that the problem of finding a suitable radial basis is non-trivial. Furthermore, the accuracy of the eigenenergies obtained tends to diminish significantly for higher states. For these reasons, the numerical solution of the close-coupled equations, which is equivalent to using an infinite R-basis, will remain an important technique for calculating bound state energies.

3.5.4 Angular-radial decoupling methods

We end this chapter with a description of methods which incorporate most of the ideas so far discussed. The methods rely on an adiabatic separation of the stretching motion of the van der Waals bond from internal motions in a way which is analogous to the Born-Oppenheimer (BO) separation of electronic and nuclear motion. The case of two rigid rotors will be considered; the extension to vibrotors should be straightforward, though no calculations including this degree of freedom have yet been carried out.

We partition the Hamiltonian (2.2) into the sum of a radial and angular part.

$$H = T_R + H_o\left(R \middle| \hat{\underset{\sim}{r}}_1, \hat{\underset{\sim}{r}}_2, \hat{\underset{\sim}{R}}\right) \tag{3.45}$$

where

$$T_R = -\frac{1}{2\mu R}\frac{\partial^2}{\partial R^2} R \tag{3.46}$$

is the radial kinetic energy operator. The angular (or fixed-R) Hamiltonian, is given by

$$H_o\left(R \middle| \hat{\underset{\sim}{r}}_1, \hat{\underset{\sim}{r}}_2, \hat{\underset{\sim}{R}}\right) = \frac{\underset{\sim}{l}^2}{2\mu R^2} + h_1 + h_2 + V\left(\hat{\underset{\sim}{r}}_1, \hat{\underset{\sim}{r}}_2, R\right) \tag{3.47}$$

Assuming the rotational motion is much faster than the stretching of the dimer bond, we fix R to obtain an equation analogous to the electronic wave equation in the BO approximation

$$\left(H_o - U_\alpha^{J\varepsilon}\right) f_\alpha^{J\varepsilon}\left(R \middle| \hat{\underset{\sim}{r}}_1, \hat{\underset{\sim}{r}}_2, \hat{\underset{\sim}{R}}\right) = 0 \tag{3.48}$$

The eigenfunctions of this angular equation depend parametrically on R. They may be labelled by the quantum numbers $(j_1, j_2, j_{12}, \bar{\Omega}) \equiv \alpha$. Equation (3.48) may be solved by expanding $f_\alpha^{J\varepsilon}$ in terms of the set of basis

functions $\mathcal{Y}(j_1\ j_2\ j_{12}\ \bar{n}JM\varepsilon\,|\hat{r}_1,\hat{r}_2,\hat{R})$ given in (2.15). The resulting linear equations are solved by diagonalising the H_o matrix, the elements of which have been given in the preceding chapter. This procedure is repeated on a grid of R values to obtain the angular eigenvalues $U_\alpha^{J\,\varepsilon}(R)$. These form effective isotropic potentials for the radial motion. They are independent of whether space-fixed or body-fixed (as here) basis functions are used in the expansion of $f_\alpha^{J\varepsilon}$, provided that a complete set is used. Le Roy and Carley (1980) have given a detailed presentation for atom-rotor systems using space-fixed coordinates.

The exact total wavefunction may now be expanded in terms of the $f_\alpha^{J\varepsilon}$, which form a complete orthonormal set at each R.

$$\Psi^{J\varepsilon} = \sum_\alpha \chi_\alpha(R)\, f_\alpha^{J\varepsilon}(R|\hat{r}_1,\hat{r}_2,\hat{R}) \qquad (3.49)$$

Inserting this in the Schroedinger equation (2.1) and projecting with $f_{\alpha'}^{J\varepsilon}$ yields a system of coupled equations for the radial functions χ_α :

$$\sum_\alpha \int d\hat{r}_1\, d\hat{r}_2\, d\hat{R}\ f_{\alpha'}^{*}\, T_R\, f_\alpha\, \chi_\alpha(R) + \left[U_{\alpha'}(R) - E\right]\chi_{\alpha'}(R) = 0 \qquad (3.50)$$

Because the angular eigenfunctions depend on R, the effect of T_R is given by

$$T_R f_\alpha \chi_\alpha = f_\alpha T_R \chi_\alpha + \chi_\alpha T_R f_\alpha - \frac{1}{\mu} \frac{\partial f_\alpha}{\partial R} \frac{\partial \chi_\alpha}{\partial R} \quad (3.51)$$

If the angular eigenfunctions vary slowly with R, the last two terms on the right hand side of (3.51) can be neglected. The equations then decouple to yield a one-dimensional radial Schroedinger equation

$$\left[T_R + U_{\alpha'}(R) - E \right] \chi_{\alpha'}(R) = 0 \quad (3.52)$$

The association of $U_{\alpha'}(R)$ with an effective angular potential for radial motion should now be clear.

An indication of the accuracy of this approach can be obtained by including the adiabatic (diagonal) correction term

$$\tau^{J\varepsilon}_{\alpha'}(R) = \int d\hat{r}_1 \, d\hat{r}_2 \, d\hat{R} \; f^*_{\alpha'} T_R f_{\alpha'} \quad (3.53)$$

The last term of (3.51) contributes only to non-adiabatic coupling between angular states (Holmgren et al. 1977). The adiabatically corrected radial equation is thus given by

$$\left[T_R + \tau_{\alpha'}(R) + U_{\alpha'}(R) - E \right] \chi_{\alpha'}(R) = 0 \quad (3.54)$$

Either (3.52) or (3.54) may be taken as a statement of the Born Oppenheimer Angular Radial Separation (BOARS) method, as developed by Holmgren et al. (1977). These equations are analogous to the nuclear wave equation in the BO approximation; they may be solved by numerical integration using the methods described earlier in this chapter. In their work on Ar-HCl, Holmgren et al. (1977) showed that equations (3.52) and (3.54) provide rigorous lower and upper bounds respectively to the ground state energy for each value of J. The difference between these bounds was typically 1.5 - 4.0 cm^{-1}, depending on the potential energy surface used. They used the centrifugal decoupling approximation throughout but included the coriolis terms in a subsequent paper (Holmgren et al. 1978) also on Ar-HCl. In this later paper they applied the BOARS method to the determination of a potential energy surface by least squares fitting to experimental data.

The non-adiabatic coupling between different angular states, caused by the last two terms in (3.51) is sometimes significant. This fact led Hutson and Howard (1980) to develop the Corrected Born Oppenheimer (CBO) method in which these correction terms are treated using perturbation theory. In the only diatom-diatom system studied to date, $(HF)_2$, Barton and Howard (1982) also

treated the J-dependent and Coriolis parts of the Hamiltonian by perturbation theory. This simplified the solution of the angular equation (3.48) and allowed spectroscopic observables, such as the rotational constant of the complex, to be calculated directly.

Provided the perturbation theory expansion is rapidly convergent, the CBO method produces eigenenergies comparable in accuracy with secular equation and direct numerical integration results (Hutson and Howard 1980). However, for some potential energy surfaces the angular eigenfunctions $f_{\alpha}^{J\varepsilon}$ can change rapidly with R; this can happen when the equilibrium geometry of the dimer suddenly changes due to sign changes in the anisotropic terms of the intermolecular interaction $V_{q_1\ q_2 \mu}(R)$. The Reversed Adiabatic (RA) method of Hutson and Howard (1982) circumvents this problem by separating the angular and radial motions in the opposite order to the CBO and BOARS methods. In the case of two diatoms, this involves fixing the geometry of the dimer and solving the following Schroedinger equation for the stretching of the van der Waals bond:

$$\left[-\frac{1}{2\mu R}\frac{\partial^2}{\partial R^2}R + V(\hat{\underset{\sim}{r}}_1, \hat{\underset{\sim}{r}}_2, R) - U\right]\chi(\hat{\underset{\sim}{r}}_1, \hat{\underset{\sim}{r}}_2, \hat{\underset{\sim}{R}}|R) = 0 \qquad (3.55)$$

This procedure is repeated on an angular grid to yield effective potentials for angular motion $U(\hat{\underset{\sim}{r}}_1, \hat{\underset{\sim}{r}}_2, \hat{\underset{\sim}{R}})$.

The resulting one-dimensional angular Schroedinger equation may be perturbatively corrected to account for non-adiabatic couplings between the different radial eigenfunctions of (3.55). The RA method is accurate if the radial wavefunction does not change rapidly with the geometry of the complex. In the rare gas - HCl systems to which it has been applied (Hutson and Howard 1982) this was found to be less restrictive than the conditions imposed on the CBO (and BOARS) method. The RA method, without non-adiabatic corrections, is analogous to the infinite order sudden approximation (IOSA) of scattering theory (e.g. Dickinson 1979).

CHAPTER FOUR

THE H_2 - H_2 DIMER

4.1 Introduction

Molecular hydrogen is the most abundant molecule in the interstellar medium with a typical number density of 10^6 cm^{-3} in dense molecular clouds. A knowledge of the cross sections for rotational excitation of H_2 by collisions with other H_2 molecules may be used to glean information on the physical properties of these interstellar clouds. As an example, such cross sections are a necessary handle in models of radiative cooling (Draine et al. 1983). These collisional calculations may be carried out provided an accurate intermolecular potential is available. The H_2-H_2 potential may be calculated using a variety of quantum mechanical methods. The purpose of this chapter is to investigate the usefulness of spectroscopy of the corresponding molecular dimer in assessing calculations of the potential energy surface.

In Chapters 2 and 3, the problem of calculating bound state energies of molecular dimers has been considered and a solution formulated. The solution is based on numerical integration of the close-coupled equations derived in Chapter 2. The algebra presented there is applicable to van der Waals molecules comprising any pair of distinguishable or identical heteronuclear or homonuclear $^1\Sigma$ diatomics, treated as rigid rotors. Results based on four independent calculations of the H_2 - H_2 intermolecular potential will be discussed

here.

The potential of Kochanski (1975) was computed using a hybrid technique in which the dispersion (intermolecular correlation) energy is evaluated from second-order perturbation theory and added to the SCF energy of the "supermolecule" H_2 - H_2. This approach is economical in terms of computer resources and, as such, is tractable even for heavier systems, e.g. CO-H_2 (Prissette et al. 1978, Flower et al. 1979) and OH-H_2 (Kochanski and Flower 1981).

The three remaining potentials (Burton and Senff 1982; Meyer and Schaefer 1985, Schaefer and Liu 1985; Schaefer and Meyer 1979) derive from configuration interaction (CI) calculations, in which the contribution of the dispersion energy to the total interaction potential is already included. The Meyer-Schaefer-Liu potential has been used in calculations of a wide range of physical properties for which experimental results are available. Calculations of differential cross sections have been compared with the experimental measurements of Buck (1982) and Buck et al. (1983a,b). A variety of transport properties, rotational relaxation and line broadening phenomena have also been calculated with this surface (Köhler and Schaefer 1983a,b).

We compare the results of our bound state calculations with those of Verberne and Reuss (1981), who employed a potential almost identical to that of Meyer, Schaefer and Liu. After comparing our results with the spectro-

scopic measurements of McKellar and Welsh (1974) we go on to briefly discuss the validity of using the rigid rotor approximation for this system. This chapter, therefore, complements and updates the pioneering work of Gordon and Cashion (1966) in which empirical isotropic potentials were used to analyse the earlier and less detailed spectra of Watanabe and Welsh (1964). Conclusions are drawn regarding the relative merits of all four calculations of the H_2 - H_2 potential surface, cited above.

4.2 The H_2 - H_2 interaction potential

As noted in Chapter 2, the interaction potential between two diatomic molecules may be expanded in terms of space-fixed (SF) or body-fixed (BF) coordinates. In SF coordinates,

$$V(\hat{\underset{\sim}{r}}_1', \hat{\underset{\sim}{r}}_2', \underset{\sim}{R}) = \sum_{q_1 q_2 q_{12}} A_{q_1 q_2 q_{12}}(R)\, I_{q_1 q_2 q_{12}}(\hat{\underset{\sim}{r}}_1', \hat{\underset{\sim}{r}}_2', \hat{\underset{\sim}{R}}) \qquad (4.1)$$

where

$$I_{q_1 q_2 q_{12}} = \sum_{m_1 m_2 m_{12}} C^{q_1 q_2 q_{12}}_{m_1 m_2 m_{12}}\, Y_{q_1 m_1}(\hat{\underset{\sim}{r}}_1')\, Y_{q_2 m_2}(\hat{\underset{\sim}{r}}_2')\, Y^{*}_{q_{12} m_{12}}(\hat{\underset{\sim}{R}}) \qquad (4.2)$$

in which C is a Clebsch-Gordan coefficient and Y_{qm} a spherical harmonic function; $\hat{\underset{\sim}{r}}_1'$, $\hat{\underset{\sim}{r}}_2'$ denote the orientations of the intramolecular axes and $\hat{\underset{\sim}{R}}$ is the orientation of the intermolecular vector, relative to an SF coordinate system. In BF coordinates,

$$V(\hat{\underset{\sim}{r}}_1, \hat{\underset{\sim}{r}}_2, R) = \sum_{q_1 q_2 \mu \geq 0} V_{q_1 q_2 \mu}(R)\, Y_{q_1 q_2 \mu}(\hat{\underset{\sim}{r}}_1, \hat{\underset{\sim}{r}}_2) \qquad (4.3)$$

where

$$Y_{q_1 q_2 \mu} = 4\pi \left(Y_{q_1 \mu}(\hat{r}_1) Y_{q_2 -\mu}(\hat{r}_2) + Y_{q_1 -\mu}(\hat{r}_1) Y_{q_2 \mu}(\hat{r}_2) \right) \times (1+\delta_{\mu 0})^{-1} \quad (4.4)$$

The representations (4.1) and (4.3) are related through a unitary transformation given in Chapter 2 (equation (2.27)).

Values of the coefficients A_{000}, $A_{202} = A_{022}$, A_{220}, A_{222} and A_{224} on a radial grid between R = 3 a.u. and R = 11 a.u. have been published by Schaefer and Meyer (1979), who also give the coefficients of the long range (van der Waals) interaction. We shall refer to this potential as SM79. For each value of the intermolecular distance, Schaefer and Meyer carried out a CI calculation at six angular geometries. These are shown in Figure 4.1. The energy of the $\triangle$ "geometry" is defined as the difference between the interactions calculated for the trapezoidal and parallelogram geometries. By substituting the five resultant energies in equation (4.1), a set of five linearly independent algebraic equations result. These may be solved by matrix inversion to obtain the $A_{q_1 q_2 q_{12}}$. The CI calculations were performed with the intramolecular separations, r_1 and r_2, fixed at 1.449 a.u. This corresponds to the expectation value of r in the ground rovibrational state of the isolated monomer.

It should be pointed out that the basis set superposition error is not corrected for in the SM79 potential as this was found to yield better agreement with elastic

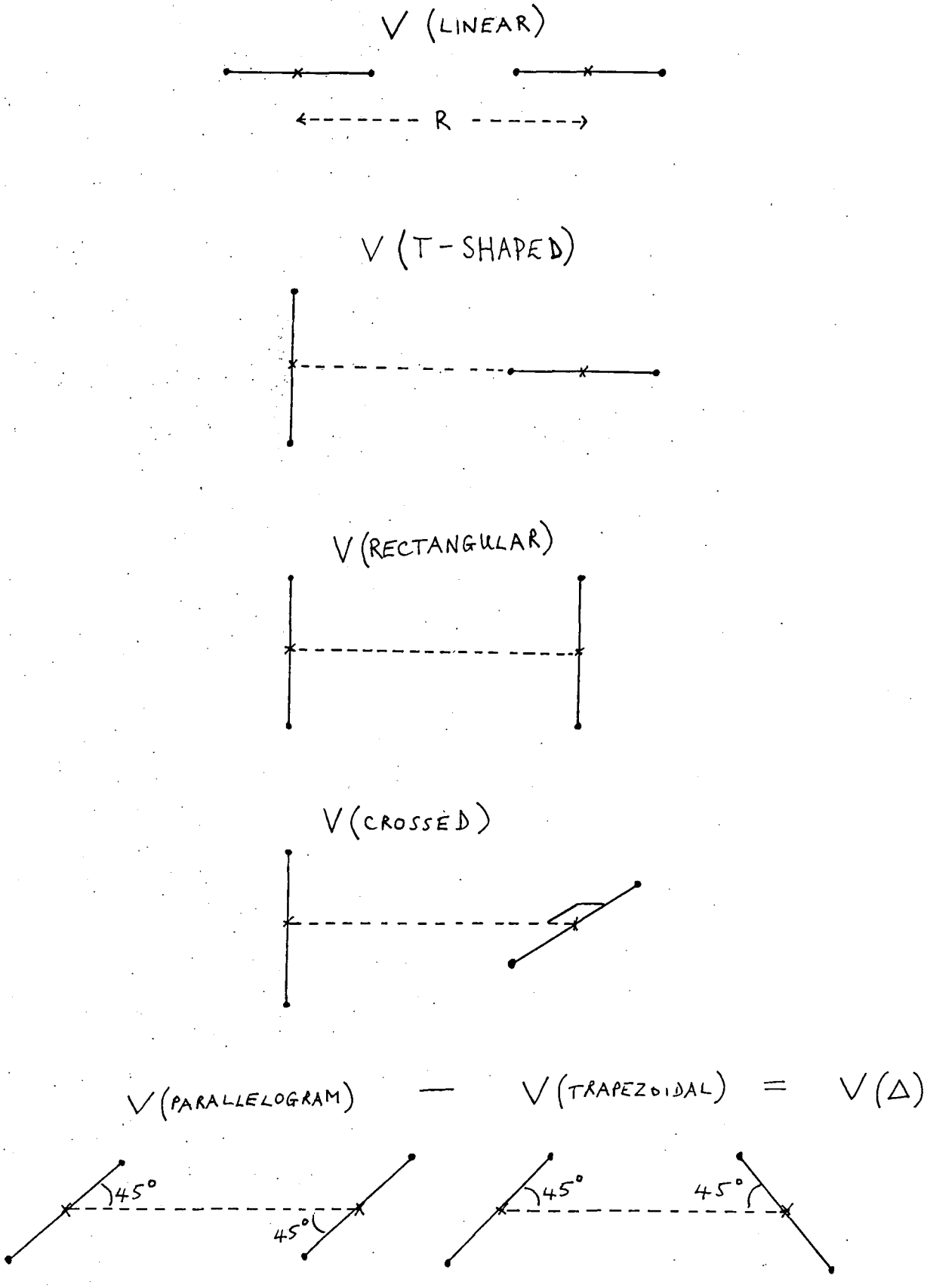

Figure 4.1

The angular geometries and corresponding interaction energies of H_2-H_2 referred to in the text. The interaction energy $V(\Delta)$ is needed to evaluate the V_{221} term in the body-fixed expansion (4.3).

scattering measurements (Schaefer and Meyer 1979).

For the SM79 potential at $R > 11$ a.u., the van der Waals coefficients of the asymptotic 1/R expansion are used. These were calculated using standard (Rayleigh-Schroedinger) perturbation theory, in which the true wavefunction is expanded as a sum of products of the wavefunctions of the isolated monomers. Details of the calculation, which used a large basis set, have been given by Meyer (1976).

From the SF potential expansion coefficients calculated by Schaefer and Meyer we have obtained the corresponding BF coefficients $V_{q_1q_2\mu}(R)$ which are plotted in Figure 4.2. The ab initio points are interpolated, as with all of the potential coefficients in this Chapter, using cubic spline polynomials (e.g. de Boor 1978). They are extrapolated for $R < 3$ a.u. by fitting $V_{q_1q_2\mu}(R)$ at R = 3 and 3.5 a.u. to the exponential form $a_{q_1q_2\mu}e^{-b_{q_1q_2\mu}}(R)$. This short range form has been shown to be appropriate (Green 1980, Ewing et al., 1978) and is a reflection of the exponential tails of the electron charge clouds.

The above CI calculations have been subsequently revised, for the same geometries and frozen bond length, by Meyer and Schaefer (1985). Furthermore, a finer radial grid was taken. The resulting potential has been termed M79 and is briefly discussed by Monchick and Schaefer (1980). It represents an improvement on the SM79 surface in that a larger electronic basis set is used to describe the molecular orbitals. Further-

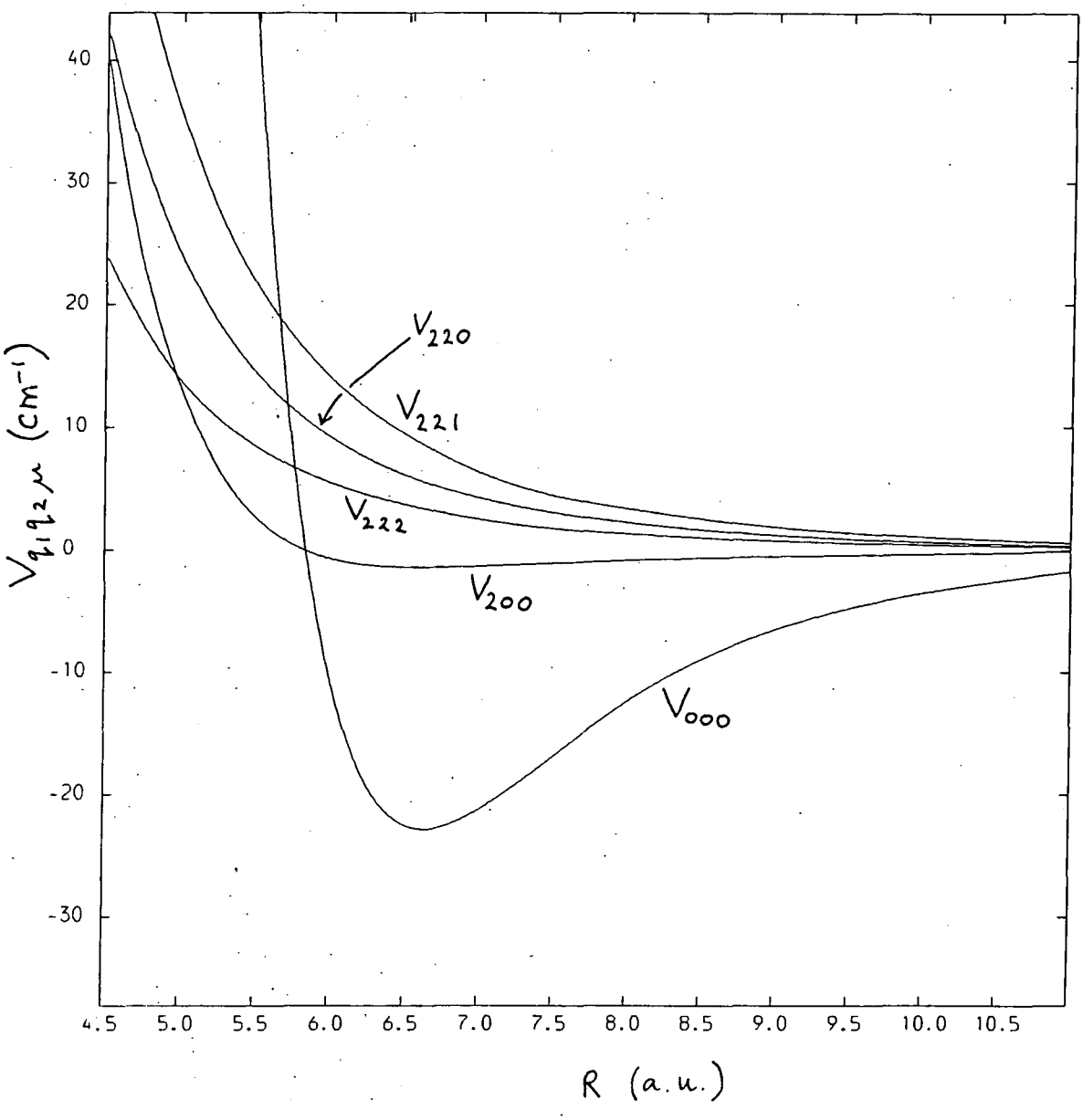

Figure 4.2

The variation with intermolecular centre-of-mass separation of the coefficients of the body-fixed expansion (cf. equation (4.3)) of the (SM79) interaction potential of Schaefer and Meyer (1979).

more,the basis set superposition error has been corrected for using the counterpoise method (Boys and Bernardi 1970). A large configuration expansion has been employed, including triple substitutions. The calculation of the dispersion interaction thus takes into account coupling between intra- and inter-molecular correlation (van der Avoird et al. 1980). The dispersion energy thus determined has been estimated to be accurate to within 5% at R = 6 a.u. (Buck et al. 1981). Further details of the potential calculation have yet to be published, though a related study on He - H_2 may be cited (Meyer et al. 1980).

The short range accuracy of the five potential expansion coefficients has been improved by Schaefer and Liu (1985). At R = 3 and 4 a.u., the CI calculations were extended to a total of 19 geometries, including those already calculated for M79. Using these additional geometries the five independent potential expansion coefficients were modified at short range. The resulting potential is termed M80. At larger R, the differences between the M79 and M80 coefficients were forced to vanish exponentially. The main result of these modifications, illustrated by Buck et al. (1983b), is that the V_{200} (or A_{202}) term is lower in the M80 potential by 16% at R = 4 a.u. The isotropic part of the potential, V_{000}, is changed by less than 1% at R = 4 a.u. The M79 and M80 potentials differ significantly only in the repulsive region. The effect on dimer bound states of these short range adjustments should be negligible.

Schaefer (1982a) has supplied us with M80 SF coefficients from R = 1.6 to 11 a.u., together with revised long range coefficients which are part theoretical (Meyer 1976, Thakkar 1977) and part numerical. The corresponding BF coefficients are plotted in Figure 4.3.

It is interesting to compare the SM79 coefficients in Figure 4.2 with the revised (M80) ones in Figure 4.3. Though the difference is small, the V_{000} term is more attractive in the SM79 potential from the minimum outwards. This is due to the basis set superposition error, which is present in the earlier calculation. Assuming that higher order terms in the potential expansion ($V_{q_1 q_2 \mu}$, q_1 or $q_2 > 2$) are negligable, then V_{200} may be associated, at large R, with the anisotropy of the dispersion interaction. This may be seen from the asymptotic forms of the BF coefficients (Flower et al. 1979, Mulder et al. 1979). The V_{200} term differs significantly for $R < 7$ a.u.; it is more negative ("softer") in the SM79 case.

The three remaining coefficients, V_{22n}, asymptotically represent the interaction between the permanent quadrupole moments of the H_2 molecules (Flower et al. 1979):

$$V_{220}(R) = \frac{6}{5}\langle H \rangle^2 R^{-5} \qquad (4.5a)$$

$$V_{221}(R) = \frac{4}{5}\langle H \rangle^2 R^{-5} \qquad (4.5b)$$

$$V_{222}(R) = \frac{1}{5}\langle H \rangle^2 R^{-5} \qquad (4.5c)$$

Indeed, Gallup (1977) has shown that, even in the region of the potential minimum, these terms may be largely described by the interaction between the quadrupole moments

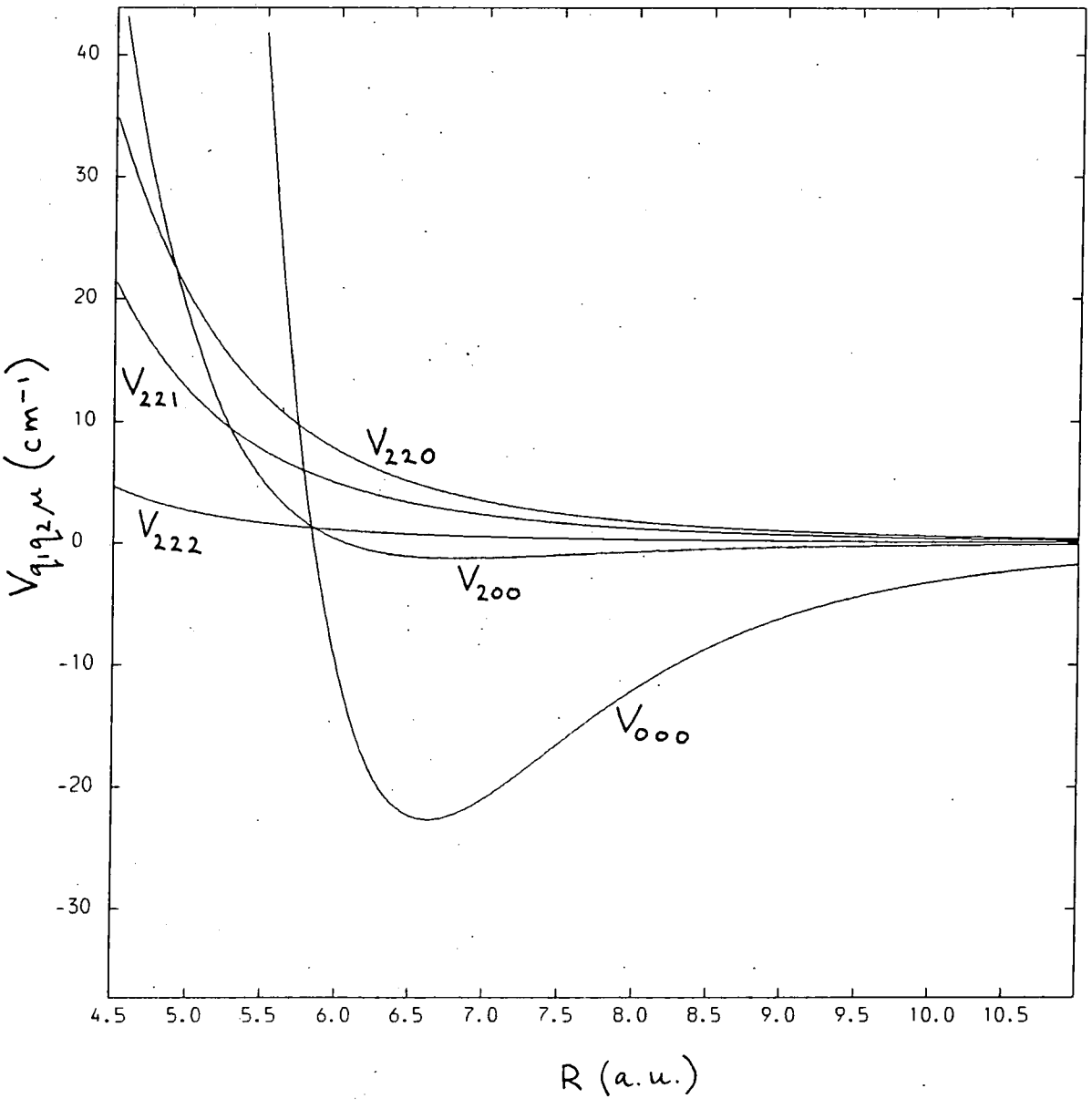

Figure 4.3

As Figure 4.2, for the M80 potential of Meyer and Schaefer (1985) and Schaefer and Liu (1985).

of the unperturbed monomers. There are large discrepancies between the V_{221} and V_{222} terms for the SM79 and M80 potentials; the former potential is incorrect asymptotically (see table 4.1). The ratio V_{220}: V_{221}: V_{222} should be 6:4:1 (equations (4.5)). At R = 11 a.u., the SM79 potential gives for this ratio 6 : 9.43 : 3.87 while the M80 behaves well with the ratio 6 : 4.00 : 0.94. Given that a relatively straightforward SCF calculation should be able to account for the interaction between permanent electrostatic moments, this discrepancy is difficult to understand. A plausible explanation is the absence of any correction for basis set superposition error in the SM79 calculation. This, as we shall see later, has a dramatic effect on the eigen-energies for ortho-H_2-ortho-H_2.

The results of CI calculations for the H_2 - H_2 system have also been reported by Burton and Senff (1982). In this paper it is claimed that the correlation energy was evaluated at two different levels of approximation, PNO-CI (Pair Natural Orbitals - Configuration Interaction) and CEPA2-PNO (Correlated Electron Pair Approximation version 2 - Pair Natural Orbitals). A description of these techniques may be found in the article by Kutzelnigg (1977a). The CEPA2 approximation includes higher-order correlation effects (quadrupole excitations) than the PNO-CI approximation, which is restricted to single and double substitutions with respect to the reference configuration. Burton (1982) expressed some preference for the CEPA2 results but noted that the magnitude of

	SM79	M80	Asymptotic
V_{220}	0.166(-5)	0.167(-5)	0.170(-5)
V_{221}	0.261(-5)	0.112(-5)	0.113(-5)
V_{222}	0.107(-5)	0.262(-6)	0.284(-6)

TABLE 4.1

Values of the potential expansion coefficients, V_{22n}(R = 11 a.u.) obtained from the SM79 and M80 ab initio calculations. Also quoted are the values obtained from the asymptotic formulae (4.5); the quadrupole moment of hydrogen was taken as 0.478 a.u. We note that the expressions given by Flower et al. (1979) are different to (4.5) due to a normalisation factor in their definition of $Y_{q_1 q_2 \mu}$. In this table, the expansion coefficients are in Hartree (1 Hartree = 219474.62 cm^{-1}). Notation : (-n) $\equiv$ x 10^{-n}.

the correlation energy may have been overestimated in the CEPA2 calculations. As we shall see below, this suspicion is confirmed by the present study of the molecular dimer. Subsequent to completion of the present calculations, the reason for this became apparent when Dr. P.G. Burton informed us that the potentials in Burton and Senff (1982) had been incorrectly designated PNO-CI and CEPA2. The correct designation is "renormalised IEPA" and "IEPA" respectively (Burton and Senff 1982, Burton 1983). This corrected designation will be used throughout the rest of this Chapter.

The Independent Electron Pair Approximation (IEPA) consists of approximating the total correlation energy as a sum of pair contributions. These are calculated independently by treating each pair in the field of the surrounding (uncorrelated) electron distribution. At intermediate and small intermolecular separations the electron pairs increasingly overlap, leading to an overestimation of the combined correlation energy (McWeeny and Pickup 1980). At very large intermolecular distances, the IEPA dispersion energy should approach that calculated by second order perturbation theory, the latter consisting also of a sum of contributions from independent electron pairs. Kutzelnigg (1977a,b) has discussed the IEPA method and its validity in some detail.

In their IEPA calculations, Burton and Senff (1982) used the same geometries as Meyer and Schaefer (Figure 4.1). They also fixed the H_2 internuclear distance at

the same value, 1.449 a.u. At each geometry, the calculated potential was shifted uniformly, by a small amount, to match the M80 potential of Meyer-Schaefer-Liu at R = 11 a.u. For R > 11 a.u. the accurate long range potential of Meyer (1976) may then be employed, as in the M80 surface.

Burton and Senff quote values for the SF coefficients, $A_{q_1 q_2 q_{12}}$. However, we chose to evaluate the BF coefficients, $V_{q_1 q_2 \mu}$, not from these, but directly from the potential; specifically, using table IV(b) and adding the shifts of table VI in Burton and Senff (1982). We did this for two reasons. The resulting BF coefficients are more accurate than the quoted SF ones, some of which are only given to one significant figure. In addition, the potential was calculated on a coarser radial grid for the two geometries contributing to the Δ energy (Figure 4.1). This contributes to the three SF coefficients A_{220}, A_{222} and A_{224} but only to one BF coefficient, V_{221}. The relation of this coefficient to the "potential of the Δ geometry" is given by

$$V_{221}(R) = \frac{2}{15}\left\{V_{\text{parallelogram}}(R) - V_{\text{trapezium}}(R)\right\} \equiv \frac{2}{15} V_{\Delta}(R) \qquad (4.6)$$

The cubic spline interpolation is thus more accurate for the IEPA potential represented by the BF expansion, the coefficients of which are plotted in Figure 4.4. The coefficients are extrapolated at R < 3 a.u. by exponential forms, fitted to the ab initio points at R = 3 and 3.5 a.u.

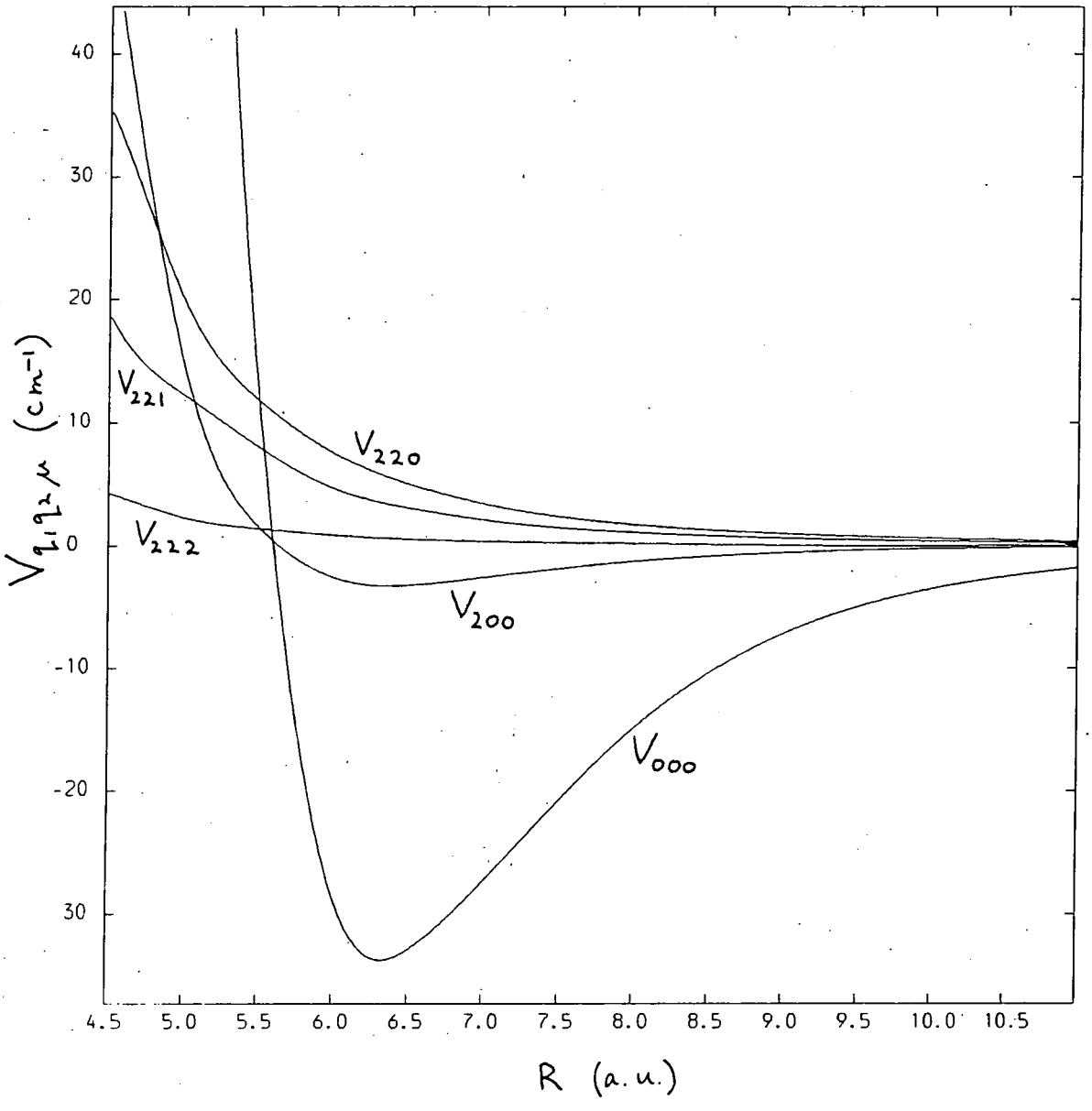

Figure 4.4

As Figure 4.2, for the IEPA potential of Burton and Senff (1982), referred to (incorrectly) in their paper as CEPA2.

The coefficients $V_{q_1 q_2 \mu}(R)$ for the fourth potential which we have employed (Kochanski 1975) are plotted in Figure 4.5. As noted above, this potential was calculated using a hybrid technique which entails a separate calculation of the intermolecular correlation energy by means of second order perturbation theory. The dispersion energy thus derived is added to the SCF energy to yield the total interaction potential, an approximate procedure whose validity should be assessed by comparison with experiment (see below).

In basic (Rayleigh – Schroedinger) perturbation theory the Hartree-Fock dispersion energy may be written, to second order, as

$$E_{disp}^{HF} = \sum_{i\neq o} \sum_{j\neq o} |\langle A_o B_o | V_{AB} | A_i B_j \rangle|^2 / (2E_o - E_i - E_j) \quad (4.7)$$

where V_{AB} is the intermolecular electronic Hamiltonian and $A_o(B_o)$ is the Hartree-Fock determinant for the ground electronic state of the isolated H_2 molecule 1(2). The wavefunction $A_i(B_j)$ is obtained by replacing one of the orbitals of $A_o(B_o)$ with an orbital corresponding to an excited state i(j). E_o, E_i and E_j are the corresponding eigenenergies of these Hartree-Fock wave functions. The approach of Kochanski (1973, 1975) differs from this simplified treatment in two ways. The ground state configuration is constructed from a fully antisymmetrized product of the individual molecular Hartree-Fock wavefunctions. In other words, $A_o B_o$ is replaced by $\mathcal{A} A_o B_o$, where the latter has the correct symmetry under interchange of electrons belonging to <u>different</u> H_2 molecules. In

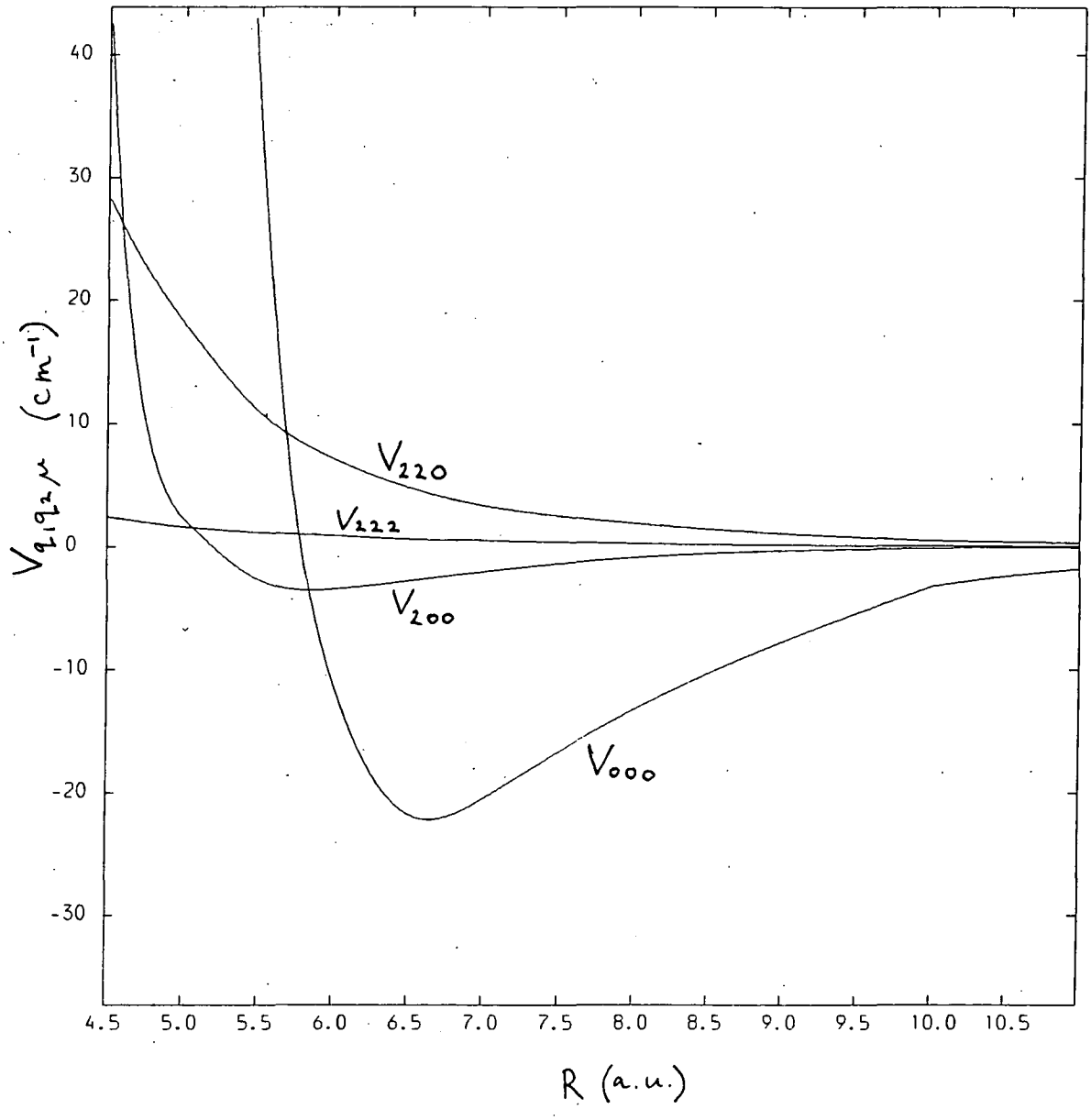

Figure 4.5

As Figure 4.2, for the Kochanski (1975) potential.

addition, an energy denominator different from the one in (4.7) is used. This corresponds to changing the partitioning of the total electronic Hamiltonian (Kutzelnigg 1977a, 1977b).

This method of calculating the dispersion energy makes three assumptions. The effect of intramolecular correlation on intermolecular correlation is neglected. Third and higher order terms in the perturbation series are ignored, though the modifications to the second order approximation introduced by Kochanski should minimise their importance. Finally, overlap between the molecular orbitals of the interacting molecules, which can lead to a decrease in the dispersion energy, is neglected.

An initial evaluation of the BF coefficients $V_{q_1 q_2 \mu}$ revealed a bump in the V_{222} term at R = 6 a.u. Kochanski (1983) subsequently informed us of an error in Table 1 of her paper (Kochanski 1975). The Hartree-Fock dispersion energy, E_{disp}^{HF}, for the rectangular geometry at an intermolecular separation of 6 a.u. should read -2.771 and not -2.671 (units in 10^{-4} Hartree). The corresponding total energy, E_{TOT}, should therefore read 0.396.

The intramolecular separation was fixed at r = 1.4 a.u. (Jaszunski et al. 1977), corresponding to the position of the minimum of the H-H interatomic potential. The rigid rotor approximation, in its simplest form, assumes that the intermolecular potential is insensitive to small changes in the intramolecular bond length. Indeed, we shall assume this to be true for the less favourable

case in which vibrational excitation of one of the monomers takes place. Nevertheless, this difference, compared with the other three ab initio potentials in our study, should be noted.

Kochanski's calculations were performed for the first four geometries of Figure 4.1. The V_{221} coefficient, as seen in equation (4.6), is not calculable from these geometries. Cubic spline interpolation of $V_{q_1 q_2 \mu}$ is used in the range of the ab initio points, 5-10 a.u. For $R > 10$ a.u., $V_{q_1 q_2 \mu}$ is fitted at $R = 10$ a.u. to the form $C_{q_1 q_2 \mu}/R^n$; the integer n is chosen to represent the correct asymptotic behaviour (Flower et al. 1979). For $R < 5$ a.u. simple exponential forms are again used, fitted to $V_{q_1 q_2 \mu}$ at the grid point $R = 5$ a.u. and the spline interpolated point $R = 5.05$ a.u.

4.3 Eigenenergies of the H_2-H_2 dimer

The problem of calculating eigenenergies of molecular dimers has been formulated earlier in this thesis, and the numerical methods employed to solve the problem have been described. In the present chapter, we shall consider the results obtained for the H_2 - H_2 dimer by means of both the R-matrix propagator and de Vogelaere algorithms.

Before comparing results derived from the four different intermolecular potentials to which reference has been made in Section 4.2, we shall briefly report our studies of the convergence properties of the algorithms which we have used. We shall also consider the convergence of the eigenvalues with respect to basis set size. Results

will be illustrated for the Meyer-Schaefer-Liu (M80) potential.

4.3.1 Convergence with respect to numerical integration parameters - de Vogelaere algorithm.

In this version of the computer programme, the wavefunctions and their derivatives are propagated, starting in the right- and left-hand classically forbidden regions, and matched near the minimum of the potential well. Numerical integration must start sufficiently far into the classically forbidden regions for the initial values of the wavefunctions to be negligibly small.

At short range, the interaction potential becomes exponentially repulsive, and the computed eigenenergies converge rapidly with respect to the inner starting point, R_{min}; this convergence is illustrated in table 4.2 for para-H_2 - para-H_2. Results accurate to four decimal places are obtained with R_{min} = 3.7 a.u.

A satisfactory value of the outer starting point, R_{max}, is more difficult to establish. At long range, there is a van der Waals tail in the potential which varies as an inverse power series in R and results in slower decay of the wavefunctions with respect to penetration into the outer classically forbidden region. As the integration range is extended, the number of integration steps per "half-range", N, must be increased to maintain numerical accuracy. The convergence of the eigenenergies with respect to these two parameters, R_{max} and N, is illustrated in table 4.3 for para-H_2 - para-H_2.

R_{min}	J = 0	J = 1
4.0	-2.41064	-0.95930
3.7	-2.41130	-0.95981
3.5	-2.41132	-0.95983
3.3	-2.41132	-0.95983

TABLE 4.2

Convergence of the computed eigenenergies of the para-H_2 - para-H_2 system with respect to the value of the inner starting point R_{min} (Bohr) of the de Vogelaere integration. The basis set consists of one rotational state (j = 0) on each H_2 molecule. The number of integration points per half-range N = 100. Energies are in cm^{-1}, relative to the dissociation energy (taken as zero throughout this chapter).

	R_{max}					
N	27	40	50	60	70	80
100	-2.40685 (-0.94005)	-2.41117 (-0.95917)	-2.41132 (-0.95983)	-2.41148 (-0.95998)		
200	-2.40685 (-0.94005)	-2.41124 (-0.95921)	-2.41124 (-0.95974)	-2.41126 (-0.95978)		
300			-2.41126 (-0.95974)	-2.41126 (-0.95978)	-2.41124 (-0.95978)	-2.41124 (-0.95978)
400						-2.41126 (-0.95978)

TABLE 4.3

Variation of the computed eigenenergies E_J of the para-H_2 - para-H_2 system with the values of the outer starting point, R_{max} (Bohr), of the de Vogelaere integration and with the number of integration points per half-range, N. The upper entries refer to J = 0, the lower entries to J = 1. The basis set employed consists of a single rotational state (j = 0) for each H_2 molecule. The energies are in units of cm^{-1}.

Results accurate to four decimal places are obtained with R_{max} = 50 a.u. and N = 200.

In the de Vogelaere method the (radial) wavefunction vanishes at the starting points of the integration. This is equivalent to placing infinite walls in the potential at R_{min} and R_{max}. Tables 4.2 and 4.3 show that as these walls move apart, the eigenenergy decreases, in line with elementary quantum mechanical arguments based on the infinite square well potential. This interpretation is aided both by the relative weakness of the H_2 - H_2 interaction and by the fact that the calculations in tables 4.2 and 4.3 are for a single (isotropic) radial Schroedinger equation.

4.3.2 Convergence with respect to numerical integration parameters - R-matrix propagator method.

As noted in Chapter 3, propagation of the R matrix, rather than both the wavefunction and its derivative, leads to greater numerical stability and to a more rapid convergence of the eigenvalues with respect to penetration into the classically forbidden regions. In particular, much smaller values of R_{max} are necessary to obtain convergence in the right-hand classically forbidden region. However, as R-matrix propagation involves local approximations to the potential, more integration steps are required than in the equivalent de Vogelaere calculation (compare tables 4.3 and 4.4).

These convergence tests are for para-H_2 - para-H_2 with H_2 restricted to its ground rotational state, and are hence uncomplicated by angular coupling. We are

N	R_{max}	
	27	40
100	-2.41161 (-0.96022)	
200	-2.41135 (-0.95981)	
300	-2.41130 (-0.95972)	-2.41152 (-0.96009)
400	-2.41128 (-0.95970)	-2.41141 (-0.95996)

TABLE 4.4

As Table 4.3, but obtained using the R-matrix propagator method.

thus able to note that the eigenvalues calculated using the R-matrix propagator method are lower than those using de Vogelaere, for fixed R_{max}, because of the effect of the infinite wall boundary conditions of the latter algorithm. Compare, for example, the eigenenergies at N = 200, R_{max} = 27 a.u. in table 4.3 with the values for N = 400, R_{max} = 27 a.u. in table 4.4.

Analogous tests, using the M80 potential, were carried out for the ortho-H_2 - para-H_2 and ortho-H_2 - ortho-H_2 systems. Similar conclusions regarding the accuracy of the eigenenergies were drawn. All results using the M80 potential, in this chapter, are accurate to three decimal places. There may be a small error in the third decimal place for results using the potentials of figures 4.2, 4.4 and 4.5 for which less detailed convergence tests were performed.

4.3.3 Convergence with respect to basis set size

Calculations have been carried out using one, two and three rotational basis functions on each H_2 molecule, i.e. a maximum of j = 0,2,4 for para-H_2 and j = 1,3,5 for ortho-H_2. A representative sample of the results obtained, using the R-matrix propagator method, is presented in table 4.5.

The H_2 molecule is light and has a large rotational constant (following Verberne and Reuss (1981), we take the reduced mass μ = 1837.14 a.u. and the rotational constant in the ground vibrational state B_o = 59.341 cm^{-1}), and we expect that the correspondingly rapid motion will

	J^{ε}	1	2	3
p-p	0^+	-2.41135	-2.43018	-2.43018
	1^-	-0.95981	-0.97471	-0.97471
o-p	0^+	-1.25177	-1.27627	-1.27629
o-o	0^+	-2.47477	-2.49692	-2.49694
	0^-	-0.66455	-0.66896	-0.66896

TABLE 4.5

Eigenenergies, in units of cm^{-1}, of states J of para-H_2 - para-H_2, ortho-H_2 - para-H_2 and ortho-H_2 - ortho-H_2; J is the total angular momentum and ε the parity of the state. The R-matrix propagator method was used. Columns 1, 2 and 3 contain results obtained with one, two and three rotational states, respectively, on each H_2 molecule.

not be greatly hindered by the weakly anisotropic H_2-H_2 interaction. The results in table 4.5, which illustrate the rapid convergence of the eigenvalues with respect to the size of the H_2 rotational basis set, confirm this expectation.

Inspection of the matrix elements of the potential between angular basis states (equation (2.29)) shows that terms in the potential expansion (4.3) with q_1 and/or $q_2 = 4$ are required to change the H_2 angular momentum by four units. There is thus no direct coupling of the bound states with states involving hydrogen molecules with $j = 4$ or 5. The similarity of columns 2 and 3 of table 4.5 reflects the weakness of indirect coupling via the $j = 2$ or 3 states of H_2. We conclude that $j = 0,2$ for para-H_2 and $j = 1, 3$ for ortho-H_2 are sufficient. When advantage is taken of the interchange symmetry of identical molecules, to be discussed in the next section, this basis set leads to a maximum of 26 coupled equations.

An interesting aside concerns the use of the reduced atomic mass, in line with Verberne and Reuss (1981), rather than the reduced nuclear mass, which is consistent with the Born-Oppenheimer approximation (Le Roy 1971). Bunker (1979a, page 201) has suggested that more accurate answers may be obtained by using the reduced atomic mass as this allows for the mass of the electrons and partly compensates for the breakdown of the Born-Oppenheimer approximation. In support of this he cites the work of Oka and Morino (1961) who studied the effect of electrons on the moment of inertia of molecules.

4.3.4 Comparison with the calculations of Verberne and Reuss

Verberne and Reuss (1980, 1981) have calculated the hydrogen dimer spectrum by solving a secular equation, i.e. by diagonalising a suitable representation of the total Hamiltonian matrix. The intermolecular vibrational basis functions were solutions of the Schroedinger equation:

$$\left\{-\frac{1}{2\mu}\frac{d^2}{dR^2} + \frac{l(l+1)}{2\mu R^2} + V_{000}(R) - E(n,l)\right\}\psi_{n,l}(R) = 0 \qquad (4.8)$$

where l is the end-over-end rotational quantum number and $V_{000}(R)$ the isotropic part of the intermolecular potential. This numerically generated basis set is truncated after the first term; $(n,l) = (0,0)$ or $(0,1)$ depending on the dimer states in question. Refer to the discussion in Section 3.5.3, especially following equation (3.44). As noted by Verberne and Reuss (1981), states with $l > 1$ are dissociative. The angular basis set includes these higher l values, where allowed by the coupling of the angular momenta of the H_2 molecules.

Verberne and Reuss (1981) employ a rotational basis consisting of a single eigenfunction on each H_2 molecule ($j = 0$ for para-H_2, $j = 1$ for ortho-H_2). They also consider the hyperfine structure of the dimer, but this will not concern us here. It is sufficient to say that their experimental measurements of the hyperfine spectra (Verberne and Reuss 1980) yield quantitative information on the leading anisotropic component of the potential $V_{200}(R)$. Their conclusions will be briefly discussed later.

They employed the M79 potential of Meyer and Schaefer (1985). In the region of the potential between the classical turning points, which determines the bound states, the M79 surface is almost indistinguishable from the M80 potential of Meyer-Schaefer-Liu (Verberne and Reuss 1981).

As the para-para (p-p) and ortho-ortho(0-0) systems consist of identical bosons, the total wavefunction must be symmetric under exchange of the constituent molecules. When the hydrogen molecules are both in their ground rotational states, this leads to the requirement that $(-1)^{j_{12}} + \ell + I_{12} = +1$ where $\underset{\sim}{j}_{12} = \underset{\sim}{j}_1 + \underset{\sim}{j}_2$ and $\underset{\sim}{I}_{12} = \underset{\sim}{I}_1 + \underset{\sim}{I}_2$ (cf. equation (2.33)). For the 0-0 system, this requirement leads to a separation of the total Hamiltonian matrix into two blocks, corresponding to $I_{12} = 0,2$ and $I_{12} = 1$ (i.e. symmetric and asymmetric functions, respectively, of the nuclear spin coordinates). As shown in Chapter 2, a corresponding advantage accrues from exploiting this symmetry property when solving coupled differential equations; the equations separate into blocks of a given interchange symmetry (cf. table 2.1).

In Table 4.6, we compare the dimer spectrum computed by Verberne and Reuss (1980, 1981) with the results of our own calculations, with one and two rotational states per H_2 molecule. Our two-rotor state results for the o-p and 0-0 systems are plotted in Figure 4.6. Also shown are the pure ℓ states to which they correlate in the isotropic limit. These levels correspond to the one-rotor state calculations on para-H_2 - para-H_2. The

System	J	ε	i	Verberne and Reuss	One-rotor	Two-rotor
p-p	0	1	1	-2.40	-2.41	-2.43
p-p	1	-1	-1	-0.953	-0.960	-0.975
o-p	1	-1		-2.42	-2.43	-2.45
o-p	0	1		-1.30	-1.25	-1.28
o-p	1	1		-0.778	-0.822	-0.836
o-p	2	1		-0.998	-0.996	-1.01
o-o	0	1	1	-2.47	-2.47	-2.50
o-o	1	1	-1	-2.42	-2.41	-2.43
o-o	2	1	1	-2.54	-2.55	-2.56
o-o	0	-1	1	-0.573	-0.665	-0.669
o-o	1	-1	1	-1.14	-1.10	-1.12
o-o	1	-1	-1	-1.50	-1.49	-1.51
o-o	1	-1	-1	-0.875	-0.918	-0.932
o-o	2	-1	1	-0.921	-0.929	-0.941
o-o	2	-1	-1	-0.798	-0.854	-0.862
o-o	3	-1	-1	-1.10	-1.10	-1.11

TABLE 4.6

Comparison of our own calculations of the hydrogen dimer spectrum with those of Verberne and Reuss (1980, 1981). The states are denoted by the total angular momentum, J, the parity, ε, and the molecular interchange symmetry, i (where applicable). In the one-rotor calculations, only the j = 0 (j = 1) state is retained for para-(ortho-) H_2, whereas j = 0, 2 (j = 1, 3) are retained in the two-rotor calculations. The eigenenergies are in units of cm^{-1}. As noted in the text, the p-p J = 1 state does not occur in nature.

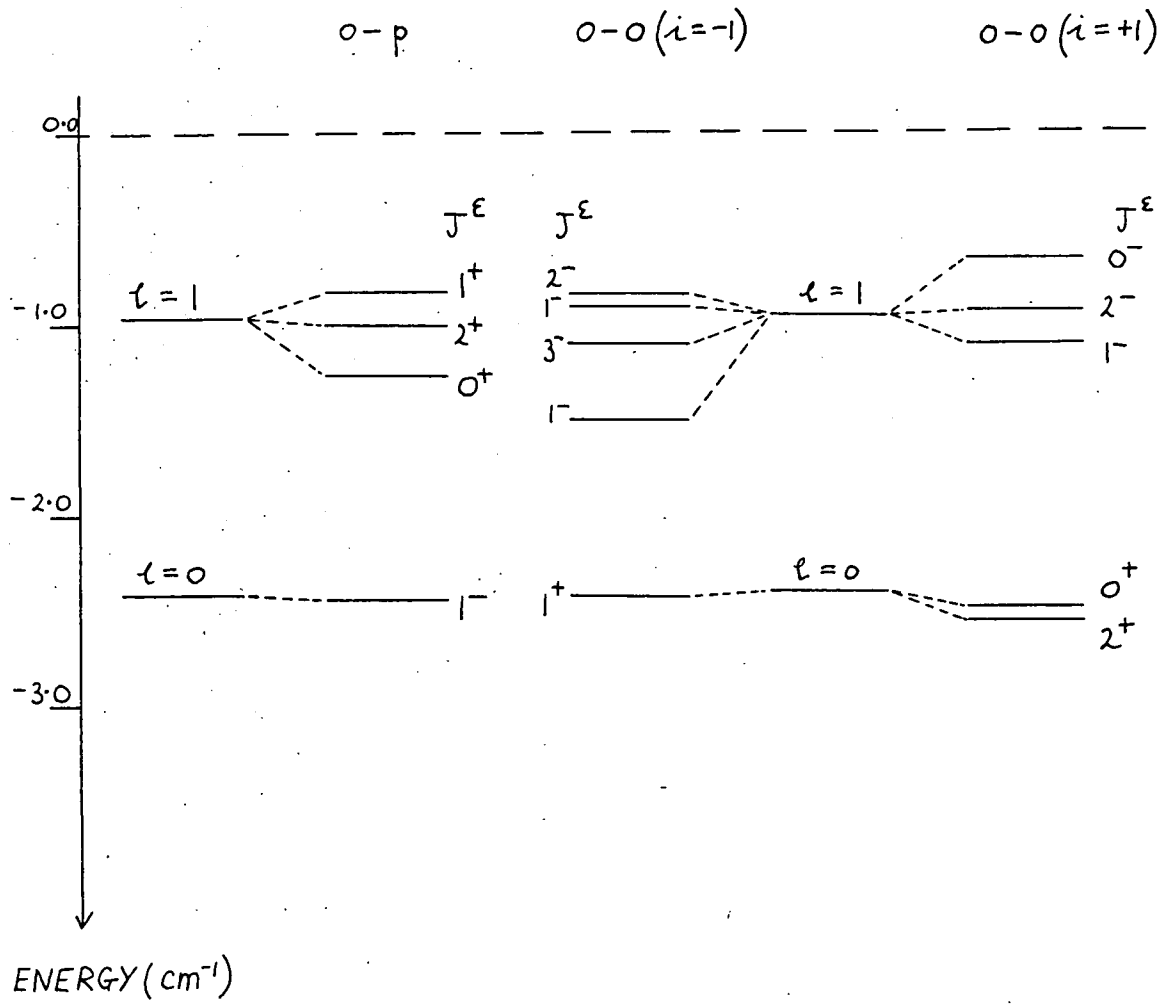

Figure 4.6

The bound states of ortho-H_2-para-H_2 and ortho-H_2-ortho-H_2 using the M80 potential of Meyer, Schaefer and Liu (Figure 4.3). The results were obtained with two rotational states on each H_2. Also shown are the one-rotor state para-H_2-para-H_2 eigenvalues, for which l is good, to which they correlate when the potential anisotropy is "switched off".

levels are designated by the values of the total angular momentum, J, the total parity, $\mathcal{E} = (-1)^{j1 + j2 + \ell}$, and the interchange symmetry, $i = (-1)^{j12 + \ell}$. We note that the level J = 1, $\mathcal{E}$ = -1, i= -1 in the p-p system, where $I_{12} = 0$, does not occur in nature owing to the requirement that $(-1)^{j12 + \ell + I12} = +1$ (see above).

The calculations of Verberne and Reuss are seen to be in better agreement with our single- than our double-rotational state results; this was to be expected, as Verberne and Reuss neglect all H_2 states higher than j = 0 or j = 1. The overall agreement between results obtained by solving the secular equation and by numerical integration of the coupled differential equations is satisfactory. Verberne and Reuss truncated the vibrational basis set, defined as the solutions of equation (4.8), after one term. This procedure is satisfactory owing to the weak anisotropy of the H_2-H_2 potential and the large value of the H_2 rotational constant.

4.3.5 Comparison of results obtained using four different H_2-H_2 ab initio potentials.

In Table 4.7, we compare the results of calculations, using the R-matrix propagator method, based upon the four ab initio potentials discussed in Section 4.2 above. As pointed out there, the V_{221} potential coefficient may not be derived from the results of Kochanski (1975), as she considered an insufficient number of interaction geometries. As a consequence, we do not present results obtained with her potential for the 0-0 system, the

SYSTEM	J	ε	i	1	2	3	4
p-p	0	1	1	-2.430	-6.218	-3.008	-2.732
p-p	1	-1	-1	-0.975	-4.316	-1.486	-1.235
o-p	1	-1		-2.447	-6.341	-3.065	-2.776
o-p	0	1		-1.276	-5.409	-2.099	-1.704
o-p	1	1		-0.836	-3.799	-1.215	-1.035
o-p	2	1		-1.013	-4.494	-1.575	-1.307
o-o	0	1	1	-2.497	-6.559		-3.785
o-o	1	1	-1	-2.431	-6.315		-2.486
o-o	2	1	1	-2.561	-6.632		-3.359
o-o	0	-1	1	-0.669	-3.122		
o-o	1	-1	1	-1.120	-4.903		
o-o	1	-1	-1	-1.505	-5.861		
o-o	1	-1	-1	-0.931	-4.178		
o-o	2	-1	1	-0.941	-4.249		
o-o	2	-1	-1	-0.862	-3.901		
o-o	3	-1	-1	-1.111	-4.771		

TABLE 4.7

Eigenenergies of the H_2-H_2 dimer, in units of cm^{-1}, as derived from the potentials of : 1, Meyer, Schaefer and Liu (M80); 2, Burton and Senff (1982); 3, Kochanski (1975); 4, Schaefer and Meyer (SM79). In these calculations, two rotational states (j = 0,2 or j = 1,3) were retained on each H_2 molecule. Results are quoted to the numerical precision of the R-matrix propagator method.

Note: There is a printing error in the corresponding Table (6) of Danby and Flower (1983). The eigenenergy for the M80 potential for o-o, $J^{\varepsilon i} = 1^{--}$ should read 6.857 rather than 6.867 (units $-x10^{-6}$ Hartree). 1 Hartree = 219474.62 cm^{-1}.

V_{221} coefficient intervening directly in these calculations.

In Section 4.2 we expressed reservations concerning the accuracy of the quadrupole-quadrupole terms, V_{22n}, for the SM79 potential of Schaefer and Meyer (1979). We quote results for the p-p and o-p systems, for which these terms intervene only through coupling to energetically distant excited rotational states of the H_2 molecules. The three lowest eigenenergies, correlating to $\ell = 0$, for the o-o system are given as an illustration of a situation where the V_{22n} terms appear in the diagonal elements of the coupling matrix. We immediately see that the relative order of these states differs from that obtained with the Meyer-Schaefer-Liu M80 and Burton-Senff potentials. Specifically, the $J^{\varepsilon i} = 0^{++}$ and 2^{++} levels are interchanged. For the SM79 potential, the V_{221} coefficient is the largest anisotropic term. In Figure 4.7 we demonstrate the effect on the eigenvalues of multiplying V_{221} by a constant, ANIS. Both the absolute values and relative ordering of the three $\ell = 0$ states are seen to be highly sensitive to the potential anisotropy. Similar calculations with the V_{220} and V_{222} terms showed that the ordering was unaltered over a range $0.0 < \text{ANIS} < 1.3$. The eigenenergies were also less sensitive to these terms. We conclude that a consistent ordering of the levels is obtained for values of ANIS between 0.67 and 0.8. V_{221} thus needs to be reduced in the SM79 potential, in line, qualitatively, with the results of the M80 and Burton-Senff potentials.

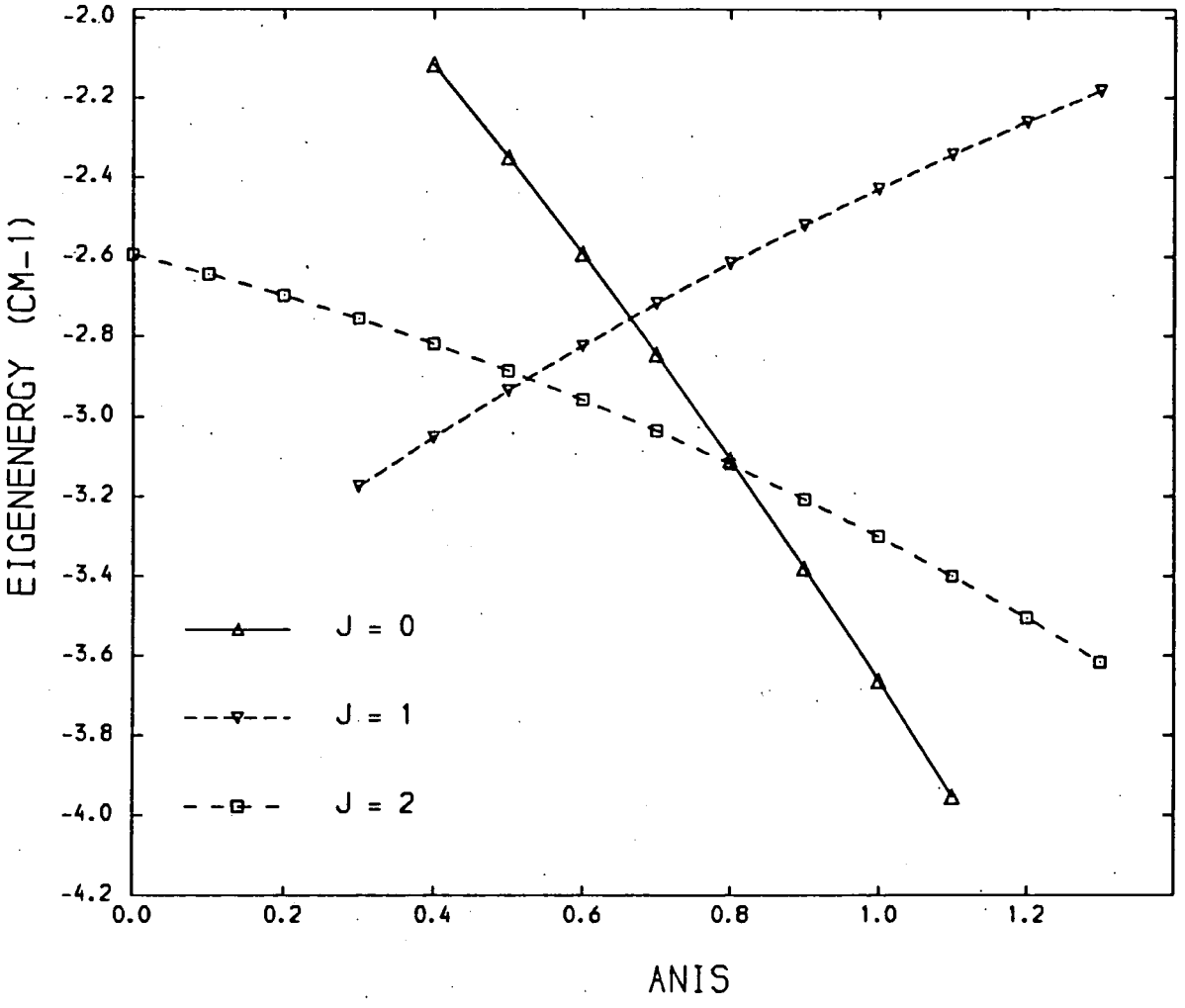

Figure 4.7

The effect of scaling the V_{221} term in the SM79 potential by a constant (ANIS) on the bound states of H_2-H_2. The bound states shown are the three ℓ = 0 levels of the ortho-ortho modification. These calculations were performed with only one rotational state (j = 1) per H_2; the results differ from the corresponding two rotor state runs by 2-3% for ANIS = 1.

Taking Table 4.7 as a whole, the salient feature is the relatively good agreement between the results of calculations based on the Meyer-Schaefer-Liu (M80) and Kochanski potentials. Results for the published potential of Schaefer and Meyer (SM79) lie in between, notwithstanding the qualifications concerning the V_{22n} terms. The eigenvalues calculated with the Burton-Senff potential are much larger in absolute magnitude, though the relative ordering of all the states agrees with the M80 calculations. The Burton-Senff potential predicts an additional bound level of the p-p system ($J = 2$, $\mathcal{E} = 1$, $i = 1$) at an energy of $-0.771\ cm^{-1}$, which is not observed. These points will be discussed further in the following section.

4.3.6 Comparison with spectroscopic measurements

McKellar and Welsh (1974) have observed absorption spectra in H_2-H_2 which comprise transitions within the fundamental band ($v'' = 0 \rightarrow v' = 1$) of H_2 accompanied by end-over-end rotational transitions of the H_2-H_2 dimer. The transitions are attributable to the induced dipole of the H_2-H_2 molecule (Poll and van Kranendonk 1961, Watanabe and Welsh 1964) and fall in the near infrared part of the spectrum.

In the final (upper) state of the transition, the vibrational states of the two H_2 molecules differ. It follows from the form of the interchange symmetrized vibrotor basis states (2.51) that there is no restriction on ℓ', the end-over-end rotational quantum number, even in the p-p system. To show this, we note that for two

para-H_2 molecules in their lowest rotational states, $j_1 = j_2 = j_{12} = \bar{\Omega} = 0$. The electronic states of the H_2 molecules are symmetric ($^1\Sigma_g^+$) and the resultant nuclear spin, $I_{12} = 0$, also gives a symmetric contribution to the overall wavefunction. We may thus write the basis states, (2.51), in the abbreviated form

$$\phi \propto \phi(v_1 v_2) + \varepsilon \phi(v_2 v_1) \qquad (4.9)$$

where normalisation factors have been ignored and the (spatial) interchange symmetry $i = {}^+1$ for the two boson monomers. The parity $\varepsilon = (-)^{\ell}$ and for the upper state of the fundamental band with $j_1 = j_2 = 0$, $v_1 = 1$ and $v_2 = 0$. Thus,

$$\phi \propto \phi(1\,0) + (-)^{\ell} \phi(0\,1) \qquad (4.10)$$

which is non-zero for both odd and even ℓ. It is less rigorous, though convenient, to regard the monomers as being distinguishable when their internal states differ. This is fully consistent with the results of Section 2.5.

We note that transitions involving $\ell', \ell'' = 0,1$ were observed to be sharp, whereas, for $\ell', \ell'' > 1$, the lines were broader than the resolution of 0.15 cm^{-1}. The evident conclusion, drawn by McKellar and Welsh (1974), is that states with $\ell > 1$ are pseudo-bound (i.e. bound only by the centrifugal barrier in the effective intermolecular potential). This observation conflicts with the prediction of a state with $\ell = 2$ by the Burton-Senff potential, as mentioned in the preceding section.

In order to make as direct a comparison as possible with the calculations reported in Section 4.3.5, let us consider the Q branches of the observed transitions, in which no change occurs in the rotational states of the H_2 molecules. Such a transition is $Q_1(o)$ $l'' = 0 \longrightarrow l' = 1$, the subscript 1 denoting the fundamental band ($\Delta V = 1$) and the 0 in brackets the initial (and for Q transitions the final) rotational state of one of the interacting H_2 molecules. The other H_2 molecule does not undergo any transition; this "null" transition may be denoted $Q_0(0)$. Using similar notation for the accompanying l transition of the dimer, this line is referred to as the R(0) component of the $Q_1(0)$ branch (Le Roy and van Kranendonk 1974). The observed frequency may be expressed in the form (McKellar and Welsh 1974)

$$\nu_R = \nu_{H_2} + \nu(l' - l'') \qquad (4.11)$$

In the absence of perturbations from surrounding molecules, ν_{H_2} is the vibrational frequency of an isolated H_2 molecule, $\nu^f_{H_2}$. If the interaction potential is assumed to be the same in the initial and final states, the experiment yields the separation of the $l = 0$ and $l = 1$ levels directly. This assumption has been applied to the N_2-N_2 dimer by Tennyson and van der Avoird (1982a) and Brocks and van der Avoird (1985). H_2-H_2 is a less favourable case because of the larger amplitude of vibration of the lighter H_2 molecules.

An estimate of the perturbed H_2 vibrational frequency,

ν_{H_2}, may be obtained from the mean value of the observed frequencies of the R(0) ($\ell'' = 0 \rightarrow \ell' = 1$) and P(1) ($\ell'' = 1 \rightarrow \ell' = 0$) components of the $Q_1(1)$ branch, see Figure 4.8. The P(1) line is of course absent in the $Q_1(0)$ spectrum because of the symmetry restrictions discussed in Section 4.3.4. McKellar and Welsh (1974) thus obtained values of 1.74 cm^{-1} and 1.62 cm^{-1} for the $\ell = 0 - 1$ energy separation, from observations of the $Q_1(0)$ and $Q_1(1)$ branches respectively. As the spectral resolution of their experiment in the region of the H_2 fundamental band ($2.0 < \lambda < 2.4\,\mu m$) was 0.15 cm^{-1}, we shall adopt a mean value of 1.68 cm^{-1} for the $\ell = 0 - 1$ energy difference.

The value of the vibrational frequency shift, $\nu_{H_2} - \nu^f_{H_2}$, deduced from the $Q_1(1)$ spectrum, was - 0.35 cm^{-1}. Its origin lies in perturbations on the vibrational motion of an H_2 monomer due to its interaction, $V(\underset{\sim}{r}_1, \underset{\sim}{r}_2, R)$, with a neighbouring molecule. The additional restoring force contributing to the vibration of monomer 1 is $-\partial V/\partial r_1$. For the low temperatures ($\sim$ 17K) of the McKellar and Welsh (1974) experiment, the attractive region of the intermolecular potential is dominant. The dispersion interaction between H_2 molecules increases with r due to an increase in the polarisability of H_2 (Le Roy et al. 1977, Ishiguro et al. 1952). Thus $-\partial V/\partial r_1$ is positive, leading to a reduction in the restoring force and hence a negative frequency shift (May et al. 1961, 1964).

In Table 4.8, we list the frequencies of the optically allowed transitions, as deduced from the eigenenergies

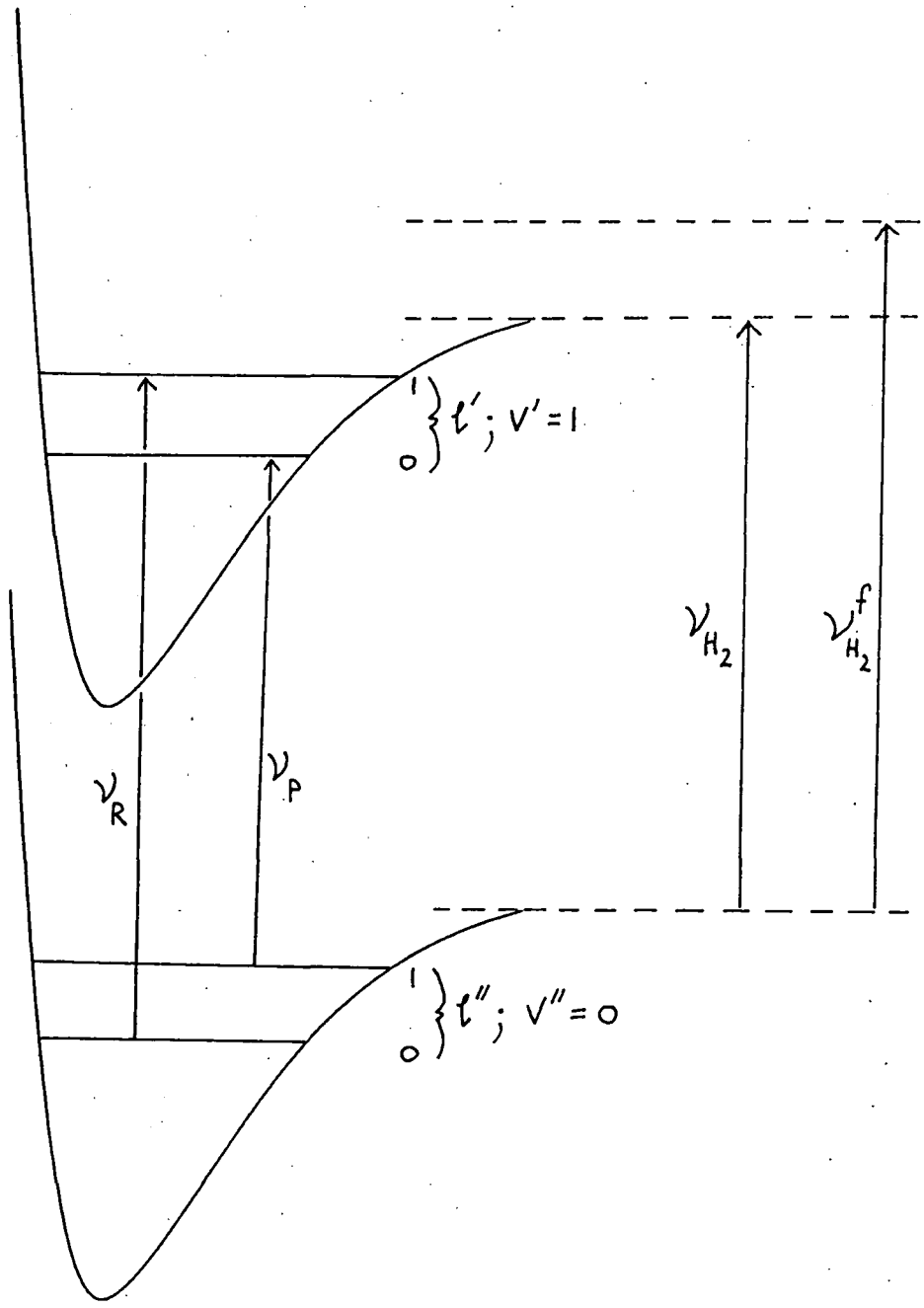

Figure 4.8

Experimental R(0) and P(1) components of the $Q_1(1)$ branch, schematically represented. $\nu_{H_2}{}^f$ is the frequency of excitation of a free H_2 molecule from V = 0 to V = 1 (4155.26 cm^{-1}). An estimate of the ℓ = 0 - 1 separation is given by $(\nu_R - \nu_p)/2$. The vibrational frequency shift, $\nu_{H_2} - \nu_{H_2}{}^f$, is approximated by replacing ν_{H_2} with $(\nu_R + \nu_p)/2$. The shift thus obtained is used to obtain the ℓ = 0 - 1 separation from the $Q_1(0)$ spectrum for which only the R(0) component is observed.

SYSTEM	J"	ε"	i"	⟶	J'	ε'	i'	MEYER – SCHAEFER – LIU M80 GHz	MEYER – SCHAEFER – LIU M80 cm–1	BURTON – SENFF IEPA GHz	BURTON – SENFF IEPA cm–1	KOCHANSKI GHz	KOCHANSKI cm–1	SCHAEFER – MEYER SM79 GHz	SCHAEFER – MEYER SM79 cm–1
P–P	0	1	1		1	−1	−1	43.6	1.46	57.0	1.90	45.6	1.52	44.9	1.50
O–P	1	−1			0	1		35.1	1.17	27.9	0.93	29.0	0.97	32.1	1.07
	1	−1			1	1		48.3	1.61	76.2	2.54	55.5	1.85	52.2	1.74
	1	−1			2	1		43.0	1.43	55.4	1.85	44.7	1.49	44.1	1.47
O–O	0	1	1		1	−1	1	41.3	1.38	49.7	1.66				
	0	1	1		1	−1	−1	29.7	0.99	20.9	0.70				
	0	1	1		1	−1	−1	46.9	1.57	71.4	2.38				
	1	1	−1		0	−1	1	52.8	1.76	95.7	3.19				
	1	1	−1		1	−1	1	39.3	1.31	42.3	1.41				
	1	1	−1		1	−1	−1	27.8	0.93	13.6	0.45				
	1	1	−1		1	−1	−1	45.0	1.50	64.1	2.14				
	1	1	−1		2	−1	1	44.7	1.49	61.9	2.07				
	1	1	−1		2	−1	−1	47.0	1.57	72.4	2.41				
	2	1	1		1	−1	1	43.2	1.44	51.9	1.73				
	2	1	1		1	−1	−1	31.7	1.06	23.1	0.77				
	2	1	1		1	−1	−1	48.9	1.63	73.6	2.45				
	2	1	1		2	−1	1	48.6	1.62	71.5	2.38				
	2	1	1		2	−1	−1	50.9	1.70	81.9	2.73				
	2	1	1		3	−1	−1	43.5	1.45	55.8	1.86				

TABLE 4.8

Frequencies of dipole transitions predicted by means of the four ab initio potential energy surfaces discussed in the text. The interchange symmetry selection rule has been relaxed since, in the relevant experiment, the interacting monomers have different vibrational quantum numbers after absorption of a photon. Note that two different levels with the quantum numbers $J = 1$, $\varepsilon = -1$, $i = -1$ occur in the o–o system (cf. Table 4.7).

of Table 4.7 and the electric dipole selection rules : $\Delta J = 0, \pm 1 (0 \nleftrightarrow 0)$, change of parity. In order to make the comparison with experiment more direct, the selection rule, no change in i, has been relaxed, thus treating the monomers as distinguishable. By considering the symmetry of the induced dipole moment of the dimer under the operations of the molecular symmetry group, and by applying the vanishing integral rule (Section 2.6), Bunker (1979b) has shown that pure Δl transitions, where the internal states of the H_2 molecules are unchanged, are only allowed for o-p $(H_2)_2$. Physically, this is because there is no collision induced dipole moment in ground state o-o and p-p systems (Brocks and van der Avoird 1985). The far infrared $Q_o(o)$ and $Q_0(1)$ spectra will therefore be considerably simpler than the observed $Q_1(o)$ and $Q_1(1)$ spectra. The predicted spectrum of optically allowed transitions is presented in Figure 4.9 for the two potentials (Meyer-Schaefer-Liu (M80); Burton-Senff) for which complete calculations are possible. Each line represents a theoretical estimate of the experimentally determined $l = 0 - 1$ separation. The spread in the calculated lines is due to the potential anisotropy, an effect not observed experimentally.

Inspection of Figure 4.9 shows that the predictions of the Meyer-Schaefer-Liu potential are in distinctly better agreement with experiment than the predictions of the IEPA potential of Burton and Senff (1982). Given the spectral resolution of 0.15 cm^{-1} in the experiment of McKellar and Welsh (1974), the rotational splitting

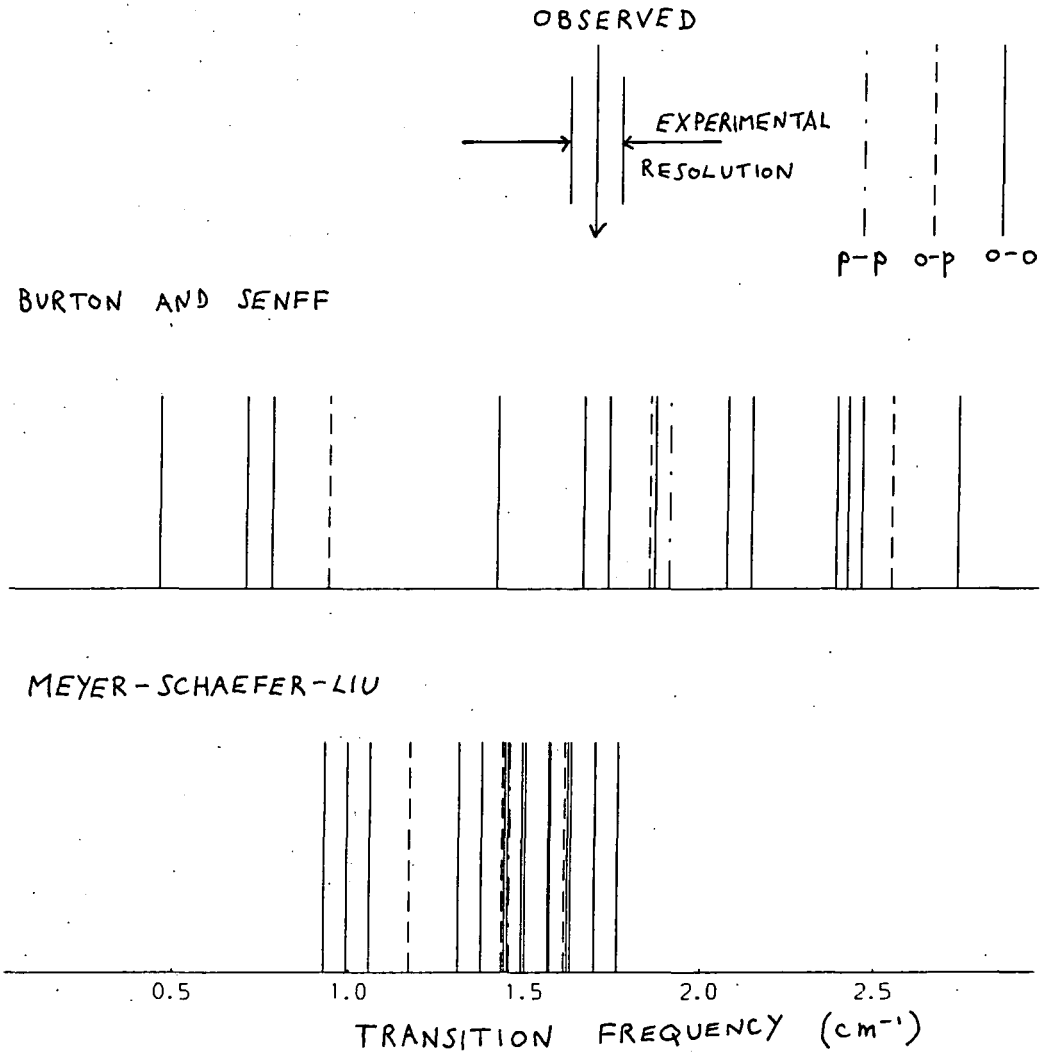

Figure 4.9

Predictions of the H_2-H_2 absorption spectrum in the fundamental band of H_2. Results are according to the ab initio potentials displayed in Figures 4.3 and 4.4. Also shown is the observed separation of the end-over-end rotational levels and the experimental resolution (McKellar and Welsh 1974). In "normal" hydrogen, the absorption in 0-0 transitions is enhanced by a factor of three relative to 0-p and nine relative to p-p transitions owing to the 3 : 1 ortho : para abundance ratio. The H_2 molecules have been treated as being distinguishable to make a more direct comparison with experiment (see the text and Table 4.8).

of the $\ell = 0$ and $\ell = 1$ states would probably have been observed if the IEPA potential were an accurate representation of reality. As the rotational splitting reflects the anisotropy of the potential, we conclude that the IEPA potential is too anisotropic in the region of the potential well. Referring to Figures 4.3 and 4.4, we see that the discrepancies between the potentials arise from differences in the magnitude of the V_{200} coefficient of the potential expansion (4.3). Similar conclusions may be drawn from the more limited comparison with experiment of results obtained from the Kochanski (1975) potential and the SM79 potential of Schaefer and Meyer (1979).

The separation of the $\ell = 0$ and $\ell = 1$ states is determined by the end-over-end rotational constant. Figure 4.9 shows this (mean) separation to be overestimated by the IEPA potential and probably underestimated by the Meyer-Schaefer-Liu potential. In terms of the end-over-end rotational constant, these results imply that the IEPA potential underestimates the H_2-H_2 equilibrium separation and hence overestimates the rotational constant. We conclude that the isotropic part V_{000} of the IEPA potential is too attractive.

The discrepancy with the H_2-H_2 equilibrium separation predicted by the Meyer-Schaefer-Liu potential may be removed by a shift of the isotropic potential minimum, towards the origin, by about 0.2Å. A simple analysis based on the p-p system predicts a somewhat larger shift

(see Figure 4.10); the fact that a simple leftward shift also raises, unphysically, the potential from the minimum outwards may account for this. Since a shift in V_{000} changes the classical turning points, and hence the relevant part of the anisotropic interaction, the other terms in the potential expansion should, by implication, be shifted also. It is interesting that the analysis of differential scattering data suggests that the zero of the isotropic potential should be shifted (in the same sense), with a concomitant shift in the anisotropic terms, by 0.1Å (Buck 1982; Buck et al. 1981, 1983b). A similar shift has been deduced from the analysis of second virial coefficient data (Schaefer and Watts 1982).

As mentioned in section 4.3.4, Verberne and Reuss (1981) have shown that the hyperfine spectrum of the H_2-H_2 dimer yields information on the potential anisotropy. Measurements on the o-p system yield an estimate of the quantity

$$\langle V_2 \rangle \propto \left| \int_0^\infty \psi_{0,2}(R)\, V_{200}(R)\, \psi_{0,0}(R)\, dR \right| \qquad (4.12)$$

where $\psi_{0,2}$ and $\psi_{0,0}$ are the radial wavefunctions corresponding to the $l = 2$ and $l = 0$ states of the dimer. $\langle V_2 \rangle$ may also be calculated theoretically; the Meyer-Schaefer-Liu potential yields a value too small compared to experiment (Waaijer et al. 1981). Geraedts et al. (1982a) and Waaijer et al. (1981) decided to constrain the V_{200} term at short and long range. The long range form of the potential is the result of an accurate cal-

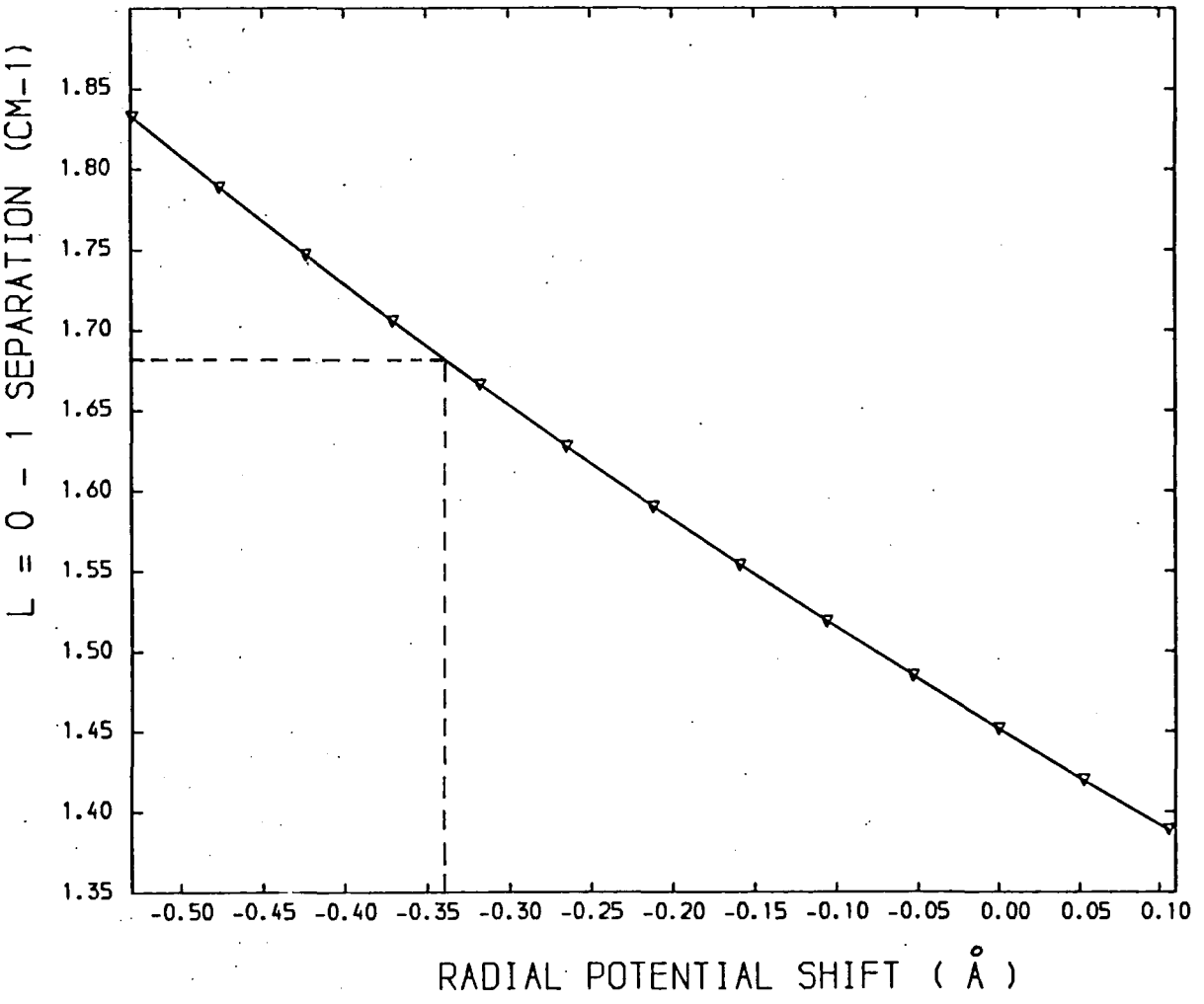

Figure 4.10

The effect of shifting the potential on the $\ell = 0 - 1$ separation for para-para $(H_2)_2$. Only one rotational state ($j = 0$) was retained on each H_2. To reproduce the experimental separation (1.68 cm^{-1}) would require a leftward shift of 0.34 Å, rather greater than that predicted when the lines from the other two dimer modifications are taken into account.

culation by Meyer (1976). At short range, the ratio V_{200}/V_{000} is fixed by inelastic differential cross section measurements (e.g. Buck et al. 1983b). To increase $\langle V_2 \rangle$ it was therefore necessary to deepen the well in V_{200} by the addition of a "blister". The resulting behaviour is closer to that of the Burton-Senff potential. Based on the results of our calculations, we are therefore unable to support the adjustments suggested by Geraedts et al. (1982a) and Waaijer et al. (1981).

4.4 The Meyer-Schaefer-Liu vibrotor potential

The M80 calculations of Meyer, Schaefer and Liu, described in Section 4.2, have been repeated with the H_2 internuclear distance fixed at a new value, 1.28 a.u. (Köhler and Schaefer 1983a). For para- and ortho-H_2, the vibrationally averaged internuclear distance, r^o, is 1.449 a.u. and 1.451 a.u. respectively. The intermolecular potential for 0-p and 0-0 systems can be obtained by fitting to the results for the two r values, 1.28 and 1.449 a.u.

Schaefer (1983) has carried out rigid rotor calculations on the bound states of the 0-p and 0-0 dimers, taking into account the difference in vibrationally averaged distances, r^o. He assumes that j_1, j_2, j_{12} and ℓ are all good quantum numbers, and his calculations thus involve solving the bound state problem for single Schroedinger equations. Consider now full close coupling calculations with H_2 restricted to one rotor state ($j = 0$ or 1). For the 0-p and 0-0 systems, there are four cases where this basis leads to a single Schroedinger equation.

Our one-rotor state calculations for these levels are thus directly comparable with those of Schaefer (1983) (see table 4.9(a)). The difference between these results of $\leqslant 0.004$ cm^{-1} is not significant. It could be attributable to the use of a slightly different reduced mass (1836.12 a.u.) by Schaefer. Therefore, our use of the same rigid rotor surface for all three dimer modifications is justified.

In table 4.9(b), we compare more one-rotor state results, these involving the solution of small systems of coupled equations, with the single Schroedinger equation results of Schaefer. The agreement is still rather good, with typical differences of less than 0.1 cm^{-1}. We see that the Schaefer results are all higher. This could reflect the fact that our results are variationally more accurate allowing, as they do, for coupling to higher ℓ states.

For the 0-0 system, there are two bound states of the same symmetry, $J^{\varepsilon i} = 1^{--}$. For this symmetry, the basis $j_1 = j_2 = 1$ leads to three coupled equations, the channels of which are defined by $(j_{12}, \pi) = (0,0)$, $(2,0)$ and $(2,1)$. Inspection of the matrix elements given in chapter 2 shows that (0,0) and (2,0) are coupled by anisotropic terms in the potential, while (2,0) and (2,1) are coupled by coriolis terms. It is not surprising, therefore, that there is a significant discrepancy with Schaefer's results; these assume that j_{12} and ℓ can both be rigorously defined (Table 4.9(c)). This inter-

	System	J	$\mathcal{E}$	i	cc	j_{12}	ℓ	sc	sc-cc
(a)	o-p	0	1		-1.252	1	1	-1.248	0.004
	o-p	1	1		-0.822	1	1	-0.819	0.003
	o-o	0	-1	1	-0.665	1	1	-0.667	-0.002
	o-o	1	-1	1	-1.103	1	1	-1.107	-0.004
(b)	o-p	1	-1		-2.425	1	0	-2.407	0.018
	o-p	2	1		-0.996	1	1	-0.985	0.011
	o-o	0	1	1	-2.475	0	0	-2.438	0.037
	o-o	1	1	-1	-2.415	1	0	-2.403	0.012
	o-o	2	1	1	-2.550	2	0	-2.417	0.133
	o-o	2	-1	1	-0.929	1	1	-0.924	0.005
	o-o	2	-1	-1	-0.854	2	1	-0.772	0.082
	o-o	3	-1	-1	-1.102	2	1	-1.022	0.080
(c)	o-o	1	-1	-1	-1.492	2	1	-1.364	0.128
	o-o	1	-1	-1	-0.918	0	1	-1.328	-0.41

TABLE 4.9

A comparison of eigenenergies (cm^{-1}) calculated using the close-coupling (cc) method and the M80 potential ($r_1 = r_2 = 1.449$ a.u.) with the results of Schaefer (1983) using the vibrotor surface. The latter results correspond to single channel (sc) rigid rotor calculations, with r = 1.449 a.u. for p-H_2 and r = 1.451 a.u. for o-H_2, for which j_{12} and ℓ are exact quantum numbers. Both the cc and sc calculations assume that j_1 and j_2 are exact. In (a) the cc results involve the solution of a single Schroedinger equation; in (b) and (c) they involve coupling to states correlating with respectively higher and the same ℓ .

pretation has been confirmed by Verberne and Reuss (1981) who calculated admixture coefficients for the equivalent space-fixed channels.

With vibrational excitation of an H_2 monomer comes a much larger increase in the mean bond length. For $V = 1$, $r^o = 1.545$ a.u. (Le Roy and van Kranendonk 1974). In the preceding section, we have assumed that this increase does not affect the potential. An extension of the ab initio potential calculations, together with further close coupling calculations of the nuclear dynamics, are needed to assess the accuracy of this approximation.

4.5 Conclusions

The results of this chapter illustrate the importance of spectroscopic measurements of van der Waals molecules in determining intermolecular potentials. Information may be derived from these measurements on the behaviour of both the isotropic and anisotropic terms in the potential in the region of the well. Studies of the molecular dimer complement the analysis of low-energy scattering data, which tend to be sensitive to the repulsive part of the interaction, from the minimum upwards.

Our specific conclusions regarding the H_2-H_2 dimer are:

(i) That the IEPA potential of Burton and Senff (1982) is too strongly attractive and overestimates the magnitude of the V_{200} coefficient in the BF expansion of the potential. Electron correlation makes too large a contribution to the IEPA potential, as suspected by

Burton and Senff.

(ii) The potential of Kochanski (1975), in which the dispersion energy is evaluated using second-order perturbation theory, satisfactorily predicts the isotropic part of the interaction, V_{000}, but again overestimates the magnitude of the V_{200} coefficient. This reflects errors in describing the anisotropy of the dispersion interaction. Taking into account other criteria, such as computer time requirements, this method remains attractive, particularly for applications to heavier systems.

(iii) In calculations on the p-p and O-p systems, the published potential of Schaefer and Meyer (1979) yields better results than both the Burton-Senff and Kochanski potentials. The quadrupole-quadrupole coefficients, V_{22n}, which intervene directly only in the O-O system, are in error; this potential should not be used in calculations involving this modification of the dimer.

(iv) The CI potential of Meyer and Schaefer (1985) and Schaefer and Liu (1985) is undoubtedly the best of the four ab initio potentials studied. The anisotropy is found to concord with the failure to resolve rotational splitting of the dimer energy levels. The agreement with the observed separation of the $\ell = 0$ and $\ell = 1$ end-over-end rotational levels would be improved by a small negative shift of the isotropic potential minimum.

The physical significance of this empirical modification is open to question. As Schaefer (1982a) has pointed out, such a shift requires an increase in the correlation

energy of 30% in the region of the zero of V_{000}. This is difficult to justify given the large number of configurations employed in this calculation. A possible explanation may be that the bond length of the H_2 molecules may decrease at shorter intermolecular separations, leading to an effective softening of the repulsive wall of the potential.

The blister in the V_{200} coefficient, postulated by Geraedts et al. (1982a) and Waaijer et al. (1981), conflicts with our findings. The short range constraints on the potential which forced its introduction may be invalid. These issues can only be resolved by fully variational bound state calculations, treating the H_2 molecules as vibrotors, in conjunction with near infrared spectroscopic measurements at improved resolution.

CHAPTER FIVE

THE D_2 - D_2 DIMER

5.1 Introduction

In the present chapter we report the results of our calculations on the D_2 - D_2 dimer. The motivation for studying this system derives from the result of the Born-Oppenheimer approximation that the electronic potential energy surface is unchanged by isotopic substitution. Furthermore, since the diatom centre of mass is unshifted, unlike HD, we may use the same potential expansion coefficients, $V_{q_1 q_2 \mu}(R)$, as we did for H_2 - H_2 (Kreek and Le Roy 1975, Liu et al. 1978). The D_2 molecule has a smaller vibrationally averaged internuclear separation than H_2; for D_2 and H_2 in their j = 0 states, r^o = 1.435 a.u. and 1.449 a.u. respectively (Le Roy and van Kranendonk 1974). The results of Section 4.4 lead us to expect that this difference will be unimportant. This assumption has also been made in scattering calculations on H_2 - H_2 and D_2 - D_2 (Ramaswamy et al. 1977). We use the rigid rotor potential which was found in Chapter 4 to give the best agreement with spectroscopic measurements, namely the M80 surface of Meyer and Schaefer (1985) and Schaefer and Liu (1985).

The reduced mass of D_2 - D_2 is approximately twice that of H_2 - H_2. This results in a lower zero point energy of the complex, and hence more bound states. The rotational constant of the dimer is also consequently smaller leading to a stronger interaction between the bound states. The smaller rotational constant of the

D_2 molecule should increase the effect of including excited rotational states in the close coupling calculations. The overall result of the mass difference is to increase the relative importance of the potential anisotropy. In the scheme of Ewing (1976), D_2 - D_2 is a more strongly coupled complex than H_2 - H_2.

In Section 5.2 we present results for the bound states of D_2 -D_2 lying below the dissociation limit of the dimer. We shall see in the section that follows that bound states correlating to rotationally excited D_2 are also possible. These calculations were performed using the R-matrix propagator method, in conjunction with Richardson h^2-extrapolation. Results for dimers comprising D_2 in either of its two distinct modifications, ortho (j = 0,2...) and para (j = 1,3...), will be given. The measurements of McKellar and Welsh (1974) yield more detailed spectra for D_2 - D_2 than for H_2 - H_2, the results for dimers of ortho-D_2 showing the most structure. Throughout the rest of the chapter we shall concentrate on the experimentally more interesting ortho-ortho (0-0) system. In Section 5.3 we calculate the bound states and resonances correlating to one of the (indistinguishable) monomers being in its first rotationally excited state (j = 2). The resonance energies and widths have been obtained using the method of Ashton et al. (1983) in conjunction with the molecular scattering code of Launay (1977, 1978). The effect of tunnelling between equivalent states will be seen to be marked in many instances. Furthermore, we shall attempt to

rationalise this behaviour in terms of simple two-level degenerate perturbation theory. These calculations will allow us to predict the, as yet unobserved, far infrared $S_o(0)$ spectrum of the dimer.

We go on, in Section 5.4, to consider the overlapping $S_1(0)$ and $Q_1(0) + S_o(0)$ spectra of 0-0 $(D_2)_2$, observed by McKellar and Welsh (1974). Full close coupling calculations on the upper states of these transitions would involve taking into account the dependence of the potential on the stretching of the monomer bond. We shall attempt to model reality by using a rigid rotor calculation with appropriate adjustments to the channel energies, enabling us to take into account the interaction between the upper levels of the single and double transitions cited above. The emphasis will be on interpretation of the spectra, rather than assessment of the potential as in Chapter 4. This is justified given that we use an ab initio potential surface which is widely regarded (e.g. Verberne and Reuss 1980, Buck et al.1983b, Köhler and Schaefer 1983b) to be the best available. The chapter ends with a summary of our conclusions both on the interaction potential and on the spectroscopic assignments.

5.2 Bound States

Methods for calculating the bound state energies of molecular dimers have been discussed in Chapter 3. In the present work we integrate the close coupled equations using the R-matrix propagator method. Richardson extrapolation is used to accelerate the convergence of the eigenenergies with respect to the number of integration steps. By way of example we give, in Table 5.1, results for the

R_{min}, R_{max}		2,27	2,40	1,80
(a) N = 50		-6.019871	-6.025452	-6.030053
100		-6.022423	-6.023029	-6.029809
200		-6.023217	-6.023388	-6.024178
400		-6.023403	-6.023444	-6.023656
800		-6.023450	-6.023461	-6.023511
extrapolation :	50-100	-6.023274	-6.022222	-6.029728
	100-200	-6.023481	-6.023507	-6.022301
	200-400	-6.023465	-6.023463	-6.023482
	400-800	-6.023466	-6.023466	-6.023463
(b) N = 50		-0.457799	-0.470535	-0.541119
100		-0.455748	-0.458302	-0.476370
200		-0.455327	-0.455992	-0.459731
400		-0.455215	-0.455397	-0.456343
800		-0.455187	-0.455251	-0.455485
extrapolation :	50-100	-0.455064	-0.454224	-0.454787
	100-200	-0.455187	-0.455222	-0.454184
	200-400	-0.455178	-0.455199	-0.455214
	400-800	-0.455178	-0.455202	-0.455199

TABLE 5.1

Convergence of the computed eigenenergies (cm^{-1}) of the ortho-D_2-ortho-D_2 system with respect to integration parameters. The limits of the integration range are R_{min} and R_{max} (Bohr); 2N is the total number of sectors. The improved convergence attainable using Richardson extrapolation (equation (3.36)) is demonstrated. The basis set consists of one rotational state (j = 0) on each D_2. The total angular momentum is (a) J = 0 and (b) J = 3.

lowest and highest of the bound states of ortho-D_2-ortho-D_2 measured relative to the dissociation limit of the dimer. This table illustrates the convergence with respect to the integration parameters: integration range, R_{max}-R_{min}, and the number of steps per half range, N. We conclude that applying Richardson extrapolation to the eigenenergies obtained with (R_{min}, R_{max}, N) = (2,27,50) and (2,27,100), yields results converged to within 0.0002 cm^{-1}. Following Bishop and Shih (1976) the reduced mass in these calculations is taken to be μ = 3670.48 a.u.

The rotational constant of D_2 is half that of H_2 and it is of more interest to examine the effect of this on convergence with respect to basis set size. In Table 5.2 we present results using a maximum of three rotational states on each D_2 molecule : j = 0,2,4 for ortho-D_2 and j = 1,3,5 for para-D_2. The sample of results quoted corresponds to that obtained for H_2 - H_2 (Table 4.5), with which it may be compared. The channel energies were obtained from the results of Bishop and Shih (1976). The addition of a second rotor state (j = 2 or 3) shifts the levels downwards, as expected from the variational principle, by $\lesssim$ 0.08 cm^{-1}. This shift is larger than the corresponding one obtained for H_2 - H_2, reflecting the smaller separation between the monomer energy levels. The addition of a third (j = 4 or 5) rotor state does not alter the results which are quoted with a precision consistent with the numerical accuracy. This is partly because these rotor states are energetically more distant, but largely because the expansion of the potential,

System	$J^{\varepsilon i}$	1	2	3
0 - 0	0^{++}	-6.0233	-6.0819	-6.0819
	1^{--}	-5.0467	-5.1026	-5.1026
p - 0	0^{+}	-5.5831	-5.6672	-5.6672
p - p	0^{++}	-6.1732	-6.2459	-6.2459
	0^{-+}	-4.4711	-4.4903	-4.4903

TABLE 5.2

Eigenenergies (cm^{-1}) of states $J^{\varepsilon i}$ of ortho-D_2-ortho-D_2, para-D_2-ortho-D_2 and para-D_2-para-D_2; J is the total angular momentum, ε the parity and i the interchange symmetry (for identical molecules). Columns 1, 2 and 3 contain results obtained with one, two and three rotational states respectively on each D_2 molecule.

equation (4.3), is truncated at $q_1 = q_2 = \mu = 2$. This means that dimer levels correlating to j_1, $j_2 = 0$ or 1 do not couple directly to excited monomer states j' where $j' - j > 2$. On the basis of energy separation alone, second order perturbation theory would predict any shift due to a third rotor state to be three times smaller than the two rotor state shift. We conclude that the two rotor state results are accurate to within 0.02 cm^{-1} and that basis set size, rather than numerical convergence, is the limiting factor.

In Table 5.3 we give two rotor state results for the bound states of 0 - 0 $(D_2)_2$, obtained from the M80 potential using the numerical parameters determined above. Following Bishop and Shih (1976), the energy of the j = 2 level of D_2 is taken as 179.078 cm^{-1}. For completeness, the energy and width of the $J(\ell) = 4$ shape resonance is also given. This was calculated using the methods to be discussed in more detail in the following section. The molecular scattering code of Launay (1977, 1978) was used to calculate the eigenphase sum, which in this single open channel case corresponds to the scattering phase shift. This is fitted to a Breit-Wigner form, assuming a linear background phase shift.

The deuteron is a boson of unit nuclear spin. Under interchange of deuterons, the deuterium molecule may thus either have a symmetric spin function with I = 0,2 or an antisymmetric spin function with I = 1. The former molecule is the ortho modification, the latter the para

J	ε	i	l	E(cm^{-1})	Γ(cm^{-1})
0	1	1	0	-6.082	0.0
1	-1	-1	1	-5.103	0.0
2	1	1	2	-3.194	0.0
3	-1	-1	3	-0.495	0.0
4	1	1	4	2.601	0.55

TABLE 5.3

The eigenenergies of 0-0 $(D_2)_2$. Also given is the energy and (FWHM) width, Γ, of the J = 4 shape resonance. The calculations were performed with two rotor states on each D_2. E(j = 2) = 179.078 cm^{-1}. The energies are measured relative to the dissociation limit of the dimer. The good quantum numbers of the levels are given : viz. the total angular momentum (J), parity (ε) and inter-change symmetry (i). Also quoted is the value of the end-over-end rotation, l.

(Rose 1957). For two D_2 molecules in the same rotational state, the symmetry of the total nuclear spin - rovibrational wavefunction under molecular exchange is given by $i(-)^{I_{12}} = (-)^{j_{12} + l + I_{12}} = +1$. For two ortho molecules, the total nuclear spin may take even or odd values, $I_{12} = 0,1,2,3,4$. All of the levels in table 5.3 are therefore allowed, contrary to the statement made by Gordon and Cashion (1966). The results of these pedestrian arguments have been confirmed by Bunker (1979b) who calculated the statistical weights for all symmetries of $(D_2)_2$ and found none of them to be zero.

Because the bound states in Table 5.3 correspond very closely to both molecules in their isotropic $j = 0$ states, they should behave according to a simple nonrigid rotor model of the form (McKellar and Welsh 1972 , Kudian and Welsh 1971):

$$E = E_o + B_l l(l+1) - D_l \left(l(l+1)\right)^2 \qquad (5.1)$$

E_o is the zero point ($l = 0$) energy; B_l and D_l respectively the rotational and centrifugal distortion constants of the dimer. Performing a least squares fit to the bound states of Table 5.3, we arrive at the values, $B_l = 0.495$ cm^{-1} and $D_l = 2.4 \times 10^{-3}$ cm^{-1}. These may be compared with the values obtained by McKellar and Welsh (1974) from their observations of the dimer spectrum in the $Q_1(0)$ region of pure ortho-D_2. The experimental results are $B_l = 0.525$ cm^{-1} and $D_l = 3.5 \times 10^{-3}$ cm^{-1}. This confirms the conclusion of Chapter 4, that the Meyer-Schaefer-Liu

potential underestimates the dimer rotational constant. The effective intermolecular separation, implied by the theoretical and experimental values of the rotational constant, is 4.11 Å and 3.99 Å respectively. This suggests a negative shift of the Meyer-Schaefer-Liu potential of 0.12 Å is required, in broad agreement with the results of Chapter 4.

In Table 5.4, the transition frequencies deduced from Table 5.3 are compared with the values obtained by McKellar and Welsh (1974) from the $Q_1(0)$ spectrum of 0-0 $(D_2)_2$. The experimental estimate of the ℓ = 0-3 energy separation is based on observations of the $S_1(0)$ spectrum where anisotropy effects are important (see Section 5.4). No $0 \leftrightarrow 3$ transitions (N and T branches) are observed in the $Q_1(0)$ spectrum as these would violate the electric dipole selection rules. The $\ell'' = 3 \rightarrow \ell' = 4$ and $\ell'' = 4 \rightarrow \ell' = 3$ lines were only partly resolved due to broadening. McKellar and Welsh (1974) conclude that the $\ell = 4$ state is pseudobound. The $0 \leftrightarrow 1$, $1 \leftrightarrow 2$ and $2 \leftrightarrow 3$ lines are all sharp, consistent with our conclusion that the $(D_2)_2$ dimer has 4 (ℓ = 0,1,2,3) bound states. The statement in McKellar and Welsh (1974) that ℓ = 3 is also pseudobound should be disregarded, though McKellar (1983) points out that pseudobound levels just above the dissociation limit in H_2 - rare gas complexes can give rise to sharp lines. In passing we add that no experimental evidence exists for the presence of levels involving excited vibrations of the van der Waals bond.

Transition ($\ell' - \ell''$)	Theory	Experiment
1 - 0	0.98	1.04
2 - 1	1.91	2.00
3 - 2	2.70	2.85
4 - 3	3.10	3.50
3 - 0	5.59	(6.94)

TABLE 5.4

The separation (in cm^{-1}) between end-over-end rotational states of ortho-ortho D_4. The theoretical results are obtained from the bound state energies of Table 5.3. The experimental result for the 3-0 separation was estimated from measurements of the $S_1(0)$ spectrum for which angular anisotropy may be expected to be important. The remaining experimental values were obtained from the unambiguously assigned R and P components of the $Q_1(o)$ spectrum in pure ortho-D_2.

This is not surprising given that the lowest bound state is 16 cm^{-1} above the minimum of the isotropic potential V_{000}.

Two rotor state calculations have also been performed on the p - 0 and p - p systems of $(D_2)_2$. The energies of all bound states lying below the dissociation limit are given in Tables 5.5 and 5.6. The energy of the j = 3 rotor state of para-D_2 is taken as 297.546 cm^{-1}, measured relative to E(j = 1) (Bishop and Shih 1976). For completeness, the energies and widths of two shape resonances of p - p $(D_2)_2$ are also given in Table 5.6 so that all states correlating with ℓ = 0,1,2,3 are calculated. The results of these tables are plotted in Figure 5.1. Comparison with the analogous diagram for $(H_2)_2$, viz Figure 4.6, shows that rotational splitting is more marked in $(D_2)_2$. The ℓ-correlations are also illustrated; though all of these are self-evident from considerations of parity and angular momentum coupling, they were all checked by carrying out (1 - rotor state) calculations allowing the potential anisotropy to decrease linearly. The magnitude of the splitting for some of the p - p levels indicates that ℓ is not a good quantum number in these cases. This space-fixed quantum number is still a convenient one to use for labelling purposes and it is the one employed by McKellar and Welsh (1974) for their experimental line assignments. We note, however, that the body-fixed quantum number $\bar{\Omega}$ could in principle have been used; the correlations

J	ε	l	ENERGY (CM-1)	WIDTH (CM-1)
1	-1	0	-6.149	0.0
0	1	1	-5.667	0.0
1	1	1	-4.839	0.0
2	1	1	-5.201	0.0
1	-1	2	-3.415	0.0
2	-1	2	-2.942	0.0
3	-1	2	-3.300	0.0
2	1	3	-0.664	0.0
3	1	3	-0.274	0.0
4	1	3	-0.593	0.0

TABLE 5.5

The eigenenergies of p-o $(D_2)_2$. The calculations were performed with two rotor states on each D_2. The corresponding channel energies were taken as 0.0, 297.546 for para-D_2 and 0.0, 179.078 for ortho-D_2. All energies are quoted in cm^{-1}. All states correlating with the end-over-end rotation, l=0-3, are bound, as is evident from the zero widths.

J	ε	i	l	ENERGY (CM-1)	WIDTH (CM-1)
0	1	1	0	-6.246	0.0
1	1	-1	0	-6.114	0.0
2	1	1	0	-6.545	0.0
0	-1	1	1	-4.490	0.0
1	-1	1	1	-5.379	0.0
1	-1	-1	1	-6.321	0.0
1	-1	-1	1	-5.169	0.0
2	-1	1	1	-5.058	0.0
2	-1	-1	1	-5.191	0.0
3	-1	-1	1	-5.521	0.0
0	1	1	2	-1.242	0.0
1	1	1	2	-5.327	0.0
1	1	-1	2	-2.843	0.0
2	1	1	2	-3.335	0.0
2	1	1	2	-2.389	0.0
2	1	-1	2	-3.458	0.0
3	1	1	2	-3.409	0.0
3	1	-1	2	-3.118	0.0
4	1	1	2	-3.545	0.0
1	-1	-1	3	0.212	0.1174
2	-1	1	3	-0.255	0.0
2	-1	-1	3	-1.415	0.0
3	-1	1	3	-0.728	0.0
3	-1	-1	3	-0.623	0.0
3	-1	-1	3	0.360	0.0126 *
4	-1	1	3	-0.412	0.0
4	-1	-1	3	-0.725	0.0
5	-1	-1	3	-0.768	0.0

TABLE 5.6

The eigenenergies of p-p $(D_2)_2$. The calculations were performed with two rotational states on each D_2. All levels correlating to $l = 0,1,2,3$ were calculated. Two of the $l = 3$ states are pseudo-bound; their energies and widths were calculated using the methods of section 5.3

* At the time of writing, a 2-rotor state result was unavailable for this resonance. The energy quoted here was obtained with one rotational state ($j = 1$) on each D_2.

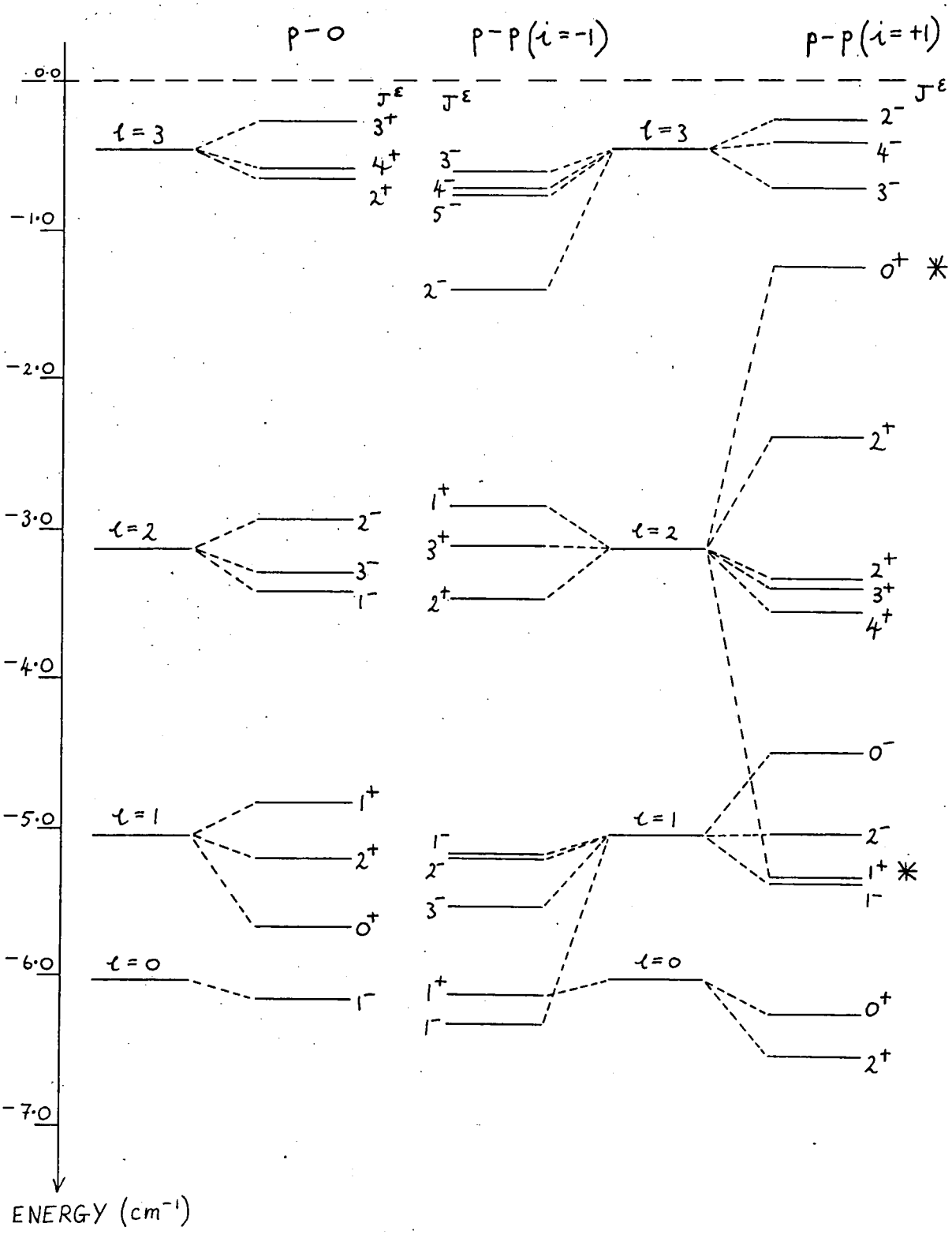

Figure 5.1

The bound states of para-D_2-ortho-D_2 and para-D_2-para-D_2. Also shown are the four end-over-end rotational states to which these levels correlate. The two shape resonances in the p-p system which correlate to $l = 3$ are not shown. A comparison with the analogous figure for H_2-H_2 (Figure 4.6) demonstrates the greater role played by rotational anisotropy in the heavier dimer.

* A brief discussion of these two strongly split levels appears in the text.

would then be obtained by multiplying the coriolis coupling terms as well as the potential coupling terms by a factor between 0 and 1. The V_{200} term in the potential expansion is responsible for the rotational splitting of the p-0 levels, the higher order V_{22n} terms contributing only via coupling to excited rotational monomer states. All of the terms in the potential expansion can directly contribute to rotational splitting in the p-p system.

The interpretation of the splitting is simplified if we note that one rotor state results differ from the two rotor state results quoted here by $\ll 0.08\ cm^{-1}$. With the restriction $j_1 = j_2 = 1$, the basis set for the strongly split p-p level $J^{\mathcal{E}i} = 1^{++}$, correlating with $\ell = 2$, consists of only one term: $(j_{12}, \Omega) = (2,1)$. For this example, the interpretation is the same whether we consider this basis or the equivalent space-fixed one, $(j_{12}, \ell) = (2,2)$. Evaluation of the potential matrix elements, equation (2.28), allows us to define an "effective radial potential":

$$\langle j_1 j_2 j_{12} \Omega | V(\hat{r}_1, \hat{r}_2, R) | j_1' j_2' j_{12}' \Omega' \rangle_{\hat{r}_1, \hat{r}_2}$$

$$= V_{000}(R) + 0.44 V_{200}(R) - 0.40 V_{220}(R) - 0.42 V_{221}(R) \qquad (5.2)$$

The anisotropic terms in the potential expansion all provide, in the region of the well, negative contributions, resulting in the marked downward shift. In the language of perturbation theory (Le Roy and van Kranendonk 1974) this is a first-order splitting. Unlike the case of two ortho-D_2 molecules, where all parts of the potential surface have an equal weighting, we can think of the two

rotating para molecules as sampling a more restricted region of the surface determined by vector coupling arguments. A similar interpretation of the rotational splitting of the $J^{\mathcal{E}\,i} = 0^{++}$ level, correlating with $\ell = 2$, may also be given; in this example two channels are involved in a one rotor state calculation, namely $(j_{12},\Omega) = (0,0)$ and $(2,0)$. Potential coupling between these leads to an additional (second-order) shift. The absence of coriolis coupling between these two channels avoids any ambiguity in the interpretation of the space-fixed shift as illustrated in Figure 5.1.

McKellar and Welsh (1974) have observed the absorption spectrum of the $(D_2)_2$ dimer in normal deuterium in the region of the $Q_1(1)$ and $Q_1(0)$ transitions. All three dimer modifications contribute, though the intensity of any p-p lines will be reduced due to the 2:1 ratio of ortho to para deuterium. This could partly explain why McKellar and Welsh were able to interpret their spectrum in terms of pure $\Delta\ell$ transitions, given that rotational splitting in the p-O system is relatively small. Some perturbation of the line frequencies was observed, however. This could be due either to rotational splitting effects, or to the interaction of the upper states corresponding to the $Q_1(1)$ and $Q_1(0)$ transitions of the p-o dimer as suggested by McKellar and Welsh. These upper states are only coupled by the dependence of the potential on intramolecular stretch. The bound states of table 5.5 could be used to predict the p-o contribution to the spectrum by neglecting this coupling and evaluating the

transition frequencies to two identical sets of upper levels, separated by the difference between the $Q_1(1)$ and $Q_1(0)$ band origins (5.914 cm^{-1}). Additionally, the $Q_1(1)$ and $Q_1(0)$ contributions from respectively the p-p and 0-0 systems could be superimposed. In the absence of line intensity information, the resulting densely packed stick spectrum is of limited use, and we do not plot it here. For the rest of this chapter we shall concentrate on the dimer absorption spectra found in pure ortho-deuterium.

5.3 The $S_o(0)$ spectrum of ortho-D_2-ortho-D_2.

The channel potentials, for two rotor state calculations on 0-0 $(D_2)_2$, are schematically illustrated in Figure 5.2. The lower states of the $S_o(0)$ absorption spectrum, which lie near to the dimer dissociation limit, were calculated in the preceding section. In this section we are interested in calculating the upper states which correlate to $(V_1, j_1, V_2, j_2) = (0,2,0,0)$ or $(0,0,0,2)$. Such states, lying below threshold, may either be internal-rotationally predissociating Feshbach resonances (Le Roy et al. 1982) or <u>bound</u> states. The latter occur when there are no open channels present in the calculations. To show the conditions under which this occurs, we first note that the fully symmetrized body-fixed (equation 2.35) and space-fixed basis functions may both be written in the abbreviated form:

$$|j_1 j_2 i\rangle \propto |j_1 j_2\rangle + i\varepsilon(-)^{j_{12}} |j_2 j_1\rangle \qquad (5.3)$$

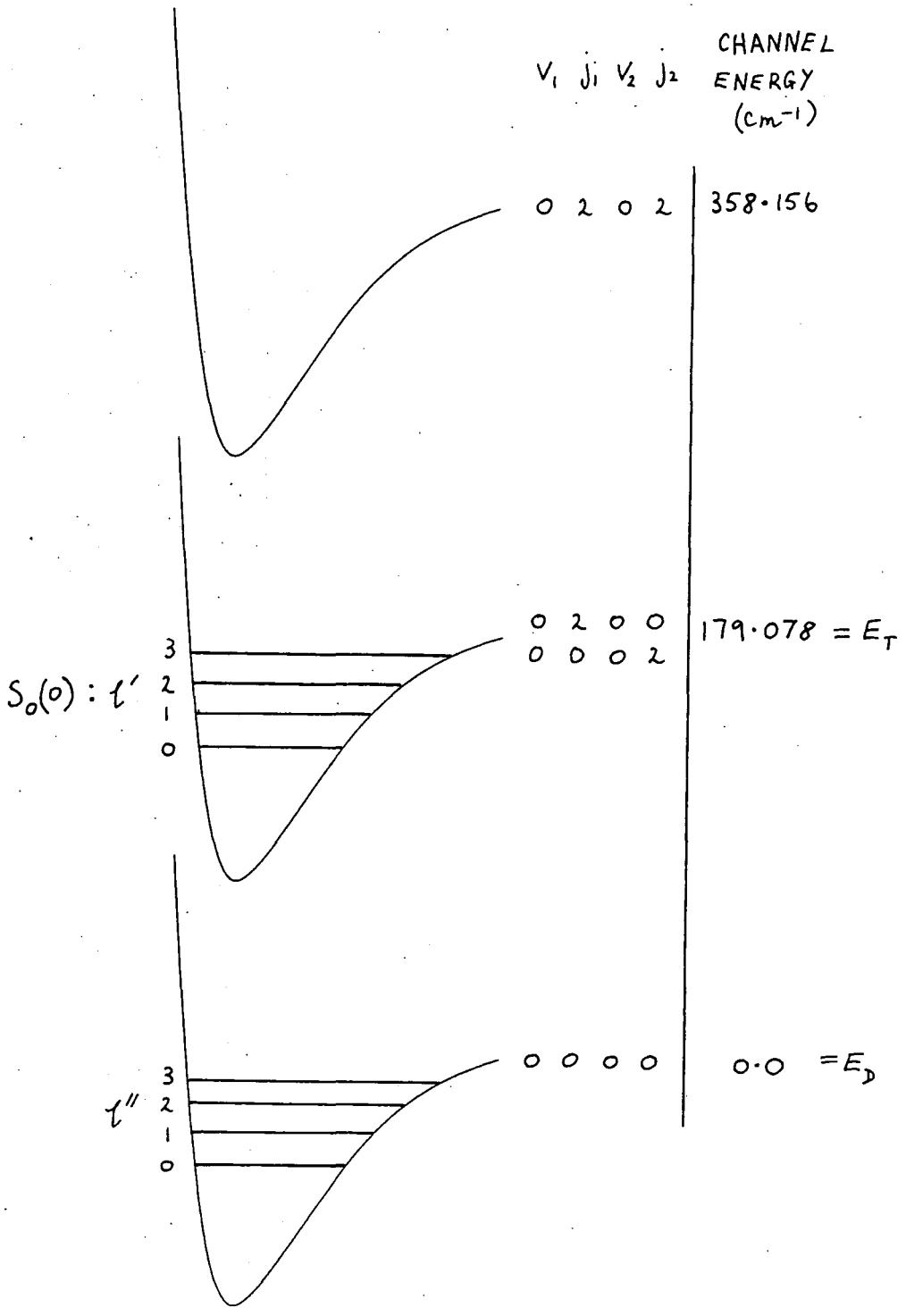

Figure 5.2

Details of the basis set and channel energies used in calculations of the $S_0(0)$ spectrum of o-o $(D_2)_2$. E_T is the $S_0(0)$ threshold energy and E_D the dissociation limit of the dimer. Only one of the four (ℓ = 0,1,2,3) effective potential energy curves, for each set of D_2 quantum numbers, is shown in this schematic representation.

The open channels are states correlating with $(V_1, j_1, V_2, j_2) = (0,0,0,0)$ and for these the parity is given by

$$\mathcal{E} = (-)^{j_1 + j_2 + l} = (-)^{l} \equiv (-)^{J} \qquad (5.4)$$

The final result of (5.4) is true for both the space-fixed and body-fixed versions of (5.3). Substituting (5.4) into (5.3) we deduce that $i = (-)^J$ for non-vanishing open channels. When j_1 and j_2 differ, as they do for the upper states of the $S_o(0)$ transition, both interchange symmetries exist. There is no coupling to the lower states either if $\mathcal{E} = (-)^{J+1}$ or $i = (-)^{J+1}$. Such states cannot predissociate by transferring their internal rotational energy to the van der Waals bond and are thus bound. Their energies have been calculated using the methods described in the preceding section, with the same numerical integration parameters.

States which do not couple to the lower levels but which lie above the $S_o(0)$ threshold, behind a centrifugal barrier, are shape (or orbiting) resonances. These predissociate by tunnelling through the barrier. All of the resonances were found by using the molecular scattering code of Launay (1977, 1978) to obtain the (real) reactance matrix, $\underset{\sim}{K}$. This is defined by the behaviour of the radial solution matrix in the asymptotic region (e.g. Balint-Kurti 1975, Dickinson 1979):

$$F_{\beta\gamma}(R) \underset{R\to\infty}{=} \delta_{\beta\gamma}\left\{k_\beta R\, j_{l_\beta}(k_\beta R)\right\} + K_{\beta\leftarrow\gamma}\left(\frac{k_\gamma}{k_\beta}\right)^{1/2}\left\{k_\beta R\, n_{l_\beta}(k_\beta R)\right\} \qquad (5.5)$$

Here, j and n are the spherical Bessel functions (Abramowitz and Stegun 1965) and l_β (l_γ) is the end-over-end angular momentum quantum number in the channel denoted by β (γ); k is a wavevector. The Launay programme integrates the coupled equations in the body-fixed frame, for reasons of numerical efficiency. At large R the solutions are then converted into space-fixed form, using the inverse of the unitary transformation given in equation (2.11); a space-fixed K matrix, as defined above, may thus be obtained (Launay 1976, Heil and Kouri 1976). This procedure is preferable to obtaining a body-fixed K matrix since the equations in this frame decouple more slowly at large R due to Coriolis terms which decay as R^{-2} (Lester 1976). The boundary conditions in equation (5.5) can be restated in terms of the S and T matrices, related to the K matrix in the following way:

$$\underset{\sim}{S} = (\underset{\sim}{I} + i\underset{\sim}{K})(\underset{\sim}{I} - i\underset{\sim}{K})^{-1} \qquad (5.6a)$$

$$\underset{\sim}{T} = \underset{\sim}{I} - \underset{\sim}{S} \qquad (5.6b)$$

Having solved the scattering equations at some trial energy, the K matrix is diagonalised ($\underset{\sim}{K}^D$) and the <u>eigenphase sum</u>, Δ, obtained:

$$\Delta(E) = \sum_\alpha \delta_\alpha = \sum_\alpha \tan^{-1}\left(K^D_{\alpha\alpha}\right) \qquad (5.7)$$

This is the multi-channel analogue of the elastic scattering phase shift (Lester 1976, Hazi 1979). The eigenphase sum is obtained at a number of trial energies in the

region of a resonance and fitted to a Breit-Wigner form, assuming a linear background, to obtain the resonance energy, E_r, and the full width at half-maximum, Γ :

$$\Delta(E) = a + bE + \tan^{-1}\left\{\frac{\Gamma}{2(E_r - E)}\right\} \qquad (5.8)$$

This method, which is due to Ashton et al. (1983), is a convenient way to calculate resonance energies and widths as only a straightforward modification of standard scattering codes is necessary to implement it (Hutson 1983b). A number of packages exist for performing least squares fits to non-linear functions of the form (5.8); we chose the NAG routine E04FDF (NAG 1984). An automatic programme for locating and fitting Breit-Wigner resonances from tables of eigenphase sums, which also uses E04FDF, has been written by Tennyson and Noble (1984). This code was used to fit many of the resonances discussed in this chapter. In a few cases, generally when the resonance was either just above a threshold or overlapped with another, a more manual approach was necessary to get a good fit. Any such problems were overcome by appropriate adjustments to the energy range over which the fit was made; the energy should also always be scaled by a constant factor to give it the same order of magnitude as the eigenphase sum.

For repeated calculation of the K matrix over a range of energies, a piecewise analytic method such as the R-matrix propagator is generally reckoned to be the most efficient approach. The Launay scattering code

uses the approximate solution de Vogelaere method. However, this code is a particularly efficient implementation, taking advantage of the presence of zero elements in the body-fixed coupling matrix (Launay 1976). Furthermore the results of chapters three and four show that there is no inconsistency in using the R-matrix propagator for bound states and the de Vogelaere for scattering calculations; the two methods can be made to agree to any desired accuracy.

5.3.1 Convergence tests

We outline the results of numerical convergence tests for the Feshbach resonance $J^{\mathcal{E}i} = 0^{++}$ correlating with $\ell = 2$. The behaviour of the eigenphase sum for this resonance is illustrated in Figure 5.3. Two rotor states are retained on each D_2. The relevant parameters for the de Vogelaere method are the integration range and, in Launay's implementation, FPT which is the number of integration steps per half-wavelength. Here the de Broglie wavelength is determined from the sum of the well depth and the collision energy relative to the lowest channel. In Tables 5.7 and 5.8 we show respectively the variation of the resonance energy and width with respect to these integration parameters. We conclude that $(R_{min}, R_{max}, FPT) = (2,27,10)$ is sufficient to obtain a resonance energy and width accurate to five significant figures. Similar convergence tests were carried out on the eigenphase sum in the vicinity of the resonance (0.04Γ from the resonance energy); the error in Δ

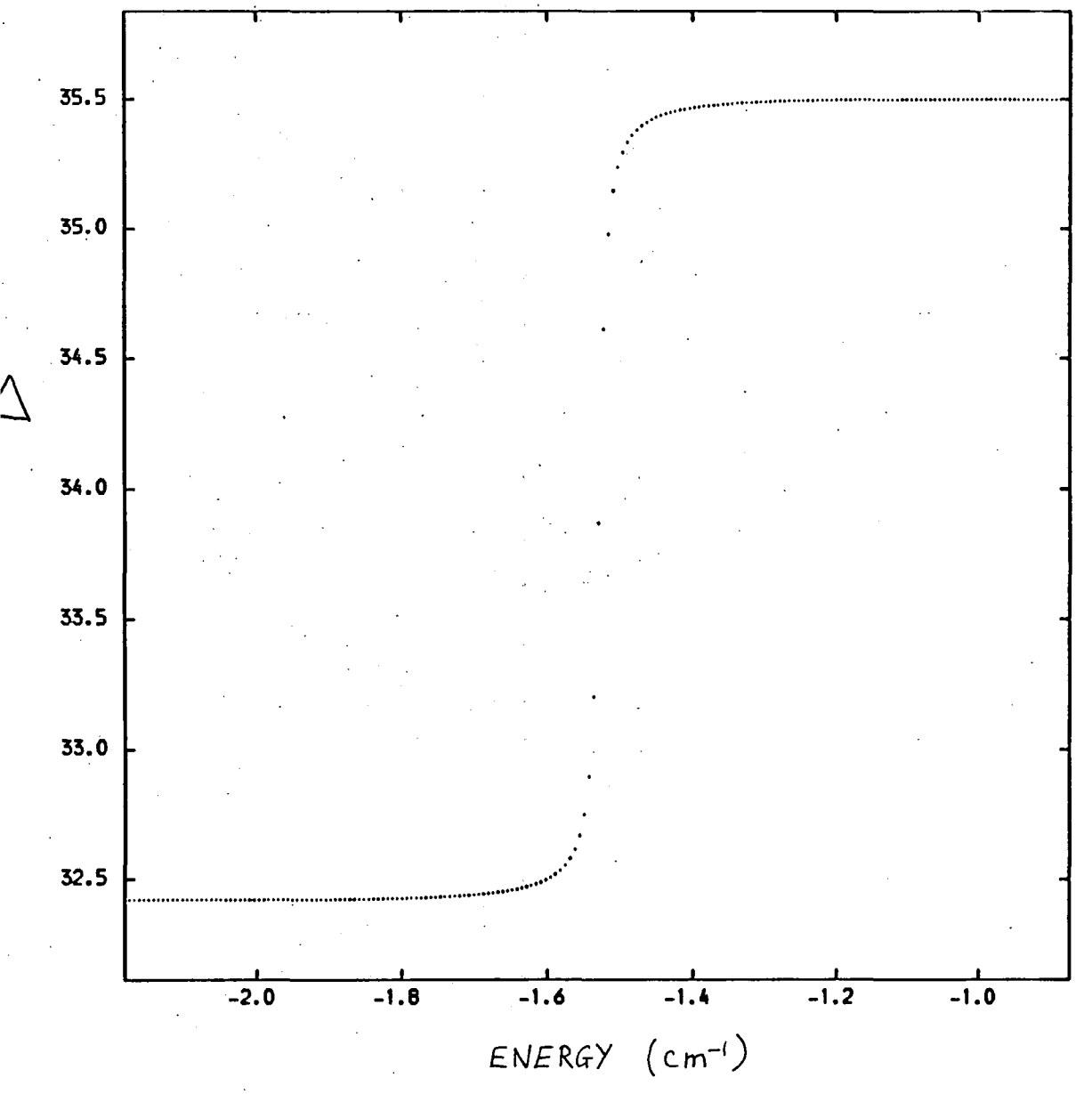

Figure 5.3

The behaviour of the eigenphase sum, Δ , in the region of the $J^{\mathcal{E}i} = 0^{++}$ Feshbach resonance correlating with $(j_1, j_2, \ell) = (2,0,2)$ or $(0,2,2)$. The energy is measured relative to the $S_o(0)$ threshold.

Resonance energy (cm^{-1}) relative to E_T

(a) FPT = 10

RFN \ RDB	1	2	3
20		-1.52878	
27		-1.52881	
40	-1.52881	-1.52881	-1.52881

(b) FPT = 20

RFN \ RDB	1	2	3
20		-1.52880	
27		-1.52882	
40	-1.52882	-1.52882	-1.52882

TABLE 5.7

The energy of the $J^{\varepsilon i} = 0^{++}$ resonance, correlating with $(j_1, j_2, \ell) = (0,2,2)$ or $(2,0,2)$, for different values of the de Vogelaere integration parameters. RDB ($\equiv R_{min}$) and RFN ($\equiv R_{max}$) determine the integration range, in a.u., in the Launay (1977, 1978) scattering programme. Twice as many steps are taken in (b) than in (a) (parameter FPT). Energies are quoted in cm^{-1}, relative to threshold : 179.078 cm^{-1}. The calculations were performed with two rotational states on each D_2.

Resonance width (cm^{-1}).

(a) FPT = 10

RFN \ RDB	1	2	3
20		0.0153732	
27		0.0153726	
40	0.0153723	0.0153725	0.0153722

(b) FPT = 20

RFN \ RDB	1	2	3
20		0.0153728	
27		0.0153724	
40	0.0153724	0.0153725	0.0153724

TABLE 5.8

The full width at half maximum of the $J^{\varepsilon i} = 0^{++}$ resonance, correlating with $(j_1, j_2, \ell) = (0,2,2)$ or $(2,0,2)$, for different values of the de Vogelaere integration parameters. Refer to the analogous resonance energy results (Table 5.7).

was found to be 0.003 for the chosen parameters. The overall accuracy of the results, for the given potential surface, will be determined by basis set truncation which we now briefly illustrate.

In Table 5.9, results are given for 2-rotor and 3-rotor state calculations of resonances and bound states correlating with $(j_1, j_2) = (0,2)$ or $(2,0)$. Coupling to the $j_1 = j_2 = 0$ state is responsible for predissociation. This channel is not present in the calculations which yield the bound states. The addition of a third rotor state ($j = 4$) to each D_2 shifts the bound state/ resonance energy downwards by $\lesssim 0.02$ cm^{-1}. For resonances lying below threshold (negative energies) the widths given by the two-rotor runs are accurate to 2 significant figures.

The error in the width is somewhat greater for the $J^{\varepsilon i} = 1^{--}$ resonance lying just above threshold. The increased error is due to fitting difficulties arising from a change in the background eigenphase sum on crossing the $S_o(0)$ threshold. In a multi-channel analogue of Levinson's theorem (e.g. Child 1974) the eigenphase sum is continuous across a threshold, though its derivative with respect to energy is in general not. The eigenphase sum for this resonance is illustrated in Figure 5.4. The fitting error was investigated by carrying out a number of fits for which the energy range and grid were varied. Changes in E_r and Γ of up to 0.0007 and 0.001 cm^{-1} respectively were found. The values quoted in Table 5.9 are those which gave the lowest mean residue (Tennyson

$J^{\varepsilon i}$	2-rotor states (cm^{-1})		3-rotor states (cm^{-1})	
	energy	width	energy	width
0^{++}	-1.5288	0.0154	-1.5421	0.0156
1^{--}	-5.9127	0.00419	-5.9332	0.00423
1^{--}	0.1040	0.0374	0.0942	0.0336
0^{+-}	-5.9359	0.0	-5.9607	0.0
1^{-+}	-6.2359	0.0	-6.2594	0.0
1^{-+}	-0.8051	0.0	-0.8181	0.0
2^{--}	-5.1426	0.0	-5.1579	0.0
2^{--}	-1.3403	0.0	-1.3531	0.0

TABLE 5.9

Convergence with respect to basis set size for resonances and bound states correlating to (j_1, j_2) = (0,2) or (2,0). Energies are quoted relative to the first excited rotational state of D_2, viz. E(j = 2) = 179.078 cm^{-1}. For the bound states, which have zero width, (j_1, j_2) = (0,0) is not present in the close-coupled equations.

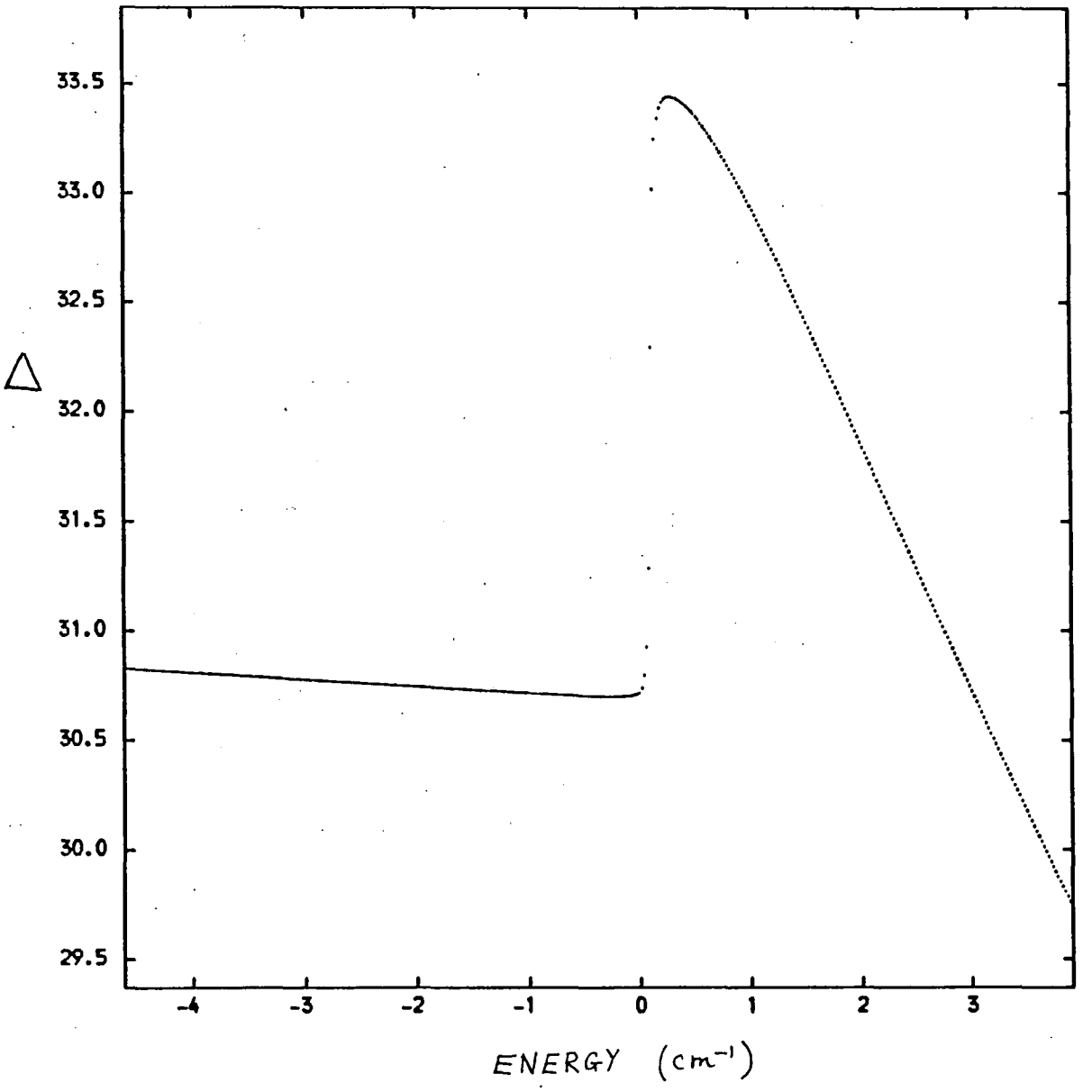

Figure 5.4

The behaviour of the eigenphase sum, Δ(radians), in the region of the $J^{\varepsilon i} = 1^{--}$ resonance correlating with $(j_1, j_2, \ell) = (2,0,3)$ or $(0,2,3)$. Since the resonance lies just above the $S_o(0)$ threshold (zero on our energy scale) it has dual Feshbach/Shape character. Note also the change in the background Δ on crossing threshold.

Noble 1984). It is interesting to note that this resonance has dual Feshbach/Shape character. It can predissociate either by transferring D_2 rotational energy to the van der Waals bond, or by tunnelling through the centrifugal barrier of the effective channel potential. We consider only the total width here, but this dual character could be quantified by calculating the partial widths; these may be found from the energy dependence of the individual eigenphases, δ_α (Hazi 1979).

Close coupling calculations with two rotor states per D_2 will be adequate, though we note that direct potential coupling to j = 4 states is thus neglected. Inclusion of j = 4 on each D_2 would involve integrating up to 64 (for $J^{\varepsilon i} = 6^{++}$) coupled equations even when interchange blocking is taken into account.

5.3.2 Results

Results for all levels correlating with $\ell = 0 - 4$ and $(j_1, j_2) = (0,2)$ or $(2,0)$ are given in table 5.10. These levels form the upper states of the $S_o(0)$ absorption spectrum; they are separated from the lower states, given in Table 5.3, by 179.078 cm^{-1}. The levels are all split into interchange doublets. Below threshold, one or both members of each doublet are bound, according to the rules discussed above. All of the states correlating with $\ell = 4$ are resonances. For these the separation of individual doublet members is less than the predissociation width. The Launay scattering code, which does not symmetrize with respect to interchange, does not resolve these. An estimate of E_r and Γ can be obtained by treating

J	ε	i	l	ENERGY (CM-1)	WIDTH (CM-1)
2	1	1	0	-6.36581	0.00459
2	1	-1	0	-6.42676	0.0
1	-1	1	1	-6.23589	0.0
1	-1	-1	1	-5.91269	0.00419
2	-1	1	1	-4.82906	0.0
2	-1	-1	1	-5.14265	0.0
3	-1	1	1	-5.43477	0.0
3	-1	-1	1	-5.36931	0.00564
0	1	1	2	-1.52881	0.01537
0	1	-1	2	-5.93589	0.0
1	1	1	2	-4.89587	0.0
1	1	-1	2	-1.97800	0.0
2	1	1	2	-2.63566	0.00285
2	1	-1	2	-3.83546	0.0
3	1	1	2	-3.36465	0.0
3	1	-1	2	-2.82761	0.0
4	1	1	2	-3.41717	0.00579
4	1	-1	2	-3.49852	0.0
1	-1	1	3	-0.80507	0.0
1	-1	-1	3	0.10467	0.03638
2	-1	1	3	0.32812	0.01503
2	-1	-1	3	-1.34028	0.0
3	-1	1	3	-1.02916	0.0
3	-1	-1	3	0.11618	0.00323
4	1	1	3	-0.12884	0.0
4	-1	-1	3	-0.69098	0.0
5	-1	1	3	-0.75170	0.0
5	-1	-1	3	-0.66645	0.00490
2	1	$\pm$1	4	2.51540	0.41700
3	1	$\pm$1	4	2.20813	0.85595
4	1	$\pm$1	4	2.36177	0.76816
5	1	$\pm$1	4	2.58124	0.61453
6	1	$\pm$1	4	2.40566	0.37311

TABLE 5.10

Two-rotor state results of resonance and bound state calculations on the upper states of the $S_0(o)$ absorption spectrum. Level energies are quoted relative to E(j = 2) = 179.078 cm^{-1}. Note that the levels are split into doublets, differing only in the interchange quantum number, i. Where i = $\pm$ 1 is listed this splitting is much smaller than the predissociation width.

these doublets as single resonances.

In addition to the scattering calculations on the ℓ = 0 - 3 resonances, we attempted to calculate the energies using our bound state programme. These resonance energies could all be found to within 0.008 cm^{-1} in this way. The bound state code also yields additional levels due to the continuum, made discrete by the bound state boundary conditions imposed on the wavefunction at short and long range. Probably the easiest way to distinguish resonance from continuum states would be to repeat the calculations with the $j_1 = j_2 = 0$ channel removed. Another possible application of the bound state approach is in the extrapolation to zero of the matching determinant (equation 3.32) to obtain the position of shape resonances.

Returning to the results of Table 5.10, we note that the width of the $J^{\varepsilon i} = 0^{++}$, $\ell = 2$ resonance is at least 2.7 times greater than any of the other Feshbach resonances lying below threshold. A similar result was found by Le Roy et al. (1982) in an analogous study of the Ar - H_2 dimer. The J = 0, ℓ = 2 resonance for that system was over twice as broad as any other correlating with j = 2 (and V = 1). the reason for this may be found in the angular potential matrix elements between rotational basis functions (Hutson and Le Roy 1983). Inspection of the potential matrix elements given in Chapter two shows that only the $V_{200}Y^i_{200}$ term in the potential expansion (equation 2.37) is responsible for internal-rotational predissociation of the $S_o(0)$ levels in D_4. Measurements

of line widths, though currently not feasible for these narrow resonances, may therefore, be expected to yield useful information on the potential anisotropy.

Consider now the tunnelling doubling of states which differ only in their interchange symmetry. This splitting can be rationalised in terms of first order degenerate perturbation theory. To illustrate this, we shall make a number of simplifications. All levels, including the resonances, are treated as discrete states. In addition we assume that the total wavefunction of any member of a J multiplet may be represented by $|n\rangle\,|j_1 j_2 \ell\, J\rangle$, where this is shorthand for $\frac{1}{R}F(j_1 j_1 j_{12}\, \ell\, JM\varepsilon\,|\,R)\,\mathcal{Y}(j_1 j_2 j_{12}\, \ell\, JM\varepsilon\,|\,\hat{\underset{\sim}{r}}_1', \hat{\underset{\sim}{r}}_2', \hat{\underset{\sim}{R}})$ (see equation 2.10 for further details). In other words j_1, j_2, j_{12} and ℓ are treated as good quantum numbers and space-fixed basis functions are appropriate. The degeneracy of the $|n\rangle\,|20\,\ell\, J\rangle$ and $|n\rangle\,|02\,\ell\, J\rangle$ states is removed by potential coupling, which we treat as the perturbation. The Hamiltonian for nuclear motion is partitioned thus:

$$H = H^{o} + V^{c} \tag{5.9}$$

where

$$H^{o} = h_1 + h_2 - \frac{1}{2\mu}\nabla_R^2 + A_{000}I_{000} + A_{202}I_{202} + A_{022}I_{022} \tag{5.10}$$

and

$$V^{c} = A_{220}I_{220} + A_{222}I_{222} + A_{224}I_{224} \tag{5.11}$$

The functions $A_{q_1 q_2 q_{12}}$ and $I_{q_1 q_2 q_{12}}$ represent respectively the radial and geometric dependence of the potential, expanded in the space-fixed frame. Further details on the terms in the equations above may be found in Chapter two. For $\ell = 2$ and $\ell = 3$, all three A_{22n} terms contribute to the interchange splitting (for $\ell = 0$ only A_{220} contributes, and for $\ell = 1$ only A_{220} and A_{222}). The dominant term is A_{224}, being over thirty times larger in magnitude than A_{220} and A_{222} near the potential minimum. Indeed, in a recent modification of the Meyer-Schaefer-Liu potential, A_{220} and A_{222} have been left out of the expansion altogether (Norman et al. 1984). We label the states $|n\rangle |20\ell J\rangle$ and $|n\rangle |02\ell J\rangle$ by 1 and 2; matrix elements of the perturbation Hamiltonian between these are given by

$$V_{11}^c = V_{22}^c = 0 \qquad (5.12a)$$

$$V_{12}^c = V_{21}^c \approx \langle n|A_{224}(R)|n\rangle \langle 20\ell J | I_{224}(\hat{r}_1', \hat{r}_2', \hat{R}) | 02\ell J\rangle \qquad (5.12b)$$

It may be shown (Bransden and Joachain 1983) that the first order energy correction, $E^{(1)}$, and the corresponding wavefunction, $a|n\rangle |20\ell J\rangle + b|n\rangle |02\ell J\rangle$, are obtained by solving the linear equations

$$a(-E^{(1)}) + b V_{12}^c = 0 \qquad (5.13a)$$

$$a V_{21}^c + b(-E^{(1)}) = 0 \qquad (5.13b)$$

With the normalisation of the wavefunctions an additional condition, two solutions are obtained:

$$E^{(1)} = V_{12}^{c}, \quad \Psi = \frac{1}{\sqrt{2}}\left(|n\rangle|20\ell J\rangle + |n\rangle|02\ell J\rangle\right) \qquad (5.14a)$$

$$E^{(1)} = -V_{12}^{c}, \quad \Psi = \frac{1}{\sqrt{2}}\left(|n\rangle|20\ell J\rangle - |n\rangle|02\ell J\rangle\right) \qquad (5.14b)$$

The space-fixed, interchange-symmetrized wavefunction is, by analogy to equation (2.35):

$$\Psi = \frac{1}{\sqrt{2}}\left(|n\rangle|20\ell J\rangle + i(-)^{\ell}|n\rangle|02\ell J\rangle\right) \qquad (5.15)$$

By comparing (5.15) with (5.14) we can predict the dependence of the interchange splitting, $\Delta E^{i} = E(i = 1) - E(i = -1)$, on the dimer angular momentum, ℓ :

$$\Delta E^{i} = \begin{Bmatrix} + \\ - \end{Bmatrix} 2 V_{12}^{c} \quad \text{for} \quad \begin{Bmatrix} \text{even} \\ \text{odd} \end{Bmatrix} \ell \qquad (5.16)$$

In Table 5.11, the value of ΔE^{i}, deduced from the full close coupling results, is compared with $2 \times \langle 20\ell J|I_{224}|02\ell J\rangle$ for $\ell = 2$ and 3. These quantities have been scaled such that for one member of each J multiplet (constant ℓ) they agree in magnitude. This is tantamount to assuming that the radial matrix element, $\langle n|A_{224}|n\rangle$, is constant for states correlating to the same ℓ. Noting that A_{224} is always positive (Schaefer 1982b), we see that perturbation theory correctly predicts the sign and gives broad agreement with the relative magnitude of the interchange splitting. The angular matrix elements were evaluated from the expression given by Green (1975), which is the space-fixed analogue of the body-fixed expression given earlier in this thesis (equation 2.29). We mention in passing that if the radial matrix element is approximated

	J^{ε}	ΔE^i	$2x\langle 20\ell J \mid I_{224} \mid 02\ell J\rangle$
(a) $\ell = 2$			
	0^+	1 (4.407)*	1 (0.09659)*
	1^+	-0.66	-0.67
	2^+	0.27	0.29
	3^+	-0.12	-0.07
	4^+	0.02	0.008
(b) $\ell = 3$			
	1^-	-1 (-0.910)*	1 (0.03220)*
	2^-	1.83	-1.50
	3^-	-1.26	1.00
	4^-	0.62	-0.33
	5^-	-0.09	0.05

TABLE 5.11

A comparison of the interchange splitting, ΔE^i, of the levels in Table 5.10 with (twice) the angular matrix element, $\langle 20\ell J \mid I_{224} \mid 02\ell J\rangle$. Perturbation theory predicts that these quantities should be proportional, differing in sign for odd ℓ (see text). The quantities have been scaled to agree in magnitude for the lowest J member of each multiplet corresponding to (a) $\ell = 2$ and (b) $\ell = 3$.

* Actual (i.e. unscaled) values are given in brackets.

by the value of A_{224} at the effective radial separation, $R_{eff} = 4.1\text{Å}$, determined from the rotational constant in the preceding section, then the absolute value of the splitting of the $J^{\varepsilon} = 0^+$ level is correctly predicted to within 10%. While this is far from rigorous (choosing A_{224} near the potential minimum, $R \approx 3.5\text{Å}$, results in a splitting twice as large) it does at least indicate that the size of the tunnelling doubling is reasonable.

To summarise, the interchange splitting discussed here is due to the interaction between the electrostatic quadrupole moments of the D_2 molecules. Experimental measurements of transitions involving these levels would yield information mainly on the A_{224} coefficient in the space-fixed potential expansion or the V_{220} and V_{221} terms in the body-fixed. Choosing the two most widely split states as examples, V_{220} breaks the degeneracy of the $J^{\varepsilon} = 0^+$ ($\ell = 2$) level and V_{221} that of $J^{\varepsilon} = 1^+$($\ell = 2$).

To deduce the $S_o(0)$ absorption spectrum, we need to know the electric dipole selection rules for transitions between the upper levels of table 5.10 and the lower levels of Table 5.3. Allowed transitions occur between states whose irreducible representations are connected by that of the dipole moment. The selection rules derived by Brocks and van der Avoird (1985), using group theoretical arguments, are consistent with the standard electric dipole selection rules, namely: change in parity, no change in interchange symmetry, and $\Delta J = 0, \pm 1$ ($0 \nleftrightarrow 0$). The latter rule comes from vector coupling

arguments.

In Table 5.12 we give the transition frequencies for the dimer spectrum accompanying the far infrared $S_o(0)$ transition of the free D_2 molecule:

$$(v_1'', j_1'', v_2'', j_2'') = (0,0,0,0) \longrightarrow (v_1', j_1', v_2', j_2') = (0,2,0,0) \text{ or } (0,0,0,2)$$

The transition frequencies are given relative to the unperturbed $S_o(0)$ quadrupole frequency of a D_2 molecule. The linewidth is the sum of the widths of the two levels participating in the transition. The table labels the initial and final states by the good quantum numbers J, ε and i together with the value of ℓ to which they correlate. The results are plotted in Figure 5.5. The band origin is taken as the zero of frequency. Lines of finite width are represented by Lorentzian profiles of unit normalisation, i.e.

$$L(\nu) = \frac{1}{2\pi} \frac{\Gamma}{(\nu-\nu_0)^2 + \Gamma^2/4} \qquad (5.17)$$

and

$$\int L(\nu)\, d\nu = 1 \qquad (5.18)$$

Here, ν_o is the line frequency and Γ the linewidth as given in Table 5.12. The constant normalisation of the Lorentzians means that we are assuming, in the absence of quantitative intensity information, that the total energy absorbed in each line is equal. See, for example, the discussion on the absorption cross-section in Merzbacher (1961). Contributions from overlapping lines are simply

J"	ε"	i"	l"	-->	J'	ε'	i'	l'	FREQUENCY (CM-1)	WIDTH (CM-1)
0	1	1	0		1	-1	1	1	-0.1538	0.0
0	1	1	0		1	-1	1	3	5.2770	0.0
1	-1	-1	1		0	1	-1	2	-0.8331	0.0
1	-1	-1	1		1	1	-1	2	3.1248	0.0
1	-1	-1	1		2	1	-1	0	-1.3240	0.0
1	-1	-1	1		2	1	-1	2	1.2673	0.0
1	-1	-1	1		2	1	0	4	7.6182	0.4170
2	1	1	2		1	-1	1	1	-3.0415	0.0
2	1	1	2		1	-1	1	3	2.3893	0.0
2	1	1	2		2	-1	1	1	-1.6347	0.0
2	1	1	2		2	-1	1	3	3.5225	0.0150
2	1	1	2		3	-1	1	1	-2.2404	0.0
2	1	1	2		3	-1	1	3	2.1652	0.0
3	-1	-1	3		2	1	-1	0	-5.9317	0.0
3	-1	-1	3		2	1	-1	2	-3.3404	0.0
3	-1	-1	3		3	1	-1	2	-2.3325	0.0
3	-1	-1	3		4	1	-1	2	-3.0035	0.0
3	-1	-1	3		2	1	0	4	3.0105	0.4170
3	-1	-1	3		3	1	0	4	2.7032	0.8560
3	-1	-1	3		4	1	0	4	2.8568	0.7682
4	1	1	4		3	-1	1	1	-8.0361	0.5495
4	1	1	4		3	-1	1	3	-3.6305	0.5495
4	1	1	4		4	-1	1	3	-2.7302	0.5495
4	1	1	4		5	-1	1	3	-3.3531	0.5495

TABLE 5.12

Transition frequencies and line widths of the $S_0(o)$ dimer spectrum in pure ortho-deuterium. Frequencies are quoted relative to the $j'' = 0 \rightarrow j' = 2$ quadrupole transition of a free D_2 molecule.

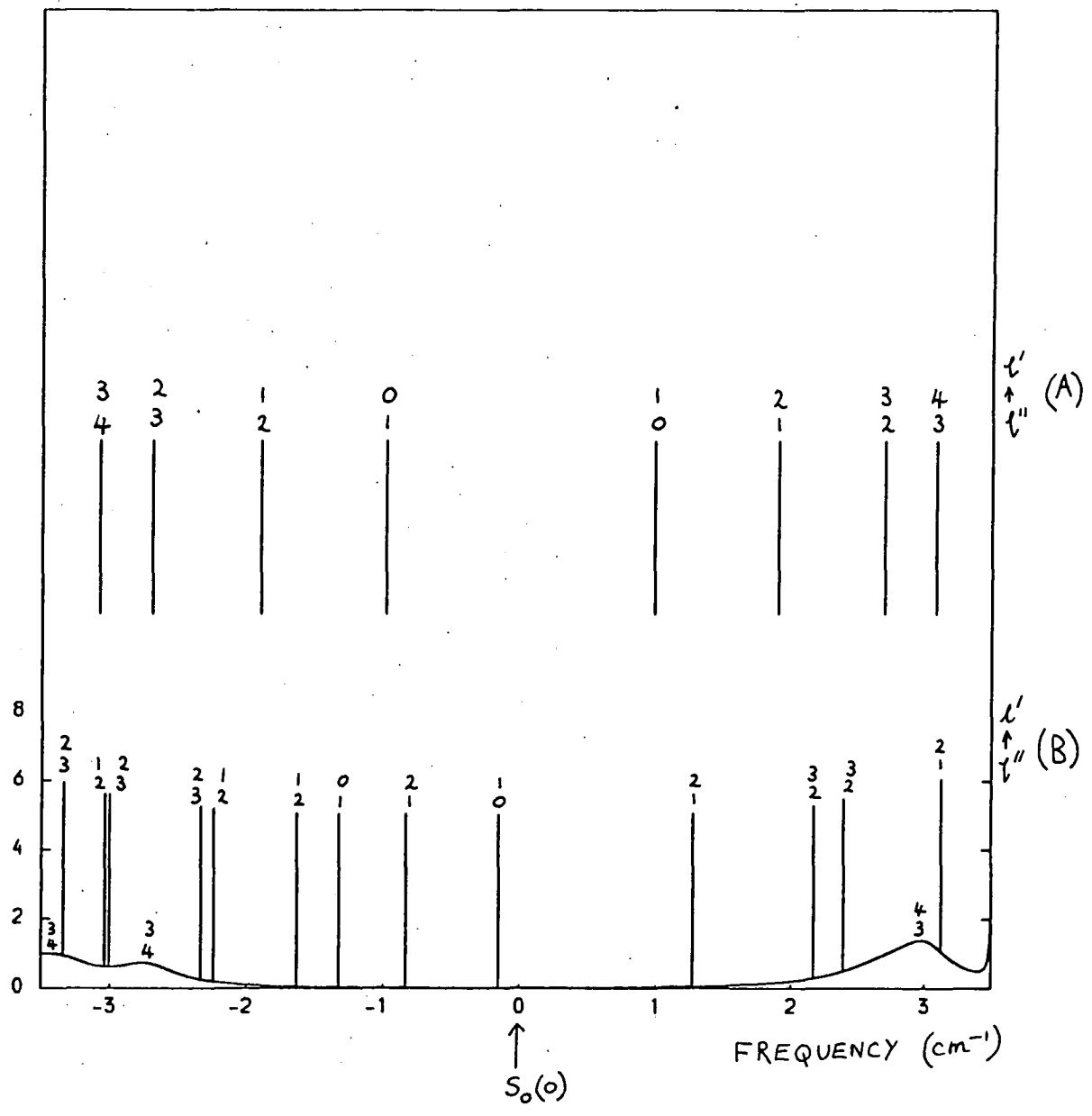

Figure 5.5

The dimer structure accompanying the far infrared $S_0(0)$ monomer transition in pure ortho-deuterium. (A) shows the results obtained using a purely isotropic interaction V_{000}. These lines are labelled by the pure $\ell'' \rightarrow \ell'$ transitions to which they correspond. These serve as markers for the full close coupling results, shown in (B), which are labelled according to the ℓ states to which the initial and final levels correlate. The units of the vertical scale are arbitrary.

summed. For transitions between bound states, the plotting convention leads to delta functions (radiative lifetimes are assumed to be infinite); these we represent by sticks of equal height. We also do this for any lines with widths, $\Gamma < 0.007$ cm^{-1}, for ease of plotting.

In the upper part of Figure 5.5 are plotted theoretical pure ℓ transitions, deduced from 1-rotor state calculations on 0-0 $(D_2)_2$. Comparison of the predicted spectrum with these pure ℓ lines illustrates the departure of the system from potential isotropy. Note the random pattern of the spectrum, particularly with regard to the labelling of the transitions based on the ℓ correlations of Table 5.12. The importance of the potential anisotropy is such that two lines ($\ell'' = 1 \rightarrow \ell' = 2$ and $\ell'' = 0 \rightarrow \ell' = 1$) are shifted across the band origin; ℓ alone is clearly insufficient to label the transitions.

No observations of dimer structure in the far infrared spectrum have been reported. It is pertinent, however, to consider what information on the intermolecular potential could be gleaned from any such spectra. One line of interest, as has already been mentioned, is $J^{\varepsilon i} = 1^{--} \rightarrow 0^{+-}$ ($\ell = 1 \rightarrow 2$) which lies about 0.83 cm^{-1} below the band origin. The interchange splitting of the final state is large, yielding information either on the space-fixed A_{224} coefficient or the body-fixed V_{220}. This line is flanked by two transitions between $\ell = 0$ and 1 states; it is therefore useful to consider the relative intensity of these three lines to determine whether the one of interest is likely to be observed or "swamped" by those

adjacent to it. Detailed information on line intensities requires a knowledge of both the wavefunctions of the initial and final states and the dipole moment function. The collision-induced dipole $\underset{\sim}{\mu}$ of the dimer can be expanded in either the space-fixed (Poll and van Kranendonk 1961) or body-fixed (Brocks and van der Avoird 1985) frame in much the same way as the potential, though a difference arises in that $\underset{\sim}{\mu}$ is a vector and the potential a scalar. As we employ the end-over-end rotation ℓ in our analysis, we consider the space-fixed expansion.

For the two rigid rotors, the dipole is a function of the dimer geometry and the intermolecular separation. The spherical components ($\nu = 0, \pm 1$) of $\underset{\sim}{\mu}$ are given by an expression of the form (Poll and Hunt 1976, 1981; Moraldi et al. 1984):

$$\mu_\nu(\hat{r}_1', \hat{r}_2', R) = \frac{(4\pi)^{3/2}}{(2r+1)^{1/2}} \sum_{\lambda_1\lambda_2\lambda_{12}L} B_{\lambda_1\lambda_2\lambda_{12}L}(R)\, Y^{r\nu}_{\lambda_1\lambda_2\lambda_{12}L}(\hat{r}_1', \hat{r}_2', \hat{R}) \qquad (5.19)$$

The function Y is a vector contraction of tensors (Rose 1957) similar in form to equation (2.10). For a dipole field, the rank r = 1. Frommhold et al. (1984) have shown that in the H_2 - H_2 dimer the most important components of $\underset{\sim}{\mu}$, accounting for 98% of the total intensity in the $S_0(0)$ region, are B_{0223} and B_{2023}. The same conclusion should hold for D_2 - D_2 which has a similar electronic structure. These coefficients are due to the dipole induced in one molecule by the permanent quadrupole of its neighbour:

$$B_{0223}(R) = -B_{2023}(R) \approx \sqrt{3}\, \propto \Theta / R^4 \qquad (5.20)$$

α and Θ are respectively the spherically averaged polarisability and quadrupole moment of the identical molecules. The transition strength of a spectral line is found from the matrix element of the dipole operator between the initial and final states (Geraedts et al. 1982b, Nicholls and Stewart 1962). The angular contribution to the matrix element consists essentially of a product of 3-j symbols, together with some weighting factors (Frommhold et al. 1984). The properties of these 3-j symbols lead to selection rules for the individual terms in the dipole expansion. The presence of the 3-j symbol $\begin{pmatrix} \ell'' & L & \ell' \\ 0 & 0 & 0 \end{pmatrix}$ leads to the conclusion that $\ell = 0 \leftrightarrow 1$ transitions cannot be driven by the dominant quadrupole-induced dipole for which L = 3 (equation 5.20). These transitions will be allowed by weaker components of the dipole function, subject to the general dipole selection rules.

It should be stressed that the intensity arguments above do not account for the mixing of different values of ℓ caused by the potential anisotropy. Nevertheless, we expect that the $\ell'' = 1 \rightarrow \ell' = 2$ line under consideration should be relatively prominent, being flanked by two lines of much weaker intensity. There should therefore, be little difficulty in identifying this line if sufficiently sensitive experiments were to be performed. A combination of longer path lengths, lower temperatures and lower gas densities, than those hitherto employed in gas cell absorption experiments, is needed.

5.4 The $S_1(0)$ and $Q_1(0) + S_o(0)$ spectra of ortho-D_2-ortho-D_2

While no observations of dimer structure at far infrared wavelengths have yet been obtained, McKellar and Welsh (1974) have reported a detailed absorption spectrum in the near infrared accompanying the single $S_1(0)$ and double $Q_1(0) + S_o(0)$ transitions of ortho-D_2. The upper states of the dimer in this region can be calculated using the rigid rotor formalism of Chapter two, if a number of assumptions are made. All coupling of monomer vibrational states is neglected. Thus we ignore vibrational predissociation from $(V_1,V_2) = (1,0)$ or $(0,1)$ to $(V_1,V_2) = (0,0)$. Work on complexes of Ar with D_2 or H_2 suggests that this assumption is valid; the widths for vibrational predissociation are much smaller than those for rotational (Hutson et al. 1983, Kidd and Balint-Kurti 1985). Furthermore, the sets of states with $(V_1,V_2) = (1,0)$ and $(0,1)$ are assumed to be decoupled. All dimer levels correlating to one vibrationally excited monomer will be split into (we assume) unresolvable interchange doublets. This assumption has also been made by Brocks and van der Avoird (1985) in their study of the N_2-N_2 dimer. Its validity rests upon the relative insensitivity of the intermolecular potential to monomer vibration, though qualifications to this statement will have to be made when we come to discuss the resonance widths. The approximation that the potential remains unchanged under rotational

as well as vibrational excitation of the interacting monomers continues to be made. Under the above conditions, the problem reduces to that of two distinguishable rigid rotors and the treatment of Section 2.2. applies. Within these constraints, rotational splitting in the J multiplets is the only cause of any departure of the calculated level energies from the isotropic ℓ states.

The channel energies used in the calculations are given in Figure 5.6. The monomer vibrational quantum numbers given there are for labelling purposes only; they do not enter explicitly into the close coupling calculations . The zero of energy is, in actuality, shifted upwards relative to that of the initial states in table 5.3 by the fundamental frequency of D_2, viz 2993.962 cm^{-1} (Bishop and Shih 1976). Note also that the states, $|n\rangle |20\ell J\rangle$ and $|n\rangle |02\ell J\rangle$, are no longer degenerate when the potential coupling is removed. As indicated in Figure 5.6, the calculations were carried out with two rotor states ($j = 0,2$) on each monomer. Inclusion of $j = 4$ would involve solving systems of up to 114 (for $J = 6^+$) close coupled equations. The numerical integration parameters employed are those determined earlier in this chapter. Parity conservation results in a few bound states, though it should be noted that these will in reality be vibrationally predissociative. The remaining states can decay by rotational predissociation.

The calculated energies and widths, together with the monomer states and ℓ levels to which they correlate, are given in Table 5.13. The levels correlating to the

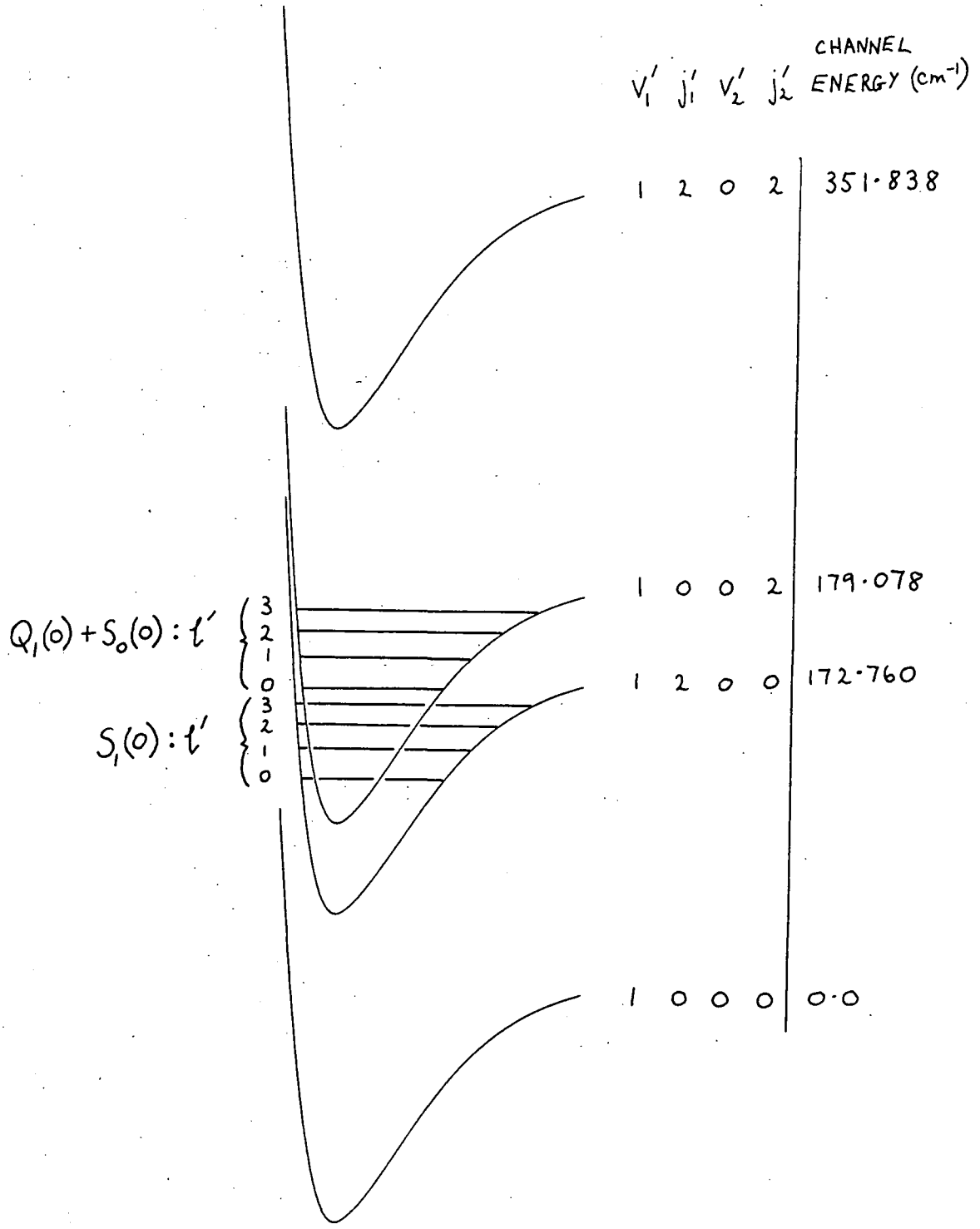

Figure 5.6

The basis set and channel energies used in our modelling of the $S_1(0)$ and $Q_1(0) + S_0(0)$ spectra of o-o $(D_2)_2$. The fundamental frequency of D_2 (2993.962 cm^{-1}) was taken as the zero of energy in the close-coupling calculations. As indicated (schematically) the final l' levels of the single and double monomer transitions are closely spaced and will interact strongly. The lower l'' states, corresponding to the channel with $(v_1'', j_1'', v_2'', j_2'')$ = (0,0,0,0), do not participate because vibrational coupling is neglected in our model.

			(a) $S_1(0)$ STATES		(b) $Q_1(0)+S_o(0)$ STATES	
J	ε	I	ENERGY (CM-1)	WIDTH (CM-1)	ENERGY (CM-1)	WIDTH (CM-1)
2	1	0	-6.28325	0.00295	-0.49536	0.00126
1	-1	1	-5.72214	0.00372	1.74747	0.30487
2	-1	1	-4.90821	0.0	1.63318	0.06446
3	-1	1	-5.33292	0.00333	0.81693	0.00774
0	1	2	-4.37193	0.00454	3.27660	0.73509
1	1	2	-3.72840	0.0	3.19176	0.32173
2	1	2	-3.24786	0.00142	3.81358	0.70219
3	1	2	-3.05703	0.0	3.65990	0.39297
4	1	2	-3.41411	0.00325	2.92680	0.31260
1	-1	3	-1.96870	0.00020	5.87366	0.35816
2	-1	3	-0.91053	0.0	5.93074	0.20677
3	-1	3	-0.53010	0.00068	5.70968	0.32700
4	-1	3	-0.39061	0.0	5.71137	0.30362
5	-1	3	-0.68249	0.00266	5.53068	0.04425
2	1	4	2.37408	0.21109	8.90568	0.70289
3	1	4	2.17542	0.22770	8.98279	0.73221
4	1	4	2.49895	0.26460	8.97057	0.71819
5	1	4	2.67862	0.59765	8.93221	0.62089
6	1	4	2.46589	0.45394	8.73831	0.43298

TABLE 5.13

Two-rotor state results for the (interacting) upper states of the (a) $S_1(o)$ and (b) $Q_1(o) + S_o(o)$ absorption spectra. All levels correlating to the first five ℓ states are listed, the energies measured relative to the $S_1(o)$ threshold (3166.722 cm^{-1}). With the approximations made (see text), each level is a rigorously degenerate interchange doublet ($i = \pm 1$) and purely vibrationally predissociative states are bound.

singly and doubly excited dimer are mixed by the same terms in the potential expansion responsible for tunnelling doubling in the $S_o(0)$ spectrum. With only two exceptions, the widths of the $Q_1(0) + S_o(0)$ upper states are greater than their $S_1(0)$ counterparts. This is due to additional predissociation pathways for the former set of levels; the rotational energy of one monomer can transfer to the other, vibrationally excited, molecule. One of the two exceptions is the $J^{\varepsilon} = 2^+$, $\ell = 0$ pair, where both states lie below the asymptote of the effective channel potential for $(V_1, j_1, V_2, j_2) = (1,2,0,0)$.

As before, we may use the electric dipole selection rules to predict the near infrared absorption spectrum for which these levels are the final states. Each of the upper levels will be finely split into a doublet, the members of which differ only in the interchange quantum number, i. One member of the doublet will contribute to any particular line providing the transition satisfies the selection rules: change of parity and $\Delta J = 0, \pm 1$ $(0 \not\leftrightarrow 0)$. What can be thought of as a relaxation of the "no change in i" rule is consistent with the results of Brocks and van der Avoird who used symmetry arguments and the vanishing integral rule (Bunker 1979a). Thus we predict, in Table 5.14(a), the $S_1(0)$ near infrared absorption spectrum of D_2 - D_2, using the results of Tables 5.13 and 5.3:

$(V_1'', j_1'', V_2'', j_2'') = (0,0,0,0) \rightarrow (V_1', j_1', V_2', j_2') = (1,2,0,0)$

J"	ε"	i"	I"	⟶	J'	ε'	i'	I'	(a) $S_1(0)$ TRANSITIONS FREQUENCY (CM-1)	(a) $S_1(0)$ TRANSITIONS WIDTH (CM-1)	(b) $Q_1(0)+S_0(0)$ TRANSITIONS FREQUENCY (CM-1)	(b) $Q_1(0)+S_0(0)$ TRANSITIONS WIDTH (CM-1)
0	1	1	0		1	-1	1	1	0.3599	0.0037	7.8295	0.3049
0	1	1	0		1	-1	1	3	4.1134	0.0002	11.9557	0.3582
1	-1	-1	1		0	1	-1	2	0.7309	0.0045	8.3794	0.7351
1	-1	-1	1		1	1	-1	2	1.3744	0.0	8.2946	0.3217
1	-1	-1	1		2	1	-1	0	-1.1804	0.0030	4.6074	0.0013
1	-1	-1	1		2	1	-1	2	1.8549	0.0014	8.9164	0.7022
1	-1	-1	1		2	1	-1	4	7.4769	0.2111	14.0085	0.7029
2	1	1	2		1	-1	1	1	-2.5278	0.0037	4.9418	0.3049
2	1	1	2		1	-1	1	3	1.2257	0.0002	9.0680	0.3582
2	1	1	2		2	-1	1	1	-1.7139	0.0	4.8275	0.0645
2	1	1	2		2	-1	1	3	2.2838	0.0	9.1251	0.2068
2	1	1	2		3	-1	1	1	-2.1386	0.0033	4.0113	0.0077
2	1	1	2		3	-1	1	3	2.6643	0.0007	8.9040	0.3270
3	-1	-1	3		2	1	-1	0	-5.7882	0.0030	-0.0003	0.0013
3	-1	-1	3		2	1	-1	2	-2.7528	0.0014	4.3086	0.7022
3	-1	-1	3		2	1	-1	4	2.8691	0.2111	9.4007	0.7029
3	-1	-1	3		3	1	-1	2	-2.5620	0.0	4.1550	0.3930
3	-1	-1	3		3	1	-1	4	2.6705	0.2277	9.4779	0.7322
3	-1	-1	3		4	1	-1	2	-2.9190	0.0032	3.4219	0.3126
3	-1	-1	3		4	1	-1	4	2.9940	0.2646	9.4656	0.7182
4	1	1	4		3	-1	1	1	-7.9343	0.5528	-1.7844	0.5572
4	1	1	4		3	-1	1	3	-3.1315	0.5502	3.1083	0.8765
4	1	1	4		4	-1	1	3	-2.9920	0.5495	3.1100	0.8531
4	1	1	4		5	-1	1	3	-3.2839	0.5522	2.9293	0.5937

TABLE 5.14

Transition frequencies and line widths of the near infrared dimer absorption spectrum in pure ortho-deuterium. Frequencies are quoted relative to the V", j" = 0, $0 \longrightarrow V'$, j' = 1,2 transition of a free D_2 molecule; this quadrupole transition was not observed in the experiments of McKellar and Welsh (1974). For convenience only, the lines are additionally classified according to whether the final state corresponds to an (a) $S_1(o)$ or (b) $Q_1(o) + S_o(o)$ transition. The interchange of the final state, i', is assigned according to the electric dipole selection rules.

Similarly, we give in Table 5.14(b) the dimer spectrum for the case where one D_2 molecule undergoes a vibrational transition ($Q_1(0)$) while the other is simultaneously excited rotationally ($S_o(0)$):

$$(v_1'', j_1'', v_2'', j_2'') = (0,0,0,0) \longrightarrow (v_1', j_1', v_2', j_2') = (1,0,0,2)$$

All transition frequencies are quoted relative to the unperturbed $S_1(0)$ frequency of D_2.

5.4.1 The $S_1(0)$ region

The predicted spectrum in the region of the $S_1(0)$ transition of D_2 is illustrated in the lower part of Figure 5.7. As with the $S_o(0)$ spectrum, represented earlier, Lorentzians normalised to unity are used to plot all lines of width > 0.007 cm^{-1}. The lines are labelled according to the values of ℓ to which the initial and final states correlate. Overlapping $Q_1(0) + S_o(0)$ lines are also plotted. The importance of the potential anisotropy is illustrated by the departure of this computed spectrum from the pure ℓ markers which are plotted above; these are obtained from the solution of single isotropic Schroedinger equations.

At the top of Figure 5.7 are given the experimental line positions obtained by McKellar and Welsh (1974). These are plotted relative to the free quadrupole frequency of D_2. It should be noted, however, that there will be a small negative vibrational frequency shift. An estimate of this is provided by the value deduced by McKellar and Welsh from the $Q_1(0)$ spectrum, viz - 0.15 cm^{-1}. We could (but don't) simulate the effect of perturbations on the free D_2 frequency by negatively shifting all

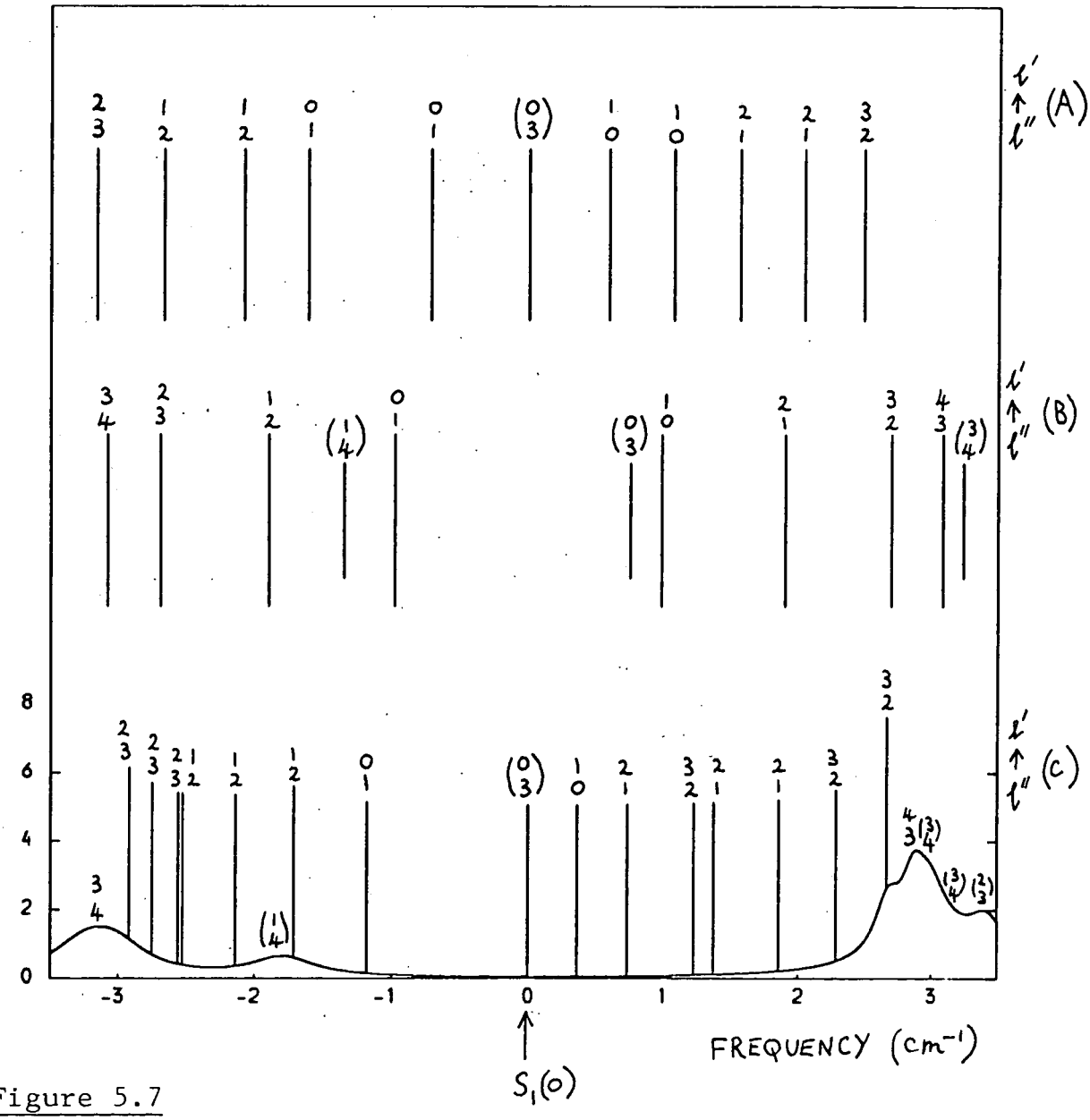

Figure 5.7

The dimer structure in the region of the near infrared $S_1(0)$ monomer transition in pure ortho-deuterium. (A): Line positions and assignments derived from the measurements of McKellar and Welsh (1974). The brackets around the $l'' = 3 \rightarrow l' = 0$ line denote that this is a $Q_1(0) + S_o(0)$ feature. The experimental resolution was 0.25 cm^{-1}. (B) : Theoretical results obtained assuming an isotropic potential. The labelling quantum number l is good in this approximation. $Q_1(0) + S_o(0)$ lines are shorter with assignments in brackets (C) : Theoretical spectrum obtained from Table 5.14.

experimental lines by this amount; this approximation would ignore any l (McKellar and Welsh 1971) or j (May et al. 1961) dependence of the shift. The actual spectrum shows marked differences in intensity between lines; this will be due partly to different individual transition strengths, and partly to the net contribution of lines too closely spaced to be resolved. The experimental resolution was 0.25 cm^{-1} in the D_2 fundamental region, $3.1 < \lambda < 3.3$ μm.

The l quantum number is clearly insufficient to uniquely label the lines in the theoretical spectrum. The same conclusion holds also for the experimental spectrum, as can be seen from the need of McKellar and Welsh to assign doublets to the l transitions $0 \leftrightarrow 1$ and $1 \leftrightarrow 2$. Even without direct reference to the theoretical spectrum, we can deduce, from considerations of angular momentum coupling and the dipole selection rules, that neither of the $0 \leftrightarrow 1$ transitions can be a doublet. The initial l levels are, for the 0 - 0 system, all singlets. The final state of the $l'' = 1 \rightarrow l' = 0$ transition is also a singlet with good quantum numbers denoted by $J^{\varepsilon} = 2^{+}$. The $l' = 1$ upper state is a triplet but only $J^{\varepsilon} = 1^{-}$ can contribute to the $l'' = 0 \rightarrow l' = 1$ transition due to the selection rule on J.

Furthermore, an intensity problem arises when we try to match these lines to our results. Reference to Figure 3 of McKellar and Welsh (1974) shows that each experimental $0 \leftrightarrow 1$ "doublet" consists of one strong and

one weak line, the strong members being immediately on either side of an intense $Q_1(0) + S_o(0)$ $l'' = 3 \rightarrow l' = 0$ feature. This feature is near to the band origin, and is close to the corresponding theoretical position (refer to Figure 5.7). Assuming this "reference" assignment to be correct, our results indicate that the genuine $0 \longleftrightarrow 1$ transitions should be assigned in both cases to the strong members of the experimental "doublets". However, arguments based on the strength of the collision induced dipole components, similar to those presented for the $S_o(0)$ spectrum, imply that the $S_1(0)$ $0 \longleftrightarrow 1$ lines should be very weak (Watanabe and Welsh 1964). These arguments assume l is a good quantum number, and mixing of upper levels with states of the same symmetry, but different l, could partly account for the discrepancy. Another possible explanation for this conflict is that, despite the dearth of neighbouring lines, there is still some scope for overlap, particularly of the (theoretical) $l = 0 \rightarrow 1$ line with an adjacent $l = 1 \rightarrow 2$ transition. There is a need to test the sensitivity of the relative position of the lines in the region of the band origin to variations in the potential energy surface. A recently modified version of the M80 potential (Norman et al. 1984) could provide a starting point.

Reservations about the $0 \longleftrightarrow 1$ lines apart, the remaining assignments of McKellar and Welsh are reasonable, though more than one l transition is likely to contribute to some of the observed lines. An example of this behaviour is provided by two closely spaced lines, $l = 2 \rightarrow 1$ and $l =$

$3 \longrightarrow 2$, calculated to lie near - 2.5 cm^{-1}. When the experimental resolution and the approximations inherent in our calculations are taken into account, there is reasonable accord between the theoretical and observed spectra. Increased resolution should yield more structure, and when this is achieved l could be used, in conjunction with J (and in some cases one would also need j_{12}), to make unique assignments. This has already been done for dimers of D_2 with rare gas atoms (McKellar 1982).

Finally, if we ignore the $Q_1(0) + S_o(0)$ lines that appear in the $S_1(0)$ region of the spectrum, and compare with the $S_o(0)$ far infrared spectrum of figure 5.5, we see that the results are very different. The figures extend over the same frequency range relative to the respective band origins. There are two reasons for the difference : firstly there is no double transition in the far infrared analogous to that in the near infrared, the upper states of which can perturb the spectrum. Secondly, tunnelling in the $S_o(0)$ upper states is relatively easy since it involves an exchange of rotational quantum numbers; we neglect it in the $S_1(0)$ spectrum as vibrational quantum numbers would have to be exchanged, and the dependence of the potential on intramolecular stretch is smaller than that on the relative orientation of the interacting monomers.

5.4.2 The $Q_1(0) + S_o(0)$ region

The near infrared spectrum results of Table 5.14 are plotted for higher frequencies in Figure 5.8. As in Figure 5.7, the frequencies are plotted relative to

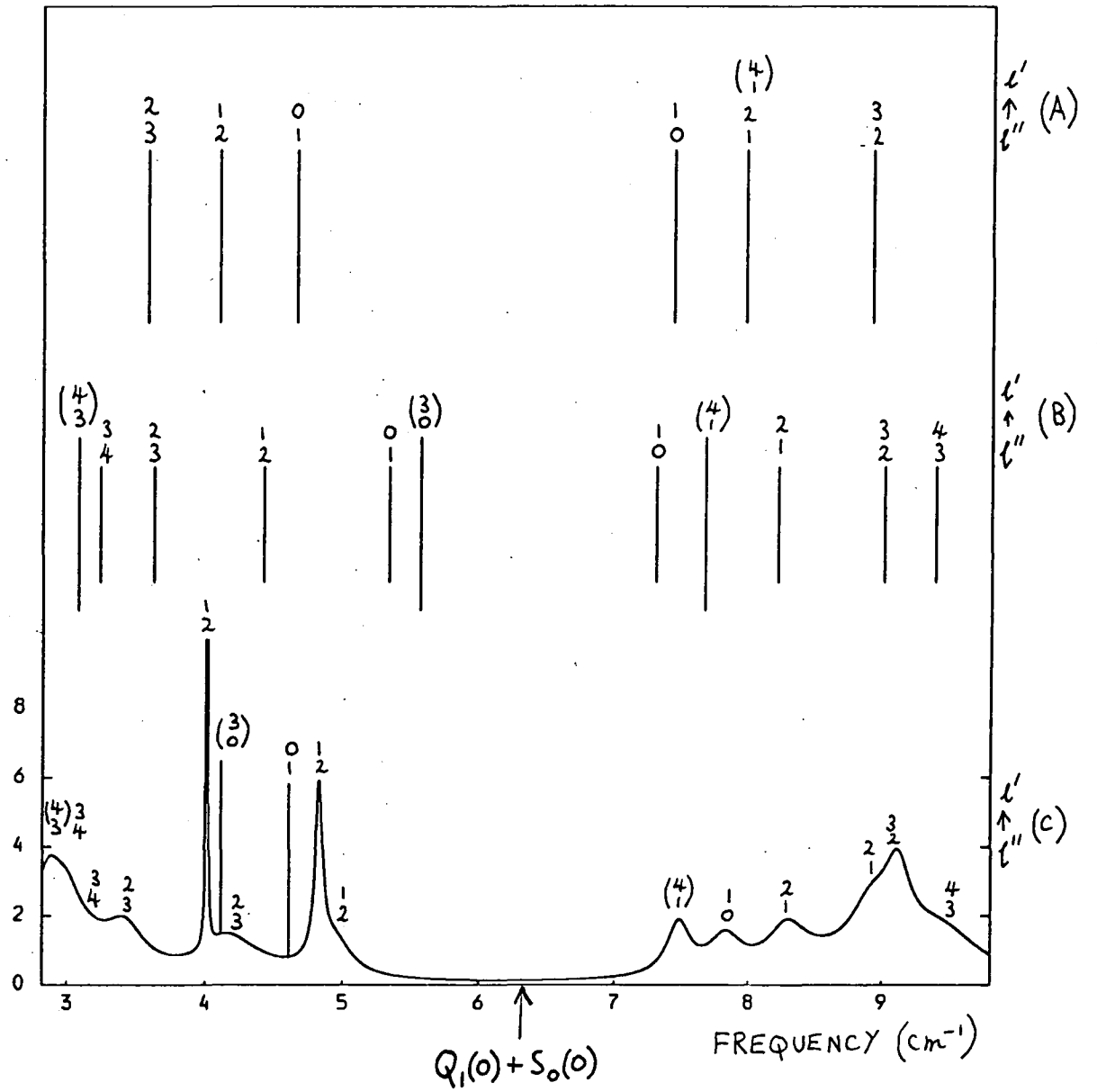

Figure 5.8

The dimer structure centred on the near infrared $Q_1(0)$ + $S_o(0)$ double transition in pure ortho-deuterium. This figure is an extension of Figure 5.7, a fact emphasised by the same horizontal scale (measured relative to the $S_1(0)$ frequency). (A) : Experimental line positions and assignments of McKellar and Welsh (1974). Here, brackets indicate $S_1(0)$ transitions. (B) : Pure ℓ markers, the $S_1(0)$ lines being longer with assignments in brackets. (C) : Theoretical spectrum obtained from Table 5.14.

the $S_1(0)$ band origin and the two plots overlap. The spectrum in Figure 5.8 is centred on the $Q_1(0) + S_o(0)$ band origin which, on this scale, lies at 6.318 cm^{-1}. There is good qualitative agreement between the theoretical and experimental spectra, though it again appears likely that different ℓ transitions will contribute to most of the experimental lines.

We now comment on the assignments of McKellar and Welsh (1974), taking each of the six observed lines in turn from left to right. We thus compare the top and bottom parts of Figure 5.8. The experimental $\ell = 3 \longrightarrow 2$ assignment is confirmed by theory. There is also agreement for the $\ell = 2 \longrightarrow 1$ line, though we note that theory predicts an adjacent $S_1(0)$, $\ell = 0 \longrightarrow 3$ line, separated by less than the experimental resolution of 0.25 cm^{-1}. The observed line marked $1 \longrightarrow 0$ probably consists of contributions from $2 \longrightarrow 1$ and $1 \longrightarrow 0$ transitions; the latter, as has already been argued, should be weak. To the right of the band origin, McKellar and Welsh observed three lines, assigning two transitions to one of them. Theory predicts four lines. If we neglect the $\ell = 0 \longrightarrow 1$ transition, which should be relatively weak, an alternative interpretation is reached. The experimental $\ell = 0 \longrightarrow 1$ line would thus be reassigned $S_1(0)$, $\ell = 1 \longrightarrow 4$. There is a second reason for thinking this could be so; a comparison of the theoretical $\Delta\ell$ markers with the predicted spectrum shows that the ordering of the $1 \longrightarrow 4$ and $0 \longrightarrow 1$ lines is reversed from what is expected on the basis of a simple nonrigid rotor model. With this interpretation,

the line doubly assigned by McKellar and Welsh should only be labelled $\ell = 1 \longrightarrow 2$. Finally, experiment and theory agree on the $\ell = 2 \longrightarrow 3$ assignment though this probably also contains some $1 \longrightarrow 2$ character. While our corrections to the original assignments may be tentative, they do at least show that consistent assignments can be made without invoking $\ell = 0 \longleftrightarrow 1$ transitions. Some of the "intensity anomalies" to which McKellar and Welsh (1974) refer are presumably due to incorrect attribution of two lines to $0 \longleftrightarrow 1$ transitions.

In contrast to the $S_1(0)$ case, this region of the spectrum is governed more by predissociation than experimental resolution. An improvement in the latter may, however, still yield further structure than hitherto observed. The calculated linewidths for the transitions above the $Q_1(0) + S_o(0)$ band origin range from about 0.2 to 0.4 cm^{-1}. This may be compared with estimates of between 0.2 and 0.6 cm^{-1} for the analogous lines observed by McKellar and Welsh. This agreement is encouraging, particularly in the light of work conducted by Le Roy et al. (1982) on the H_2 - Ar dimer. They carried out similar close coupling calculations to the ones described here, using the rigid rotor approximation. The level widths were found to be highly sensitive to vibrational averaging over the H_2 intramolecular motion; this is attributable to the sensitivity of the potential anisotropy to intramolecular stretch. The isotropic part of the potential was found to be relatively insensitive to changes in the H_2 bond length. Nevertheless, increasing the

bond length to a value appropriate to vibrationally excited H_2 did have a significant effect on the H_2 - Ar level energies. It should be noted, however, that for the discussion in this section, the important measure is the relative positions of the levels.

5.5 Conclusions

Close coupling rigid rotor calculations on the bound and rotationally predissociating states of the molecular dimer, D_2 - D_2, have been performed and the results presented in this Chapter. The interaction potential was assumed to be the same as that for H_2 - H_2; the M80 potential of Meyer, Schaefer and Liu being chosen. The larger reduced mass of the deuterated dimer leads to four (ℓ = 0, 1, 2, 3) bound states in the ortho-ortho system, twice as many as the analogous para-para $(H_2)_2$ dimer. Analysis of these results lead us to conclude that the rotational constant of the dimer is underestimated by the M80 potential, confirming the result of Chapter 4. The predicted centrifugal distortion constant is also too small. The bound state calculations on the para-ortho and para-para systems demonstrated the increased importance of potential anisotropy in the heavier $(D_2)_2$ dimer.

The rest of the Chapter was devoted to ortho-ortho $(D_2)_2$. The results of calculations on the bound states and resonances corresponding to one of the monomers in its first rotationally excited state were given. It was pointed out that some of the resonances have dual Feshbach and Shape character, a consequence of the weakness

of the D_2 - D_2 interaction. These results enabled us to predict the far infrared $S_o(0)$ absorption spectrum. Observation of this would yield information mainly on the quadrupole - quadrupole interaction as this is responsible for the significant interchange doubling of the final states. The magnitude and sign of this splitting were shown to be consistent with first order degenerate perturbation theory.

The near infrared spectrum, in the region of the $S_1(0)$ and $Q_1(0) + S_o(0)$ transitions of ortho-D_2, has been observed and was modelled theoretically by treating the monomers as distinguishable rigid rotors. In making assignments to the observed lines McKellar and Welsh (1974) treated the dimer as a pseudodiatomic molecule. We have demonstrated that this fails in the $S_1(0)$ region because of rotational splitting of the pure ℓ levels. The increased role of the rotational anisotropy in D_4 is illustrated by the fact that no such rotational splitting effects have been observed in the analogous $S_1(0)$ spectrum of H_2 - H_2. Some differences between the observed and theoretical spectral patterns are evident and will in part be due to errors in the anisotropic interaction. However, no clear information on this can be deduced until either further experiments have been performed at higher resolution, or quantitative line intensities have been calculated. The latter requires a knowledge of the collision induced dipole moment function, details of which have been published by Moraldi et al. (1984).

The absorption spectrum in the overlapping $Q_1(0)$ + $S_o(0)$ region is simpler. Comparison of observed linewidths with those calculated in this chapter, lead us to conclude that this is due to the spectrum being predissociation limited. It has proved possible to offer alternative line assignments to those given by McKellar and Welsh (1974) which may explain some of the "intensity anomalies" reported by these authors. Taking the near infrared spectrum as a whole, it is clear that more than one transition contributes to many of the observed lines.

Finally, we note that the $S_o(0)$ and $S_1(0)$ spectra are significantly different and the former cannot be inferred from observations of the latter. The source of this difference lies in the shift of channel energy on interchanging the rotational quantum numbers of monomers in different vibrational states.

CHAPTER SIX

THE $S_0(0)$ AND $S_1(0)$ SPECTRA OF THE H_2 - H_2 DIMER

6.1 Introduction

The near-infrared $S_1(0)$ and $S_1(1)$ spectra of the H_2-H_2 dimer have been observed in absorption in the laboratory by McKellar and Welsh (1974). On the basis of these spectral measurements, McKellar (1984) subsequently suggested that spectral features in the far-infrared spectra of Jupiter and Saturn (Gautier et al. 1983) might be attributable to $S_0(0)$ and $S_0(1)$ transitions in the H_2-H_2 dimer. In the preceding chapter we showed that the $S_0(0)$ spectrum of D_2-D_2 is expected to be quite different in appearance from the observed $S_1(0)$ spectrum. This is partly due to interchange splitting of the upper states in the $S_0(0)$ spectrum by the angular dependence of the potential. In the $S_1(0)$ spectrum the upper states can interact, via the same angular dependence, with the upper states of the double transition $Q_1(0) + S_0(0)$. Though the latter of these two effects is much less important in the H_2-H_2 case, due to the greater energy separation of the interacting upper states, we decided to test the validity of inferring the Hydrogen far-infrared spectrum from the near-infrared.

Frommhold et al. (1984) have computed the $S_0(0)$ and $S_0(1)$ absorption spectra of the H_2-H_2 dimer and compared their results with the observations of Jupiter and Saturn. Though their calculations provided information on line intensities, they completely neglected the effects of

potential anisotropy. In the light of our experience with D_2-D_2 it was judged useful to investigate this further.

In the present chapter, we present results of calculations of the frequencies of the $S_0(0)$ transitions of the para-H_2 -- para-H_2 dimer. These computations take into account the rotational splitting of both the bound and pseudo-bound (predissociating) levels of the dimer. The interchange symmetry of the para-H_2 molecules is also taken into account in order to assess the importance of interchange splitting of the dimer energy levels. The analogous $S_1(0)$ spectrum has also been calculated in order to make direct comparison with the laboratory measurements of McKellar and Welsh (1974).

6.2 The lower states

The $S_0(0)$ and $S_1(0)$ absorption spectra have in common the same lower states. These are calculated by the theoretical and numerical methods discussed in chapters 2 and 3. The coupled radial equations are integrated by means of the R-matrix propagator method, and the technique of Richardson extrapolation is used to accelerate convergence of the computed eigenenergies (Chapter 3). In the calculations reported here, a two-rotor basis ($j = 0,2$) was used to represent each para-H_2 molecule.

As noted in Chapter 4, the para-para system consists of identical bosons and the total wavefunction must be symmetric under exchange of the constituent molecules,

i.e. the interchange symmetry $i = +1$. It follows that $(-1)^{j_{12} + l + I_{12}} = +1$ when $j_1 = j_2$, where $\underset{\sim}{j}_{12} = \underset{\sim}{j}_1 + \underset{\sim}{j}_2$ and $\underset{\sim}{I}_{12} = \underset{\sim}{I}_1 + \underset{\sim}{I}_2$ are the resultant rotational and (nuclear) spin angular momenta of the dimer and l is the relative angular momentum of the two molecules. In the para-para system, where $I_1 = I_2 = I_{12} = 0$, we require that $(-1)^{j_{12} + l} = +1$ when $j_1 = j_2$.

In Table 6.1, we present the calculated eigenenergies of the para-para states correlating with $v_1 = v_2 = 0$ and $j_1 = j_2 = 0$. Details of these calculations have been given in Chapter 4. Following Bishop and Shih (1976) we use $\mu = 1836.15$ a.u. for the reduced mass of the dimer and $E(j = 2) = 354.397\ cm^{-1}$. These small changes in the constants of motion do not affect our results, compared with Chapter 4, to the accuracy quoted here. All computed energies are given, although, as noted above, levels with $i = -1$, for which l is odd, do not occur in nature. The interaction potential employed is that found in Chapter 4 to give the best representation of the H_2-H_2 interaction, namely the M80 potential of Meyer, Schaefer and Liu. Our results are compared with those of Frommhold et al. (1984), who used the isotropic, semi-empirical potential of McConville (1981). There is reasonable agreement in the absolute magnitudes of the bound state eigenenergies and better agreement in their separations.

				Present work		Frommhold et al.	
J	ε	i	ℓ	E	Γ	E	Γ
0	1	1	0	-2.43	0	-2.91	0
1	-1	-1	1	-0.97	0	-1.35	0
2	1	1	2	1.3	0.9	1.2	0.6
3	-1	-1	3	5.0	5	5	6
4	1	1	4	10.6	13		

TABLE 6.1

Computed eigenenergies of states of para-H_2-para-H_2 correlating with $v_1 = v_2 = 0$, $j_1 = j_2 = 0$. The total angular momentum (J), parity (ε), interchange (i), and relative angular momentum (ℓ) quantum numbers are listed. Also given are the positions and full widths at half-maximum intensity, Γ, of the shape resonances. Results of the present work are compared with those obtained by Frommhold et al. (1984). As noted in the text, states of negative interchange symmetry, i = -1, do not occur in nature for the para-para system. Units are cm^{-1}.

Also listed in Table 6.1 are the positions and widths of the predissociating states, which were determined using the molecular scattering code of Launay (1976, 1977). The eigenphase sums (Ashton et al. 1983) were fitted to Breit-Wigner forms using the algorithm of Tennyson and Noble (1984). The computed positions and widths of the resonances agree well with the calculations of Frommhold et al. (1984).

6.3 The upper states

Table 6.2 contains results of calculations on those states, correlating with $v_1 = v_2 = 0$ and $j_1 = 0$, $j_2 = 2$ or $j_1 = 2$, $j_2 = 0$, which form the upper states of the $S_0(0)$ spectrum. These eigenenergies are shifted compared with those in Table 6.1 by the energy separation of the $j = 0$ and $j = 2$ levels of H_2, namely 354.397 cm^{-1}.

Coupling of the relative angular momentum, $\underset{\sim}{l}$ with the resultant rotational angular momentum, $\underset{\sim}{j}_{12}$, gives rise to the splitting into J multiplets shown in the table. The magnitude of this splitting, neglected by Frommhold et al. (1984), is a few tenths of a wavenumber. Of further interest is the interchange splitting of levels which differ only in the value of i. This splitting was also neglected by Frommhold et al. on the grounds that the molecules are distinguishable when in different rotational states. Evidently, this statement is only an approximation to reality, as the

J	ε	i	ℓ	E (cm^{-1})	Γ (cm^{-1})
1	-1	1		- 1.33	0
1	-1	-1		- 1.27	0.0034
3	-1	-1	1	- 1.06	0.0031
3	-1	1		- 1.06	0
2	-1	-1		- 0.90	0
2	-1	1		- 0.82	0
5	-1	$\pm$1		5.1	2.8
2	-1	$\pm$1		5.1	3.6
1	-1	$\pm$1	3	5.1	3.8
4	-1	$\pm$1		5.2	3.1
3	-1	$\pm$1		5.3	3.6

TABLE 6.2

Computed eigenenergies of states of para - H_2-para - H_2 correlating with $v_1 = v_2 = 0$, and $j_1 = 0$, $j_2 = 2$ or $j_1 = 2$, $j_2 = 0$. Only the states of odd parity, $\varepsilon = -1$ which are associated with odd values of ℓ, are listed, as only these states contribute to the S_o (0) spectrum (cf. Table 6.4).

States of negative energy and finite width, Γ, are Feshbach resonances. Note that states of negative interchange symmetry, i = - 1, do not occur in nature but are tabulated to illustrate the magnitude of the interchange splitting; where i = $\pm$ 1 is listed the interchange splitting is much smaller than the predissociation width.

indistinguishability of the two molecules is attributable to their being identical boson systems, regardless of their internal rotational angular momentum states. States differing in the value of i are split into an "interchange doublet", of which only the $i = +1$ component occurs in nature. As may be seen from Table 6.2, the magnitude of this splitting is small for those levels contributing to the $S_0(0)$ spectrum of the para-H_2 -- para-H_2 dimer, but it should not be concluded that the effect is always negligible. Indeed, for other levels of the H_2-H_2 dimer the interchange splitting is significant. By way of example, the state $J^{\epsilon} = 0^+$, correlating with $(v_1, v_2; j_1, j_2; l) = (0, 0; 2, 0; 2)$ or $(0, 0; 0, 2; 2)$, is split by 1.6 cm^{-1}. However, the $i = +1$ member of this interchange doublet does not contribute to the dipole $S_0(0)$ spectrum because the spin statistics of H_2-H_2 forbid lower states of negative parity (odd l). For other systems such as D_2-D_2, HF-HF (Barton and Howard 1982) and N_2-N_2 (Tennyson and van der Avoird 1982a, Brocks and van der Avoird 1985), the interchange splitting measurably affects the predicted spectra.

The upper states of the $S_1(0)$ spectrum correlate with $(v_1, v_2; j_1, j_2) = (1, 0; 2, 0)$ or $(0, 1; 0, 2)$. In precise analogy to Chapter 5 we neglect the vibrational dependence of the interaction potential and hence the coupling between these equivalent states. The system

is thus treated as two distinguishable rigid rotors. The resulting basis set expansion is the same as in the $S_0(0)$ calculations except that $v_1 = 0$ is replaced by $v_1 = 1$. The channel energies are altered accordingly, measured relative to $(v_1, v_2; j_1, j_2) = (1, 0; 0, 0)$. Note that we include (rotational) coupling to the higher levels $(v_1, v_2; j_1, j_2) = (1, 0; 0, 2)$, which correspond to the upper states of the double $Q_1(0) + S_0(0)$ transition. The eigenenergies of upper states contributing to the $S_1(0)$ spectrum are shown in Table 6.3. The energies are quoted relative to the $S_1(0)$ threshold, $E(v, j = 1,2) = 4498.739\ cm^{-1}$ (Bishop and Shih 1976).

In Table 6.4, we list the computed frequencies and widths of the optically allowed transitions in the $S_0(0)$ spectrum of the para-H_2 - para-H_2 dimer, expressed relative to the frequency of the $\ell' = 1 \leftarrow \ell'' = 0$ transition. Our results are arithmetic means of allowed transitions to the computed energy multiplets in Table 6.2. The level of agreement with the calculations of Frommhold et al. (1984) is satisfactory, bearing in mind that different interaction potentials have been used.

In Table 6.4, we also compare our computations of the $S_1(0)$ spectrum, analogously obtained from Tables 6.1 and 6.3, with the laboratory measurements of McKellar and Welsh (1974). The agreement between theory and experiment is seen to be satisfactory. The two lines originating

J	ε	l	E (cm^{-1})	Γ (cm^{-1})
1	-1		- 1.19	0.0024
3	-1	1	- 1.04	0.0018
2	-1		- 0.84	0
1	-1		5.09	4.7
2	-1	3	5.26	4.9
3	-1		5.43	4.9

TABLE 6.3

Computed eigenenergies of states of para-H_2-para-H_2 correlating with $v_1 = 1$, $v_2 = 0$, and $j_1 = 2$, $j_2 = 0$. We list only those states which contribute to the $S_1(o)$ spectrum. The two levels $J = 4$ and $J = 5$, associated with $l = 3$, have not been calculated as the dipole moment operator will couple these only to the very broad $l = 4$ shape resonance (Table 6.1).

		$S_o(o)$		$S_1(o)$	
$\ell' \leftarrow \ell''$		PW	FSB	PW	MW
1	2	-3.47±0.7	-4.11±0.3	-3.56±0.6	-4.25±0.6
1	0	0 ± 0	0 ± 0	0.000±0.002	0.00±0.15
3	2	2.8 ±2.0	2.2 ±3.0	2.7 ±3.0	2.9 ±1.0
3	0	6.5 ±2.0	6.4 ± 3.0	6.3 ±2.0	7.3 ±2.0

TABLE 6.4

A comparison of the computed positions and half-widths (cm^{-1}) of lines in the $S_o(o)$ spectrum of para-H_2 - para-H_2; PW: present work; FSB: Frommhold et al. (1984). Frequencies (cm^{-1}) are expressed relative to the $\ell' = 1 \leftarrow \ell'' = 0$ transition. Our computed results for the corresponding transitions in the $S_1(o)$ spectrum are also given and compared with the laboratory measurements of McKellar and Welsh (1974) (MW). Half-widths attributed to MW have been estimated from their published spectrum, which had a resolution of 0.15 cm^{-1}.

from the lower l'' = 2 state are triplets, but the separation is smaller than the individual line widths due to predissociation. This explains why the experiment failed to resolve rotational fine structure. Furthermore, the positions and widths of the corresponding transitions in the $S_0(0)$ and $S_1(0)$ spectra are very similar, justifying McKellar's use of his near-infrared $S_1(0)$ spectrum to identify $S_0(0)$ features in the far-infrared spectra of Jupiter and Saturn.

6.4 Conclusions

In this Chapter, computed frequencies of the $S_0(0)$ transitions between bound and pseudo-bound levels of the para-H_2 - para-H_2 dimer have been presented. The calculations accounted for the interchange symmetry of the H_2 molecules. Analogous calculations of the $S_1(0)$ spectrum were found to be in satisfactory agreement with the laboratory measurements of McKellar and Welsh (1974). Further experiments at increased resolution are unlikely to observe the small rotational splitting due to intrinsic predissociation effects.

The $S_0(0)$ and $S_1(0)$ spectra have been shown to be very similar, in marked contrast to the case of the D_2-D_2 dimer. There are three reasons for this. Firstly, the rotational splitting is smaller in H_2-H_2 than in D_2-D_2. Secondly, the interchange, or tunnelling, doubling is also smaller for H_2-H_2; where it is large the affected

levels do not contribute to the spectrum. This latter effect is due to the different spin statistics of the two isotopic systems, there being no restriction on the spatial interchange symmetry of D_2-D_2 states. Thirdly, the perturbation on the upper states of the $S_1(0)$ spectrum, due to interactions with the corresponding $Q_1(0) + S_o(0)$ levels, is much less important in H_2-H_2 due to the greater energy separation (17.7 cm^{-1}) between them, a fact noted by McKellar and Welsh (1974).

The results of this chapter lend support to the proposed identification of features in the far infrared spectra of Jupiter and Saturn with $S_o(0)$ transitions of the H_2-H_2 dimer.

CHAPTER SEVEN

DISCUSSION AND FUTURE WORK

7.1 Methods

The main purpose of this thesis has been to develop methods of calculating the bound state energies of molecular dimers. The energies and widths of internal-rotationally predissociating resonances have also been obtained, using the method of Ashton et al. (1983). The results of these calculations can be used in conjunction with spectroscopic measurements to discriminate between different potential energy surfaces. We have been able, as a consequence, to interpret the experimental near infrared spectra of the hydrogen and deuterium dimers in more detail than was hitherto possible. In Chapter two, a quantum mechanical close coupling formalism was presented and the symmetrization of the basis functions discussed in some detail. This symmetrization was also cast explicitly into the language of group theory, which provides a powerful tool for the extension of these methods to more complex systems. The problem reduces to the solution of sets of coupled second order differential equations, the boundary conditions depending on whether the individual channels are open or closed at large values of the intermolecular separation. We have opted to solve these equations using numerical integration which we showed, in Chapter three, to be an easy and accurate way of determining bound state energies. This is not to say that other techniques such as the secular equation and BOARS methods do not have their place. Indeed, maximum physical insight will be achieved by using a diverse

range of methods. Those which have been used in bound state calculations of van der Waals molecules were discussed in Chapter three. There we noted that perturbation theory has been used to improve on the BOARS approximation; more recently the shortcomings of the secular equation approach have been similarly overcome (Hutson and Le Roy 1985).

While the de Vogelaere and R-matrix propagator methods agree to very high accuracy (up to 7 significant figures), the latter has proved to be particularly suitable for adaptation to bound state problems. The R-matrix propagator method is numerically stable in the classically forbidden regions and a smaller integration range, than that dictated by the "infinite wall" boundary conditions of the de Vogelaere method, is required. Furthermore, since the R-matrix propagator method is based on the piecewise analytic principle, much of the work done for the first trial energy may be saved for subsequent energies. Its one major drawback, slow convergence with respect to the number of integration steps, can be overcome using Richardson extrapolation. Further improvement could be achieved by using propagators corresponding to a linear, rather than a constant, coupling matrix $\underset{\sim}{W}(R)$ in the individual sectors. These propagators are more complex, involving the evaluation of the Airy functions. Step length algorithms of the type discussed by Stechel et al. (1978) could also be used. These attempt to maximise the step length within constraints

imposed by input tolerances. For a constant reference potential in each sector, these tolerances are related to the derivative of the coupling matrix elements, and to the departure from constancy of the transformation which diagonalises $\underset{\sim}{W}(R)$ in each sector. The problem with such algorithms is that, while they may give reasonably accurate answers with a relatively small number of steps, the error does not in general vary monotonically with respect to changes in the input tolerances. This precludes the use of Richardson extrapolation. As pointed out in Chapter three, we divide the integration range into two parts which meet near the potential minimum. An equal number of sectors is used in each of these parts; longer steps are therefore taken in the wider region beyond the minimum where the potential is more slowly varying. An additional problem may afflict the more complex step length algorithms in any future calculations of predissociation using the R-matrix propagator method. If one or more of the variable step lengths become equal to a multiple of half the de Broglie wavelength in any channel, a large round-off error can result, leading to a greatly increased global error. This was called the "magic π instability" by its discoverers, Mattson et al. (1983).

Despite the obvious utility of the numerical integration approach to bound state problems, it should be worthwhile to explore ways of improving efficiency so that it can be conveniently applied to a greater

variety of systems. Calculating the eigenenergies corresponds to finding the zeroes of a matching determinant, and it would be desirable to improve the efficiency of this search. In the simplest version of the computer programme, the matching determinant is evaluated on a grid of trial energies. An iteration is started when the determinants for two adjacent points on this grid differ in sign. It is straightforward to distinguish a sign change due to an eigenenergy from one caused by a pole, for which the determinant becomes infinitely large. Nevertheless, it would be worthwhile to investigate ways of eliminating such poles altogether from the energy dependence of the determinant. Berrington and Seaton (1985) have succeeded in doing this for calculations of the electronic bound states of atomic ions using an L^2 R-matrix method. It is worth noting here that the choice of stabilisation matrix determines the positions of poles in the de Vogelaere method. Performing duplicate sets of preliminary (small basis set) de Vogelaere calculations, differing only in stabilisation method, should minimise the risk of missing any energy levels due to the presence of poles.

In the early stages of this work, some exploratory model calculations, based on the oxygen dimer (Cashion 1966), were constructed to yield evenly degenerate eigenvalues. In such cases the matching determinant is zero at the eigenenergy but has the same sign on either side. Evenly degenerate eigenvalues also sometimes occur

in correlation tests. For these eigenvalues, iteration was found to be much more rapid using the logarithm of the matching determinant, $\log_{10}|\det|$. The speed of iteration to an eigenenergy in the general case could also be easily improved by using this function, multiplied by $\pm$ 1 depending on the sign of det.

A more radical way of improving the efficiency of the numerical integration method is suggested by the success in scattering calculations of the method of Thomas (1979, 1982). Computer time is saved by propagating only one solution vector, instead of the usual matrix, and iteratively matching this to the correct boundary conditions. It was suggested in Chapter three that Thomas's method may most naturally be extended to bound state calculations using the artificial channels approach. Thus, larger sets of coupled equations, needed for the extension of our work to strongly coupled dimers, could be integrated in this way.

An alternative to integrating increasing numbers of equations is to choose a more realistic basis expansion. For the weakly coupled hydrogen and deuterium dimers studied in this thesis, an angular basis consisting of vector coupled spherical harmonics rapidly converged with respect to the addition of more terms. In scattering calculations on strongly coupled atom-molecule systems, Clary (1983, 1984) has shown that by multiplying the spherical harmonic basis by an exponential "localisation function", an improvement over the conventional expansion

can be obtained. With such bases, the expressions for the coupling matrix elements are different from those given in Chapter two. The extension of this technique to heavier diatom-diatom systems should nevertheless be relatively straightforward, especially in cases where the centrifugal decoupling approximation is valid. For semi-rigid complexes, a hindered rotor basis, of the kind applied by Kidd et al. (1981) to the water molecule, may be preferable. Starting with a large number of conventional angular functions, a Hamiltonian matrix is obtained with all radial coordinates fixed at values corresponding to the equilibrium geometry. The hindered rotor basis is defined by the combinations of the original functions which diagonalise this Hamiltonian. This new basis set may be truncated significantly without prejudicing the accuracy of the calculated eigenenergies.

We end our discussion on methods with brief comments on the fitting and location of Breit-Wigner resonances. The fitting procedure for resonances just above threshold could be improved by assuming two different, smoothly connected, background eigenphase sums on either side of the threshold. The fact that the resonances just above threshold were generally found to be quite narrow meant that a single (linear) background could be assumed provided the fit was performed over an energy range no wider than a few resonance widths.

Resonance calculations, like those for bound states, require a search for characteristic behaviour over an

energy grid. Since the eigenphase sum is only defined modulo π, this grid must be at least equal to the width of the narrowest resonance to ensure all are found. Truhlar and Schwenke (1983) have shown how to define an absolute eigenphase sum, which allows resonances to be located using a much broader grid. Their approach, which involves calculating a K-matrix at the end of each integration step, should not be difficult to implement with standard scattering codes.

7.2 Assessment of interaction potentials using spectroscopy

The methods discussed above have been applied to the bound and resonance states of the lightest molecular dimer, $H_2 - H_2$, and its isotopic sister $D_2 - D_2$. In Chapter four, the bound states of H_4 were calculated using four different ab initio calculations of the potential energy surface. In the ortho-para and ortho-ortho modifications, rotational splitting of the levels, denoted by the end-over-end rotation l, leads to a spread of values for the $l = 0 - 1$ energy separation. The results are sensitive to the potential used. Only one $l = 0 - 1$ line has been observed in the experiments of McKellar and Welsh (1974) due to limited resolution. We deduced that the best potential was the M80 surface of Meyer, Schaefer and Liu. For this potential, the spread of the $l = 0 - 1$ frequencies is sufficiently small to be consistent with the failure of experiment to find any anisotropy effects. The main fault with the M80 potential is that it predicts too small a value

for the end-over-end rotational constant, B_ℓ, a fact confirmed by bound state calculations on the D_4 system in Chapter five. The potential could be empirically improved by negatively shifting the isotropic part, and by implication the anisotropic terms also, by 0.1 - 0.2Å. We can assert that this is a potential effect with some confidence, rather than a consequence of our assumption that the potential is insensitive to the stretching of the monomer bonds. Strictly speaking, the experiment yields information on the average of two potentials: one corresponding to both monomers in their ground vibrational (V = 0) states, the other to one H_2 in its V = 1 state. B_ℓ for the latter surface should be somewhat smaller since the repulsive wall is pushed outwards from the considerations of Chapter two. Bound state calculations based on a perfect ground state potential would thus give a <u>larger</u> B_ℓ than that deduced from experiment.

A further alteration to the M80 potential has been suggested by Waiijer et al. (1981) based on measurements of the hyperfine spectrum of H_4. Their modification to the V_{200} term in the potential expansion brings it closer to that of the Burton-Senff potential which we have shown is too anisotropic. Future work on H_4 should include bound state calculations on the shifted M80 potential, with and without the "blister" in V_{200}, the form of which has been given by Waiijer et al. (1981).

The purpose of these runs will be to check our preliminary conclusion that the blister leads to results inconsistent with near infrared measurements.

7.3 Simulation of absorption spectra

In addition to the bound levels of D_4 we have also reported calculations on rotationally predissociating states. The upper states of the $S_o(0)$ absorption spectrum are split due to tunnelling doubling, involving the exchange of the rotational quantum numbers of identical monomers. This splitting was found to be consistent with Rayleigh-Schroedinger perturbation theory, which treats the levels as being discrete. This assumption appears to be justified since we were able to accurately reproduce the energies of the $S_o(0)$ resonances using our bound state code.

The spectroscopic measurements so far carried out on D_4 have been in the (near infrared) region of the fundamental band of deuterium. By neglecting vibrational predissociation, we attempted to model the dimer structure accompanying the $S_1(0)$ and $Q_1(0) + S_o(0)$ transitions in pure ortho-D_2. McKellar and Welsh (1974) have listed three shortcomings in their theoretical analysis of this spectrum. They ignored both the effects of potential anisotropy and the perturbation it causes between the upper states corresponding to the single and double transitions cited above. We have included both of these factors in our analysis, the latter one by treating the interacting monomers as distinguishable rigid rotors

and altering the channel energies accordingly. The third shortcoming mentioned by McKellar and Welsh is also present in our analysis; this is the treatment of the vibrational frequency shift. Like McKellar and Welsh, we still have to either ignore this shift or rely on a simple elimination by treating its effect on all levels as being equivalent to a change in the asymptotic energy of the relevant channel (refer to Figure 4.8). Even with a knowledge of the variation of the potential with monomer stretch, upon which it depends, there are considerable theoretical difficulties in modelling this shift (Hutson and McCourt 1984). Further experiments with lower gas pressure and longer path lengths should help to minimise this problem.

Calculations of both the near and far infrared spectra of para-H_2, completely analogous to those on ortho-D_2, have also been reported. The results were presented in Chapter six. The $Q_1(0) + S_o(0)$ channels were present in the calculations of the $S_1(0)$ spectrum, but the energies and widths of the corresponding states were not evaluated.

Of current astrophysical interest is the far infrared $S_o(0)$ spectrum of the hydrogen dimer. Results were presented for the para-para modification. We have shown that the isotropic model of the dimer, used by Frommhold et al. (1984) in their interpretation of the Jovian $S_o(0)$ spectrum, is reliable. This is despite the presence of interchange splitting, because of the weak coupling and the zero statistical weights of some of the levels. It is desirable to extend our calculations to include the $S_o(0)$ spectrum for the ortho-para modification,

as ortho-H_2 is also present in the Jovian atmosphere. These calculations differ from the para-para case in that many more resonances have to be located and fitted; this is due to the angular momentum coupling of $j_1 = 1$ and $j_2 = 2$ to give three possible values of j_{12}. Furthermore, interchange symmetry effects will be absent in this modification. This means, for example, that initial states of the $S_o(0)$ spectrum with odd values of l are allowed only in the ortho-para modification. The relative intensity of lines in the $S_o(0)$ spectrum could thus in principle provide information on the ratio of ortho to para hydrogen in the Jovian atmosphere. Frommhold et al. (1984) have been able to obtain some indication of the value of this ratio. Precise information is difficult to obtain, both because they have neglected the effects of potential anisotropy and because the spectrum is not well resolved.

In addition to information on statistical weights, the production of simulated spectra relies on the calculation of three properties of each spectral line : its frequency, width and intensity. The analysis of the far infrared H_4 spectrum of Jupiter and that of the near infrared H_4 and D_4 laboratory spectra both provide motivation for the extension of our calculations to take the intensity factor into account. The simulation of the spectra of anisotropic van der Waals molecules has already been considered by various authors. Brocks and van der Avoird (1985) and Dunker and Gordon (1978)

have calculated line intensities for the spectra of N_2-N_2 and Ar-H_2 respectively. These calculations ignored predissociation, however, and assumptions were made regarding the linewidths. In the only examples of fully simulated spectra of which the author is aware, Kidd and Balint-Kurti (1984) and Beswick and Shapiro (1982) both used the artificial channels method. The systems studied by these authors were respectively Ar-HD and Ar-N_2.

Future work could involve investigating the extension of our methods to include intensity information and hence simulate the spectra of H_4 and D_4. The problems involved in calculating the needed eigenfunctions were briefly addressed in Chapter three. The relevant collision induced dipole moment is already available (Moraldi et al. 1984). We could also try using the secular equation method; this produces the bound state eigenfunctions easily, though continuum wavefunctions are difficult to reproduce well. It may prove possible to combine the information we already have on the linewidths with intensities calculated using a secular equation approach in which open channels are omitted. Finally we note that the width of each line may be increased by a suitable amount to take pressure broadening into account. Doppler broadening is included by convoluting the resulting Lorentzian with a Gaussian profile (e.g. Pine et al. 1984, Minguzzi and Di Lieto 1985).

7.4 Vibrotor calculations

All of the calculations in this thesis could usefully be repeated treating the molecules as vibrotors, using the formalism presented in Chapter two. However, given the large number of coupled equations, which arise due to the monomer rotational levels which must be included with each vibrational state, it is best to be selective. There is widespread motivation for such calculations, most apparently to improve the accuracy of the calculated dimer spectrum. Of particular interest are the line positions near the $S_1(0)$ band origin of ortho-ortho $(D_2)_2$. Since linewidths are expected to be highly sensitive to variations of the potential anisotropy with monomer excitation, it would also be useful to confirm that the observed spectrum in the $Q_1(0) + S_o(0)$ region of ortho-D_2 is predissociation limited.

The close coupling scattering calculations, used in the interpretation of measurements of the total differential cross-sections of D_2-H_2 (Buck et al. 1981), made the rigid rotor approximation. However, as pointed out in Chapter four, there may be a significant change in monomer bond length during the course of the collision. A vibrotor analysis may provide an explanation for the proposed negative shift of the repulsive wall of the M80 potential. The need to postulate a 30% increase in the dispersion interaction, in the region of the potential zero, would thus be avoided. Furthermore, the hyperfine spectra measured by Verberne and Reuss (1980) probe the repulsive region less sensitively than

the relatively high energy scattering experiments of Buck et al. If the short range constraint imposed on the rigid rotor surface by the latter experiments is relaxed, the need for Waaijer et al. (1981) to introduce a blister in the well region of the V_{200} coefficient could be avoided. In short, the motivation for vibrotor calculations on H_4 and D_4 is to isolate the error intrinsic in the ab initio determination of the potential from the effects of monomer stretch.

There probably already exists sufficient information on the potential to begin the calculations just suggested. We have already mentioned, in section 4.4, that M80 potential calculations have been performed for two values of the H_2 internuclear separation. Taking into account the latest improvements to the M80 surface (Norman et al. 1984), this provides the basic information needed. A fit to this data over the whole coordinate space (i.e. including r_1 and r_2 as well as $\hat{\underset{\sim}{r}}_1$, $\hat{\underset{\sim}{r}}_2$ and R) could be attempted by assuming a suitable model for the potential (Raich et al. 1976). This kind of approach has produced satisfactory results for the H_2-CO system, even though only the potential for equilibrium monomer bond lengths was available (Poulsen 1982).

Qualitative checks on any such complete H_2-H_2 vibrotor potential could be performed in a number of ways. Ree and Bender (1979) have reported CI and SCF calculations of the r ($1.3 < r < 1.5$ a.u.) dependence of the H_2 - H_2

interaction for small intermolecular separations ($1.5 < R < 5.0$ a.u.). In addition, we know from measurements of Raman frequency shifts (May et al. 1961) that the behaviour of the H_2-H_2 interaction, with respect to changes in the H_2 bond lengths, is intermediate between that of He-H_2 and Ar-H_2. Detailed information on the r dependence of the potentials for these systems is already available (Senff and Burton 1985, Schaefer and Köhler 1985, Le Roy et al. 1982). Finally, we note that some qualitative information on the r dependence of the isotropic potential, V_{000}, may be deduced from the unambiguously assigned $Q_1(0)$ spectrum of D_4. This yields the energy separation between the l states: 1-0, 2-1, 3-2 and 4-3 (see Table 5.4). A simultaneous least squares fit to the bound states calculated for two potentials, V_{000} ($V_1 = 1$, $V_2 = 0$) and V_{000} ($V_1 = V_2 = 0$), could be performed. A wide range of isotropic model potentials is available (Maitland et al. 1981). However, since we can only have a maximum of 4 adjustable parameters we would be restricted, for the sake of argument, to using two Lennard-Jones type potentials. Initial guesses for the four parameters could be obtained by a fit to the ab initio M80 potential.

7.5 The H_2 - CO dimer

A most obvious area for future work is in the study of different molecular dimers. H_2-CO is an astrophysically significant system amenable both to calculations and experiment. Large differences exist between the available

ab initio potentials (e.g. Flower et al. 1979, Poulsen 1982, van Hemert 1983 and Schinke et al. 1984). This highlights the difficulties in electronic structure calculations, which lie far behind the methods for nuclear dynamics from the point of view of accuracy. Differences between the H_2-CO potentials will allow some discrimination even with the low resolution gas cell absorption measurements that have been made to date. Kudian et al. (1967) have noted the similarity of the H_2-CO and H_2-N_2 spectra. Measurements of the latter were subsequently repeated at improved resolution, yielding evidence for 7 or 8 end-over-end rotational bound states (McKellar and Welsh 1971). The situation should improve with the molecular beam measurements currently being made by N. Halberstadt and Ph. Brechignac.

The rotational constant of CO ($1.9cm^{-1}$) is thirty times smaller than that of H_2. The H_2-CO potential is also more anisotropic than that of H_2-H_2. The H_2-CO dimer is thus by far the more strongly coupled of the two. It will be interesting to see how the methods used in this thesis will fare with this heavier system. The relative importance of the potential anisotropy makes it worthwhile to consider using the centrifugal decoupling (CD) approximation. Though the reverse is true, it does not follow that the success of the CD approximation in scattering calculations (e.g. Schinke et al. 1984) will lead to it being valid for bound states. A theoretical study of the H_2-CO dimer should provide

an opportunity to implement many of the other alternative methods, and improvements to the existing ones, discussed in this chapter.

REFERENCES

Abramowitz, M., and Stegun, I.A., 1965, Handbook of Mathematical Functions (New York : Dover).

Alexander, M.H., 1984, J. Chem. Phys., 81, 4510-6.

Alexander, M.H., and De Pristo, A.E., 1976, J. Chem. Phys. 65, 5009-16.

Alexander, M.H., and De Pristo, A.E., 1977, J. Chem. Phys. 66, 2166-72.

Arthurs, A.M., and Dalgarno, A., The Theory of Scattering by a Rigid Rotor, 1960, Proc. R. Soc. A 256, 540-51.

Ashton, C.J., Child, M.S., Hutson, J.M., 1983, J. Chem. Phys. 78, 4025-39.

Atkins, P.W., 1983, Molecular Quantum Mechanics (2nd Edition) (Oxford : Oxford University).

Balint-Kurti, G.G., 1975a, Adv. Chem. Phys. 30, 137-83.

Balint-Kurti, G.G., 1975b, International Review of Science, Physical Chemistry Ser. 2, 1, 283-326.

Baluja, K.L., Burke, P.G., and Morgan, L.A., 1982, Comput. Phys. Commun. 27, 299-307.

Barton, A.E., and Howard, B.J., 1982, Discuss. Faraday Soc. 73, 45-62.

Bender, C.F., and Davidson, E.R., 1966, J. Phys. Chem. 70, 2675-85.

de Bernardis, P., Masi, S., Malagoli, A., and Melchiorri, F., 1985, Astrophys. J. 288, 29-31.

Berns, R.M., and van der Avoird, A., 1980, J. Chem. Phys. 72, 6107-16.

Berrington, K.A., and Seaton, M.J., 1985, J. Phys. B. 18, 2587-99.

Beswick, J.A., and Shapiro, M., 1982, Chem. Phys. 64, 333-41.

Bishop, D.M., Shih, S., 1976, J. Chem. Phys. 64, 162-9.

Blaney, B.L., and Ewing, G.E., 1976, Ann. Rev. Phys. Chem. 27, 553-86.

Boardman, A.D., O'Connor, D.E., and Young, P.A., Symmetry and its applications in Science, 1973, (London : McGraw-Hill),

Bocchetta, C.J., and Gerratt, J., 1985, J. Chem. Phys. 82, 1351-62.

de Boor, C., 1978, A Practical Guide to Splines, (Berlin : Springer Verlag).

Boys, S.F., and Bernardi, F., 1970, Mol. Phys. 19, 553-66.

Bransden, B.H., and Joachain, C.J., 1983, Physics of Atoms and Molecules, (New York : Longman).

Brocks, G., and van der Avoird, A., 1985, Mol. Phys. 55, 11-32.

Brocks, G., van der Avoird, A., Sutcliffe, B.T., Tennyson, J., 1983, Mol. Phys. 50, 1025-1043.

Buck, U., 1982, Discuss. Faraday Soc. 73, 187-203.

Buck, U., Huisken, F., Maneke, G., Schaefer, J., 1983a, J. Chem. Phys., 78, 4430-8.

Buck, U., Huisken, F., Kohlhase, A., Otten, D., and Schaefer, J., 1983b, J. Chem. Phys. 78, 4439-50.

Buck, U., Huisken, F., Schleusener, J., Schaefer, J., 1981, J. Chem. Phys. 74, 535-44.

Buckingham, A.D., 1967, Adv. Chem. Phys. 12, 107-42.

Bunker, P.R., Molecular symmetry and spectroscopy, 1979a, (New York : Academic Press).

Bunker, P.R., 1979b, Can. J. Phys. 57, 2099-105.

Burton, P.G., 1982, private communication.

Burton, P.G., 1983, Chem. Phys. Lett. 100, 51-8.

Burton, P.G., Gray, P.D., and Senff, U.E., 1982, Mol. Phys. 47, 785-809.

Burton, P.G., and Senff, U.E., 1982, J. Chem. Phys. 76, 6073-87.

Burton, P.G., and Senff, U.E., 1983, J. Chem. Phys. 79, 526-7.

Cashion, J.K., 1968, J. Chem. Phys. 48, 94-103.

Child, M.S., 1974, Molecular Collision Theory, (New York : Academic Press).

Clary, D.C., 1983, Chem. Phys. 76, 331-41.

Clary D.C., 1984, Mol. Phys. 51, 1311-9.

Coleman, J.P., and Mohamed, J., 1978, Math. of Computat. 32, 751-62.

Coleman, J.P., and Mohamed, J., 1979, Comput. Phys. Comm. 17, 283-300.

Cooley, J.W., 1961, Math. of Computat. 15, 363-74.

Cowan, R.D., The Theory of Atomic Structure and Spectra, 1981, (California : California University).

Dalgarno, A., 1975, Atomic and Molecular Processes in Astrophysics Ed. M.C.E. Huber and H. Nussbaumer (Geneva : Geneva Observatory), 1-98.

Danby, G., Theoretical Studies of van der Waals molecules : general formulation, 1983, J. Phys. B : At. Mol. Phys. vol. 16, 3393-3410.

Danby, G., and Flower, D.R., 1983, J. Phys. B. 16, 3411-22.

De Vries, P.L., and George, T.F., 1980, Mol. Phys. 39, 701-7.

Dickinson, A.S., 1979, Comput. Phys. Comm. 17, 51-80.

Draine, B.T., Roberge, W.G., and Dalgarno, A., 1983, Astrophys. J., 264, 485-507.

Dunker, A.M., and Gordon, R.G., 1976a, J. Chem. Phys. 64, 4984-94.

Dunker, A.M., and Gordon, R.G., 1976b, J. Chem. Phys. 64, 354-63.

Dunker, A.M., and Gordon, R.G., 1978, J. Chem. Phys. 68, 700-25.

Dyke, T.R., Howard, B.J., Klemperer, W., 1972, J. Chem. Phys. 56, 2442-54.

Edmiston, C., and Krauss, M., 1966, J. Chem. Phys. 45, 1833-9.

Eisberg, R.M., 1961, Fundamentals of Modern Physics (New York : Wiley).

Ewing, G.E., 1976, Can. J. Phys. 54, 487-504.

Ewing, T.F., Detrich, J., Conn, R.W., 1978, J. Chem. Phys. 69, 4662-8.

Ezra, G.S., 1982, Symmetry properties of molecules (Berlin : Springer-Verlag).

Flower, D.R., Launay, J.M., Kochanski, E., and Prissette, J., 1979, Chem. Phys. 37, 355-62.

Foglia, C., 1984, Comput. Phys. Comm. 32, 209-13.

Fox, L., 1960, Boundary value problems and differential equations Ed. R.E. Langer (Madison : Wisconsin : Wisconsin University) 243-55.

Frommhold, L., Borysow, A., Moraldi, M., Meyer, W., and Birnbaum, G., 1985, 14th International Conference on the Physics of Electronic and Atomic Collisions (Palo Alto : ICPEAC 1985), 636.

Frommhold, L., Samuelson, R., Birnbaum, G., 1984, Astrophys. J. 283, L79-82.

Gallup, G.A., 1977, Mol. Phys. 33, 943-53.

Gautier, D., Marten, A., Baluteau, J.P., Bachet, G., 1983, Can. J. Phys. 61, 1455-61.

Geraedts, J., Waayer, M., Stolte, S., and Reuss, J., 1982a, Discuss. Faraday Soc. 73, 375-86.

Geraedts, J., Stolte, S., and Reuss, J., 1982b, Z. Phys. A. 304, 167-75.

Gianturco, F.A., 1980, Atomic and Molecular Collision Theory Ed. F.A. Gianturco (New York : Plenum), 315-92.

Gioumousis, G., and Curtiss, C.F., 1961, J. Math. Phys. 2, 96-104.

Gordon, R.G., 1969, J. Chem. Phys. 51, 14-25.

Gordon, R.G., 1971, Meth. Comput. Phys. 10, 81-109.

Gordon, R.G., and Cashion, J.K., 1966, J. Chem. Phys. 44, 1190-5.

Gray, C.G., 1968, Can. J. Phys. 46, 135-9.

Green, S., 1974, in Atomic and Molecular Physics and the Interstellar Matter, Les Houches, session XXVI, (Amsterdam : North-Holland). pp.83-133.

Green, S., 1975, J. Chem. Phys. 62, 2271-7.

Green, S., 1977, J. Chem. Phys. 67, 715-7.

Green, S., 1980, J. Chem. Phys. 73, 2740-50.

Green, S., Ramaswamy, R., and Rabitz, H., 1978, Astrophys. J., 483-96.

Green, S., and Thaddeus, P., 1976, Astrophys. J., 205, 766-85.

Gush, H.P., 1981, Phys. Rev. Lett. 47, 745-8.

Hajj, F.Y., 1980, J. Phys. B. 13, 4521-8.

Hamermesh, M., 1962, Group Theory (Reading : Addison-Wesley).

Hanel, R., Conrath, B., Flasar, M., Kunde, V., Lowman, P., Maguire, W., Pearl, J., Pirraglia, J., Samuelson, R., Gautier, D., Gierasch, P., Kumar, S., and Ponnamperuma, C. 1979, Science 204, 972-6.

Hartree, D.R., 1958, Numerical Analysis (Oxford : Oxford University).

Hazi, A.U., 1979, Phys. Rev. A. 19, 920-2.

Heil, T.G., Green, S., Kouri, D.J., 1978, J. Chem. Phys. 68, 2562-83.

Heil, T.G., and Kouri, D.J., 1976, Chem. Phys. Lett. 40, 375-80.

Herman, R.M., and Short, S., 1968, J. Chem. Phys. 48, 1266-72.

Herzberg, G., Molecular Spectra and Molecular Structure. I. Spectra of diatomic molecules, 1950, 2nd edition (New York : Van Nostrand).

Hobza, P., and Zahradnik, R., 1980, Top. Current Chem. 93, 53-90.

Holmgren, S.L., Waldman, M., Klemperer, W., 1977, J. Chem. Phys. 67, 4414-22.

Holmgren, S.L., Waldman, M., Klemperer, W., 1978, J. Chem. Phys. 69, 1661-9.

Howard, B.J., 1981, Discuss. Faraday Soc. 71, 23-9.

Humphries, C.M., and Horton, B.H., 1977, unpublished work.

Hutson, J.M., 1983a (private communication).

Hutson, J.M., 1983b (private communication).

Hutson, J.M., 1984, J. Chem. Phys. 81, 2357-62.

Hutson, J.M., Ashton, C.J., and Le Roy, R.J., 1983, J. Phys. Chem. 87, 2713-20.

Hutson, J.M., and Howard, B.J., 1980, Mol. Phys. 41, 1123-41.

Hutson, J.M., and Howard, B.J., 1982, Mol. Phys. 45, 769-90.

Hutson, J.M., and Le Roy, R.J., 1983, J. Chem. Phys. 78, 4040-3.

Hutson, J.M., and Le Roy, R.J., 1985, J. Chem. Phys. 83, 1197-203.

Hutson, J.M., and McCourt, F.R., 1984, J. Chem. Phys. 80, 1135-49.

Ishiguro, E., Arai, T., Mizushima, M., Kotani, M., 1952, Proc. Phys. Soc. (London) A65, 178-87.

Jaszunski, M., Kochanski, E., Siegbahn, P., 1977, Mol. Phys. 33, 139-46.

Johnson, B.R., and Secrest, D., 1968, J. Chem. Phys. 48, 4682-93.

Kidd, I.F., and Balint-Kurti, G.G., 1984, Chem. Phys. Lett. 105, 91-4.

Kidd, I.F., and Balint-Kurti, G.G., 1985, J. Chem. Phys. 82, 93-105.

Kidd, I.F., Balint-Kurti, G.G., and Shapiro, M., 1981, Discuss. Faraday Soc. 71, 287-300.

Klemperer, W., 1977, Discuss. Faraday Soc. 62, 179-84.

Kochanski, E., 1973, J. Chem. Phys. 58, 5823-31.

Kochanski, E., 1975, Theor. Chim. Acta, 39, 339-46.

Kochanski, E., 1983, (private communication).

Kochanski, E., and Flower, D.R., 1981, Chem. Phys. 57, 217-25.

Köhler, W.E., and Schaefer, J., 1983a, J. Chem. Phys. 78, 4862-74.

Köhler, W.E., and Schaefer, J., 1983b, J. Chem. Phys. 78, 6602-10.

Kreek, H., and Le Roy, R.J., 1975, J. Chem. Phys. 63, 338-44.

Kreyzig, E., 1972, Advanced engineering mathematics (3rd edition) (New York : Wiley).

Kudian, A.K., and Welsh, H.L., 1971, Can. J. Phys. 49, 230-42.

Kudian, A., Welsh, H.L., and Watanabe, A., 1967, J. Chem. Phys. 47, 1553-4.

Kutzelnigg, W., 1977a, Methods of electronic structure theory ed. H.F. Schaefer III (New York : Plenum) 129-88.

Kutzelnigg, W., 1977b, Discuss. Faraday Soc. 62, 185-96.

Launay, J.M., 1976, J. Phys. B. 9, 1823-37.

Launay, J.M., 1977, J. Phys. B. 10, 3665-72.

Launay, J.M., 1978, D.E.S. Thesis (University of Paris VII).

Leavitt, R.P., 1980, J. Chem. Phys. 72, 3472-82.

Le Roy, R.J., 1971, J. Chem.Phys. 54, 5433-4.

Le Roy, R.J., and Carley, J.S., 1980, Adv. Chem. Phys. 42, 353-420.

Le Roy, R.J., Carley, J.S., and Grabenstetter, J.E., 1977, Discuss. Faraday Soc. 62, 169-78.

Le Roy, R.J., Corey, G.C., and Hutson, J.M., 1982, Discuss. Faraday Soc. 73, 339-55.

Le Roy, R.J., and van Kranendonk, J., 1974, J. Chem. Phys. 61, 4750-69.

Lester, W.A., 1968, J. Comput. Phys. 3, 322-6.

Lester, W.A., 1971, Meth. Comput. Phys. 10, 211-41.

Lester, W.A., 1976, Dynamics of molecular collisions, part A. ed. W.H. Miller (New York : Plenum), 1-32.

Levy, D.H., 1981, New Scientist 1234, 15-7.

Light, J.C., 1971, Meth. Comput. Phys. 10, 111-41.

Light, J.C., 1983, (private communication).

Light, J.C., Walker, R.B., 1976, J. Chem. Phys. 65, 4272-82.

Light, J.C., Walker, R.B., Stechel, E.B., and Schmalz, T.G., 1979, Comput. Phys. Comm. 17, 89-97.

Liu, W.K., Grabenstetter, J.E., Le Roy, R.J., and McCourt, F.R., 1978, J. Chem. Phys. 68, 5028-31.

Longuet-Higgins, H.C., 1963, Mol. Phys. 6, 445-60.

Löwdin, P.O., 1955, Phys. Rev. 97, 1474-89.

McConville, G.T., 1981, J. Chem. Phys. 74, 2201-5.

McKellar, A.R.W., 1982, Discuss. Faraday. Soc. 73, 89-108.

McKellar, A.R.W., 1983 (private communication).

McKellar, A.R.W., 1984, Can. J. Phys. 62, 760-3.

McKellar, A.R.W., and Welsh, H.L., 1971, J. Chem. Phys. 55, 595-609.

McKellar, A.R.W., and Welsh, H.L., 1972, Can. J. Phys. 50, 1458-64.

McKellar, A.R.W., and Welsh, H.L., 1974, Can. J. Phys. 52, 1082-9.

McWeeny, R., and Pickup, B.T., 1980, Rep. Prog. Phys. 43, 1065-144.

Magnus, W., 1954, Commun. Pure Appl. Math. 7, 649-73.

Maitland, G.C., Rigby, M., Smith, E.B., and Wakeham, W.A., 1981, Intermolecular Forces (Oxford : Clarendon Press).

Mattson, T.G., and Anderson, R.W., 1984, Mol. Phys. 52, 319-44.

Mattson, T.G., Mitchell, M.R., Anderson, R.W., 1983, Mol. Phys. 50, 251-74.

May, A.D., Degen, V., Stryland, J.C., Welsh, H.L., 1961, Can. J. Phys. 39, 1769-83.

May, A.D., Varghese, G., Stryland, J.C., Welsh, H.L., 1964, Can. J. Phys. 42, 1058-69.

Merzbacher, E., 1961, Quantum Mechanics (New York : Wiley).

Messiah, A., Quantum Mechanics, 1962, volume 2 (Amsterdam : North-Holland).

Metropoulos, A., 1981, Chem. Phys. Lett. 83, 357-61.

Metropoulos, A., and Chiu, Y-N., 1978, J. Chem. Phys. 68, 5607-14.

Metropoulos, A., and Chiu, Y-N, 1980, Chem. Phys. 47, 359-67.

Meyer, W., 1976, Chem. Phys. 17, 27-33.

Meyer, W., Hariharan, P.C., and Kutzelnigg, W., 1980, J. Chem. Phys. 73, 1880-97.

Meyer, W., and Schaefer, J., 1985, (to be published).

Millar, T., and Williams, D., 1985, New Scientist 1451, 12-6.

Minguzzi, P., and Di Lieto, A., 1985, J. Molec. Spec. 109, 388-94.

Mohamed, J.L., 1984, J. Comput. Phys. 54, 457-67.

Monchick, L., and Schaefer, J., 1980, J. Chem. Phys. 73, 6153-61.

Moraldi, M., Borysow, A., and Frommhold, L., 1984, Chem. Phys. 86, 339-47.

Mulder, F., van der Avoird, A., and Wormer, P.E.S., 1979, Mol. Phys. 37, 159-80.

NAG 1984, Fortran Library Manual Mark 11, 3.

Nicholls, R.W., and Stewart, A.L., 1962, Atomic and Molecular Processes Ed. D.R. Bates (New York : Academic Press), 47-78.

Norman, M.J., Watts, R.O., and Buck, U., 1984, J. Chem. Phys. 81, 3500-4.

Oka, T., and Morino, Y., 1961, J. Mol. Spectr. 6, 472-82.

Pine, A.S., Lafferty, W.J., and Howard, B.J., 1984, J. Chem. Phys. 81, 2939-50.

Poll, J.D., and Hunt, J.L., 1976, Can. J. Phys. 54, 461-70.

Poll, J.D., and Hunt, J.L., 1981, Can. J. Phys. 59, 1448-58.

Poll, J.D., and van Kranendonk, J., 1961, Can. J. Phys. 39, 189-204.

Pople, J.A., 1982, Discuss. Faraday. Soc. 73, 7-17.

Poulsen, L.L., 1982, Chem. Phys. 68, 29-40.

Prissette, J., Kochanski, E., and Flower, D.R., 1978, Chem. Phys. 27, 373-80.

Rabitz, H., 1975, J. Chem. Phys. 63, 5208-15.

Raich, J.C., Anderson, A.B., and England, W., 1976, J. Chem. Phys. 64, 5088-94.

Ramaswamy, R., Rabitz, H., and Green, S., 1977, J. Chem. Phys. 66, 3021-30.

Ree, F.H., and Bender, C.F., 1979, J. Chem. Phys. 71, 5362-75.

Riley, M.E., and Kuppermann, A., 1968, Chem. Phys. Lett. 1, 537-8.

Rose, M.E., 1957, Elementary Theory of Angular Momentum, (New York : Wiley).

Rosenthal, A., and Gordon, R.G., 1976, J. Chem. Phys. 64, 1621-9.

Schaefer, H.F., 1972, The Electronic Structure of Atoms and Molecules : A Survey of Rigorous Quantum Mechanical Results (Reading : Addison-Wesley).

Schaefer, J., 1982a, Discuss. Faraday. Soc. 73, 410-3.

Schaefer, J., 1982b, (private communication).

Schaefer, J., 1983, (private communication).

Schaefer, J., and Köhler, W.E., 1985, Physica A. 129A, 469-502.

Schaefer, J., and Liu, B., 1985 (to be published).

Schaefer, J., and Meyer, W., 1979, J. Chem. Phys. 70, 344-60.

Schaefer, J., and Meyer, W., 1983, 13th International Conference on the Physics of Electronic and Atomic Collisions (Berlin : ICPEAC 1983), 702.

Schaefer, J., and Watts, R.O., 1982, Mol. Phys. 47, 933-44.

Schinke, R., Meyer, H., Buck, U., and Diercksen, G.H.F., 1984, J. Chem. Phys. 80, 5518-30.

Schneider, B.I., and Walker, R.B., 1979, J. Chem. Phys. 70, 2466-70.

Scott, M.R., 1973, Invariant imbedding and its applications to ordinary differential equations. An introduction (Reading : Addison Wesley).

Seaton, M.J., 1974, J. Phys. B., 7, 1817-40.

Seaton, M.J., and Wilson, P.M.H., 1972, J. Phys. B, 5, L1-3.

Secrest, D., 1979, Atom-molecule collision theory, Ed. R.B. Bernstein,(New York : Plenum), 265-99.

Secrest, D., 1983, Topics in current physics vol. 33 : Molecular Collision dynamics, Ed. J.M. Bowman, (Berlin : Springer-Verlag), 7-24.

Senff, U.E., and Burton, P.G., 1985, J. Phys. Chem. 89, 797-806.

Shapiro, M., 1972, J. Chem. Phys. 56, 2582-91.

Shapiro, M., and Balint-Kurti, G.G., 1977, Discuss. Faraday. Soc. 62, 51-3.

Shapiro, M., and Balint-Kurti, G.G., 1979, J. Chem. Phys. 71, 1461-1469.

Spitzer, L., and Morton, W., 1976, Astrophys. J., 204, 731-49.

Stechel, E.B., Walker, R.B., Light, J.C., 1978, J. Chem. Phys. 69, 3518-31.

Storey, J.W.V., and Cheung, A.C., 1978, Astrophys. Lett. 19, 89-91.

Takayanagi, K., 1965, Adv. At. Mol. Phys. 1, 149-94.

Tennyson, J., 1982, Chem. Phys. Lett. 86, 181-4.

Tennyson, J., 1983, Comput. Phys. Comm. 29, 307-19.

Tennyson, J., 1984, Comput. Phys. Comm. 32, 109-14.

Tennyson, J., and Noble, C.J., 1984, Comput. Phys. Commun. 33, 421-4.

Tennyson, J., and Sutcliffe, B.T., 1982, J. Chem. Phys. 77, 4061-72.

Tennyson, J., and Sutcliffe, B.T., 1983a, J. Chem. Phys. 79, 43-51.

Tennyson, J., and Sutcliffe, B.T., 1983b, J. Molec. Spec. 101, 71-82.

Tennyson, J., and Sutcliffe, B.T., 1984, Molec. Phys. 51, 887-906.

Tennyson, J., and van der Avoird, A., 1982a, J. Chem. Phys. 77, 5664-81.

Tennyson, J., and van der Avoird, A., 1982b, Discuss. Faraday. Soc. 73, 118-21.

Tennyson, J., and van der Avoird, A., 1982c, J. Chem. Phys. 76, 5710-18.

Tennyson, J., and van der Avoird, 1984a, J. Chem. Phys. 80, 2986-6.

Tennyson, J., and van der Avoird, 1984b, Chem. Phys. Lett. 105, 49-53.

Thakkar, A.J., 1977, Chem. Phys. Lett. 46, 453-6.

Thomas, L.D., 1979, J. Chem. Phys. 70, 2979-85.

Thomas, L.D., 1982, J. Chem. Phys. 76, 4925-31.

Thomas, L.D., Alexander, M.H., Johnson, B.R., Lester, W.A., Light, J.C., McLenithan, K.D., Parker, G.A., Redmon, M.J., Schmalz, T.G., Secrest, D., and Walker, R.B., 1981, J. Comput. Phys. 41, 407-26.

Truhlar, D.G., and Schwenke, D.W., 1983, Chem. Phys. Lett. 95, 83-6.

Vanden Bout, P.A., Steed, J.M., Bernstein, L.S., and Klemperer, W., 1979, Astrophys. J., 234, 503-5.

van der Avoird, A.D., 1982, Discuss. Faraday. Soc. 73, 33-44.

van der Avoird, A., Wormer, P.E.S., Mulder, F., and Berns, R.M., 1980, Top. Current Chem. 93, 1-51.

van Hemert, M.C., 1983, J. Chem. Phys. 78, 2345-54.

Verberne, J., and Reuss, J., 1980, Chem. Phys. 50, 137-45.

Verberne, J., and Reuss, J., 1981, Chem. Phys. 54, 189-200.

de Vogelaere, R., 1955, J. Res. NBS, 54, 119-25.

Waaijer, M., and Reuss, J., 1981, Chem. Phys. 63, 263-73.

Waaijer, M., Jacobs, M., and Reuss, J., 1981, Chem. Phys. 63, 257-61.

Wagner, A.F., and McKoy, V., 1973, J. Chem. Phys. 58, 2604-20.

Watanabe, A., and Welsh, H.L., 1964, Phys. Rev. Lett. 13, 810-2.

Watanabe, A., and Welsh, H.L., 1965, Can. J. Phys. 43, 818-28.

Weissbluth, M., Atoms and Molecules, 1978, (New York : Academic Press).

Wells, B.H., and Wilson, S., 1983, Mol. Phys. 50, 1295-1309.

Wolniewicz, L., 1983, J. Chem. Phys. 78, 6173-81.